INFORMATION TO USERS

This dissertation was produced from a microfilm copy of the original document. While the most advanced technological means to photograph and reproduce this document have been used, the quality is heavily dependent upon the quality of the original submitted.

The following explanation of techniques is provided to help you understand markings or patterns which may appear on this reproduction.

1. The sign or "target" for pages apparently lacking from the document photographed is "Missing Page(s)". If it was possible to obtain the missing page(s) or section, they are spliced into the film along with adjacent pages. This may have necessitated cutting thru an image and duplicating adjacent pages to insure you complete continuity.

2. When an image on the film is obliterated with a large round black mark, it is an indication that the photographer suspected that the copy may have moved during exposure and thus cause a blurred image. You will find a good image of the page in the adjacent frame.

3. When a map, drawing or chart, etc., was part of the material being photographed the photographer followed a definite method in "sectioning" the material. It is customary to begin photoing at the upper left hand corner of a large sheet and to continue photoing from left to right in equal sections with a small overlap. If necessary, sectioning is continued again — beginning below the first row and continuing on until complete.

4. The majority of users indicate that the textual content is of greatest value, however, a somewhat higher quality reproduction could be made from "photographs" if essential to the understanding of the dissertation. Silver prints of "photographs" may be ordered at additional charge by writing the Order Department, giving the catalog number, title, author and specific pages you wish reproduced.

University Microfilms

300 North Zeeb Road
Ann Arbor, Michigan 48106

A Xerox Education Company

72-22,598

CALOYANNIDES, Michael Akylas, 1944-
A MATHEMATICAL AND EXPERIMENTAL INVESTIGATION OF MICROCYCLE SPECTRAL ESTIMATES OF SEMICONDUCTOR FLICKER NOISE.

California Institute of Technology, Ph.D., 1972
Engineering, electrical

University Microfilms, A XEROX Company, Ann Arbor, Michigan

THIS DISSERTATION HAS BEEN MICROFILMED EXACTLY AS RECEIVED.

A MATHEMATICAL AND EXPERIMENTAL INVESTIGATION OF MICROCYCLE SPECTRAL ESTIMATES OF SEMICONDUCTOR FLICKER NOISE

Thesis by

Michael A. Caloyannides

In Partial Fulfillment of the Requirements

For the Degree of

Doctor of Philosophy

California Institute of Technology

Pasadena, California

1972

(Submitted July 6, 1971)

PLEASE NOTE:

Some pages may have

indistinct print.

Filmed as received.

University Microfilms, A Xerox Education Company

ACKNOWLEDGMENTS

The author wishes to express his sincere appreciation to his advisor, Professor H. C. Martel, for his friendly guidance since this author's early undergraduate years.

The financial support of the California Institute of Technology via, among others, a California Institute Foundation Fellowship, is gratefully acknowledged.

The intellectual support which the author received during many years from Professor C. Bures in that most practical discipline, Philosophy, is gratefully acknowledged, too.

This author also wishes to acknowledge the emotional support provided by his adopted "little brother", David, whose presence and need for guidance created plenty of enthusiasm to do this research.

TABLE OF CONTENTS

PART	TITLE	PAGE
	ACKNOWLEDGEMENTS	i
CHAPTER 1.	Abstract	v
CHAPTER 2.	Introduction	1
2.1	Presentation of the Material	6
CHAPTER 3.	Spectral Estimation	9
3.1	General	9
3.2	The Estimator Used in This Experimental Work	14
CHAPTER 4.	Reliability of the Estimate	17
4.1	Exact Spectral Estimate's Variance For Prewhitened Processes	19
4.2	Spectral Variance For $k/\|f\|^{\alpha}$, $\alpha > 0$ Processes	22
4.2.1	Effect of Truncation of the Assumed Spectrum on the Variance	25
4.3	Discussion of Variance Considerations	25
CHAPTER 5.	Consideration of Specific Steps in the Estimator Used in this Work	30
5.1	Prewhiteneing and Postgreening	30
5.2	Windowing	34
5.3	Aliasing and Dealiasing	36
5.4	Removal of the Constant Mean	40
5.4.1	Effect of Removing an Inaccurately-Estimated Constant Mean	42
5.5	Treatment of Multiple Noise Sources	46

TABLE OF CONTENTS con't.

PART	TITLE	PAGE
CHAPTER 6.	Major Sources of Bias in the Estimate	59
6.1	Linear Trend Removal from the Data	70
CHAPTER 7.	Theoretical Considerations about Flicker Noise	73
7.1	Mathematically Modeling the Flicker Noise Mechanism	73
7.1.2	Experimental Justification for Such Models	81
CHAPTER 8.	Cost-Reducing Data-Taking Algorithms	87
8.1	Non-Constant but Non-Random Sampling	88
8.1.2	Mathematics Pertaining to Such Sampling	93
8.2	Alternate Cost-Reducing Data-Processing Algorithms	99
CHAPTER 9.	Low Frequency Spectral Estimation Experiments	101
9.1	General Considerations	101
9.2	Design of the Noise Sources	102
9.3	Design of the Power Supply	108
9.4	Temperature Regulation	109
9.4.1	Passive Attenuation and Internal Temperature Rise	119
9.4.2	Active Temperature Control	127
9.5	Automatic Data-Collecting Circuits	143

TABLE OF CONTENTS con't.

PART		TITLE	PAGE
CHAPTER 9. con't.			
	9.5.1	Error-Control Coding Used	156
	9.6	Auxiliary Data-Collection Circuits	159
	9.7	The Paper-Punch Recorder	160
	9.8	The Computer Program	162
CHAPTER 10.		Semiconductor Noise Experiments	165
	10.1	Mk.II and Mk.III Spectral Density Estimates	166
	10.2	Time Multiplexed Op-Amps' Spectral Density Estimates	170
	10.3	Interpretation of Significant Experimental Results of this Work	191
CHAPTER 11.		Conclusions and Further Work	206
		Appendix A	208
		Appendix B	211
		References	217
		List of Figures	227

1. ABSTRACT

The experimental portion of this thesis tries to estimate the density of the power spectrum of very low frequency semiconductor noise, from $10^{-6.3}$ cps to 1. cps with a greater accuracy than that achieved in previous similar attempts: it is concluded that the spectrum is $1/f^{\alpha}$ with α approximately 1.3 over most of the frequency range, but appearing to have a value of about 1 in the lowest decade. The noise sources are, among others, the first stage circuits of a grounded input silicon epitaxial operational amplifier. This thesis also investigates a peculiar form of stationarity which seems to distinguish flicker noise from other semiconductor noise.

In order to decrease by an order of magnitude the pernicious effects of temperature drifts, semiconductor "aging", and possible mechanical failures associated with prolonged periods of data taking, 10 independent noise sources were time-multiplexed and their spectral estimates were subsequently averaged. If the sources have similar spectra, it is demonstrated that this reduces the necessary data-taking time by a factor of 10 for a given accuracy.

In view of the measured high temperature sensitivity of the noise sources, it was necessary to combine the passive attenuation of a special-material container with active control. The noise sources were placed in a copper-epoxy container of high heat capacity and medium heat conductivity, and that container was immersed in a temperature controlled circulating ethylene-glycol bath.

Other spectra of interest, estimated from data taken concurrently with the semiconductor noise data were the spectra of the bath's controlled temperature, the semiconductor surface temperature, and the power supply voltage amplitude fluctuations. A brief description of the equipment constructed to obtain the aforementioned data is included.

The analytical portion of this work is concerned with the following questions: what is the best final spectral density estimate given 10 statistically independent ones of varying quality and magnitude? How can the Blackman and Tukey algorithm which is used for spectral estimation in this work be improved upon? How can non-equidistant sampling reduce data processing cost? Should one try to remove common trands shared by supposedly statistically independent noise sources and, if so, what are the mathematical difficulties involved? What is a physically plausible mathematical model that can account for flicker noise and what are the mathematical implications on its statistical properties? Finally, the variance of the spectral estimate obtained through the Blackman/Tukey algorithm is analyzed in greater detail; the variance is shown to diverge for $\alpha \geq 1$ in an assumed power spectrum of $k/|f|^{\alpha}$, unless the assumed spectrum is "truncated".

CHAPTER 2

INTRODUCTION

Why is flicker noise important?

Nature has been generous in displaying many kinds of noise. Semiconductors, in particular, are mainly affected by five kinds: thermal noise, generation-recombination noise, partition noise, shot noise and flicker noise. Thermal noise is well understood in principle[1] and is attributed to random collision of carriers within the lattice. Generation-recombination noise refers to the random generation and recombination of hole-electron pairs, and of carriers with traps.[2] Partition noise has been explained essentially in terms of a carrier current being split into two parts that flow to different electrodes.[1] Shot noise has had more than its share of attention for many years and has been found to be caused by the random emission of electrons and photons; more recently, a simple shot noise picture has reasonably described such effects in diodes, transistors, FET's and avalanche diodes.[1] Flicker noise refers to the noise whose spectral density is observed to increase as frequency decreases; it is also known as "excess noise", "1/f noise", "semiconductor noise", "low frequency noise", "pink noise", and "contact noise"; indeed, it is quite ubiquitous: it was discovered in tubes,[3] in quartz crystal oscillators,[4] semiconductor diodes, resistors,[5] light sources,[6] field effect transistors,[7] bipolar transistors,[8] thermistors,[8] carbon microphones,[9] thin films,[10] biological membrane potentials,[11] the frequency of the rotation of the earth,[12]

and even galactic radiation noise.[13] One is indeed very tempted to suspect the presence of an underlying physical law that would explain the existence of flicker noise in so many different physical situations.

Flicker noise is important in precise experimentation. Whereas any desired precision can be obtained for a measurement contaminated with white noise by increasing the duration of the experiment, a measurement with results whose accuracy is limited by 1/f noise may not be improved by prolonging the data-taking time.[14] In a typical application a quartz crystal was used in a slave oscillator; were it not for flicker noise which produced frequency fluctuations of at least three parts in 10^{13},[15,16] the precision of ten second interval measurements would be better than one part in 10^{14}.[17]

Several formal theories have been presented in the past trying to explain flicker noise. Experiments with germanium by McWhorter[18] showed that there exists a set of surface states with a relaxation time of the order of minutes; the physical model suggested is a plausible one and also applicable to FET's and to semiconductor filaments. Fonger[19] and Watkins[20] extended the model to junction diodes and transistors, and recently Van Der Ziel[1] further developed this theory on the model that the carriers in the material interact with trapping levels at some depth in the surface oxide by tunneling. The mathematics of it are fairly straightforward and concise, yet the underlying implication is that if one measures long enough to estimate spectra at low enough frequencies he will indeed find a leveling-off of the spectral density estimate.

Somewhat along the same vein, though concerned more with the mathematics of it, D. Halford[14] has shown that any class of "reasonable" time-dependent perturbations (such as a series of exponential decays appropriately scaled in amplitude and time) occurring at random can result into 1/f spectra for frequencies in an arbitrarily large but finite range. Schonfield and Barnes[22] have also advanced a method of generating 1/f noise which pays special attention to the shape of each of the perturbations; yet a physical explanation of an 1/f spectrum extending over more than a couple of decades of frequency would require postulating the existence of very specially shaped disturbances which would be hard to justify on physical grounds.

Mathematically inclined researchers, on the other hand, have claimed that it is the blind extrapolation of the 1/f behavior to $f = 0$ which incorrectly suggests that the total energy is infinite ("infrared catastrophe"); based on some recent experiments by J. Brophy[5] suggesting a peculiar lack of conventional stationarity in 1/f noise samples, Mandelbrot[23] conjectures that the "infrared catastrophe" paradox is a consequence of applying the usual Wiener mathematics on a sample which is not stationary and thus not eligible for that mathematics; accordingly he introduces the concept of the "conditional spectrum" to be applied to such "sporadic functions".

The mathematics of spectrum analysis is a topic in itself having gone through three or four eras of improvements. An often-used in the past and intuitively appealing way to estimate power spectral densities is by means of the "periodogram". As is discussed in Section 3.1., how-

ever, the periodogram gives an estimate of spectral density which is in some cases quite questionable; it thus proved unsatisfactory. The estimation of spectra via mean lagged products originally advanced by Blackman and Tukey,[24] instead, proved effective in answering many questions and provided insight about the essential limitations of the problem. It is via mean lagged products that the spectral estimates of the experimental portion of this thesis are arrived at. Indeed, it takes considerably fewer arithmetic operations to calculate approximately one-tenth as many mean lagged products as there are data points, and then to Fourier-transform the results, than it does to calculate all the Fourier coefficients of a time series. Yet the very straightforwardness of this approach suggests that some improvements could be made to optimize the computational operations involved such as the recording of data points which are not equally spaced in time. Such questions are considered in detail in Section 8.1.

A new algorithmic process for calculating with great computational efficiency the spectrum of a time series has been advanced by Tukey[26] under the name of the "Fast Fourier Transform". There are at least two somewhat different approaches to implementing the "Fast Fourier Transform", one due to Cooley and Tukey (the CT method), and another programmed by Sande along lines suggested in lectures by Tukey. The fast Fourier transform requires on the order of $2T\log_2 T$ arithmetic operations (where T is a power of 2) whereas the convolution operations in computing mean lagged products require approximately nT multiply-and-add operations for n data points and for a maximum lag of T. Indeed there are a variety of

potential applications of the fast Fourier transform, especially when quick estimation of the frequency content of a nonstationary signal are essential.

The theoretical analysis of the Blackman/Tukey algorithm (and of other algorithms) is incomplete in that it is not known how the quality of the final spectral density estimate deteriorates if the input data deviates from various assumptions built into the Blackman/Tukey algorithm.

On the experimental side, prior spectral estimates have not gone below the $f = 10^{-6.0}$ cps frequency; worse yet, the best available such estimate[25] is of questionable reliability at the low frequency end for reasons related to the mathematics of the spectral estimator used. The fundamental difficulty in obtaining reliable spectral density estimates at very low frequencies is that excessively long data-taking periods are required, during which all pertinent equipment must be highly stable and insensitive to environmental variables such as temperature, line voltage fluctuations, etc.; indeed, it can be readily appreciated that the experimental difficulties associated with a doubling of the data-taking period from one month to two months are considerably less than half of the difficulty involved in moving from a two-month to a four month data-taking period.

This thesis deals extensively with the above theoretical questions; it also extends the experimentally measured spectral density estimates by an octave at the low end, while concurrently giving more reliable estimates at such frequencies as the 10^{-6} cps figure mentioned above.

It appears from the foregoing that the problem of flicker noise has some very specific areas where questions are waiting for answers and mathematical procedures need improvement. Is semiconductor flicker noise such that it indeed does not go like 1/f to sufficiently low frequencies but levels off instead? Is flicker noise perhaps nonstationary in a specific measurable way? What mathematical yet physically plausible model can result in 1/f noise and be consistent with the observed statistics of the experimental portion of this thesis? How can one optimize the well-developed mean-lagged-product approach in the sense of achieving higher computational efficiency?

It is hoped that this thesis will provide considerable light on the above questions, too.

2.1 PRESENTATION OF THE MATERIAL

In a dissertation dealing with a number of interrelated topics, the particular order of presentation is, to a degree, a matter of subjective choice.

The material in the present work is presented in a way which appears most logical to this author, and which will facilitate understanding even by a reader who is not a specialist in this particular field.

Spectral estimation mathematics are discussed first with some emphasis on why this apparently well-known topic presents some difficulties in experimental practice.

A detailed exposition of the particular spectral estimator used in the experimental part of this work is presented next in order to provide

the necessary ground work on which subsequent analyses are based. This author is well aware that the reader may not be familiar with specific steps in the algorithm at this stage. Accordingly, Chapter 5 considers in adequate detail those aspects of the estimator which the reader may not see the justification for.

The reliability of the final estimate is of major importance in explaining why some, possibly unfamiliar, steps are included in the estimator; this is discussed in Chapter 4 which precedes the detailed analysis of such unfamiliar steps.

Chapter 6 points out some major sources of possible distortion of the spectral estimate as obtained experimentally.

Chapter 7 considers some mathematical and physical implications of flicker noise and compares those with the experimental evidence available.

This is followed by an application-oriented consideration of cost-reducing data-taking or data-processing algorithms; this chapter is motivated by the generally high expense involved in obtaining reliable low-frequency spectral density estimates.

This concludes the theoretical portion of this work. Chapter 9 considers the experimental set-up used in this work as well as the reasons for the particular choices made. By this time, all necessary background information has been presented for a meaningful evaluation of the actual experimental results obtained; this is done in Chapter 10 which presents and discusses experimental results in the chronological order in which they were obtained; this approach has the advantage of indicating why certain improvements were necessitated on the experimental set-up while

this work was in progress; the final spectral density estimate is thus, naturally, given last and it is accompanied by other data relevant to it.

Very little material is of clearly peripheral nature, and such material is relegated to appendices.

Except for the material on the spectral estimator for a single stochastic process and the associated elaborations on some parts of Chapter 5, this work is entirely the work of this author except for contributions in the form of thought-provoking discussions by this author's thesis advisor.

CHAPTER 3

SPECTRAL ESTIMATION

3.1 General

Before settling on a specific mathematical technique for estimating the spectral densities of the noise sources for this thesis, it was deemed worthwhile reviewing other than the latest techniques; aside from gaining insight into the specific difficulties of mathematical spectral density estimation, it was thought that some refinement of an older, intuitively "natural" approach known as the periodogram might produce a usable algorithm for a "good" estimate. Letting

$$X_T(f) = \int_0^T x(t)e^{i\omega t}\,dt \tag{1}$$

and assuming ergodicity, then the quantity

$$S_T(f) \equiv \frac{|X_T(f)|^2}{T} \tag{2}$$

called the "periodogram", appears to provide a power spectral density estimate of the random process $x(t)$, $t\varepsilon[0,T]$. In particular, letting $T \to \infty$, would (incorrectly in some cases) suggest that

$$\lim_{T\to\infty} S_T(f) = S(f) \equiv \text{True Spectral Density.}$$

This procedure has been shown[27] to fail for a large class of examples, such as for real gaussian processes. The "catch" is that although

$$\lim_{T \to \infty} E[S_T(f)] = S(f) \tag{3}$$

where E is the expectation operator, the variance

$$\sigma^2[S_T(f)] = E\{S_T(f) - E[S_T(f)]\}^2 \tag{4}$$

will not necessarily tend to zero, as $T \to \infty$. Specifically, it has been shown[27] that for a real gaussian process

$$\sigma^2[S_T(f)] \geq \{E[S_T(f)]\}^2 \tag{5}$$

for all T . It follows that the variance of $S_T(f)$ does not approach zero in the limit as $T \to \infty$ for all f such that $S(f) > 0$; that is, the estimate $S_T(f)$ does not converge in the mean to the true spectrum for any frequency except possibly those for which $S(f) = 0$.

The next logical step is to go back to the definition of the power spectral density and try to apply it to a discrete time series with the minimum of distortion. This is the Blackman and Tukey[24] type spectral estimator and it is through the use of this estimator that the experimental results of this thesis are derived. The estimator is basically a plausible finite-difference approximation to the exact definition of spectral density given by

$$S(f) \equiv \int_{-\infty}^{\infty} R(\tau) e^{i\omega t}\, dt \tag{6}$$

Since one has available at best a small number of sample functions extended in time rather than an extended number of short-duration sample functions, ergodicity of the autocorrelation and of the mean are essential assumptions. Specifically, it has been shown[28] that the necessary and

sufficient condition for the ergodicity of the mean is that

$$\lim_{T\to\infty} \frac{1}{2T} \int_{-T}^{T} R(\tau)d\tau = \eta^2 \tag{7}$$

where $R(\tau)$ is the autocorrelation function and η is the mean of the (stationary) process; the necessary and sufficient condition for ergodicity of the autocorrelation has been shown[28] to be

$$\lim \frac{1}{T} \int_{0}^{2T} (1 - \frac{\tau}{2T})\, C(\tau,\lambda)d\tau = 0 \tag{8}$$

for any given λ, where $C(\tau,\lambda)$ is the autocovariance of the process

$$x(t + \lambda)\, x(t)$$

Whereas to test for the ergodicity of the mean it is sufficient to know η (which in practice is never known exactly) and $R(\tau)$, testing for the ergodicity of the autocorrelation requires knowledge of fourth-order moments not readily available from a finite duration sample function.

Assuming ergodicity, the autocorrelation of a continuous stochastic process $x(t)$, $t\varepsilon(-\infty,\infty)$ is defined for any τ as

$$R(\tau) = \lim_{T\to\infty} \frac{1}{2T} \int_{-T}^{T} x(t + \tau)x(t)dt \tag{9}$$

The closest equivalent to this definition for a discrete time series of n samples taken at equidistant sampling intervals is

$$C(r\Delta\tau) = \frac{1}{n-r} \sum_{q=1}^{n-r} x(q\Delta\tau) \cdot x[(q+r)\Delta\tau] \tag{10}$$

$$r = 0,1,2,\ldots m < n$$

with $$C(-r\Delta\tau) \triangleq C(r\tau) \qquad (11)$$

These $C(r\Delta\tau)$'s are Blackman and Tukey's "mean lagged products", where $\Delta\tau$ is the sampling interval.

In order to have a reasonable variance for $S(f)$ at the low frequencies, it is shown below that it is necessary to restrict m to a value much less than n ; m in this work is taken equal to $n/100$ or $n/10$ depending on whether a single source or 10 noise sources are being tested.

Distortion has already been introduced by an implicit time window associated with the finite length of the sample function chosen. Forgetting momentarily such subtle issues as prewhitening, transformations and windows, the effects of which have been amply discussed in the literature,[24],[25] the Fourier transform of the function $C(r\Delta\tau)$ is needed next. The problem is that in the finite-difference approximation $C(r\Delta\tau)$ is not defined for times other than

$$t = k \cdot \Delta\tau, \; k = 0, \pm 1, \pm 2, \ldots, (n-1) \; .$$

Blackman and Tukey have selected the intuitively plausible alternative to the Fourier transform of $C(r\Delta\tau)$

$$V(f_r) = \Delta\tau[C(0)+2\sum_{q=1}^{m-1} C(q\Delta\tau)\cos\frac{qr\pi}{m} + C(m\Delta\tau)\cos r\pi)] \qquad (12)$$

where $\omega q\Delta\tau = rq\pi/m$, and $r = 1,2, \ldots m$ (13)

It is interesting to point out that Eq. (12) can be looked upon as an approximate Fourier transform of the finite-length staircase shown in Fig. 1 below.

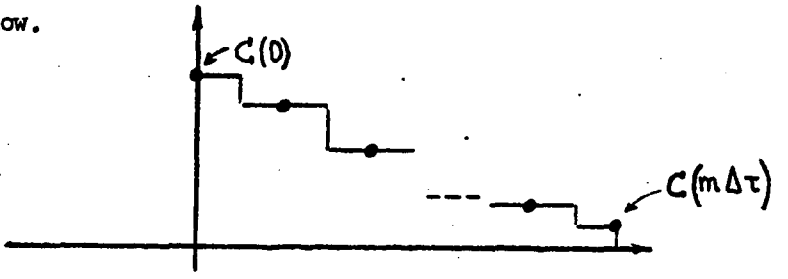

Fig. 1

Modified Autocorrelation Function

It is clearly important that this approximation is most valid if the truncated $C(q\Delta\tau)$ has nearly the same Fourier transform as the non-truncated $C(q\Delta\tau)$; this, in turn, implies the desirability that $C(q\Delta\tau)$ have a small magnitude outside the $|m\Delta\tau|$ band.

The result of Fourier-transforming this quantity is equivalent to the convolution of a "window" with unity height and width $2m\Delta\tau$, centered at the origin, convolved with $C(k\Delta\tau)$ which is in principle known over a much longer interval, $|k\Delta\tau| < n\Delta\tau$.

Then letting $V(f_r) \triangleq V_r$ for notational simplicity, V_r of Equation (12) is

$$V_r \approx \text{F.T}\left\{C(k\Delta\tau) * \text{F.T.}[D_o(\tau)]\right\} \tag{14}$$

where:

$D_o(\tau)$ is the aforementioned window

F.T. is the Fourier transform

$*$ stands for convolutions.

The well documented topic of optimal windows is discussed to some extent in Section 5.2; for the present introductory purposes, suffice it to say that a smoother window than $D_o(\tau)$ above, results in lower variance of the final spectral density estimate.

Considering that the Blackman/Tukey estimator is the best available estimator in terms of accuracy, computational economy, and conceptual simplicity, it was actually used for the data processing of the experimental part of this thesis.

3.2 The Estimator Used in this Experiment

The exact algorithm used in deriving a spectral density estimate in the experimental part of this work is that given by Blackman/Tukey's original paper[24].

The steps indicated below may not be all immediately obvious, and the reader is referred to the aforementioned original presentation; a few aspects of the algorithm which are of special interest in the present work are elaborated upon in detail in Chapter 5.

The purpose of this presentation of the algorithm at this particular stage in this work is to provide the essential definitions, symbols, and notations used throughout this work. Reference will be made to these equations in later sections.

Given n equidistant data samples

$x_i \quad i \in [1, n]$,

form the "prewhitened" set of data samples

$$z_j = \sum_{i=0}^{k} A_i \, x_{i+j}, \quad j = 1, 2, \ldots (n-k) \quad . \quad k = 9 \text{ in this work.} \qquad (15)$$

where A_i's are appropriate constants.

Form the mean-lagged products,

$$C(r\Delta\tau) \triangleq C_r = \frac{1}{(n-k)-r} \sum_{q=1}^{n-k-r} z_q \cdot z_{q+r} - \left[\frac{\sum_{q=1}^{n-k} z_q}{n-k}\right]^2 \qquad (16)$$

The mean-lagged-products equation (16) is functionally different to a small degree, from Equation (10) in that it incorporates removal of the mean as well. This rather peculiar way of removing the mean has been extensively analyzed by Blakemore, and will thus not be elaborated upon in this work.

Compute the "raw spectral density estimates"

$$V_r = \Delta\tau\left[C_o + 2\sum_{q=1}^{m-1} C_q \cos\frac{qr\pi}{m} + C_m \cos r\pi\right] \qquad (17)$$

Compute the refined ("windowed") spectral density estimates

$$U_r = a_{-1} V_{r-1} + a_o V_r + a_1 V_{r+1}, \qquad r = 2, 3, \cdots (m-1) \qquad (18)$$

Postgreen the above refined spectral estimates by dividing each U_r by $|Y_r|^2$ to obtain the aliased spectral estimates

$$\frac{U_r}{|V_r|^2} \triangleq S_A(f_r) \qquad (19)$$

where Y_r depends on the prewhitening performed earlier, which, in turn, depends on the (guessed or approximately estimated) power spectral density of the process in question.

De-alias the above aliased spectral estimates to obtain the final dealiased estimates given by

$$S(f_r) = S_A(f_r) - \sum_{q=1}^{m} \left[S\left(\frac{q}{\Delta\tau} - f_r\right) + S\left(\frac{q}{\Delta\tau} + f_r\right) \right] \qquad (20)$$

Although the S appearing in the summation should be the true spectral density, in practice it must be an estimate or an experimental value that is used to effect the dealiasing.

For notational simplicity, the above notation will be adhered to in this work, and no special symbols such as $\hat{}$ will be used to denote an estimate, unless it is not clear from the discussion whether a quantity is an estimate or not.

The significance of prewhitening, postgreening, "windowing", and de-aliasing will be dealt with to some extent in Chapter 5.

CHAPTER 4

RELIABILITY OF THE SELECTED ESTIMATOR

The estimator $V(f_r)$ given in Equation (12) is a linear function of the mean-lagged-products which, in turn, were defined to be functions of random variables (the raw data); as such, $V(f_r)$ is a random variable itself, having a mean and a variance. It is in terms of its mean and variance therefore that we can answer the pertinent question "how good an estimator is it?". The computational details have amply been explored by both Blackman and Tukey's original presentation of the estimator[24] and, subsequently, by Blakemore's review and additional analysis of some of its properties.

The reason for studying the variance of the spectral estimate is twofold:

1) We want a measure of the accuracy of the final estimate.
2) We specifically want to observe if the variance of the estimate increases for any particular shape of power spectra, and, if so, in what way.

Trying to analytically express the variance of the spectral estimate is no straightforward task. Blackman and Tukey started by calculating the covariance between the spectral estimate at two different frequencies; this approach also provides the correlation between adjacent estimates. In the interest of deriving a variance expression which is simple to use for quick evaluations, Blackman and Tukey and subsequently, Blakemore, had to resort to simplifying assumptions; such assumptions have no bearing on the eligibility of a particular stochastic

process to be analyzed by this estimator, but only imply that the variance of the estimator will then be harder to calculate. The aforementioned assumptions are that $x(t)$ is a sample function from a zero mean stationary gaussian stochastic process. The resulting covariance can be written as in Reference (24). Let $Q_i(f)^*$ denote the Fourier transform of a window $D_i(\tau)$ whose shape may or may not be rectangular; then, for the continuous data case,

$$\mathrm{Cov}_i\{S(f_1),S(f_2)\} \approx \frac{1}{4}\int_{-\infty}^{\infty}[Q_i(f+f_1) + Q_i(f-f_1)][Q_i(f+f_2) + Q_i(f-f_2)]\Gamma(f)df \tag{21}$$

where

$$\Gamma(f) = 4\int_{-\infty}^{\infty} S(f+f')S(f-f')\left[\frac{\sin(\omega' T_N)}{(\omega' T_N)}\right]^2 df' \quad . \tag{22}$$

and $T_N = n\Delta\tau$. The desired variance, thus reduces to

$$\sigma_i^2[S(f_1)] \approx \frac{1}{4}\int_{-\infty}^{\infty}[Q_i(f+f_1) + Q_i(f-f_1)]^2\Gamma(f)df \tag{23}$$

The need for some simpler-looking measure of the quality of the estimate $S(f_i)$ is obvious, and an additional simplifying assumption is thus in order. The motivation for this assumption is purely mathematical in that it greatly simplifies the actual computation of $\Gamma(f)$ given in Equation 22. Indeed, the only functional form of $S(f_i)$ for which the variance, Eq. (23), has been evaluated is the case of $S(f) = K$, where

*i is a bookkeeping index of different window shapes; see Section 5.2.

K = constant. This case is of particular interest because, as is shown later in this work, "prewhitening" of any nonconstant power spectrum is highly desirable because among other reasons it appears to result in lower variance of the estimated spectrum.

4.1 Exact Spectral Estimate Variance for Prewhitened Processes

Let the prewhitened spectrum $S(f)$ be approximated by a constant. Then

$$\Gamma(f) = 4 \int_{-\infty}^{\infty} K^2 \frac{\sin^2 2\pi T_N f'}{(2\pi T_N f')^2} df', \quad \text{where} \quad K = S_{\text{prewhitened}}$$

This integral is extensively tabulated, and its derivation will not be repeated here. The result is

$$\Gamma(f) = \frac{4K^2\pi}{2\pi T_N} = \frac{2K^2}{T_N}$$

The derivation will thus continue from this stage.

$$\text{var}[S(f_j)] = \frac{1}{4} \int_{-\infty}^{\infty} [Q_i(f+f_j) + Q_i(f-f_j)]^2 \Gamma(f) df$$

For computational simplicity the analysis will proceed with the zeroth window, D_o of width $2\,T_M = 2\,m\Delta\tau$. Substituting $i = 0$ in Eq. (23) above, yields

$$\text{var} = \frac{1}{4} \int_{-\infty}^{\infty} [Q_o(f+f_1) + Q_o(f-f_1)]^2 \Gamma(f)$$

where $\Gamma(f) = \frac{2K^2}{T_N}$ and $Q_o(f) = 2\,T_M \left(\frac{\sin 2\pi f T_M}{2\pi f T_M}\right)$

$$\therefore \text{ var} = \frac{1}{2T_N} \int_{-\infty}^{\infty} [Q_o^2(f+f_1) + Q_o^2(f-f_1) + 2Q_o(f+f_1)Q_o(f-f_1)]K^2 df$$

$$= \frac{2T_M^2K^2}{T_N} \int_{-\infty}^{\infty} \frac{\sin^2[2\pi(f+f_1)T_M]}{[2\pi(f+f_1)T_M]^2} df +$$

$$+ \frac{2T_M^2K^2}{T_N} \int_{-\infty}^{\infty} \frac{\sin^2[2\pi(f-f_1)T_M]}{[2\pi(f-f_1)T_M]^2} df +$$

$$+ \frac{4T_M^2K^2}{T_N} \int_{-\infty}^{\infty} \frac{\sin[2\pi(f-f_1)T_M] \cdot \sin[2\pi(f+f_1)T_M]}{[2\pi(f-f_1)T_M][2\pi(f+f_1)T_M]} df$$

Let the first additive term on the right hand side of the last equation be denoted by I_1, the second one by I_2 and the third by I_3.

It is well known that

$$\int_{-\infty}^{\infty} \frac{\sin^2(ax-b)}{(ax-b)^2} dx = \frac{\pi}{a}$$

and that

$$\int_{-\infty}^{\infty} \frac{\sin(ax+k)}{ax+k} \cdot \frac{\sin(ax+\ell)}{ax+\ell} dx = \frac{\pi}{a} \frac{\sin(k-\ell)}{(k-\ell)}$$

In our case

$$k = +2\pi f_1 T_M \ , \quad \ell = -2\pi f_1 T_M \ , \quad k-\ell = 4\pi f_1 T_M \ .$$

$$\text{var} \triangleq I_1 + I_2 + I_3 \ , \text{ and therefore}$$

$$\text{var} = \frac{2T_M^2K^2}{T_N} \cdot \frac{\pi}{2\pi T_M} + \frac{2T_M^2K^2}{T_N} \cdot \frac{\pi}{2\pi T_M} + \frac{4T_M^2K^2}{T_N} \cdot \frac{\pi}{2\pi T_M} \cdot \frac{\sin 4\pi f_1 T_M}{4\pi f_1 T_M}$$

$$\therefore \frac{var}{K^2} = \frac{T_M}{T_N} + \frac{T_M}{T_N} + \frac{2T_M}{T_N}\frac{\sin(4f_1\pi T_M)}{(4\pi f_1 T_M)}$$

$$= \frac{2T_M}{T_N}\left(1 + \frac{\sin 2\phi}{2\phi}\right) \quad \text{where} \quad \phi = 2f_1\pi T_M \tag{24}$$

An approximate, and simpler, way to estimate the integral

$$var[S(f_1)] \approx \frac{1}{2T_N}\int_{-\infty}^{\infty}[Q_o^2(f+f_1) + Q_o^2(f-f_1) + 2Q_o(f+f_1)Q_o(f-f_1)]K^2\,df$$

is as follows.

Avoiding the inconclusive result,

$$\lim_{T_M \to \infty} Q^2(f) = \lim_{T_M \to \infty} \frac{\sin^2(2\pi f T_M)}{\pi^2 f^2} = \text{undefined},$$

one observes that

$$\left[\frac{\sin L(f-f_j)}{L(f-f_j)}\right]^2 \triangleq F$$

is a function of a given shape which "shrinks" in width as L increases, without changing shape, as shown below.

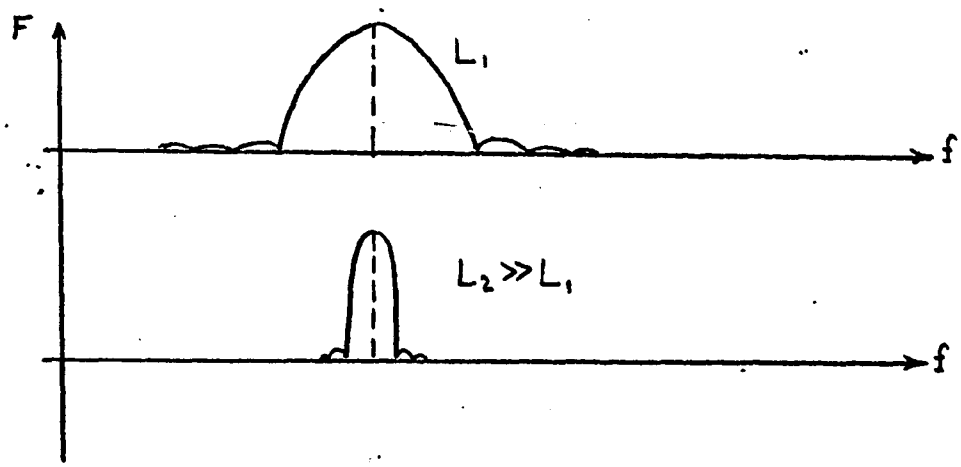

When this function F is multiplied by L^2, it becomes spike-like in behavior as a factor of an integrand; in fact, it behaves in this context as a delta function of weight

$$4T_M^2 \int_{-\infty}^{\infty} \frac{\sin^2 2\pi T_M(f-f_j)}{(2\pi T_M(f-f_j))^2}\, df = \frac{\pi}{2\pi T_M} \cdot 4T_M^2 = 2T_M$$

hence

$$\text{var}[S(f)] \cong \frac{1}{2T_N} \int_{-\infty}^{\infty} [2T_M\, \delta(f+f_1) + 2T_M\, \delta(f-f_1)]S^2(f)df$$

$$= \frac{2T_M}{T_N}\, S^2(f) \quad .$$

which agrees basically with Eq.(24).

In a similar way, one can approximately evaluate the variance for other windows. The details can be found in Ref. 24 and are not repeated here. For the commonly used windows (usually referred to as Q_1, Q_2 and Q_3) the result is:

$$\text{var}[S(f_j)] = K \frac{T_M}{T_N} S^2(f_j) \qquad (25)$$

where K is slightly less than 1, the actual value depending on both the index i and the frequency f_j.

4.2 Variance Considerations for $1/|(f)|^{\alpha}$ Processes.

The question raised next is if this spectral estimate's variance can be analytically derived for a more complicated power spectral density; the bothersome case of

$$S = K/f^1$$

is of great interest in the framework of this work.

Difficulties may be foreseen if one thinks of the problem as a regular integration of a diverging integrand; $1/f$ does diverge, after all, at $f = 0$. Arbitrary truncation of the $1/f$ behavior is a way out, although a poor one as shown below.

The two questions of significant interest are:

(a) Does the estimate's variance of an assumed $K/|f|^{\alpha}$ power spectrum diverge for certain values of α ?

(b) If so, what is the significance of "divergence" of the variance for actual experimental data-processing situations? The pertinent question thus is: which is the critical exponent, α , $\alpha > 0$ in $S \triangleq K/|f|^{\alpha}$, above which the variance of the spectral estimate diverges? The question is of practical interest in evaluating spectral estimates of unprewhitened processes; it is also of theoretical interest in that it establishes once and for all the critical value of the parameter α below which the "infrared catastrophy" does not exist as a possibility.

Letting $H_i(f;f_1) \triangleq Q_i(f+f_1) + Q_i(f-f_1)$, Equation (23) becomes

$$\text{var}_i\{S(f_1)\} = \frac{1}{4}\int_{-\infty}^{\infty}[H_i(f;f_1)]^2\Gamma(f)df$$

Substituting $S(f) = K/|f|^{\alpha}$ in

$$\Gamma(f) = 4\int_{-\infty}^{\infty} S(f+y)S(f-y)\left(\frac{\sin 2\pi y T_N}{2\pi y T_N}\right)^2 dy$$

yields $$\text{var}_i\{S(f_1)\} = \int_{-\infty}^{\infty}[H_i(f;f_1)]^2\left[\int_{-\infty}^{\infty}\frac{K}{|f+y|^{\alpha}}\cdot\frac{K}{|f-y|^{\alpha}}\cdot\left[\frac{\sin 2\pi y T_N}{2\pi y T_N}\right]^2 dy\right]df$$

It can readily be seen that the quantity in the brackets will diverge for those values of the parameter α where

$$\int_{-\infty}^{\infty}\frac{1}{|x|^{\alpha}}\,dx$$

will diverge.

It is quite clear that the above integral will diverge for $\alpha \geq 1$ but will not diverge for $0 \leq \alpha < 1$

Since the quantity in the brackets is part of the integrand of $\text{var}_i[S(f_1)]$, and since the divergence is in no way "undone" by the rest of the integrand, $\text{var}_i[S(f_1)]$ will diverge, too.

In the interest of completeness it is of interest to consider if the above results hold for sampled data systems too.

If, in the derivation of the spectral variance of sampled data systems, the appropriate mathematical changes are made to allow for the sampled nature of the input data, it has been shown[24] that for equidistant sampling

$$\operatorname{var}_i\{U_r\} = \frac{1}{4}\int_{-\infty}^{\infty} H_{iA}^2(f; \tfrac{r}{2m\Delta\tau})\Gamma_{\Delta\tau}(f)df$$

$$= \frac{1}{4}\int_{-\infty}^{\infty}\left[Q_{iA}(f + \tfrac{r}{2m\Delta\tau}) + Q_{iA}(f - \tfrac{r}{2m\Delta\tau})\right]^2\Gamma_{\Delta\tau}(f)df$$

$$= \frac{1}{4}\int_{-\infty}^{\infty}\left[\sum_{q=-\infty}^{\infty}Q_i(f + \tfrac{r}{2m\Delta\tau} - \tfrac{q}{\Delta\tau}) + \sum_{p=-\infty}^{\infty}Q_i(f - \tfrac{r}{2m\Delta\tau} - \tfrac{q}{\Delta\tau})\right]^2\Gamma(f)df$$

where

$$\Gamma_{\Delta\tau}(f) = 4\int_{-\infty}^{\infty} S(f + y)S(f - y)\left(\frac{\sin 2\pi yn\Delta\tau}{n\sin 2\pi y\Delta\tau}\right)^2 dy \quad .$$

where n, $\Delta\tau$, m, are constants. Consider $\Gamma_{\Delta\tau}(f)$ first. Let $S(f) \triangleq K/|f|^{\alpha}$

$$\Gamma_{\Delta\tau}(f) = 4\int_{-\infty}^{\infty} \frac{K}{|f+y|^{\alpha}} \cdot \frac{K}{|f-y|^{\alpha}} \cdot \left(\frac{\sin 2\pi yn\Delta\tau}{n_o\sin 2\pi y\Delta\tau}\right)^2 dy$$

Clearly, the analysis which indicated divergence for $\alpha \geq 1$ for continuous data systems applies equally well to sampled data systems.

It is important to consider, at this stage, what the implications of the above results are in an actual experimental situation. The experimental results to be presented later do imply a nearly 1/f spectrum over a remarkably wide range. However, they do not appear to be consistent with an infinite variance for the spectral estimate. It may well be that this seeming discrepancy is due to the experimental procedures used in taking data.

It does appear quite plausible, however, that some form of variance-increase must be expected if a noise source is not prewhitened prior to subsequent data processing. This will be discussed further in the final chapter of the thesis.

4.2.1 Effect of Truncation of the Assumed Spectrum on the Variance.

Assume a power spectrum of the form

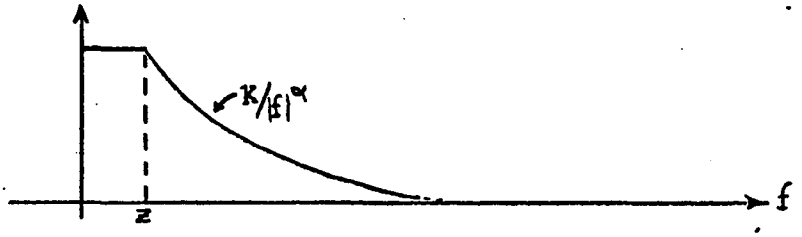

The brief analysis which indicated divergence for the nontruncated spectrum makes it trivially obvious that the estimate's variance does not diverge if the power spectrum is in reality truncated, but grows beyond any bound as the truncation frequency approaches zero.

4.3 Discussion of the Variance Considerations

The desirability for prewhitening even in actual experimental situations was indicated above*, and the spectral variance for the zeroth window was evaluated. Reference 24 includes derivations of the spectral variance for other windows.

*Variance considerations are not the only considerations pointing towards the desirability of prewhitening. Intermodulation distortion considerations, for example, are least damaging if the analyzed spectrum is relatively flat. In addition, References 24 and 25 analyze in considerable detail why the spectrum of the noise source should not vary significantly over distances of a few $\frac{1}{2T_M}$'s; these analyses will, naturally, not be repeated here.

Even these results, however, are the consequences of a set of assumptions whose violation can only increase the true estimate's variance. These assumptions are:

(a) $T_M \ll T_N$, this assumption was invoked by Blackman and Tukey in simplifying integration limits while deriving Equation 23 above. Blakemore[25] has shown that a consequence of not satisfying this inequality can be evaluated by replacing Q_i by Q_i'' in this general expression for $\text{var}_i[S(f_j)]$; Q_i'' is found to be a weighted sum of more than one "window", and the predictable effect is to increase the numerical value of the variance.

(b) A potentially serious disadvantage of time-multiplexing used to reduce the overall data-taking period is the possibility of statistical correlation among the multiplexed sources. Every effort has been made to eliminate such effects in the experimental part of this thesis, and, indeed, no such obvious correlation has been detected in the data on which the final results are based. In the worst case, that of complete correlation between noise sources, the spectral estimate's variance can increase tenfold, as shown in part 5.5.

In view of the aforementioned considerations, the evaluated expression for the spectral estimate's variance

$$\text{var}[S(f_j)] = K \frac{T_M}{T_N} S^2(f_j)$$

is too optimistic.

Although the effect of violating the $T_M \ll T_N$ assumption has not been quantitatively determined to any great accuracy, and although no means have been devised for precisely measuring the amount of correlation between noise sources, it is the opinion of this author that a value of $K = 3$ is a realistic one for the present work.

It must be stressed at this stage that it is very hard to quantitatively appreciate the degree to which the various assumptions used in deriving the above expression were satisfied; it is hard, for instance, to measure how truly "white" an unknown power spectrum has become after being prewhitened by a filter designed to prewhiten K/f^1 spectra only.

Given that $T_M/T_N \tilde{=} 1/10$ per noise source, for each and every sampling rate used in this work, and that 10 noise sources were multiplexed*, the above variance expression becomes

$$\frac{\sqrt{\text{var}[S(f_j)]}}{\bar{S}(f_j)} \approx \sqrt{\left(\frac{T_M}{T_N} = \frac{1}{10}\right)\frac{1}{10} \cdot 3} = \sqrt{,03} \approx .17$$

For a gaussianly distributed random variable $S(f_j)$ (a plausible assumption), this means that 68% of the time the estimate would be within 17 percent of its average value; we thus basically have a "17% estimator". This result is further elaborated on in Section 5.2 below.

In conclusion, Equation (25) means that if variance is important, given T_N, T_M must be kept small; but then, as will be shown in Section

---

* This is analyzed in detail in part 5.5 below. Equation (45) shows that the variance is then reduced by a factor of 10.

5.2, the time window $D_i(\tau)$ gets narrow and its transform widens; this in turn affects the frequency resolution adversely. Much has been written, some helpfully, on this point; the need to balance bandwidth of a spectrum estimate, which it is desired to make narrow, versus the estimate's statistical stability, which it is desired to make great, is commonplace. It is quite obvious that where the detection of specific frequency peaks is of interest, such as a "radar cross section" problem where each extra frequency peak may amount to an extra corner of the oncoming missile), frequency resolution is of great importance. In flicker noise measurements, on the other hand, where a reasonably smooth spectrum is almost always the case, the concern of statistical stability will be great; a happy medium is thus chosen. Obviously there is the alternative of a longer T_N, i.e., a longer data taking period which will be beneficial to both frequency resolution and statistical stability; the problems then are ones of equipment instability during the low-sampling speed runs.

CHAPTER 5

CONSIDERATION OF PARTICULAR STEPS IN THE ESTIMATOR USED IN THIS WORK

While the Blackman/Tukey estimator is used in this work, the justification for some particular aspects of it may not be immediately obvious.

This section does not attempt to repeat the entire theory behind the Blackman/Tukey estimator; specific topics are only treated to the extent necessary to justify particular choices in this thesis. For a thorough background, the reader is referred to References 24 and 25.

5.1 Prewhitening and Postgreening

Section 4.3 above has discussed some of the reasons for the desirability of prewhitening. Experimental work for this thesis indicates an increased variance of the spectral estimate if it is obtained without prewhitening; Figures 2 and 3 below show two ordinary-looking noise source outputs and the two corresponding spectral estimates for each one of them obtained with no prewhitening and with prewhitening; the increase in variance is quite evident.

What is needed is a filter $Y(f)$ such that

$$S_z(f) = |Y(f)|^2 \, S_x(f) \text{ , where } |Y(f)|^2 = |f| \text{ , } |f| \leq \frac{1}{2\Delta\tau}$$

The filter will be periodic in frequency with period $\frac{1}{\Delta\tau}$ like the aliased spectral density (aliasing is discussed in Section 5.3 below.)

Letting

Prewhitened and Non-prewhitened Spectral Estimates of Noise Source #4

Raw Output of Noise Source #4

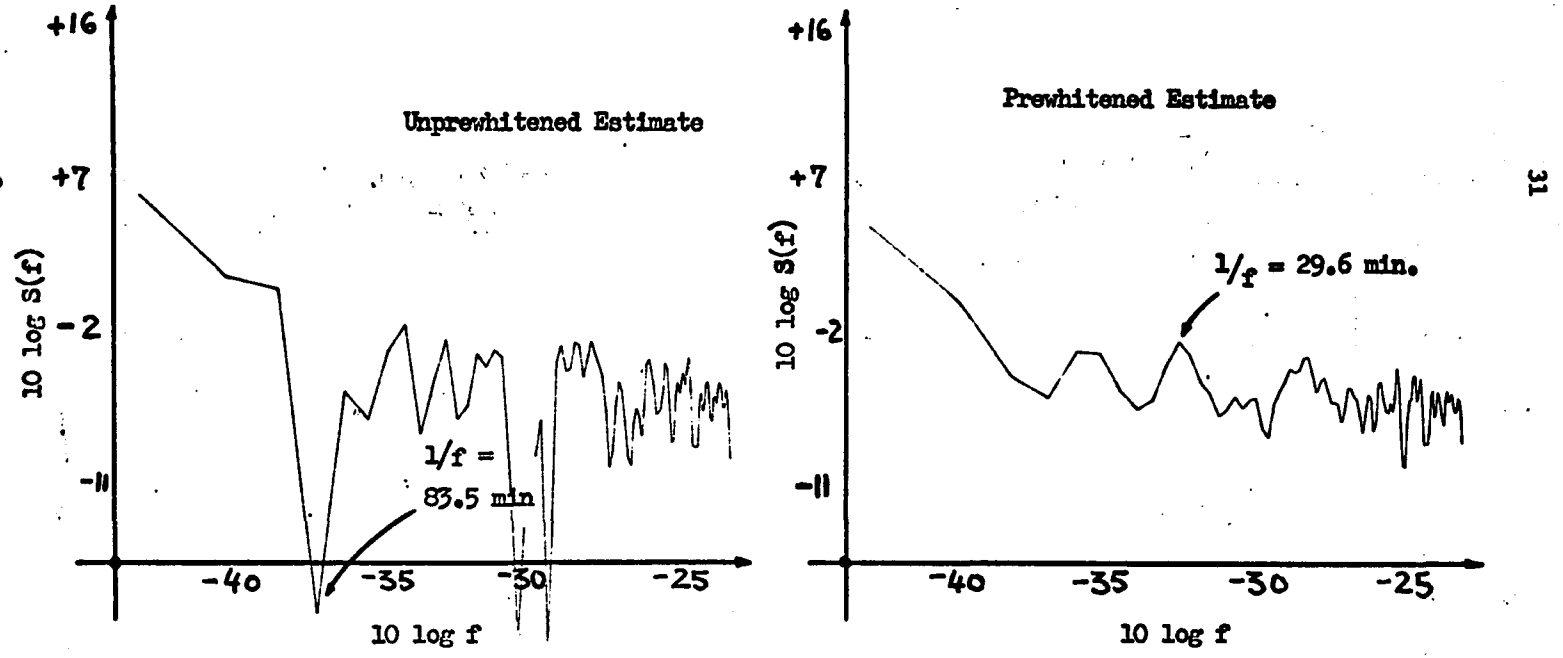

Figure 2

Prewhitened and Non-prewhitened Spectral Estimates for Noise Source #5

Raw Output of Noise Source #5

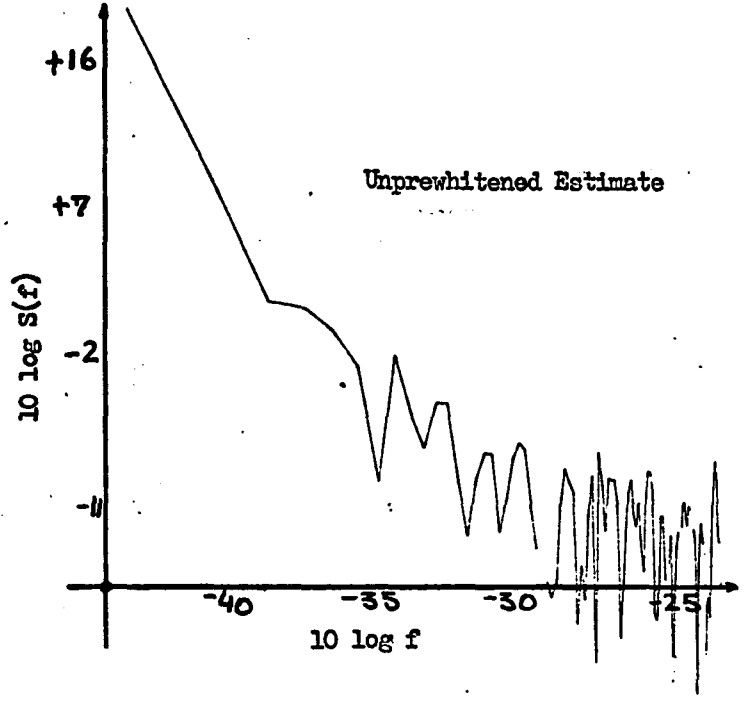

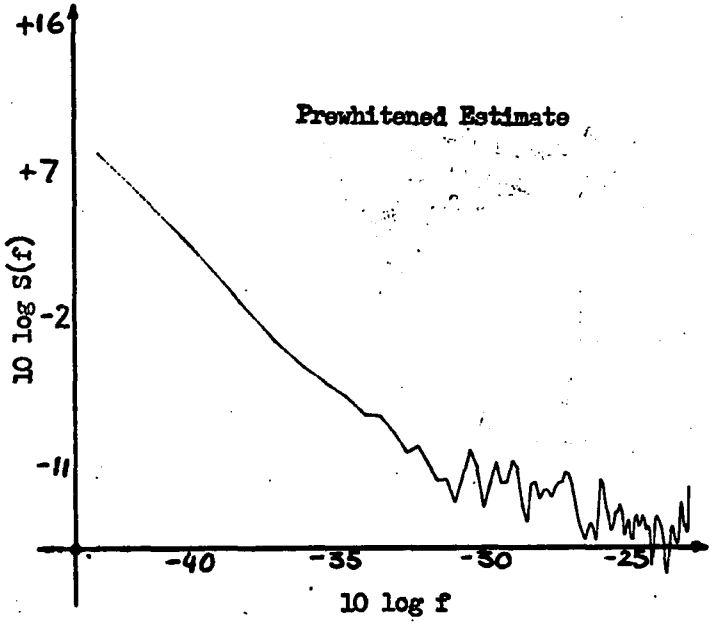

Figure 3

$$|Y(f)|^2 = B_o + 2B_1 \cos 2\pi f + 2B_2 \cos 4\pi f + \cdots$$

$$= \sum_{\ell=-k}^{k} B_\ell \cos 2\pi \ell f \qquad (26)$$

k clearly is determined by the degree of the desired accuracy, and the B_ℓ's are determined by imposing the desired analytic expression on the left hand side of this equation.

A finite summation is required for computer implementation. Furthermore, it is desired that the finite summation be zero at $f = 0$. Imposing these requirements results[25] in the following expression:

$$|Y(f)|^2 = \frac{4}{\pi^2} \sum_{\ell=1}^{k} \frac{1}{\ell^2} - \frac{4}{\pi^2} \sum_{\ell=1}^{k} \frac{1}{\ell^2} \cos(2\ell\pi f \Delta\tau) \qquad (27)$$

which defines the $(k+1)$ constants B_ℓ and hence the prewhitening filter in the frequency domain. It is only practical to prewhiten data in the time domain. One such scheme is proposed by Blackman-Tukey*: in the discrete case the prewhitened data are formed from the raw x_i's by

$$z_j = \sum_{i=0}^{k} A_i \, x_{i+j} \,, \qquad j = 1,2,\cdots,n-k$$

Blakemore has shown[25] that the A_i's can be viewed as the sampled-data version of the impulse response of a linear filter; accordingly, they are obtained from the filter characteristics, the

---

*This time domain approach is clearly preferable, since prewhitening can then be done before any subsequent data processing, as desired.

B_i's, by self-convolution, which yields

$$\begin{aligned} B_o &= A_o^2 + A_1^2 + \cdots + A_k^2 \\ B_1 &= A_o A_1 + \cdots \; A_{k-1} A_k \\ B_2 &= A_o A_2 + \cdots \; A_{k-2} A_k \\ &\vdots \\ B_k &= A_o A_k \end{aligned} \tag{28}$$

The solution of these nonlinear algebraic equations, when inverted, gives the desired A_i's . It was found by Blakemore[25] that very adequate results were obtained with $k = 9$ (i.e., 10 A_i's).

The inverse procedure, "postgreening", is quite simple in the frequency domain; we are passing the power spectrum $S_z(f)$ through a filter which is $\frac{1}{|Y(f)|^2} \triangleq \frac{1}{|f|}$; that is,

$$S_x(f) = \frac{1}{|Y(f)|^2} S_z(f) = \frac{1}{|f|} S_z(f) \tag{29}$$

The procedure thus involves simple division of each frequency-domain estimate.

5.2 "Windows"

It is desired to concentrate the main lobe of $Q_i(f)$ (see equation 21) near the zero frequency and to minimize the area under the side lobes; whereas the reduction of the side lobes of $Q_i(f)$ implies a smoothly changing time-domain window $D_i(\tau)$, the desired concentration of the main lobe implies a flat and blocky $D_i(\tau)$.

Different attempts at a happy compromise of the above conflicting requirements have resulted in different windows $D_i(\tau)$, i being just a bookkeeping index.

The original work of Blackman/Tukey has indicated that the theoretical variance of the final spectral estimate is approximately the same for all usual windows except the zeroth one, $D_o(\tau)$ which has twice the variance associated with it.

The window used in this work is the "hanning" window

$$\begin{aligned} D_2(\tau) &= \frac{1}{2}\left(1 + \cos\frac{\pi\tau}{T_M}\right) && |\tau| < T_M \\ &= 0 && |\tau| > T_M \end{aligned} \tag{30}$$

The corresponding Fourier transform is easily obtained to be

$$Q_2(f) = \frac{1}{2}\,Q_o(f) + \frac{1}{4}\left[Q_o\left(f + \frac{1}{2T_M}\right) + Q_o\left(f - \frac{1}{2T_M}\right)\right] \tag{31}$$

where

$$Q_o(f) = 2T_M\,\frac{\sin 2\pi f\,T_M}{2\pi f\,T_M} \tag{32}$$

Since multiplication in the time domain is equivalent to convolution in the frequency domain, and since convolution in sampled-data systems amounts to a discrete summation, it has been shown[24] that "windowing" is preferable in the frequency domain because it only amounts to a simple summation.

For the window chosen, we simply have

$$U_r = 0.25\,V_{r-1} + 0.50\,V_r + 0.25\,V_{r+1} \tag{33}$$

Since this is an extensively documented topic, it will not be pursued any further in this work.

5.3 Aliasing and De-Aliasing

Since one cannot tell how many wiggles a certain signal has between two successive sampled values without some a priori knowledge of its spectrum, it is possible that high frequency energy can masquerade as energy at lower frequencies. This follows trivially from the associated mathematics, as shown below, and is often referred to as "aliasing".

Applying the estimator given by Section 3.2 to an infinitely long stationary random process yields[25]

$$S_A(f_r) = \sum_{q=-\infty}^{\infty} S(f_r - \frac{q}{\Delta\tau}) \tag{34}$$

Thus

$$S_A(f_r) = S(f_r) + \sum_{q=1}^{\infty} [S(\frac{q}{\Delta\tau} - f_r) + S(\frac{q}{\Delta\tau} + f_r)] \tag{35}$$

where the notation of Section 3.2 is adhered to.

Since $S(f_r)$ is never estimated in practice at frequencies $f > \frac{1}{2\Delta\tau}$, the arguments of $S(f_r)$ above are all positive.

The sketch below indicates the aliased frequencies corresponding to an estimate-frequency f_r

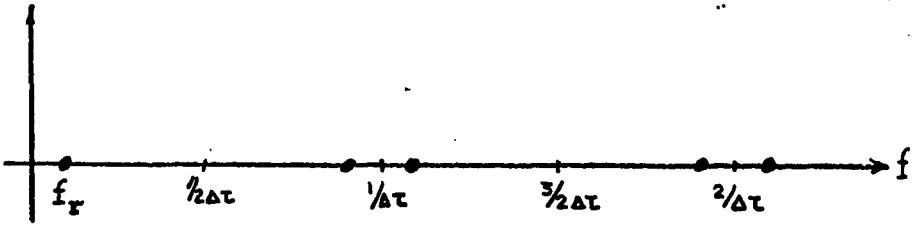

It follows that all one needs to do to remove this bias from the estimate is to subtract the quantity

$$\sum_{q=1}^{\infty} \left[S\left(\frac{q}{\Delta\tau} - f_r\right) + S\left(\frac{q}{\Delta\tau} + f_r\right)\right]$$

where the spectra at these frequencies must either be obtained through other measurements or be estimated.

For a typical K/f spectrum with $\Delta\tau = 100$ sec, $n = 10{,}000$ data points, $m = 100$ discrete frequency estimates, the estimator used in this work will provide estimates from $f = \frac{1}{2\Delta\tau} = 5 \times 10^{-3}$ cps to $\frac{1}{2[m=100]\Delta\tau} = 5 \times 10^{-5}$ cps , that is, two decades in frequency. Let us first consider the aliasing correction at the low-frequency end. Its nearest alias is at $[\frac{1}{\Delta\tau = 100} - 5 \times 10^{-5}] \simeq 10^{-2}$ cps, and has a magnitude of $K/f = K \times 10^{2}$, i.e., three orders of magnitude smaller than the spectral density at the low frequency end.

Similarly, the second nearest alias is at approximately 10^{-2} cps with magnitude

$$K \times 10^{2}$$

the third nearest alias is at approximately 2×10^{-2} cps with magnitude

$$\frac{1}{2} \times K \times 10^{2} \text{ , etc.}$$

The overall sum of aliases is therefore

$$2K[2 \times 10^{2} + 10^{2} + \cdots]$$

If only a few aliasing terms are allowed to exist, then this quantity is much smaller than

$$\frac{K}{5} \times 10^{5}$$

Appendix B discusses the effects of a large number of aliasing terms.

In the high frequency end of the estimated spectrum, aliasing results in significantly more distortion.

For a highest frequency estimate at

$$f = \frac{1}{2\Delta\tau} = 5 \times 10^{-3} \text{ cps}$$

with magnitude

$$\frac{K}{7} = \frac{K \times 10^3}{5}$$

the first alias is at 5×10^{-3}cps with magnitude $\frac{1}{5}(K \times 10^3)$. The second alias is at 15×10^{-3}cps with magnitude $\frac{1}{15}(K \times 10^3)$, etc. The total aliasing is thus

$$\frac{K \times 10^3}{5} + \frac{K \times 10^3}{15} + \frac{K \times 10^3}{15} + \frac{K \times 10^3}{25} + \frac{K \times 10^3}{25} + \cdots$$

which is a growing number as more terms are added. This shows that aliasing is a definite problem even for $1/f$ spectra, and even more of a problem for $1/|f|^{\alpha}$, $\alpha < 1$ spectra.

It also shows the de-aliasing algorithm. From simple mathematical considerations, the sum of the aliases will not diverge however, for spectra of the type $1/|f|^{\alpha}$, $\alpha > 1$.

A low-pass filter to cut off the high frequencies at a rate faster than $1/f$ is, thus, clearly desirable. Given the cutoff frequency of the low pass filter associated with the process being measured, the above equations provide the de-aliasing algorithm; this algorithm was, in fact, used in de-aliasing spectral estimates of this work. A detailed example of the procedure is given in Appendix B.

Since an ideal low-pass filter is unrealizable, a single RC filter was, instead, used in this work. Ideally, different RC filters with appropriately scaled timed-constants ought to be used for different sampling rates; this is not essential, however, for two reasons:

(a) The aliasing effect is always a measurable quantity.

(b) The above "appropriate" time constants can amount to very sizable capacitors for the lowest sampling rate runs. If, for example, $\Delta\tau = 10{,}000$ sec, the highest frequency estimate is at $\frac{1}{2} \times 10^{-4}$ cps; an appropriate RC filter would then have to have

$$\tau = RC \simeq 2 \times 10^{4} \text{ sec}$$

Keeping in mind that it is desirable to keep noise pickup to a minimum, and that the input impedance of the voltmeter ought to be much larger than the series resistor R, one can select

$$R = 1 \text{ megohm}$$

in which case $C = 1/5$ Farad, which is an outrageously large value for any realizable capacitor.

It is of interest to point out that in reality, of course, there exists an effective built-in low-pass filter in any semiconductor, since there is always a frequency above which the semiconductor is capacitive in nature. It is desirable for practical purposes, however, not to depend on the unknown capacitive nature of the semiconductor for de-aliasing purposes.

The particular choices of low pass filters used in the experimental part of this thesis are discussed logically together with the experimental results themselves. Further discussion on de-aliasing is

relegated to Appendix B.

5.4 Constant Mean Removal

Most derivations concerning stochastic processes are traditionally carried out for zero-mean processes for notational simplicity; ordinarily there is no loss of generality in so doing, since one can always redefine a new set of processes through a simple linear transformation

$$\overline{X_{new}}(t) = \overline{X_{old}}(t) - \overline{M} \tag{36}$$

where $\overline{X}(t)$ is an n-dimensional vector in the most general case.

Unfortunately, there may actually be a loss of generality if a complicated sequence of linear and nonlinear transformations is performed on the zero mean process; the original stochastic processes do not appear explicitly in the final result, and a final substitution of the type given by Eq. (36) is thus out of the question. There are two options at that stage; one either rederives the algorithm for a non-zero-mean process and is thus able to analytically account for the bias which may appear at the end, or one simply takes the mean out of the random function before any data processing.

All the stochastic processes treated experimentally in this work had nonzero means; in fact, in the case of the ten multiplexed noise sources, different nonzero means were actually imposed on each, for purposes of identification.

The question of what is the best estimate of the mean comes first. It would be the sample mean if the noise process was a sample from a normal distribution of known variance; it would be a

conditionally unbiased, sufficient and consistent estimator of the true mean. But the process isn't always gaussian. Experimental results where a sizable linear trend or a low-frequency sinusoidal variation were superimposed on the data are discussed in Section 6.1 below. The conclusions drawn there are that the final result is practically unaffected despite the imposed distortion, and they strongly support the intuitive belief that any estimator of the mean which is more refined than the sample mean is totally unnecessary.

The estimated mean can be removed from the data at any of many stages of the Blackman/Tukey algorithm; it can be removed from each data point $\overline{x_i}(t)$ by simple subtraction,

$$\overline{n_i}(t) = \overline{x_i}(t) - \overline{M} \quad , \tag{37}$$

its square can be removed from the computed correlation function $R_x(\tau)$,

$$R_n(\tau) = R_x(\tau) - M^2 \tag{38}$$

or an appropriate more complicated function of it can be removed from the raw spectral estimates or from any other stage of the algorithm, in principle. Blakemore[25] has worked out the computational details indicating that either of the two approaches suggested by Eqs. (37) and (38) give, predictably, very comparable results in terms of bias; indeed, there appears to be little reason, if any, to consider removing some complicated function of the mean from still some other stage of the overall algorithm. As can be readily seen from Eq. (16), the mean was removed in the experimental results by a method very analogous

to that suggested by Eq. (38).

Since the quantity removed from the data is really an approximation to the true mean, one is concerned what the effect of an inaccurately approximated mean removal is.

5.4.1 Effect of removing an inaccurately estimated constant mean

If the data $x(t)$ is indeed a sample from a stationary zero mean noise process $n(t)$ plus an additive constant M ; that is, if

$$x(t) = n(t) + M \tag{39}$$

then the correlation functions are

$$R_x(\tau) = R_n(\tau) + M^2 \tag{40}$$

and removing (M^2) from the approximately one hundred mean lagged products is on the average equivalent to removing (M) from the approximately ten thousand data points usually recorded for each run.

The quantity (M), however, is a random variable and its computed value need not coincide with the true mean of the process $x(t)$; it is of interest, therefore, to have an understanding of the effect of a poor estimate of the true mean of the process $x(t)$ on the corresponding spectral density estimate for that process as obtained by the Blackman-Tukey algorithm.

An estimate of the true mean which is smaller or larger in absolute value than the true mean, will result in mean-lagged-products which are correspondingly larger or smaller in algebraic value than the true values. This effect can be easily modeled mathematically by letting

$$C_r^{\text{actual}} = C_r^{\text{true}} + \Delta \tag{41}$$

when: C_r^{actual} = mean-lagged-products computed using the estimated value of the mean of the process in subtracting M^2 .

C_r^{true} = corresponding coefficients obtained by using the (unknown) true mean of the process.

Δ = the unwanted additive constant resulting from a poor estimate of the mean of the process; it can be positive or negative.

The actual algorithm for spectral estimation will now be used to trace the pernicious effects of the above quantity Δ .

The raw spectral density estimates are computed according to the formula

$$V_r = \Delta\tau \left[C_o + 2 \sum_{q=1}^{q=m-1} C_q \cos \frac{qr\pi}{m} + C_m \cos r\pi\right]$$

For all estimates in this research, $m = 100$. If the C_i^{actual} , $i \in [0,m]$, above are replaced by the corresponding $C_i^{\text{true}} + \Delta$, then

$$V_r^{\text{estimated}} = \Delta\tau \left[C_o + 2 \sum_{q=1}^{99} C_q \cos \frac{qr\pi}{m} + \Delta \cos \frac{qr\pi}{m} + \right.$$

$$\left. C_m \cos r\pi + \Delta \cos r\pi\right] = \Delta\tau \left[C_o + 2 \sum_{q=1}^{99} C_q \cos \frac{qr\pi}{m} + C_m \cos r\pi\right] +$$

$$\{\Delta_\tau[\Delta + 2\Delta \sum_{q=1}^{99} \cos \frac{qr\pi}{100} + \Delta \cos r\pi]\} \quad . \quad \text{Thus,}$$

$$V_r^{\text{estimated}} = V_r^{\text{true}} + \{(\Delta) \cdot \Delta\tau[1 + 2 \sum_{q=1}^{99} \cos \frac{qr\pi}{100} + \cos r\pi]\}$$

Let: $\frac{1}{2}(1 + \cos r\pi) \triangleq K_r$; this can be either zero or one.

Let: $[1 + 2 \sum_{q=1}^{99} \cos \frac{qr\pi}{100} + \cos r\pi] = G_r$

The quantity within the braces is of interest. Given specific constant values for the error Δ and the sampling period $\Delta\tau$, the frequency dependence of the error is given by table 1 below.

The error introduced is of alternating sign, hence the distortion of the final result cannot be an overall increase or decrease of the true magnitude of the spectral density.

The magnitude of this distortion can be appreciated by assigning typical numerical values to the parameters involved. For a sampling period of $\Delta\tau = 100$ sec. and a plausible error of mean estimation of ≈ 0.2 volts*, the additive error G_1 at the low frequency end of the estimate is

$$G_1 \approx (4 \times 10^{-2})(10^2)(1.725 \times 10^{-4}) = 6.9 \times 10^{-4} \text{ volt}^2 \text{ sec}$$

The corresponding typical numerical value $V_1^{\text{estimated}}$ determined experimentally for that sampling period is approximately 7db or

$$V_1^{\text{estimated}} = \text{antilog}_{10}(0.7) \approx 5.01 \text{ volt}^2 \text{ sec.}$$

which is four orders of magnitude larger; minor inaccuracies in mean estimation are thus of no consequence for high sampling rates.

For a sampling period of $\Delta\tau = 10{,}000$ sec. and a plausible error of $\pm$ 0.2 volts, the worst additive error, G_1 is

*This value is based on the noise amplitude values actually recorded after adequate amplification, and is consistent with the rest of this discussion which is based on the same values.

TABLE (1). Error Coefficients Resulting from Inaccurate Estimation of the Noise Source's Mean.

r	K_r	G_r	r	K_r	G_r	r	K_r	G_r
1	0.000	0.000172541	34	1.000	-0.000156425	67	0.000	0.000098854
2	1.000	-0.000172079	35	0.000	0.000153504	68	1.000	-0.000093952
3	0.000	0.000170365	36	1.000	-0.000157088	69	0.000	0.000099108
4	1.000	-0.000171289	37	0.000	0.000150904	70	1.000	-0.000096068
5	0.000	0.000170618	38	1.000	-0.000148624	71	0.000	0.000088155
6	1.000	-0.000175834	39	0.000	0.000159256	72	1.000	-0.000086501
7	0.000	0.000171378	40	1.000	-0.000150114	73	0.000	0.000083700
8	1.000	-0.000171691	41	0.000	0.000144497	74	1.000	-0.000085667
9	0.000	0.000167906	42	1.000	-0.000143524	75	0.000	0.000078753
10	1.000	-0.000171691	43	0.000	0.000157326	76	1.000	-0.000081301
11	0.000	0.000166163	44	1.000	-0.000138123	77	0.000	0.000076219
12	1.000	-0.000173166	45	0.000	0.000132259	78	1.000	-0.000078782
13	0.000	0.000166252	46	1.000	-0.000144396	79	0.000	0.000072807
14	1.000	-0.000170037	47	0.000	0.000138646	80	1.000	-0.000077561
15	0.000	0.000164792	48	1.000	-0.000135256	81	0.000	0.000062332
16	1.000	-0.000167012	49	0.000	0.000153490	82	1.000	-0.000072137
17	0.000	0.000161916	50	1.000	-0.000133760	83	0.000	0.000051886
18	1.000	-0.000168040	51	0.000	0.000130784	84	1.000	-0.000070542
19	0.000	0.000163257	52	1.000	-0.000127656	85	0.000	0.000060454
20	1.000	-0.000167549	53	0.000	0.000121428	86	1.000	-0.000042573
21	0.000	0.000161469	54	1.000	-0.000134949	87	0.000	0.000034839
22	1.000	-0.000167355	55	0.000	0.000126265	88	1.000	-0.000048473
23	0.000	0.000163645	56	1.000	-0.000112813	89	0.000	0.000031009
24	1.000	-0.000161573	57	0.000	0.000121854	90	1.000	-0.000037953
25	0.000	0.000165001	58	1.000	-0.000122886	91	0.000	0.000028998
26	1.000	-0.000164151	59	0.000	0.000109389	92	1.000	-0.000043869
27	0.000	0.000160307	60	1.000	-0.000121966	93	0.000	0.000007167
28	1.000	-0.000165850	61	0.000	0.000114530	94	1.000	-0.000031784
29	0.000	0.000158861	62	1.000	-0.000130273	95	0.000	-0.000001177
30	1.000	-0.000159353	63	0.000	0.000125423	96	1.000	-0.000017032
31	0.000	0.000153229	64	1.000	-0.000104591	97	0.000	-0.000004858
32	1.000	-0.000159517	65	0.000	0.000107236	98	1.000	-0.000009224
33	0.000	0.000156879	66	1.000	-0.000104114	99	0.000	0.000008404

$$G_1 \approx (4 \times 10^{-2})(10^4)(1.725 \times 10^{-4}) \approx 6.9 \times 10^{-2} \text{ volt}^2 \text{ sec.}$$

The corresponding numerical value observed experimentally for this new sampling period is approximately 20 db or

$$V_1^{\text{estimated}} = \text{antilog}_{10}\,(2) = 100 \text{ volt}^2 \text{ sec.}$$

again, four orders of magnitude larger.

It follows that accurate mean estimation is unnecessary when the amplitude of the noise source measured is of the order observed in this research.

5.5 Multiple Noise Source Treatment

As Chapter 9, which deals with the experimental setup, discusses in detail, 10 different noise sources were time-multiplexed for the final spectral density estimate.

The following questions are of immediate interest:

a) What is the best estimation technique if the individual spectral estimates of 10 independent noise sources are available?*

b) How is the answer to the first question modified if the 10 noise sources are correlated?

---

* An essential set of assumptions for a meaningful combination of estimates from multiple noise sources is that:
a) The noise sources are statistically independent.
b) The noise sources have power spectra which may only differ by a multiplicative constant.
Assumption (b) is satisfied to a reasonable degree as evidenced by individual spectral density estimates of various noise sources. Assumption (a) is also satisfied to an extent discussed both theoretically below, and experimentally later.

In trying to answer the first question, the conditional maximum likelihood estimator of the mean[30] approach is a likely candidate for an estimator. For purely algebraic convenience and for lack of any evidence to the contrary, it may be assumed that the 10 available estimates $S_j(f_i)$ at each discrete frequency (i) are samples from a normal distribution having some variance σ_j^2 . In accordance with the definition of the maximum likelihood estimator, one wants to maximize

$$p(\mu|\vec{S}) = \frac{p(\vec{S}/\mu)p(\mu)}{p(\vec{S})}$$

where μ is the unknown mean, $\vec{S}$ is a 10-dimensional vector, and $p(\mu)$ is a measure of any available a priori information concerning the value of what is wanted; in the absence of any such information, the solution of[31]

$$\frac{\partial}{\partial\mu} \log p(\vec{S}/\mu) = 0 \quad . \tag{42}$$

leads to the conditional maximum likelihood estimator of μ . Doing the algebra, yields:

$$\begin{aligned} \log p(\vec{S}/\mu) &= \log[(2\pi\sigma_j^2)^{-10/2} \exp \frac{-\sum_{j=1}^{10}(S_j-\mu)^2}{2\sigma_j^2}] \\ &= -\frac{10}{2} \log 2\pi\sigma_j^2 - \frac{1}{2\sigma_j^2} \sum_{j=1}^{10}(S_j-\mu)^2 \end{aligned} \tag{43}$$

Setting the derivative equal to zero and solving for μ ,

$$\frac{\partial \log p(\vec{S}/\mu)}{\partial \mu} = 0 = \frac{1}{\sigma_j^2} \sum_{j=1}^{K} (S_j - \mu) \Big|_{\mu=\mu(\vec{S})}$$

$$= \frac{1}{\sigma_j^2} [S_1 - \mu) + (S_2 - \mu) + \ldots] \tag{44}$$

yields

$$\mu(\vec{S}) = \frac{1}{10} \sum_{j=1}^{10} S_j \tag{45}$$

This is all very nice and seems to validate one's intuitive feeling that this should be the case; if the real data are considered, however, certain doubts are raised. Figure 4 is a plot of the raw data obtained from the 10 noise sources used in part of the experimental part of this thesis for a particular sampling rate. As can be seen from that figure, the individual outputs appear to vary considerably in relative amplitude; the corresponding individual spectral estimates are thus, quite predictably, shifted in magnitude from each other. The simple averaging of Equation (45) would then, in essence, attenuate the contributions of the least noisy sources, and at the same time amplify the overall trend and random spectral fluctuations of the "noisy" noise sources; this would in turn invalidate any claim that the variance of the estimated mean $\mu(\vec{S})$ is one-tenth that of just "any" individual spectral estimate $S_j(f_i)$.

The noise observed as raw data from each noise source is, as will be discussed in Section 9.2, essentially that of the first stage of a high gain d.c. amplifier. An off-the-shelf remedy for the above observed nonuniformity of the output amplitudes of the individual noise sources would then be to scale them all through appropriate multiplicative

Recorded Raw Noise Output.

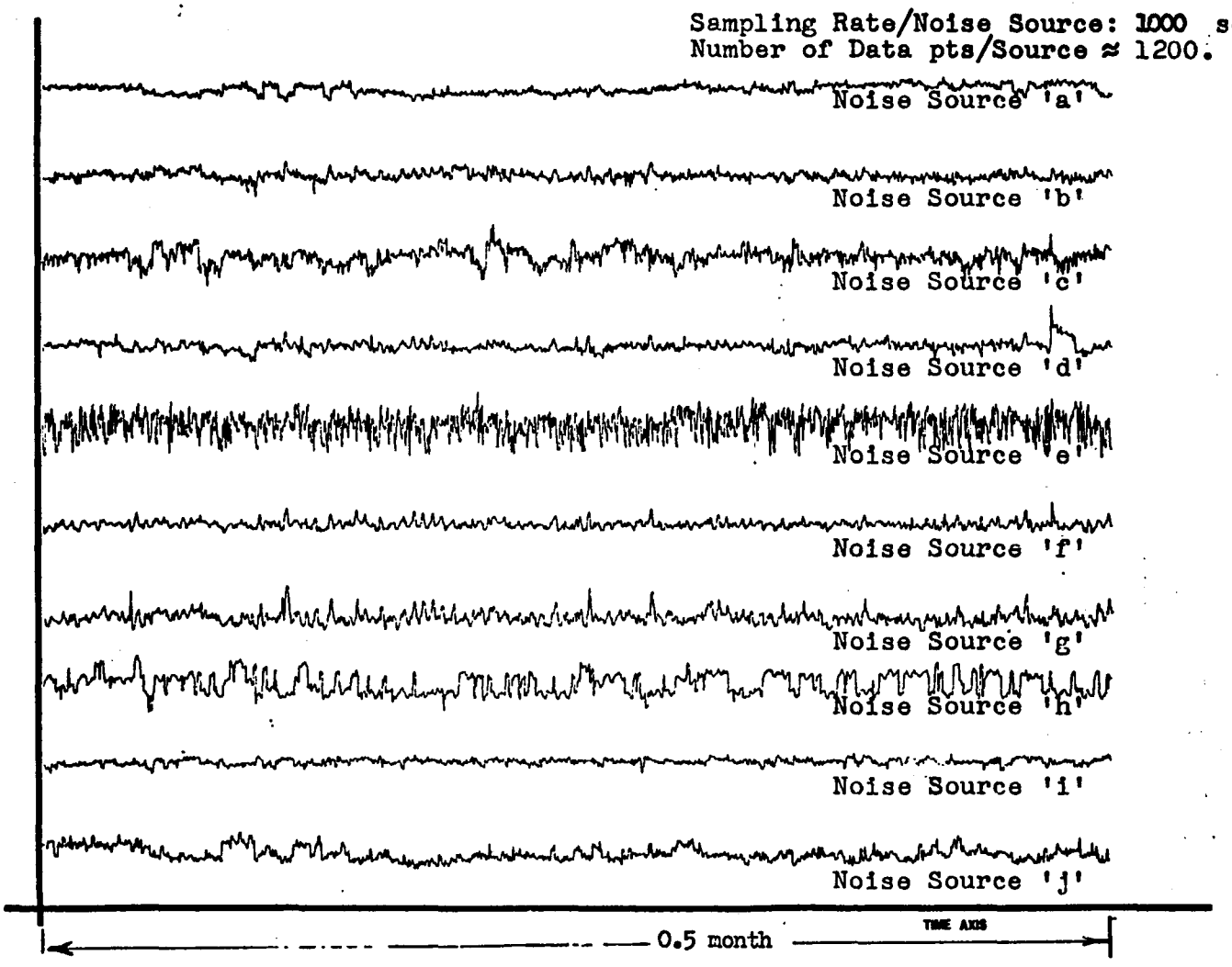

Figure 4

constants; this can be done either on the raw data itself, or on the individual spectral estimates $S_j(f_i)$; the latter is preferable because of the highly reduced amount of computational work involved, and also because it eliminates the likely possible need for an iterative procedure where a noise gain is guessed from the raw data, and the effect on the spectrum is then observed in preparation for the next guess.

A closer look at the data plot of Figure 4, however, indicates that over and above the aforementioned difficulty, the individual noise sources display outputs which are significantly different in nature; noise source #h is "popcorning"* with a time constant of a few hours; noise sources #e,h, deviate considerably from their sample mean, while other sources display still different behavior. One is thus left with the impression that perhaps some noise sources ought to be attenuated and others amplified in inverse proportion to their "quality". Quality should be measurable then, and the only sensible yardstick is how close each particular noise source comes to the mathematical model used in deriving the spectral estimator.

In developing the estimator in Section 3.1, it was found necessary to assume: (a) Fourth order stationarity of the noise source. (b) Ergodicity of the mean and of the autocorrelation.

The first requirement (on which the second is essentially dependent) is at best hard to check; even second order ("wide-sense")

---

*
"Popcorning" refers to an output whose mean fluctuates between two or more well-defined levels; the Hausition times can be random with different transition probabilities associated with each state.

stationarity which is all that is required for ergodicity of the mean is hard enough to verify experimentally. The fundamental difficulty involved here is that one must agree on a minimum time span over which stationarity can be expected. It is mentioned earlier in connection with Figure 4 that noise source #h is "popcorning" with a time constant often exceeding 6 hours; it follows that for that particular source, stationarity is not an accurate assumption for experimental runs shorter than a few times the above time constant; thus, noise source #h would be of relatively poor quality for the short duration runs but not necessarily so for the long duration (low sampling rate) ones.

Checking for ergodicity of the mean is relatively simple if the analytic expression of the autocovariance or of the autocorrelation is available. Specifically, it has been shown that if

$$\lim_{\tau \to \infty} R(\tau) \neq \eta^{2*} \tag{46}$$

the ergodic theorem is not satisfied.

No such scheme is as yet available for checking for the ergodicity of the autocorrelation.

As can be deduced from the above discussion, checking the "quality" of each noise source is a rather subjective matter, basically based on:

(a) How stationary is the mean of that source during that particular run?*

*This is not easy to check in an experimental situation.

(b) How smooth is the corresponding estimated spectrum?

These criteria are by no means complete; as was shown earlier, they are at best usable guidelines in assessing the "quality" of a particular noise source.

Figure 5 shows histograms of the absolute value of the amplitude distributions of each of 10 noise sources used in deriving preliminary estimates in experimental work, in an attempt to assess the stationarity of each, somewhat less subjectively.** The presence of a gaussian shape, or absence thereof, is of no great significance in this context, since the only place where a gaussian assumption was used was as a mathematical simplification in deriving a simple-looking property of the estimator, namely its variance. A significant feature observable in these figures is that the shape of the distribution of the amplitudes of the first half of some noise sources differs from that of the second half; does this imply nonstationarity? Not necessarily: stationarity has no built-in time interval during which it must be displayed. Stationarity is, thus, difficult to check, even through the use of such histograms. It appears that the only valid conculsions that may be drawn from Figure 5 for the time being are that a particular recording of a run at a particular time is not as useful as it could have been at another time. Reference will be made later on, to these figures in Section 7.1.2 in connection with the

*This is a measure of quality in the sense that, for example, a popcorning source with just one level shift during the run in question is not a good source.

**The statistical properties of the sources will be examined later in this work.

***This is a relevant measure of quality for reasons related to the spectral variance. (See Blakemore[25] for details).

Statistical Fluctuations In Amplitude Probability Distributions between Different Noise Sources, and between Two Successive Halves of Each Noise Source, for Different Sampling Rates.

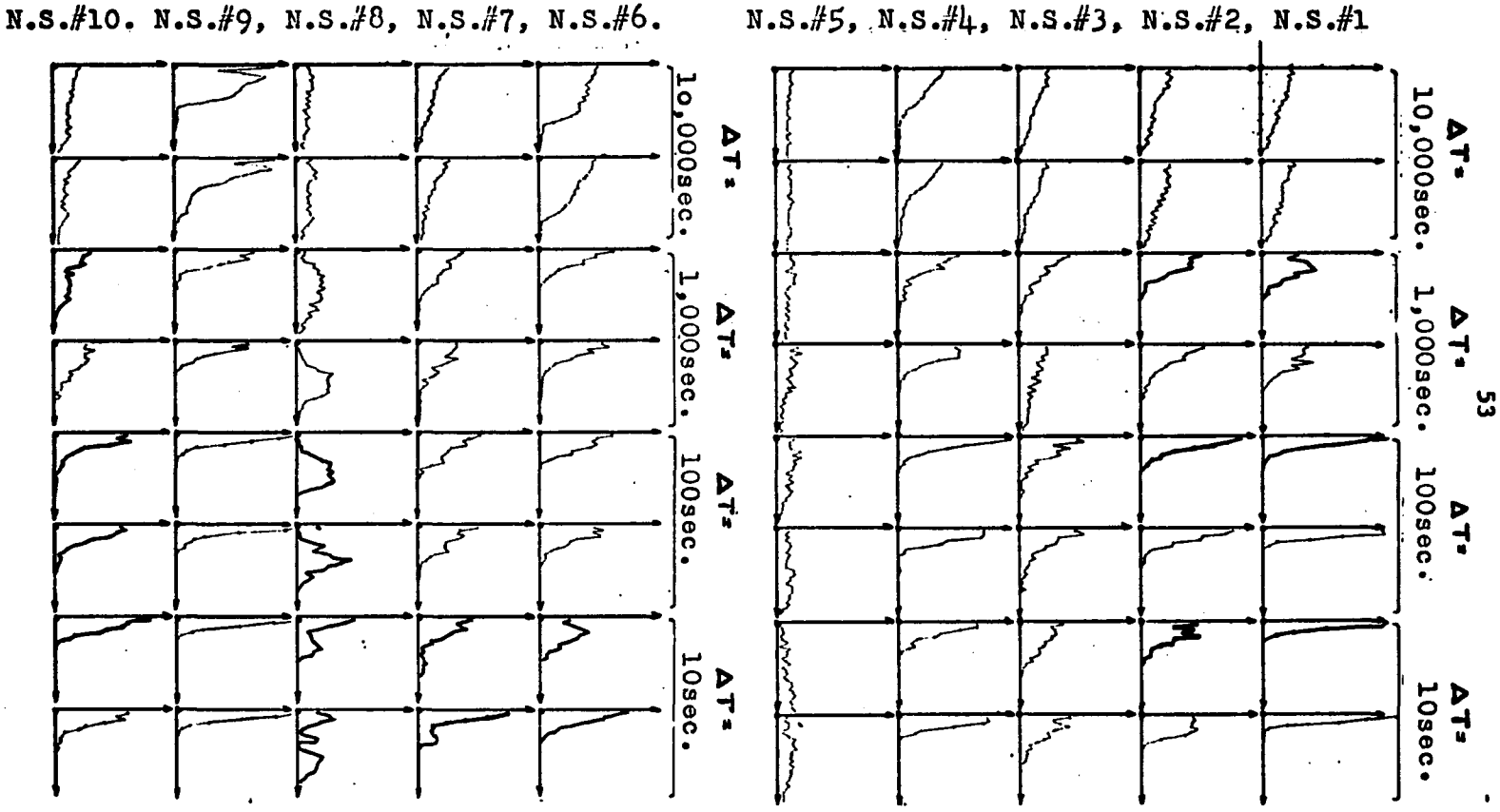

Figure 5

expected statistics from a postulated mathematical model of flicker noise.

A highly relevant point of interest is the question "at what frequency (for each run) should the weighted averaging be attempted?". The high frequency end is a poor choice in that it is most affected by aliasing; the low frequency end is also a poor choice in that it is very susceptible to bias. A rational and convenient, however arbitrary, choice is a frequency near the middle of the range for which that particular run has provided spectral estimates.

The scheme actually used in averaging the 10 individual spectra in this work involved the following steps:

1. Find the average value of the ten spectra at $f = f_c$ where f_c is the frequency in the middle of the range available.
2. At that one frequency find the appropriate 9 multiplicative factors α_K, $K\epsilon[2,10]$ such that all 10 individual spectra have the same magnitude as one of them.
3. Repeat steps 1 and 2 for $f = f_c + \frac{1}{4}\Delta F$ and $f = f_c - \frac{1}{4}\Delta F$ where ΔF is the total frequency span available. Record the new multiplicative constants obtained as β_K and γ_K.
4. The quantities $\delta_K \equiv \frac{\alpha_K + \beta_K + \gamma_K}{3}$, $K\epsilon[2,10]$ are the unweighted multiplicative factors sought.
5. Through good judgment based on the discussion of the present section assign weights $0.8 < \xi_K < 1.2$, $K\epsilon[1,10]$ to the 10 noise sources respectively.

6. The final "weighted" average spectrum is then given by

$$\frac{1}{10} \sum_{K=1}^{10} \left(\frac{\alpha_K + \beta_K + \gamma_K}{3}\right) \xi_K \cdot [S_K(f_i)], i\epsilon[1,100]^{*} \quad . \tag{47}$$

where $\alpha_1 = \beta_1 = \gamma_1 = \delta_1 \equiv 1$

A quantity of interest at this stage is the variance of the final estimate. In order that the result be a usable one, it is necessary to use Eq. (25) which gives the variance for a single noise source as a starting point; the further assumption that $\delta_K S_K(f)$, $K\epsilon[2,10]$ are samples from a gaussian distribution [not a very accurate assumption but a realistic one] simplifies the mathematics considerably. It was shown in Eq. (45) that

$$\hat{\mu}[\hat{S}[(f_i)] = \frac{1}{10} \sum_{j=1}^{10} \hat{S}_j(f_i)^{**} \quad .$$

Replacing $\hat{S}_j(f_i)$ by $\delta_j \hat{S}_j(f_i)$ in the equation above, is a step in the right direction towards approaching the assumption of gaussianly distributed spectral estimates. Hence

$$\hat{\mu}[\hat{S}(f_i)] = \frac{1}{10} \sum_{j=1}^{10} \delta_j \hat{S}_j(f_i) \quad . \tag{48}$$

---

*As explained in the experimental part of the thesis, $S_K(f_i)$ is obtained at 100 frequencies for such data

**The symbol $\hat{}$ will be used, as an exception, in this section only, to indicate an estimate because it is not always clear; this is consistent with the notation convention adopted since Section 3.2.

Since $\hat{\mu}[\hat{S}(f_i)]$ is the sum of 10 gaussian random variables, it is itself a gaussian random variable having a mean and a variance of its own. Thus[32]

$$E\{\hat{\mu}[\hat{S}(f_i)]\} = \frac{1}{10}\sum_{j=1}^{10}\hat{S}_j(f_i) \equiv \mu \equiv \overline{\hat{\mu}\,[\hat{S}(f_i)]} \tag{49}$$

and

$$E\{\{\hat{\mu}[\hat{S}(f_i)] - \mu\}^2\} = \frac{1}{10^2}\sum_{j=1}^{10}\sum_{e=1}^{10}\overline{\hat{S}_j(f_i)\hat{S}_e(f_i)} - \mu^2.$$

$$= \frac{1}{10^2}\sum_{j=1}^{10}\sum_{e=1}^{10}\overline{\hat{S}_j(f_i)\hat{S}_e(f_i)} \tag{50}$$

where E is the expectation operator, and μ was defined in Eq. (49).

Now recalling that in general

$$\sigma^2 = E[x^2] - E^2[x]$$

and that for uncorrelated gaussian random variables (therefore independent ones) having the same mean (assured by the incorporation of δ_K's in the expressions)

$$E[x_1x_2] = E[x_1]\,E[x_2] = \mu_1\mu_2 = \mu^2 \quad .$$

Equation (50) simplifies to[33]

$$\sigma^2_{\text{final}} = \frac{1}{10^2}\;10(\sigma_j^2 + \mu^2) + \frac{1}{10^2}(10^2 - 10)\mu^2 - \mu^2 = \frac{\sigma_j^2}{10}$$

where σ_j^2 is the variance of each individual spectral estimate given by Eq. (25) earlier, i.e.,

$$\text{Var}\,[\hat{S}_j(f_i)] = \mu^2[S_j(f_i)]\,\frac{T_M}{T_N} \quad .$$

In other words, the variance of the result of multiplexing 10 noise sources for time T_N is the same as the variance of the result of having 1 noise source and measuring it for time $10 \cdot T_N$, assuming that the appropriate multiplicative constants have been incorporated as above. This is so if and only if the individual noise sources are not correlated. The magnitude of the subjectively assigned coefficients ξ_i has been deliberately kept close to unity because doing otherwise would result in an increased variance of the final estimate, according to the discussion earlier in this section; in fact the very presence of these near-unity (but not always unity) multiplicative constants is part of the reason for allowing a variance of

$$\text{var}[S(f_i)] = \frac{3T_M}{T_N} \,/\, S^2(f_i)$$

For the overall final spectral estimate as opposed to the computed figure of

$$\frac{1T_M}{T_N} \,/\, S^2(f_i) \quad .$$

(for windows other than the zeroth window, as already stated.)

One additional point related to the above is a consequence of the fact that any one given noise source could exhibit a behavior which could be more acceptable for one sampling speed than for another; accordingly, no attempt was made to associate any one noise source with one subjective quality coefficient ξ_i for all sampling speeds associated with that particular source.

While the criteria and the narrow ranges related to the assignment of a particular ξ_i have been already given, the actual 50 coefficients* have not because they would be relatively meaningless without proper substantiation; such substantiation, if it were to be complete would require the insertion of 50 raw-data plots and another 50 preliminary spectral density estimates.

It must be stressed that in averaging the final spectral density estimates, it was not the logarithms of the individual spectral estimates which were linearly averaged but the actual individual spectral estimates themselves. Since the assignment of the subjective factors ξ_i required human intervention before any further computer processing, and since the individual spectral estimates were deliberately punched in data cards in logarithmic form for easy evaluation, the "averaging" computer program had to reconvert each of these numbers to their antilog equivalents, average them, and reconvert them to one final set of 100 logarithms representing the 100 discrete estimates.

---

*Corresponding to 10 coefficients for 5 different sampling rates.

CHAPTER 6

COMMON SOURCES OF BIAS IN THE ESTIMATE

If the assumptions of ergodicity, stationarity, and appropriate spectral smoothness needed in deriving the Blackman/Tukey estimator are met, if the unprewhitened power spectrum of the source is indeed $1/f$, if the raw data are not hiding a sharp spectral peak, then we can have some faith in the final estimate; but we have no usable test for checking the ergodicity of the autocorrelation and we have no test for checking high order (or any order, actually) stationarity. Applying this estimator's mathematics to the ineligible noise source may, and does, result in final estimates which are "reasonable-looking", well within the variance bounds of Eq. (25), yet heavily biased.

Experience from some hundred different spectral estimates obtained from an equivalent number of noise sources indicates that there are a few persistent and identifiable common sources of spectral estimate bias plot.

The spectral density of a disturbance which is uncorrelated with the "signal", in this case noise, is theoretically additive to the signal's spectral density; indeed, given $n(t)$ and $d(t)$ as the stochastic representation of a noise in time, and of a corresponding disturbance, then, assuming wide-sense stationarity and defining $S(t) = n(t) + d(t)$,

$$R_{ss}(\tau) = E\{[n(t) + d(t)][n(t+\tau) + d(t+\tau)]\}$$

$$= E[n(t)\, n(t+\tau)] + E[d(t)\, d(t+\tau)] = R_{nn}(\tau) + R_{dd}(\tau) \qquad (51)$$

with the cross-products vanishing in the limit. Then,

$$S_s(f) = \int_{-\infty}^{\infty} R_{nn}(\tau)\, e^{i\omega\tau}\, d\tau + \int_{-\infty}^{\infty} R_{dd}(\tau)\, e^{-i\omega\tau}\, d\tau = S_n(f) + S_d(f) \quad (52)$$

There are three points of interest at this stage:

a) A finite-duration random process $S(t)$, $t \in [0,T]$ which has a seemingly out-of-place delta function or unit step or something similar in it, cannot be called "stationary" as such. Although it could indeed have resulted from some stationary ensemble, it is not very realistic physically.

b) The algorithm used in this work for estimating spectral densities is based on many assumptions discussed already, which were imposed by the practical limitations of the actual problem; deviation from such assumptions, consequently, results in biases of various kinds. Equation (52) is thus, at best, only approximate in the experimental part of this thesis; an equivalent relation must be obtained which is based on the numerical details of the actual algorithm used in spectral estimation.

c) Spectral density estimates should not be expected to be additive on the log scale which is used in this work.

The raw data distortions most often encountered which result in bias of some form are shown in Fig. 6 below. A delta function in time, whose amplitude is much larger than the r.m.s. value of the noise, like the one simulated by the digital computer on Fig. 6a, is not too common; it can be caused by an uncorrected error in the raw data, or by an unintentionally introduced card-punching error while manually correcting for a multiplexing-synchronization error. Spectral

Typical Raw Data Distortions.

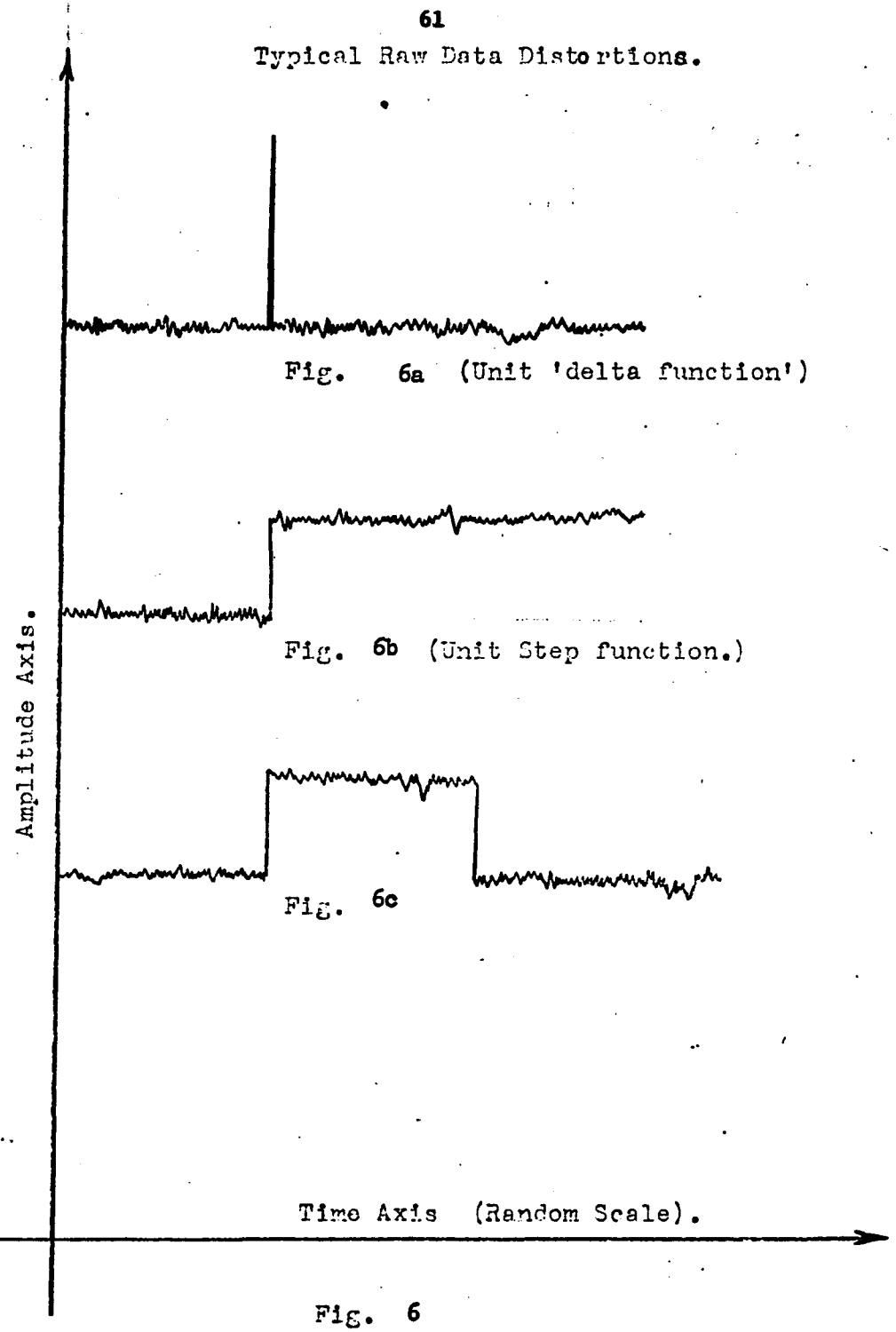

Fig. 6a (Unit 'delta function')

Fig. 6b (Unit Step function.)

Fig. 6c

Fig. 6

density estimates were obtained from all noise sources* used in the final spectral estimate, with computer-created delta functions of amplitudes of $-\frac{1}{2}$ v, -1v, and -2v ; these amplitudes are not much larger than the typical noise deviations, but are certainly representative of the situation encountered in actual experimental runs. The lower left-hand side of Fig. 7 shows the expected gradual "whitening" of the undisturbed spectral density estimate of noise source No. 1 as the amplitude of the spike in the time domain is increased.

Figures 7 through 11 indicate the anticipated result, namely that a particular disturbance such as a single data point out of 1000 being displaced by the mean by a given amount results in a specific additive spectrum; this additive spectral density is independent of the particular noise source and is, naturally, not very distinguishable if the spectral density of the noise source itself is of considerably larger magnitude.

A more common source of spectral estimate bias caused by a step type disturbance of the raw data is simulated and depicted in Fig. 6b. It is almost invariably caused by a missing data card which throws the remainder of the data off the preciously guarded multiplexing synchronization. A simple mathematical derivation of the "extra spectral density to be added" is quite misleading; assuming $f(t) = A\,U(t)$, then

$$R(\tau) = \lim_{T \to \infty} \frac{A^2}{2T} \int_{-T}^{T} U^2(t)\,dt = \lim_{T \to \infty} \frac{A^2}{2T} \int_{0}^{T} dt = \frac{A^2}{2} \qquad (53)$$

*Estimates were obtained for one only sampling speed; it is believed that this provides an adequate measure of a noise source's nature for the purposes of this section.

Figure 7

Spectral Comparisons between Controllably Distorted Variations of the Raw Noise Output of Noise Source #1.
(all superimposed distortions have a 1 volt amplitude unless otherwise specified).

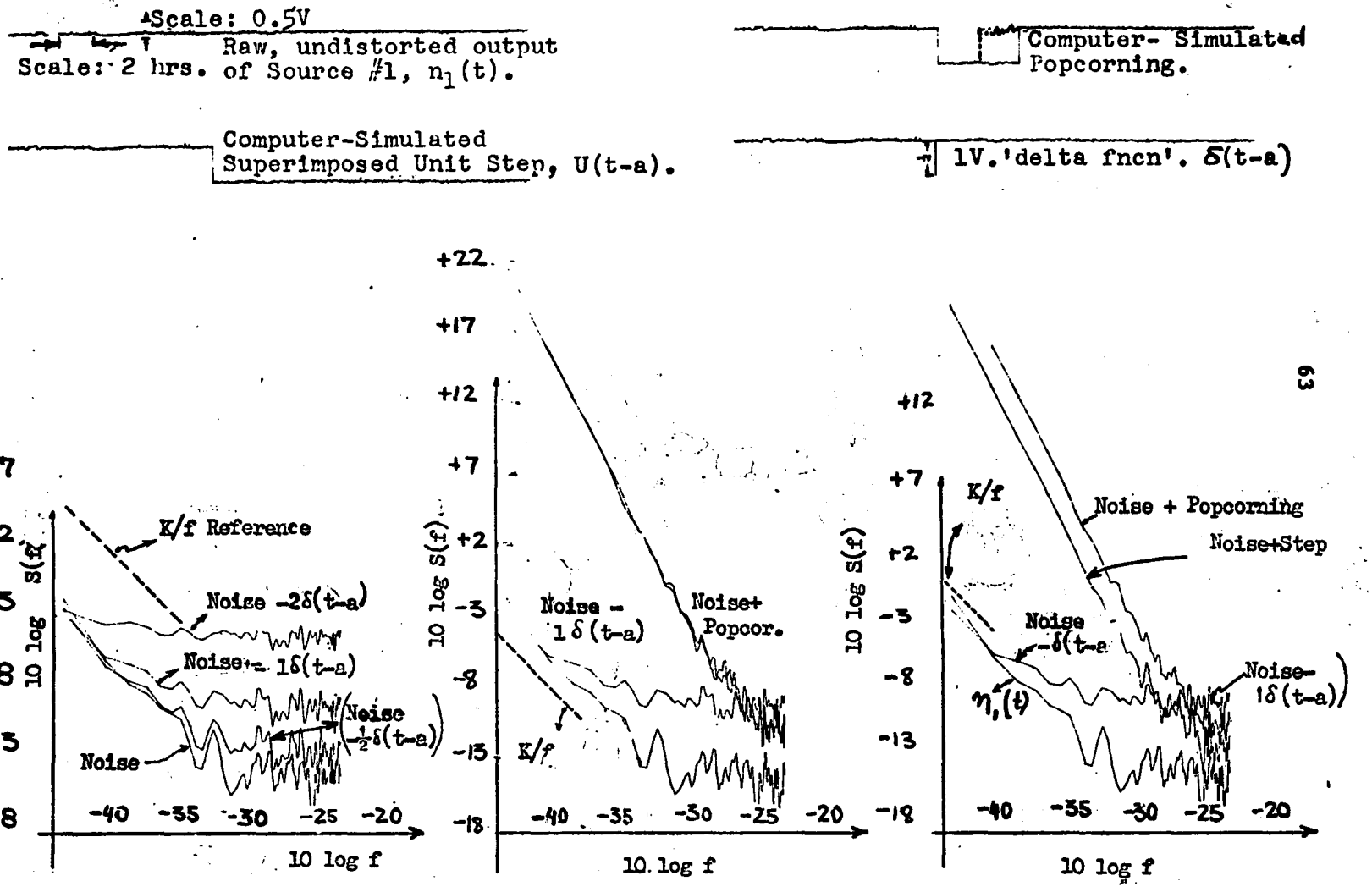

Spectral Comparisons between Controllably Distorted Variations of the Raw Noise Output of Noise Source #3.

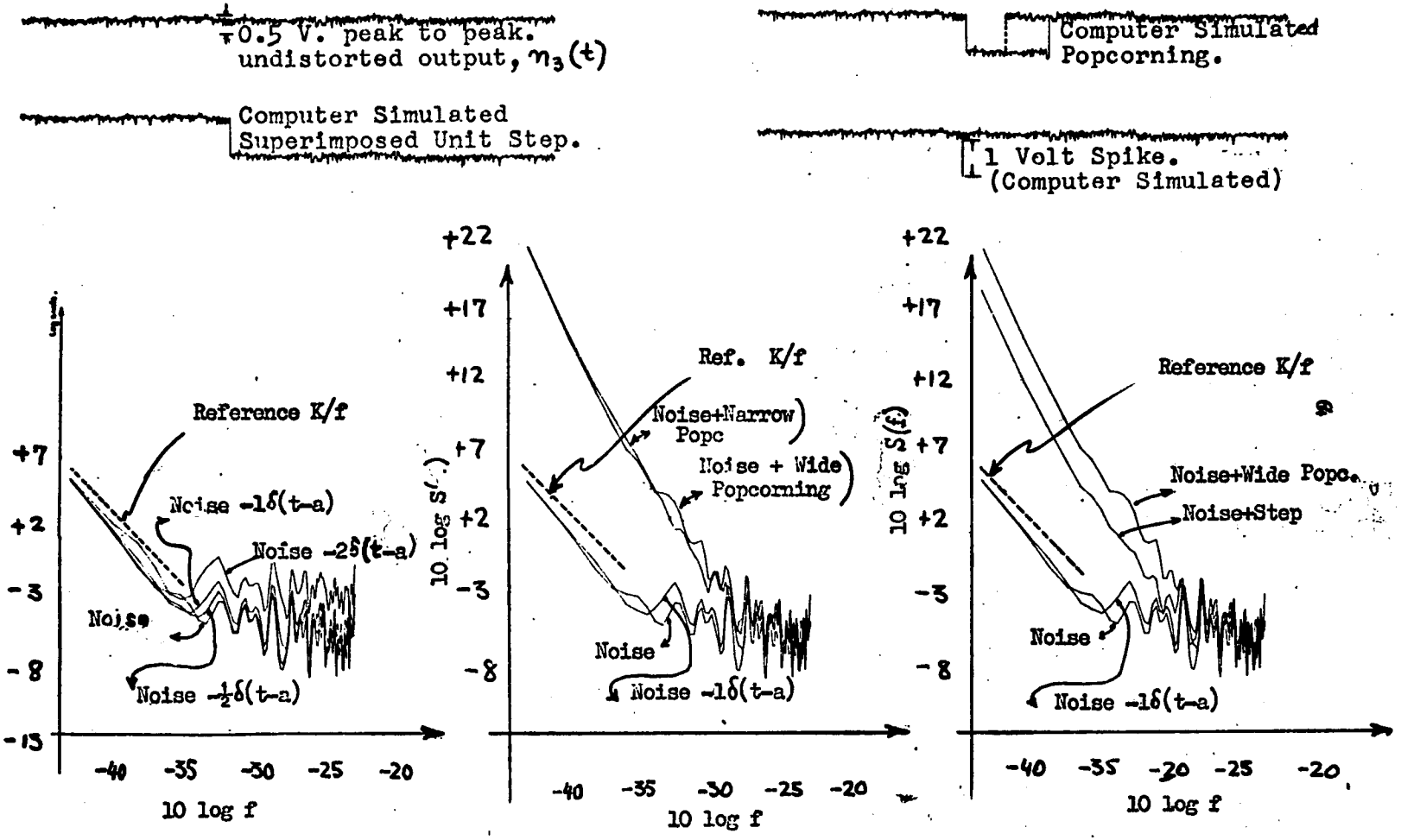

Figure 8

Spectral Comparisons Between Controllably Distorted Versions of the Raw Output of Noise Source #5.

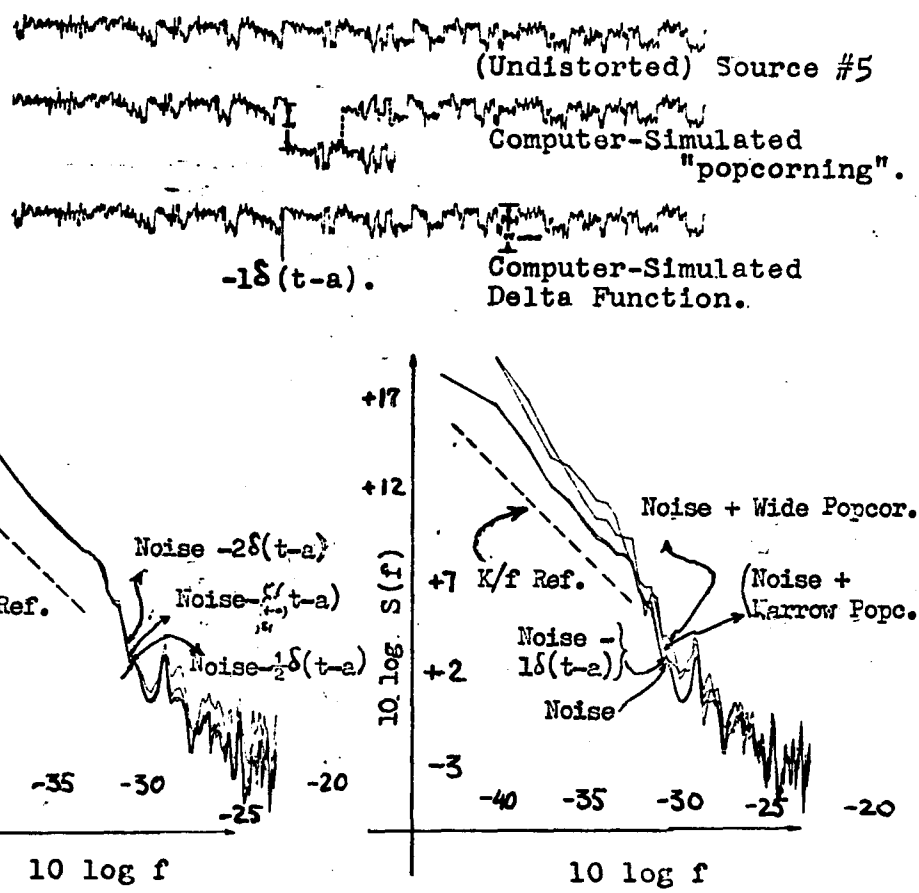

Figure 9

Spectral Comparisons Between Controllably Distorted Versions of the Raw Output of Noise Source #7.

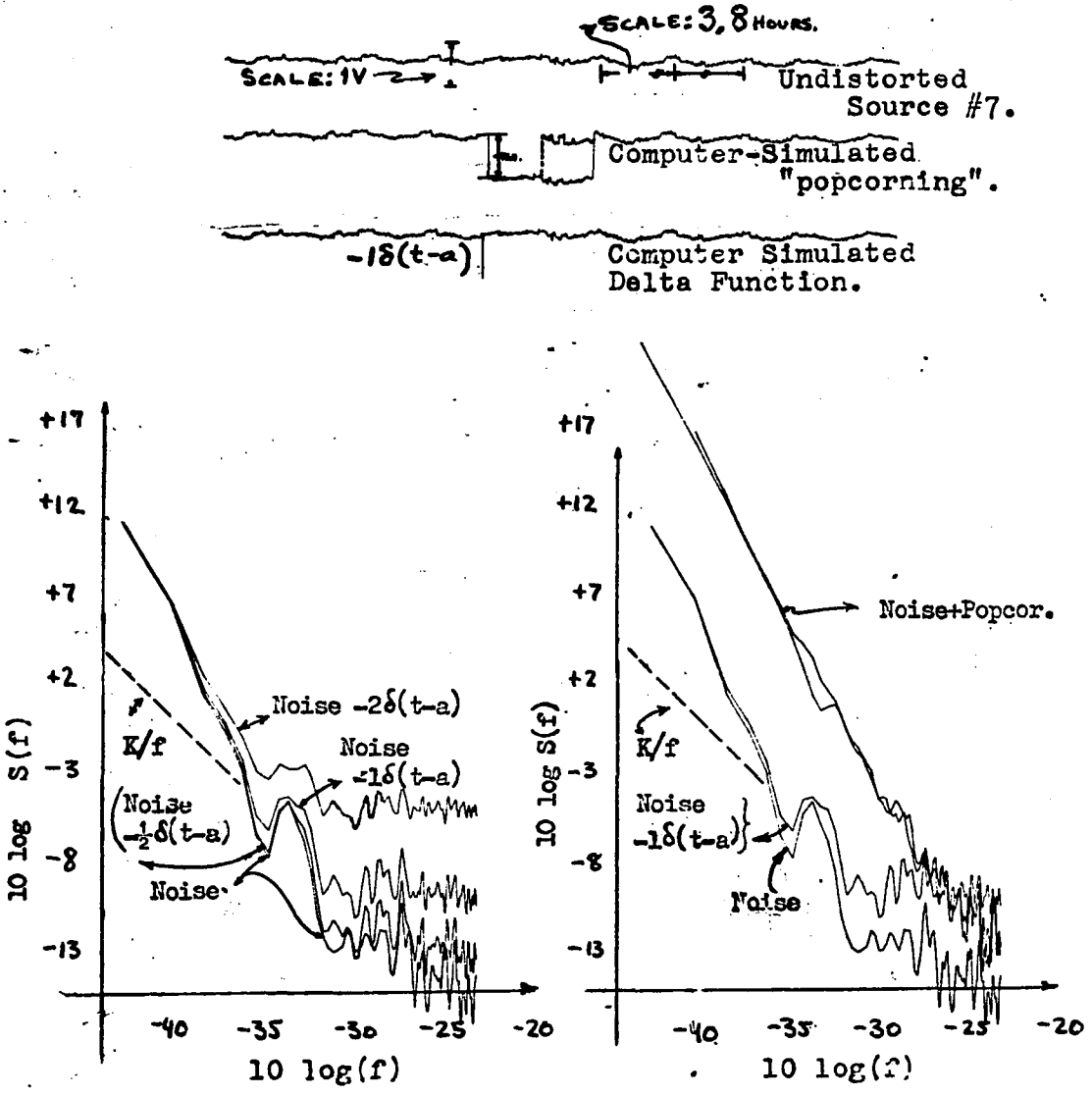

Figure 10

Spectral Comparisons Betweeen Controllably Distorted Versions of the Raw Output of Noise Source #8.

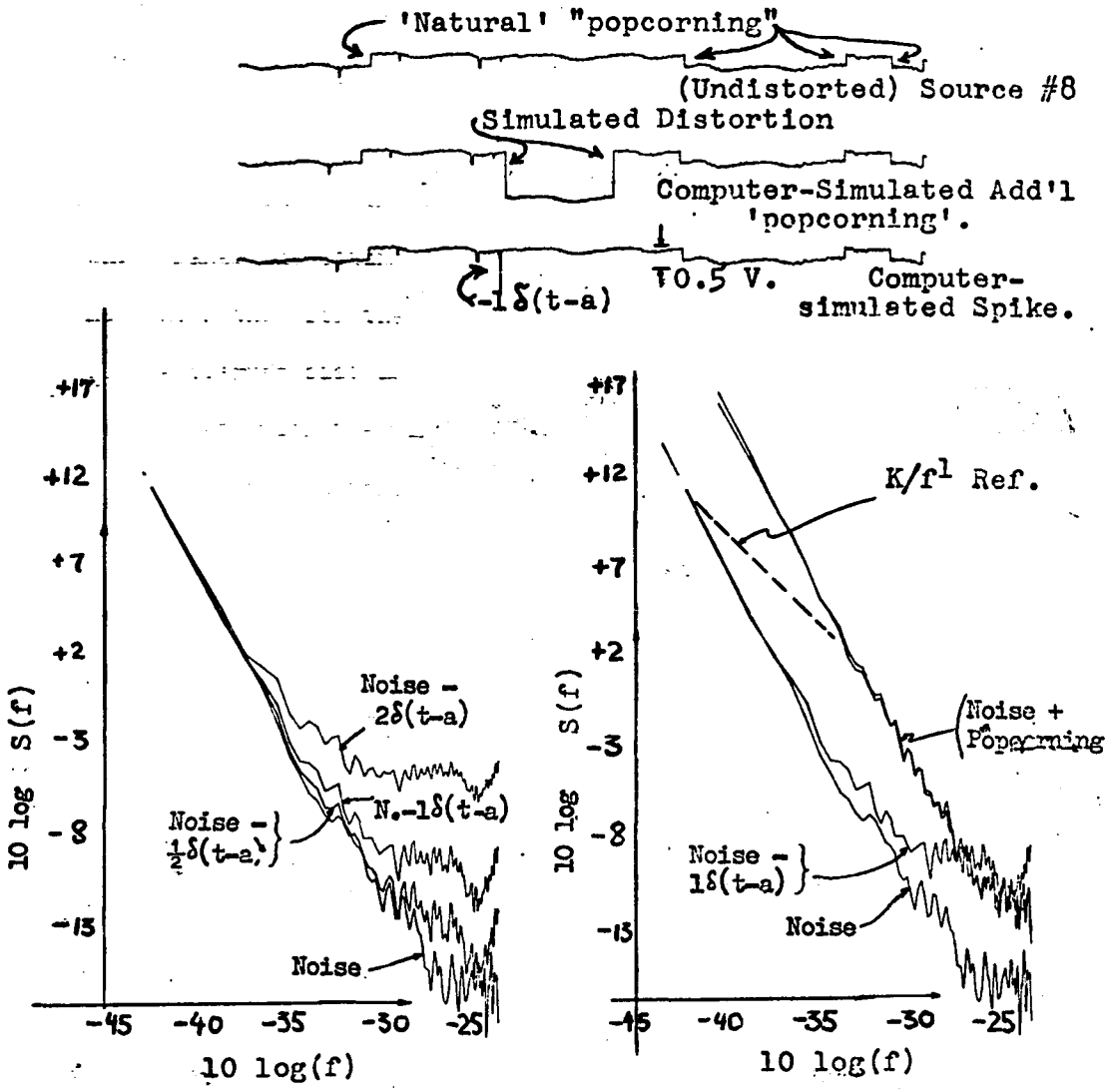

Figure 11

and $S(\omega) = \pi A^2 \delta(\omega)$.

This is certainly not the effect obtained experimentally and depicted in the lower right side of Figs. 7 and 8. What is observed there is a bias on the low frequency side of the spectral estimates which makes the estimate look steeper than it really is. Blakemore[25] has shown that for the simplified case where $A >> \sigma^2$ = variance, the above-observed bias is to be expected as a consequence of the interaction of the data with the window. This case is complicated by the fact that it arises from "interchanging" sources which means that the general noise level is different on the two sides of the step. Since such an event occurs on all 20 records it cannot escape detection.

Whereas the power spectrum for a unit step function in time is a spike at the origin, as Eq. (53) indicated, the power spectrum for the rectangular pulse $p_T(t)$ of the half-width T is not. Its Fourier transform is easily obtained by direct integration

$$F(\omega) = \frac{2\sin\omega T}{\omega}$$

hence the power spectrum

$$\frac{A^2(\omega)}{T} = \frac{4\sin^2\omega T}{T\omega^2} \qquad (54)$$

Depending on the width of the center lobe of the last equation above, one can expect anything from an additive "white" spectrum to an additive spectral density biasing mainly the low frequency edge of the unbiased spectral density estimate. This is readily confirmed by the plots in the middle of Figs. 7 and 8. As with delta-function-type disturbances,

the amount of additive spectral energy is determined by the disturbance-parameters and by the data-processing algorithm, and is independent of the particular noise source; this is readily seen in Fig. 10 which depicts a "noisy" source whose unbiased spectral density energy is sufficiently large to "mask" the additive energy of the disturbance.

One might be tempted at this stage to try to increase the "signal to noise" ratio, "signal" being the 1/f noise and "noise" being all such step-like disturbances; this way, biases of all the aforementioned kinds should vanish. This is not always possible, however; quite often, the step-like disturbance is caused by a malfunction of either the regulated power supply or the temperature regulator; this is perceived by the first stage of noise-creation, and no amount of subsequent amplification can subsequently selectively discard that disturbance only.

Fig. 11 depicts a "popcorning" source. This new type is treated in great detail in Ref. 34. A quick glance at the steepness of the spectral estimate's low frequency side might suggest the distorting presence of one (or more) superimposed rectangular pulses in the raw data, in line with all the discussion of this section; indeed, there are such pulses, only they are part of the noise. Removing them digitally would produce an artificial array of data, representing nothing physical; keeping the noise source as it is would steepen the overall final estimate; yet the latter can hardly be called "distortion" or "bias" since "popcorning" does exist in semiconductors and is as natural as flicker noise itself.

6.1 Linear Trend Removal

The question of linear trend removal from a zero mean process (averaged over the available time) will now be considered.

One is concerned with the presence of a specific and simple kind of nonconstant-in-time sample-mean: a linearly varying mean. The underlying reluctance to generalize to other forms of time dependence is the fear of throwing away low-frequency information in the process of mean removal.

Fig. 10 has shown convincingly that an obviously extraneous time dependence of the mean whose period was about one-tenth the data length had no noticeable effect on the estimate. Having removed it would certainly have caused no foreseeable deterioration of the estimate's quality.

The traditional noise source whose mean varies linearly with time is computer-simulated in Figs. 12 and 13 from two otherwise genuine noise sources of constant mean, and the spectral estimates are compared. As can be readily seen, the effect of a linear mean shift by about 50 times the standard deviation had practically no effect whatsoever on the accuracy of the result. In short, there is no need at all for removing either any reasonable linear trend or any other nonlinear trend which is slowly varying so that its main power comes from frequencies too low to affect the spectral estimate.

What is left then to worry about is a slowly varying extraneous disturbance whose characteristic time constant is at least an order of magnitude smaller than the total length of the run, and is nonlinear, too. Such a disturbance is, conveniently, rather unlikely on physical grounds; disturbances tend to be, for the most part, either abrupt, or characteristic of some aging process and hence monotonic.

Spectral Density Effect of Simulated Linear Trend on Raw Noise Output.

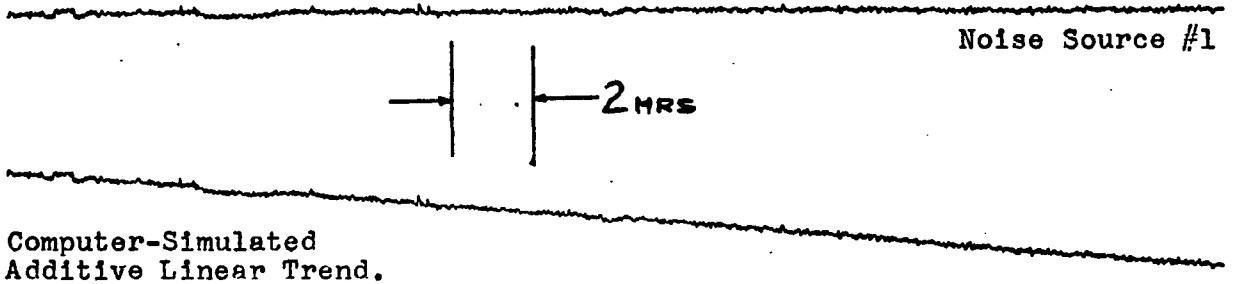

Computer-Simulated
Additive Linear Trend.

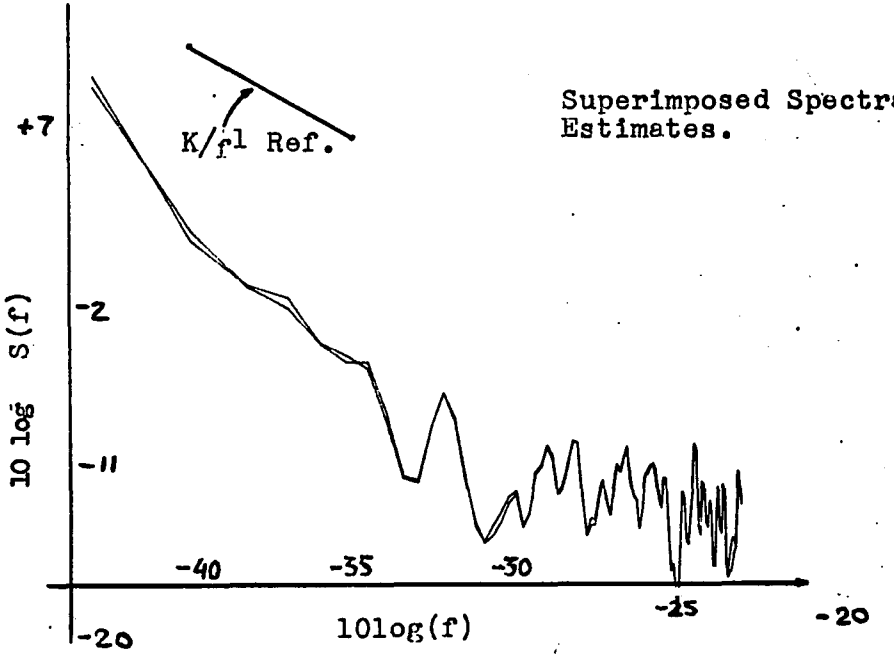

Superimposed Spectral Density
Estimates.

Figure 12

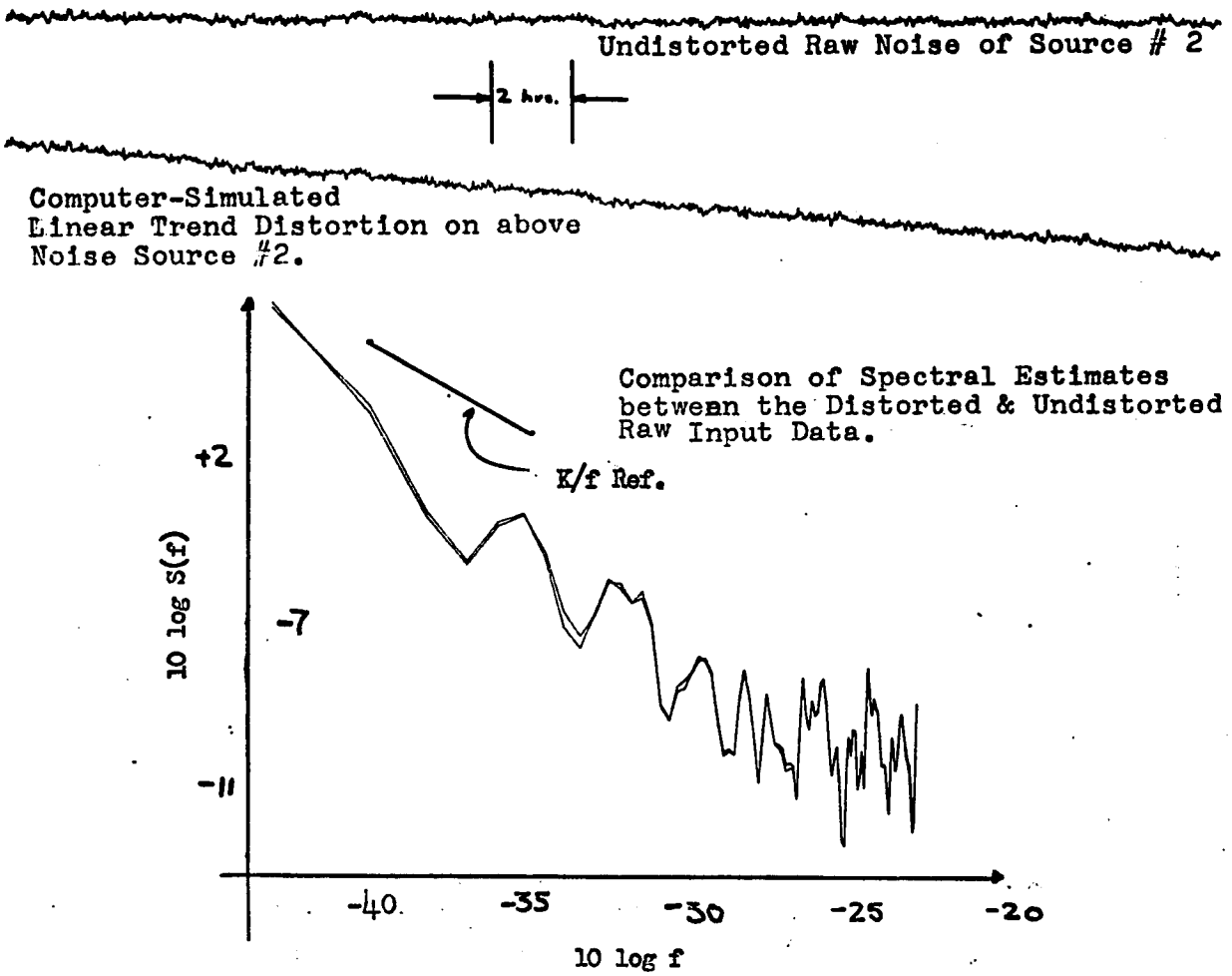
Undistorted Raw Noise of Source # 2
2 hrs.
Computer-Simulated
Linear Trend Distortion on above
Noise Source #2.
Comparison of Spectral Estimates
between the Distorted & Undistorted
Raw Input Data.
K/f Ref.
+2
-7
-11
10 log S(f)
-40
-35
-30
-25
-20
10 log f

Figure 12

CHAPTER 7

FURTHER GENERAL THEORETICAL CONSIDERATIONS

Physical reasoning, as well as experience from other kinds of noise, seem to suggest that flicker noise is the result of a superposition of a very large number of repetitive - though not periodic - disturbances. As it is not the goal of this thesis to venture into the physics of semiconductors, the emphasis in this chapter will be on the details of mathematical models.

7.1 Mathematically Modeling the Flicker Noise Mechanism

The little available literature on this topic seems to concentrate on either of two extremes: one deals exclusively with semiconductor physics, while the other deals exclusively with mathematical models having, for the most part, little contact with reality; a typical example of the latter approach is summarized very briefly below.

Given an ergodic ensemble of functions, whose ensemble average is zero and whose ensemble-autocorrelation is assumed to be

$$R_f(\tau) = A\,\delta(\tau) \tag{55}$$

hence its power spectrum is

$$S_f(\omega) = k \quad . \tag{56}$$

then if one assumes that

$$\exists \quad g(t) \quad \ni \quad \dot{g}(t) = f(t) \tag{57}$$

then utilizing the well-established relation[27]

$$S_{\dot{f}}(\omega) = |\omega|^2 \, S_f(\omega) \tag{58}$$

one obtains

$$S_g(\omega) = \frac{k}{|\omega|^2} \tag{59}$$

If one now defines $S_f^{(m)}(\omega)$ to be the m-fold integral of $f(t)$, then

$$S_f^{(m)}(\omega) = \frac{k}{|\omega|^{2m}} \tag{60}$$

and to describe flicker noise it is enough to let $2m = 1$.

This mathematical device of fractional order of integration generates flicker noise from white noise; it is due to Barnes and Allan.[22] The author of this thesis fails to see any practical use associated with fractional orders of integration.

Something much more concrete and tangible is clearly needed in providing a formal justification for flicker noise. The specific questions that this section considers are the following:

a) Can the physically plausible model of a summation of "random telegraph signals" result in 1/f noise? If so, what are the necessary constraints?

b) Does the above model imply either the existence or the absence of any specific probability distribution?

c) How do the experimental data obtained in this work compare with the anticipated predictions from the above theoretical considerations? This question is also treated in Section 7.1.2 below.

Puckett[34] has very recently worked out the mathematics giving the autocorrelation and spectrum of a single but generalized random telegraph

signal where the expected time spent in one state does not necessarily coincide with the expected time spent in the other state.

For the simpler case of a common semirandom-telegraph-signal $x(t)$ taking the values $+B$ or $-B$ with zero crossings which are Poisson distributed with an average frequency λ, many texts,[35,28] established the following relation for the associated autocorrelation:

$$R_{xx}(\tau) = \beta^2 \, e^{-2\lambda|\tau|} \tag{61}$$

The power spectrum follows trivially by Fourier-transforming the above, namely:

$$S_x(\omega) \equiv \int_{-\infty}^{\infty} \beta^2 \, e^{-2\lambda|\tau|} e^{-j\omega\tau} d\tau \tag{62}$$

$$S_x(\omega) = \beta^2 \, \frac{4\lambda}{4\lambda^2 + \omega^2} \tag{63}$$

Sketches of $R_{xx}(\tau)$ and of $S_x(\omega)$ appear in Fig. 14a below:

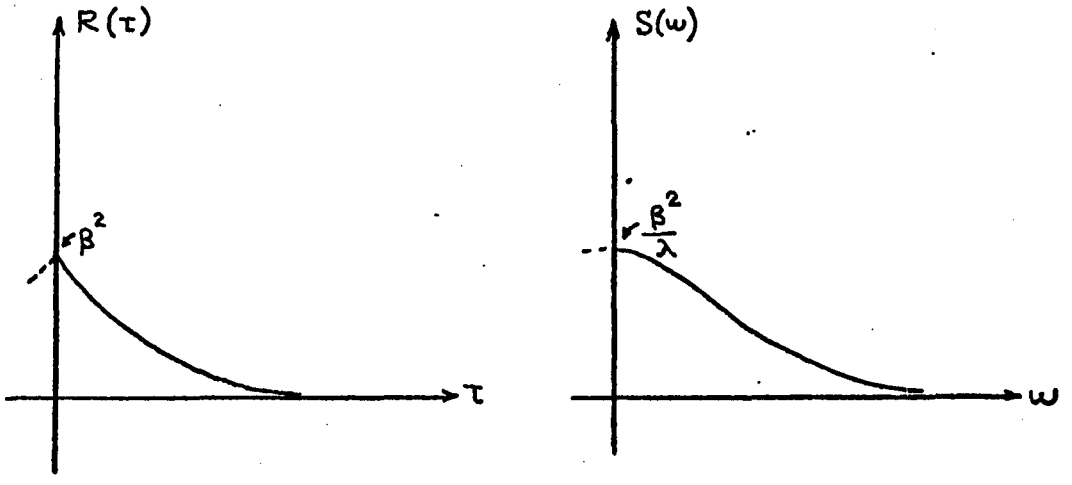

Fig. 14a

Quite clearly, there exists a point, ω_f , somewhere in between these extremes where the slope of $S_x(\omega)$ is that of some k_3/f spectrum which would pass through that point; the region "near" that point will, accordingly, be "almost" like k_3/f: Mathematically speaking, one requires that value of $\omega = \omega_f$ and of k_3 which results from the simultaneous solution of

$$S_x(\omega) = \frac{4\beta^2\lambda}{4\lambda^2 + \omega^2} = \frac{k_3}{\omega} \equiv S_y(\omega) \tag{65}$$

$$\frac{d}{d\omega}\left[S_x(\omega)\right] = \frac{d}{d\omega}\left[S_y(\omega)\right] \tag{66}$$

that is, letting $4\lambda\beta^2 = k_1$ and $4\lambda^2 = k_2$ for notational convenience, Eq. (66) becomes

$$\frac{2k_1\omega}{(k_2 + \omega^2)^2} = \frac{k_3}{\omega^2} \tag{67}$$

The positive real solution of the simultaneous equations (66) and (67) provides the desired ω_f .

It is clear now, that by superimposing many independent random telegraph signals of appropriately scaled β's and λ's one can synthesize a spectral density displaying a k_3/f behavior over arbitrarily many decades of frequency. The rule for selecting such "appropriate" parameters to artificially synthesize a k_3/f spectrum will clearly depend on the amount of "ripple" one will allow in the resulting spectrum, as illustrated in Fig. 14b;

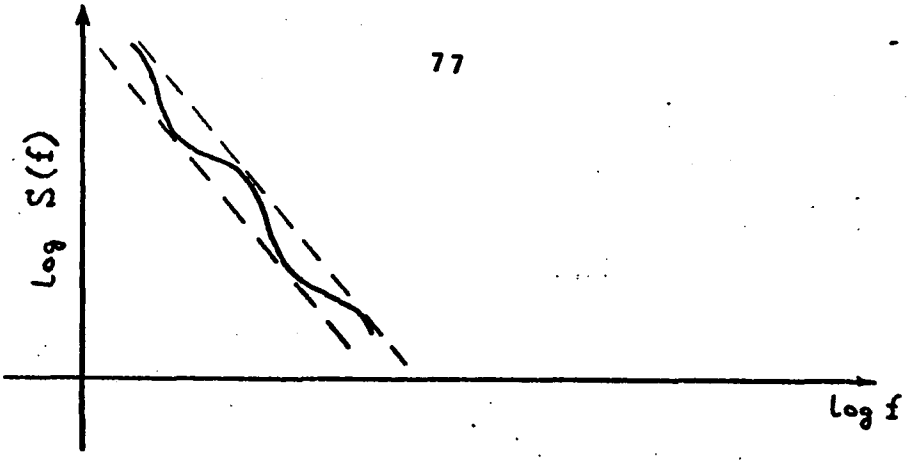

Ripple from Superposition of Many Telegraph Signals to Form a K/f Process.

Fig. 14b

The existence of such a discrete set of parameters is rather unlikely; it is physically more plausible to assume the presence of a continuous distribution in λ and β .

Any further arguments specifying physically realistic numerical upper and lower limits for the distributions of λ and β , are bound to get deeply involved with the kinetics of the oxide layers of the semiconductors; this is not the purpose of this work. It is of direct interest in the framework of this research, however, to examine the mathematical implications of the model introduced in this section.

It has been a peculiar trend in the past to misinterpret the applications of the Central Limit Theorem and to take it for granted that a summation of an infinite number of any independent random processes has a gaussian distribution. In fact, a closer look at the mathematics of the Central Limit Theorem indicates that this is patently false in some cases.

Many texts[28,36] establish the unidimensional central limit

theorem: given N statistically independent random variables $x_i, i\epsilon[1,N]$ and defining

$$z \equiv \frac{1}{\sqrt{N}} \sum_{i=1}^{N} (x_i - \bar{x}) \quad , \quad x_i - \bar{x} \equiv y_i \tag{68}$$

where $\bar{x}$ is the mean value of the x_i's , and such that $\bar{z} = 0$, and $\sigma_z^2 = \sigma_x^2 =$ (the shared variance of all random variables regardless of N), then

$$\lim_{N\to\infty} \int_a^b P_z(z)dz = \int_a^b \frac{e^{-\frac{y^2}{2\sigma_y}}}{a\pi\sqrt{\sigma_y}} dy \tag{69}$$

Indeed the central limit theorem does not at all imply that p_z approaches the gaussian density function, but that the integral of p_z between fixed limits approaches the value of the integrated gaussian density function between the same limits. In other words, the operations of limit-taking and integration are not always interchangeable. Mathematically inclined researchers[37] have pointed out that a set of sufficient conditions for $p_z(z)$ itself to be gaussian as $N \to \infty$ in Eq. (69) is that

$$\text{a)} \quad \sigma_1^2 + \ldots + \sigma_n^2 \to \infty \tag{70}$$

$$\text{b)} \quad \int_{-\infty}^{\infty} x^{\alpha} f_i(x)dx < c \equiv \text{constant}, \ \alpha > 2 \tag{71}$$

Indeed, (70) is easily satisfied if the given random variables have all equal variances. Equation (71) is satisfied if all densities

$f_1(x)$ are zero for $|x| > c_2$. (71)

What is of relevant interest in this work is not the undimensional central limit theorem which was presented above to highlight points which will subsequently be harder to pinpoint in view of the forthcoming mathematical complexity. It is the multidimensional central limit theorem which is of interest here. We have been observing a process, the output of a noise source, and have been wondering if indeed it could have resulted from a summation of many random telegraph waves; having shown that it could, we are presently trying to see if the so-modeled noise source is then gaussian, as was commonly believed,[38] or not.

We have k samplings of the noise sources output; these compose a k-dimensional vector which contains all the available information on that source; accordingly, we can think of the contributing individual telegraph signals as a set of N K-dimensional vectors, too. The development of the multivariate central limit theorem exactly mirrors the development of the corresponding one-dimensional theorem referred to earlier in this section; the development proceeds through the use of the joint characteristic function

$$M_x(\omega_1,\omega_2, \ldots\omega_k) = \int_{-\infty}^{\infty}\ldots\int P_x(x_1,x_2,\ldots x_k)e^{j\omega_1x_1+\ldots j\omega_kx_k}dx_1\ldots dx_k \quad (72)$$

and is well documented in relevant textbooks: Given

$$\vec{z} \equiv (z_1,z_2,\ldots z_n) \equiv \frac{1}{\sqrt{N}}\sum_{i=1}^{N} x_i,* \quad (73)$$

*The normalization $\frac{1}{\sqrt{N}}$ is such that the covariance matrix $[\Lambda_x] = [\Lambda_z]$.

where each k-component vector x_i is statistically independent of all others, i.e.,

$$p(x_1.x_2...x_k) = \prod_1^N p(x_i) \tag{74}$$

and assuming that each such x_i has the same density function p_{x_i}, with zero mean, covariance matrix $[\Lambda_x]$ and characteristic function M_x then

$$\lim_{N\to\infty} M_z(\vec{\omega}) = \exp[-\tfrac{1}{2}\,\vec{\omega}\,[\Lambda_z]\,\vec{\omega}^{\,T}] \tag{75}$$

and the density is obtained by taking the inverse transform of (75) above. It is of great interest that here, again, as $N\to\infty$, $p_z(z)$ does not necessarily converge to a gaussian density; the fundamental "catch" is that if p_x contains impulses, multidimensional or unidimensional, so does p_z, regardless of the numerical value of N. What does always become gaussian in the limit is the distribution function F_z.

In the interest of completeness, letting $k = 1$ in (75) above yields

$$\lim_{N\to\infty} M_z(\omega) = \exp(-\tfrac{1}{2}\,\omega\lambda_{11}\omega) = \exp(-\tfrac{1}{2}\,\omega^2\sigma^2) \tag{76}$$

which is in accord with the one-dimensional central limit result stated earlier in Eq. (69).

Can this theoretically-derived result be easily checked against available experimental evidence? The unfortunate answer is a flat "no"; given a set of time-sampled values of a noise source can only result in a histogram-looking plot of the probability density estimate; any such

histogram, by its very nature, befogs the issue as to whether or not it is an envelope of a much finer structure, and if so, what is that structure.

A histogram of that type which estimates the probability density is shedding some light on the fashionable talk about a lack of stationarity that some researchers[5] have observed in their noise sources of flicker noise.

7.1.2 Related Experiment Evidence

It has been noted[39] that the inference that the spectral power density remains inversely proportional to zero frequency implying infinite total noise power is appropriate only for stationary random processes. Reputable researchers in this field[39] have claimed that 1/f noise may not be stationary in the usual sense, but rather may possess a weaker form of conditional stationarity.

The first recorded attempt to examine the statistics of 1/f noise goes back to 1955;[40] the experiment's failure has subsequently been attributed[5] to the measurement technique's inability to detect any "conditional stationarity". A subsequent attempt by J. Brophy[5] claimed to have observed some significant statistical difference between 1/f and Nyquist noise: specifically, although the probability amplitudes of both types of noise were similar, the variances of the distributions of different samples fluctuated considerably in the case of 1/f noise. Although that experiment's published report was somewhat oversummarized, no attempt was made to duplicate it because of the enormous amount of data

handling required to obtain, for example, 100 sample variances. This thesis, having already documented the presence of "popcorning" noise sources whose time constant is occasionally of the order of 8-10 hours, makes it obvious that taking 100 "good" sample variances at 2-3 different sampling rates would take a prohibitively large amount of time and computer time.

What is of interest in the context of this work is to actually observe the probability distributions of the various raw data-sets from which the final experimental results of this thesis are obtained. Are the amplitude distributions truly gaussian? How do the shapes differ between two different halves of each unknown data-taking session? What consequence does that have on stationarity considerations? What can one infer from these amplitude distributions as to the corresponding raw data or even spectral estimate?

Figure 5 above shows the distribution of the absolute values of the amplitudes of all ten noise sources for each sampling speed used; each "run" is artificially split into two halves for stationarity observation considerations.

A bell-shaped plot of a zero-mean process which displays more than one peak is indicative of a noise source which has two or more preferred "states" and whose sample mean may be neither of those; this is typical of "popcorning" noise sources and, occasionally, of error in the multiplexing-synchronization, as explained in Chapter 9 below.

A rather "flat" plot reminiscent of low-pass-filtered white noise is suggestive of a noise source which is uniformly distributed in amplitude; this is somewhat of an oversimplified statement, however, in view

of the fact that the plots are essentially histograms which can take any of twenty discrete values.

Any striking difference in the amplitude distribution between the first and the second half of an experimental run tends to imply non-stationarity; alternatively, however, it may only imply, for example, that the noise source's intrinsic time constants are large, perhaps as large as references (1) and (18) have suggested that they may be. Approaching the stationarity question through Brophy's way[5] by making histograms of the variances of many different runs, is a venture of questionable use for two reasons:

a) Since the time constants involved from the physics of the semiconductors may be large,[1] one will have to take long-lasting runs. Time-multiplexing is inapplicable, since it is the changing statistics of only one source that one is after. If each run is one month long, getting 30 variances would require equipment of extremely good stability. Indeed, it would be next to impossible to avoid environmental influence from creeping into the system. The results would thus be highly questionable.

b) Since no physically sensible upper limit has yet been determined for the intrinsic time constants of semiconductor kinetics, one would still wonder if, perhaps, each run should have been even longer!

Normalized distribution plots of the absolute value of the amplitude were made for two noise sources on probability paper, so that the gaussian shape of the plot could be verified easier. The longest available records were selected, so that the nature of the statistics of

the sources in their most interesting regions could be studied.

Noise source #4, depicted in Fig. 15a below was selected because its linear plot (already presented in Fig. 5 earlier) appeared to resemble the familiar bell-shape to a considerable extent. Its probability-paper graph verifies this.

Noise source #9, depicted in Fig. 15b below, was selected because its linear plot displayed a peculiar dip near the peak of the bell-shaped curve. Its probability-paper graph depicts this peculiarity at point X on the graph because the integral of the bell-shaped curve increases only slightly as the area under the aforementioned "dip" is integrated.

There are two points of interest at this stage:

a) Since these graphs are graphs of the absolute value and not of the algebraic value of the amplitudes, the distribution is postulated to be symmetric around the mean. This fact is reflected on the probability-paper graphs, too.

b) Even if the curves seem truly gaussian, it is important that they have resulted from histograms. Accordingly, they are at best envelopes of a true distribution.

This section has attempted to experimentally determine the amplitude-distribution of two noise sources whose spectra are believed to be $1/f$ in nature. It has been found that, within the limits of reasonable experimental accuracy, the sources are gaussianly distributed in amplitude. This is in agreement with the theoretical discussion of Section 7.1 with the understanding that the experimentally obtained distribution curve is only the envelope of the true distribution.

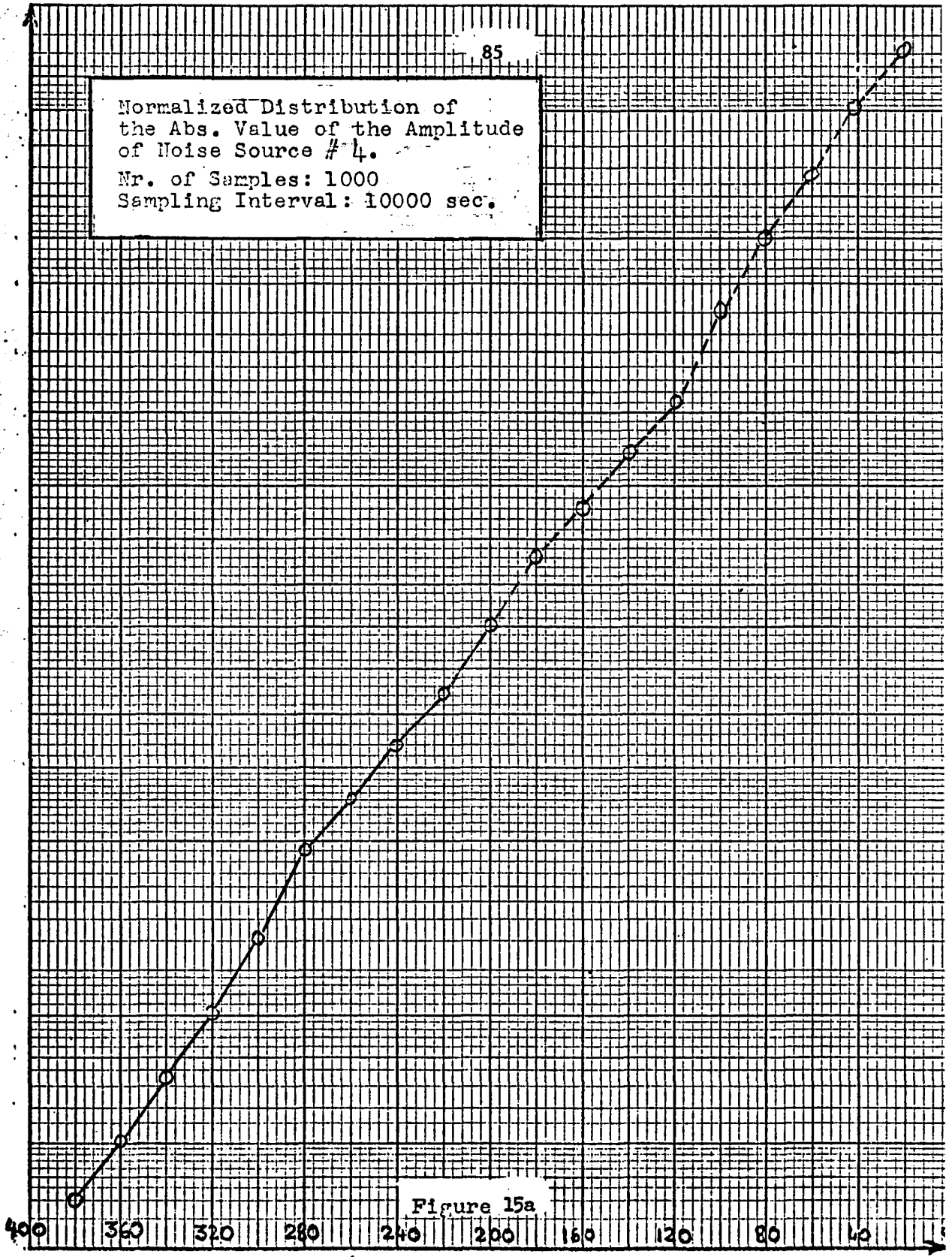
Normalized Distribution of
the Abs. Value of the Amplitude
of Noise Source # 4.
Nr. of Samples: 1000
Sampling Interval: 10000 sec.
400
360
320
280
240
200
160
120
80
40
(arbitrary scale)

Figure 15a

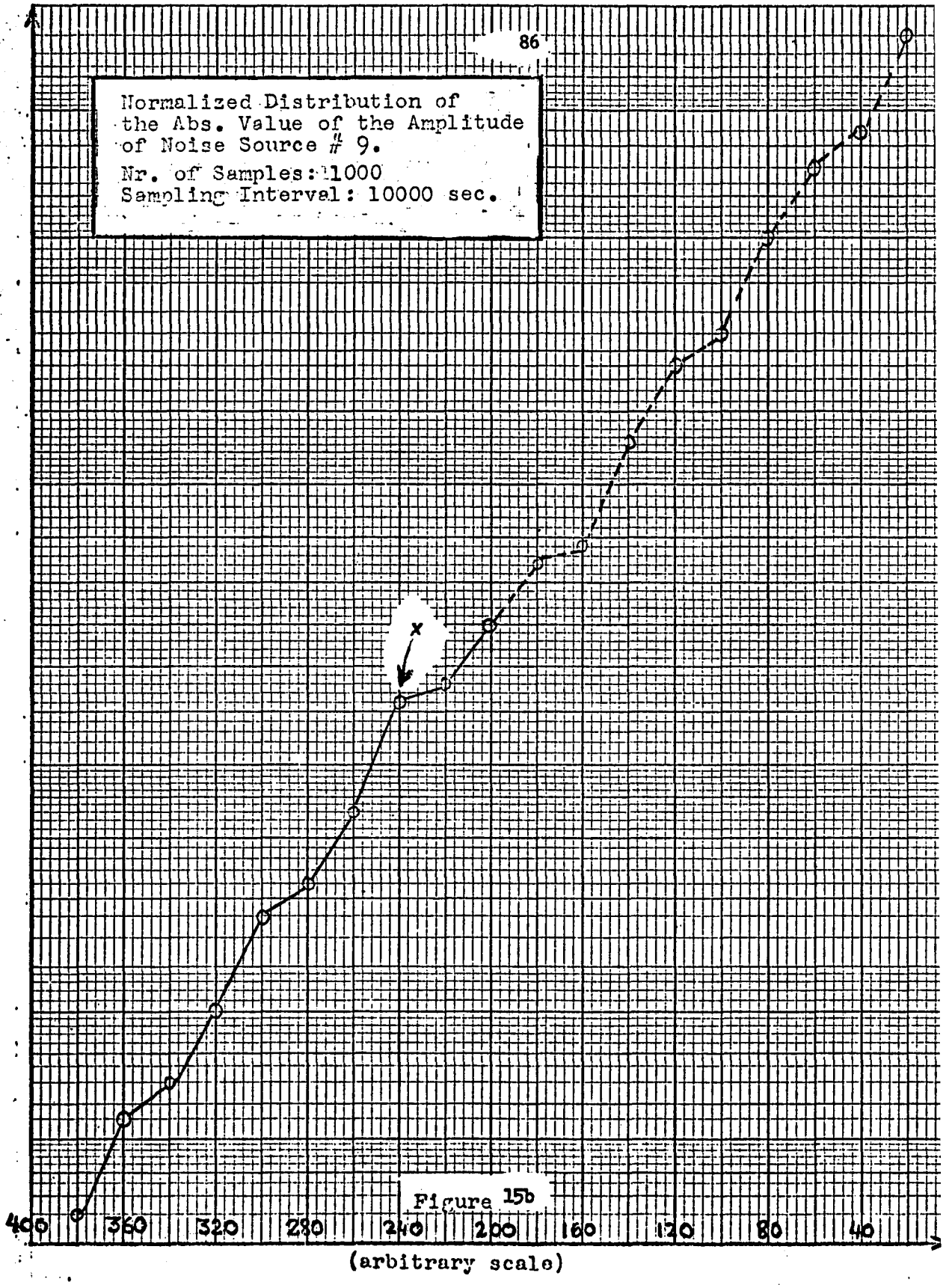
Normalized Distribution of
the Abs. Value of the Amplitude
of Noise Source # 9.
Nr. of Samples: 1000
Sampling Interval: 10000 sec.
x
400
360
320
280
240
200
160
120
80
40
(arbitrary scale)

Figure 15b

CHAPTER 8

COST REDUCING DATA-TAKING ALGORITHMS

The sampling technique discussed so far where the available samples are spaced equally in time has been motivated by sheer conceptual and computational simplicity; nowhere in the derivation was any attempt at optimization made.

The first part of this analysis deals with the following situation: Suppose it is of interest to obtain an estimate at a very low frequency by increasing drastically m of Eq. (12); this will clearly result in an estimate of very high variance, but the interesting question is the following: Since it is evident from

$$C_r = \frac{1}{n-r} \sum_{q=0}^{n-r} x[(q\Delta\tau)] \cdot x[(q+r)\Delta\tau] \tag{77}$$

that there will be, percentagewise, more terms in the sum for r small than for r large, the reliability of the low-indexed C_r's will be statistically better than the reliability of the high indexed ones; how will this reflect on the reliability of the spectral estimates at low frequencies and how at high frequencies? Is it "best" to have a constant number of terms in the summation of the aforementioned Eq. (77)?

Even in the usual cases where T_M/T_N is of the appropriate order of 1:100 or thereabouts, are we perhaps determining some of the mean-lagged products with unnecessary accuracy? Couldn't we approach the economy of the fast Fourier transform and yet stay away from its

algorithmic complexity by refining our present algorithm?

The second part of this analysis considers the following question: How can one process samples taken at a known but not constant rate? Is there any condition to be satisfied by the times at which sampling is made? Can we get alias-free sampling through this approach?

8.1 Non-Constant but Non-Random Sampling

It has been seriously hinted in the past[24,25] that the development of "the right" sampling algorithm, where samples are taken at nonequal but prescribed nonrandom intervals of time would do such wonderful things as optimize data processing, eliminate the need for de-aliasing, etc.

As the derivations and discussion below suggest, such hopes are, unfortunately, unrealizable.

It is of interest to start this discussion by expanding the fundamental equation (17) above as follows:

$$V_1 = \Delta\tau[C_0+2C_1\cos(\tfrac{1\pi}{100}) + 2C_2\cos(\tfrac{2\pi}{100}) + \cdots + C_{100}\cos(\pi)]$$

$$V_2 = \Delta\tau[C_0+2C_1\cos(\tfrac{2\pi}{100}) + 2C_2\cos(\tfrac{4\pi}{100}) + \cdots + C_{100}\cos(2\pi)] \qquad (78)$$

$$\vdots$$

$$V_{100} = [C_0-2C_1+2C_2-\cdots-2C_{99}+C_{100}] \qquad (79)$$

Indeed, "fitting cosines to the data" is a misleading oversimplification, in that every single "raw estimate" depends on all autocorrelation coefficients. The degree of dependence of any one "raw esimate" on a particular C_i is directly related to the actual power spectral density of the stochastic process being considered.

It thus follows, in answer to the question posed in the introduction to this chapter, that there is no need to reduce the reliability of the low indexed C_i's unless the cost of an excessive number of digital cross correlations becomes prohibitively expensive; indeed, it has been shown[26] that the autocorrelation is the most expensive step of the entire procedure used in this thesis; such shortcuts as the "Fast Fourier Transform" have been devised in an effort to by-pass the expensive correlation-taking. It is in such cases that the algorithms suggested below could be of use.

The motivation is to record and subsequently process no more data points than are enough to provide an almost equal number of C_i's for all desired i, $i \in [0;m]$, m to be pre-specified. Although the total number of recorded data points is kept constant for both the "old" (Tukey) and the "new" algorithms, the time span required for data-recording for the "new" algorithm is somewhat longer. Quantitative comparison is made later.

In the following sampling algorithm, for instance,

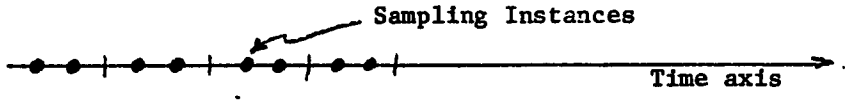

if we are to collect n points, this will take 3/2 the time it would take to collect the same number of points without any skipping.

The relative abundance of the various C_i's is now clearly

No. of C_0's	is	$100\% \cdot \eta$	
C_1's	is	$50\% \cdot \eta$	
C_2's	is	$50\% \cdot \eta$	
C_3's	is	$100\% \cdot \eta$	Assuming $\eta \gg 6$
C_4's	is	$50\% \cdot \eta$	
C_5's	is	etc. $\cdot \eta$	

The above information is plotted as "SPACING B" in Figs. 16 and 17. (In Fig. 17, m is allowed to increas indefinitely up to η, assuming $\eta = 10{,}000$. From Fig. 17 it can be seen that for large m there exists a higher abundance* of $C_{i=m}$'s than if scheme "A" (the Tukey approach) had been used. This is to be expected since we are sampling for a longer time; the price we pay, or seem to, is that some mean lagged products are not quite as reliable, (e.g., C_1, C_2, etc. are $50\% \cdot \eta$ available only).

This is not as bad as it seems to be; the difficulty can be somewhat alleviated by adjusting these unreliable values through a weighted averaging with adjacent reliable values. In so doing, we have essentially sacrificed some frequency resolution.

Along the same line of thought, one can consider similar, yet more sophisticated algorithms, e.g.,

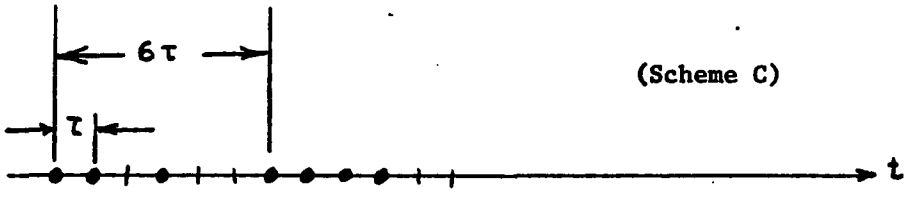

(Scheme C)

*Not relative to higher indexed ones but as compared to the Tukey algorithm.)

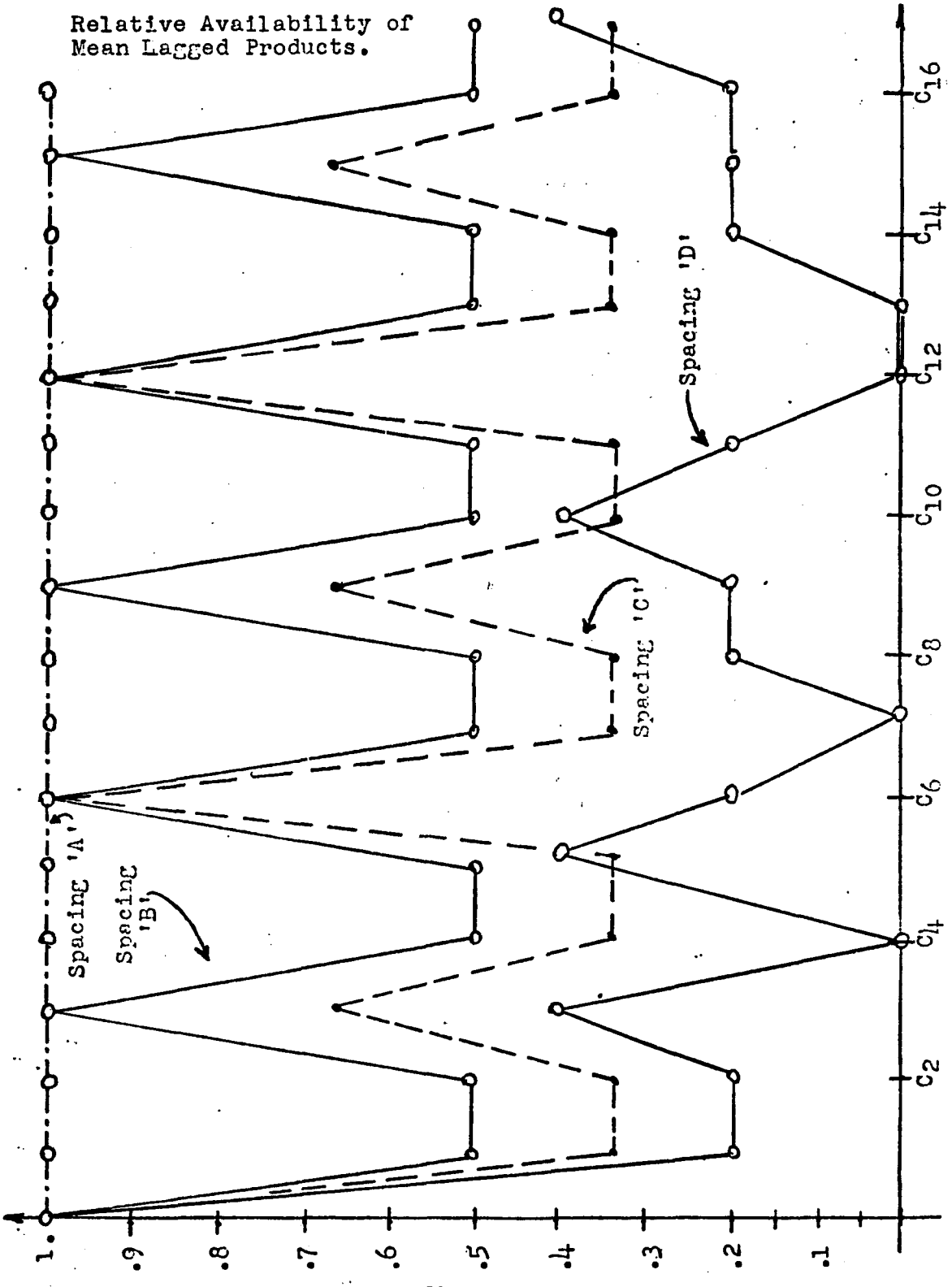
Relative Availability of
Mean Lagged Products.
Spacing 'A'
Spacing 'B'
Spacing 'C'
Spacing 'D'
1.
.9
.8
.7
.6
.5
.4
.3
.2
.1
C_2
C_4
C_6
C_8
C_{10}
C_{12}
C_{14}
C_{16}

Fig. 16

Fig. 17 .

Averaged Relative Availability of Mean Lagged Products for High-Indexed C_j's.

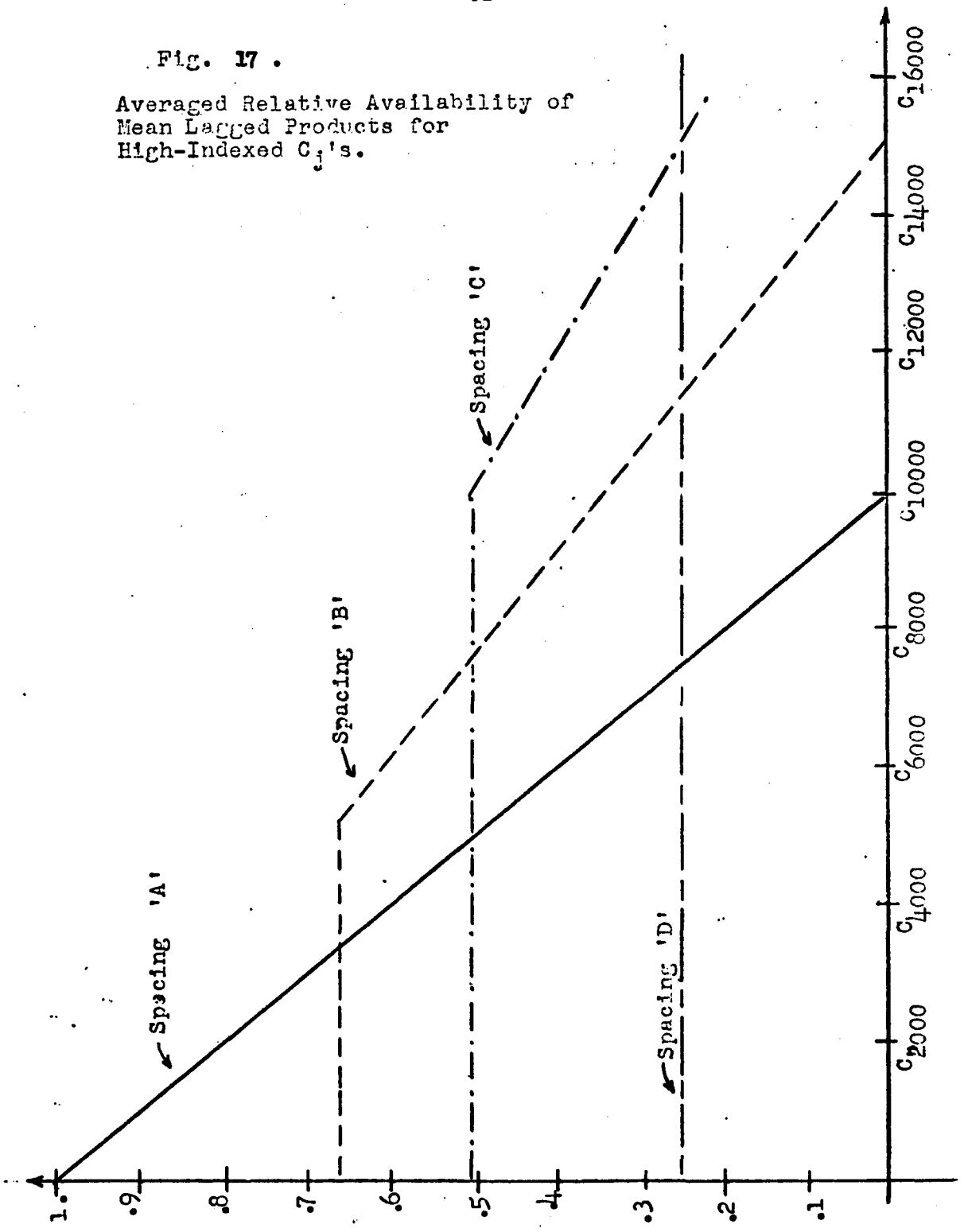

whose relative availabilities of C_i's are shown in Fig. 16 and Fig. 17; for that scheme the time factor expansion is 2/1 , that is, twice the time is needed to gather a total of η data points than if the Blackman-Tukey algorithm were used.

8.1.2. Mathematics Pertaining to Nonconstant, Nonrandom Sampling

The problem of processing data obtained at unevenly spaced, nonrandom, but known times, can always be reduced, as discussed below, to one which can be treated by the Blackman-Tukey algorithm which has been extensively discussed. The obvious penalty for so doing is the irrevocable loss of any and all potential benefits that could be inherent in a scheme where data points are not evenly spaced. A curve would thus be fitted, through simple digital processing, through the available points of $C(\tau_i)$, and the value of the resulting curve could subsequently be read at equidistant intervals, as indicated in Fig. 18 below; from that stage on, the usual algorithm, namely the sequence of

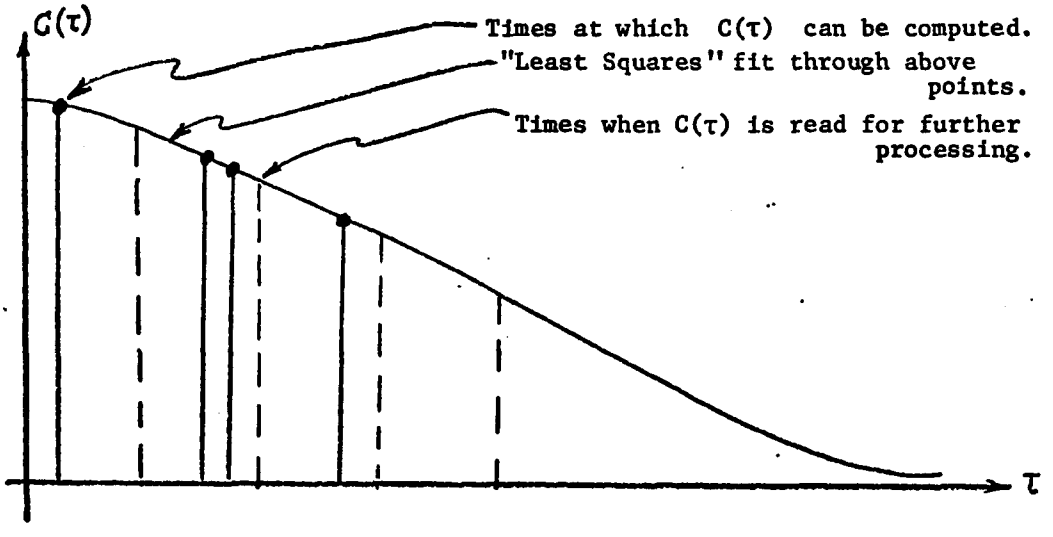

Fig. 18. Autocorrelation Sampling

steps outlined in Section 3.2, can be used as is; such an approach is not in the least disreputable, since the resulting accuracy should not be, on the average, any worse than that obtained from data collected at equally spaced time intervals.

An alternative approach will provide considerably more insight into the nature of uneven sampling.

It can be recalled from Fig. 1 that the Blackman-Tukey algorithm involved fitting a staircase-like function through $C(k\Delta\tau)$ such that the transition in the magnitude of the resulting curve occurred halfway between every two subsequent τ_i's ; the function was defined as zero at $\tau > T_M$.

Figure 19 below suggests a very analogous approach tailored for uneven sampling.

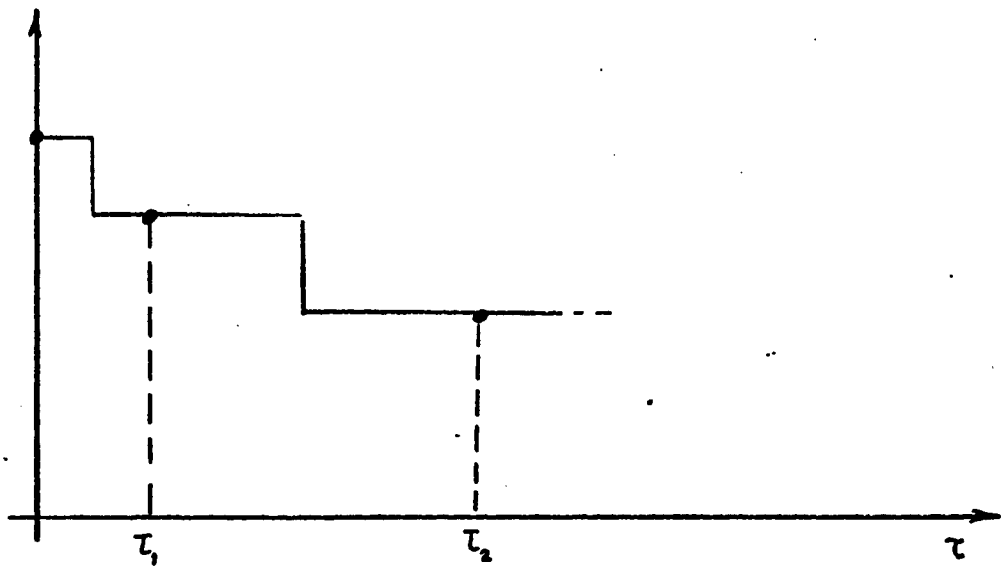

Fig. 19

The following related points of interest should be mentioned:

(a) Unless the sampling scheme is periodic with period much smaller than T_N, the record length, any one $C(\tau_i)$ will be the result of one, or at most, a very few cross-correlation multiplications, and will be very unreliable.

(b) If the sampling scheme is purposely not periodic, then the aforementioned unreliability of the lagged products can be compensated for by the greatly increased number of the now available lagged products. Indeed, if the τ_i's are not, loosely speaking, linearly related, there can be up to

$$m = \binom{\eta}{2} \frac{\eta\,!}{2(\eta-2)\,!} \tag{80}$$

such products (e.g., in the case of random sampling where time is also recorded).

For a typical $\eta = 10{,}000$ this amounts to

$$\frac{10{,}000!}{2(9{,}998)!} \simeq \frac{1}{2} \times 10^8 \text{ products}$$

As this thesis is not concerned with random sampling, a topic in itself, we will not pursue the consequences of this scheme any further.

In the following it is assumed that through a data-taking scheme such as the one described in Chapter 3, mean lagged products $C(\tau_k)$, $k \in [0,m]$ have been obtained through the use of

$$C(\tau_k) = \frac{1}{\eta_k} \sum_k x(t_i)\, x(t_i + \tau_k) \tag{81}$$

where the summation extends over all possible intervals which are τ_k in width; η_k is the number of such available intervals and depends on the particular sampling scheme used, as is obvious from this discussion, and on the record length.

Fourier transforming the function depicted in Fig. 19 yields the analytical expression of the estimator as follows

$$S(f) = \int_{-\infty}^{\infty} C(\tau)\, e^{-i\omega\tau} d\tau = \int_{-T}^{T} C(\tau)\cos\,\omega\tau\, d\tau$$

$$= 2\int_{0}^{T} C(\tau)\cos\,\omega\tau\, d\tau \simeq 2C_o\frac{\tau_1}{2} + 2\int_{\tau_1/2}^{\frac{\tau_1+\tau_2}{2}} C_1\cos(\omega\tau_1)\, d\tau$$

$$+ 2\int_{\frac{\tau_1+\tau_2}{2}}^{\frac{\tau_2+\tau_3}{2}} C_2\cos(\omega\tau_2)\, d\tau + \cdots + 2\int_{\frac{\tau_{m-1}+\tau_m}{2}}^{\tau_m} C_m\cos(\omega\tau_m)d\tau \qquad (82)$$

Carrying out the integration gives:

$$S(f) \simeq C_o\tau_1 + 2C_1\cos\,\omega\tau_1\left[\frac{\tau_1+\tau_2}{2} - \frac{\tau_1}{2}\right] + 2C_2\cos\,\omega\tau_2\left[\frac{\tau_3}{2} - \frac{\tau_1}{2}\right] +$$

$$\cdots + 2C_m\cos(\omega\tau_m)\left[\tau_m - \left(\frac{\tau_m}{2} + \frac{\tau_{m-1}}{2}\right)\right] = C_o\tau_1 + [C_1\cos(\omega\tau_1)]\tau_2$$

$$+ C_2[\cos(\omega\tau_2)](\tau_3 - \tau_1) + \cdots + C_m\cos\,\omega\tau_m(\tau_m - \tau_{m-1}) \qquad (83)$$

Defining $\tau_o \equiv 0$, and $\tau_{-i} = -\tau_i$ for notational convenience yields

$$S(f) = \tau_1 C_1 + \sum_{i=1}^{m-1} C_i \cdot\cos(\omega\tau_i)(\tau_{i+1} - \tau_{i-1}) + C_m\cos\,\omega\tau_m(\tau_m - \tau_{m-1})$$

or, letting the nonexisting $\tau_{|m|+1}$ be defined identically equal to $\tau_{|m|}$ for notational simplicity, then

$$S(f) = \int_{-T}^{T} \frac{1}{2} \sum_{-m}^{m} C_i \cos \omega\tau_i [\tau_{|i|+1} - \tau_{|i|-1}] \delta(\tau-\tau_i) d\tau \qquad (84)$$

Interchanging summation and integration gives

$$S(f) = \int_{-\infty}^{\infty} [\frac{1}{2} \sum_{-m}^{m} C_i [\tau_{|i|+1} - \tau_{|i|-1}] \delta(\tau-\tau_i)] e^{-i\omega\tau_i} d\tau \qquad (85)$$

where $\tau_{-(m+1)} \triangleq \tau_{-m}$

$\tau_{m+1} \triangleq \tau_m$

which is the estimator's expected value.

The traditional question at this stage is how this estimate $S(f)$ is related to the true power spectrum of the stochastic process. Equation (85) can be rewritten as

$$S(f) = \int_{-\infty}^{\infty} \frac{1}{2} \sum_{-m}^{m} C(\tau)\, \delta(\tau-\tau_i) [\tau_{|i|+1} - \tau_{|i|-1}] e^{-i\omega\tau_i} d\tau$$

$$= \frac{1}{2} \sum_{-m}^{m} [\tau_{|i|+1} - \tau_{|i|-1}] \int_{-\infty}^{\infty} C(\tau)\, \delta(\tau-\tau_i) e^{-i\omega\tau_i} d\tau \qquad (86)$$

and, by the convolution property of the Fourier transform,

$$= \frac{1}{2} \sum_{-m}^{m} [\tau_{|i|+1} - \tau_{|i|-1}] \cdot \{e^{i\omega\tau_i} \circledast P(f)\}$$

where $P(f) \triangleq$ F.T.$[C(\tau)]$ and is equal, to an approximation, to the "true spectral density" of the process in question.

$\circledast$ stands for convolution. Simplifying yields

$$S(f) = \frac{1}{2} P(f) \circledast \sum_{-m}^{m} (\tau_{|i|+1} - \tau_{|i|-1}) e^{-i\omega\tau_i} \tag{87}$$

This important relation, aside from implicitly evaluating how "good" $S(f)$ is, provides a necessary condition between the τ_k's such that the estimate is nontrivial, namely that

$$\sum_{-m}^{m} (\tau_{|i|+1} - \tau_{|i|-1}) e^{-i\omega\tau_i} \neq 0 \tag{88}$$

In the interest of completeness, it is easily shown below that Eq. (87) is a generalized version of the Blackman-Tukey relation given in Eq. (90). Indeed, letting $\tau_{|i|+1} - \tau_{|i|-1} = 2\Delta\tau$ and letting $\pm m \to \pm \infty$ in Eq. (86)

$$S(f) = \frac{1}{2} \cdot 2\Delta\tau \sum_{-\infty}^{\infty} \int_{-\infty}^{\infty} C_1(\tau)\, \delta(\tau - i\Delta\tau) e^{i\omega\tau}\, d\tau$$

and through the use of the transform pair

$$\Delta\tau \sum_{k=-\infty}^{\infty} \delta(t - k\Delta\tau) \Longleftrightarrow \sum_{k=-\infty}^{\infty} \delta(f - \frac{k}{\Delta\tau}) \tag{89}$$

reduces to

$$S(f) = \sum_{i=-\infty}^{\infty} P(f - \frac{i}{\Delta\tau}) \tag{90}$$

which is a restatement of Eq. (34), if $S(f)$ is replaced by $S_A(f_r)$ and $P(f)$ by $S(f_r)$.

Equation (89) could form a convenient starting point to elaborate on whether or not appropriate t_i's exist, such that alias-

free spectral estimates can be obtained through the generalized estimator of Eq. (85)

It follows from (89) that if and only if

$$\sum_{-m}^{m} (\tau_{|i|+1} - \tau_{|i|-1}) e^{-i\omega\tau_i} = k_1 \, \delta(f) \qquad (91)$$

then only

$$S(f) = k_2 \, P(f) \qquad (92)$$

where k_1 and k_2 are appropriate multiplicative constants. Equation (91) can be rewritten as

$$\sum_{-m}^{m} (\tau_{|i|+1} - \tau_{|i|-1}) \cos \omega\tau_i \stackrel{?}{=} k \, \delta(f) \qquad (93)$$

and it is quite clear that, even if $|m|$ were allowed to increase beyond any bounds, the left-hand side of Eq. (93) could not result to a single delta function.*

This result, disappointing as it may be, is of significance in that it says something about the "generalized" estimator of Eq. (85): that particular estimator as it is defined in this section cannot give unaliased estimates regardless of any elaborations such as prewhitening, statistical analyses, and the like.

8.2 Alternate Cost-Reducing Data Processing Algorithms

All the above algorithms necessitate the construction of a somewhat fancy master clock, which will determine the uneven sampling

---

*A string of ∞ delta functions can result from an infinite summation of cosines. $\sum_{k=-\infty}^{\infty} \delta(t-T_1-kT) = \frac{1}{T} + \frac{2}{T} \sum_{k=1}^{\infty} \cos k \frac{2\pi}{T}(t-T_1)$

times, and the insertion of a "flag" in the data every time the "scheme-cycle" is repeated (unless, of course, one has total faith in the infallibility of the apparatus). An alternative approach is to use even sampling and to use some very elementary statistics and process no more data than are required for a given accuracy; this approach has the advantage that it takes the burden off the lab and into the computer's hands, which are friendlier.

Statisticians[41] have observed that a very conservative limit of statistical error is given by

$$R \equiv 3 \frac{\sum_{1}^{n} |d - \bar{d}|^2}{n} \tag{94}$$

where d, in our case, can be the value of the last additive term in Eq. (77) and $\bar{d}$ is the mean so far, i.e., the (possibly unfinished) estimate for that particular mean lagged product. The main program could thus be modified somewhat to compute R every, say, 10 points after the first 100 additive terms, and compare it with the $|d - \bar{d}|$ at that time; should 10 consecutive such operations indicate that $|d - \bar{d}| < R$, the program would stop doing any more multiplications for that particular C_i.

CHAPTER 9

LOW FREQUENCY SPECTRAL ESTIMATION EXPERIMENTS

The experimental part of this thesis is concerned with obtaining reliable spectral density estimates of semiconductor flicker noise. The present section covers the designs of some of the electronics used and the motivation for their use; included are designs of noise generators, electronic implementation of automatic data collection, environmental parameter's attenuation, and auxiliary equipment design.

Specific statements as to which design was used in what stage of the experiment are made in Chapter 10 where the experimental results are presented; also discussed in Chapter 10 are the observed reasons why the various design improvements were undertaken. The final experimental results are given in Chapter 10.

9.1 General Considerations

Recent developments related to the kinetics of the oxide traps in semiconductors and the associated long time constants involved[1] have revitalized the faith that $1/f$ noise should stop being $1/f$ at some very low frequency, thereby resolving once and for all the paradox of the "infrared catastrophe" discussed in Section 2.

Concurrent developments in the realm of mathematics have pointed out that an often observed lack of the assumed stationarity and the consequent application of the traditional mathematics to an ineligible physical situation might explain the paradox of the "infrared catastrophe".

The motivation for the extensive experimental investigation of low frequency $1/f$ noise reported below is to obtain reliable experimental

evidence of the behavior of flicker noise at frequencies even lower than have been reported so far. Indeed, it is not the intent of the experimental portion of this thesis to attempt to verify any of the many flicker noise models put forth by solid state physicists or mathematicians, although some of the results of this work may help one to select the most promising models.

9.2 Noise-Source Design

The prime motivation behind the selection of the source of noise chosen has been to use a real-life semiconductor operating in a real life situation. Four years ago, when this research started, real life was somewhat different from today insofar as semiconductor technology is concerned. A d.c. amplifier, "Mark II", utilizing discrete components and a carefully matched pair of transistors in a differential input configuration was then designed by H. C. Martel; spectral density estimates (reported in Chapter 10) and measurements of this noise source, such as its temperature sensitivity, dictated the subsequent use of a 2N2060 dual-in-line package of a temperature-matched pair of bipolar transistors in the input stage. A schematic diagram of these noise sources is given in Fig. 20. Power density estimates were obtained down to $10^{-4.2}$ cps with the above improved noise source, referred to as "Mark III" hereafter. As discussed later in Chapter 10, in connection with "Mark III", it became quite apparent at this stage that the accuracy of the results would increase if the various drifts associated with temperature, supply voltage, and semiconductor "aging" were reduced through shorter data-taking periods. Time-multiplexing ten statistically independent noise sources (for a tenth of the data-

Fig. 20.

Schematics for Mark II and III

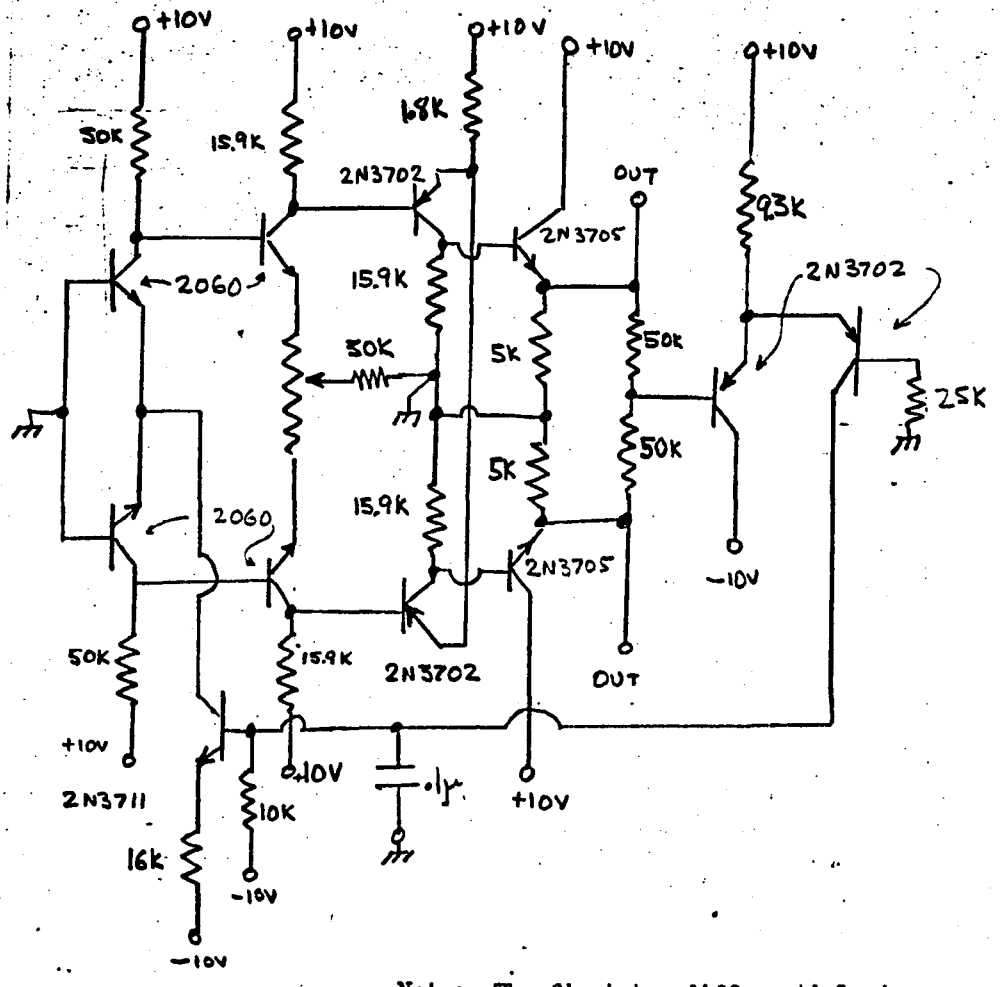

Note: The first tow differential stages utilized high gain 2N3711 transistors for the Mk II circuit.

taking time needed if only one noise source were used) would provide results of, theoretically, the same accuracy as has been shown earlier. In practice, the accuracy could be even better since the various drifts would have only a tenth of the time to display themselves.

Recent advances in integrated circuits have taken the operational amplifier out of the laboratory and into an extremely wide range of applications. Further advances in monolithic integrated circuits and hybrid thick film devices, plus startling decreases in prices, have made operational amplifiers an obvious choice in areas where they were not even considered earlier. It was, therefore, appropriate that integrated-circuit operational amplifiers be used as the ten noise sources for the best controlled spectral density estimates to be reported in this work.

It is significant that the attempt to measure the noise characteristics of one transistor alone is not entirely defeated by utilizing a grounded input differential amplifier. Indeed, if the reasonable assumption is made that each of these two paired transistors is a statistically independent sample from an ensemble, then the measured spectrum is the same as that for a single transistor except for a multiplicative constant.

In the interest of keeping up with the present state of semiconductor technology, and of avoiding repetition, a brief circuit analysis will be given for the noise source utilizing integrated circuit operational amplifiers only; many of the arguments carry through to the discrete-component noise sources with minor modifications; for specific details pertinent only to the discrete component noise source, Blakemore[25] has an adequate analysis.

Many considerations enter into the design of a noise source, not the least of which is that the final design represent a typical one rather than a laboratory attraction.

The fundamental non-inverting circuit shown in Fig. 21 is used exclusively.

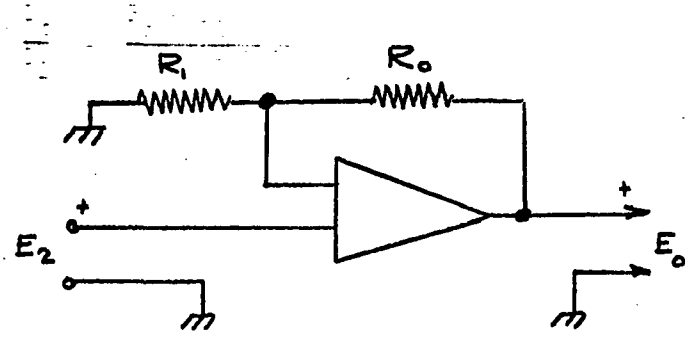

Fig. 21

Because of very high gain (approximately 100 db) required to make microvolt noise voltages large enough to be reliably read by standard laboratory equipment, drifts as well as voltage and current effects are most important in noise-source design. Input voltage offset (due to unequal base-emitter voltages in the input transistor pair despite manufacturing attempts to minimize it) is there; so is current offset, which is caused by current leaking into the input terminals of the amplifier; both vary with supply voltage, and with temperature, thereby causing voltage drift. D.C. balancing techniques are thus needed to overcome input offsets; high quality regulation of the ambient temperature and the supply voltages is also essential to minimize drift and will be discussed in Sections 9.3 and 9.4 below. Offset voltage adjusting is achieved by

simply providing the small constant d.c. bias voltage needed at the differential input. A straightforward implementation of this idea is shown in Fig. 22. The complete schematic of the noise source is shown in Fig. 23.

The gain is easily obtained to be

$$\frac{E_o}{E_1} = \frac{R_o + R_1 + R_3}{R_1 + R_3} \tag{96}$$

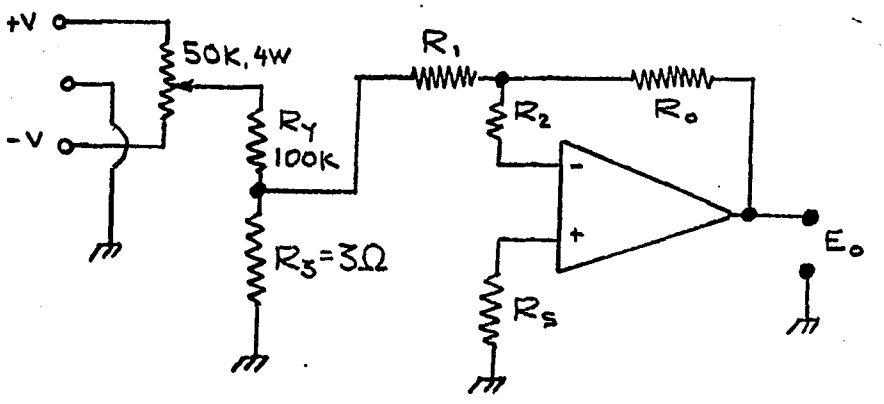

Fig. 22

and the total offset voltage-adjustment range from the cascaded voltage divider is $\pm V \frac{R_3}{R_y}$ (referred to the input).

The effect of having assumed infinite bandwidth and zero output impedance are of very little consequence for the specific purposes of this experimental work; in fact, a low controllable bandwidth is highly desirable if aliasing is to be minimized; h.f. spurious oscillations are also

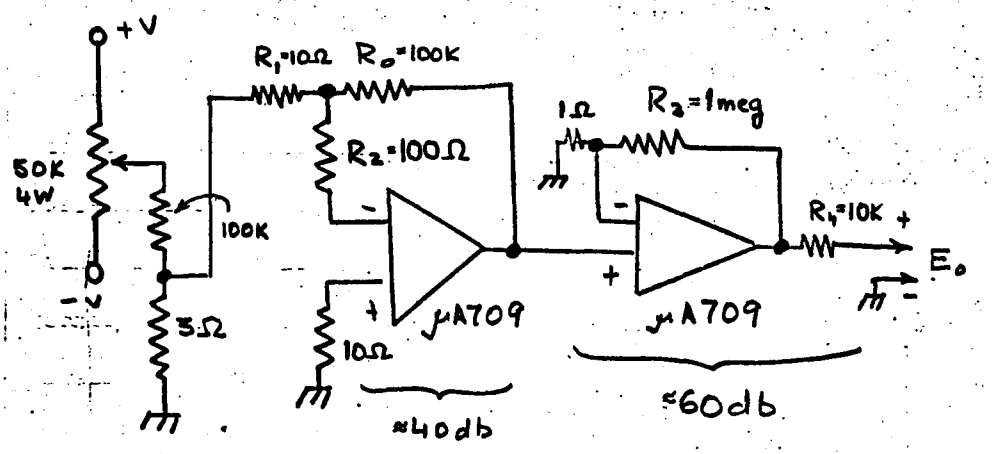

Frequency Compensation Not Shown.
See Fairchild Corp. Data Sheet.

Fig. 23

Schematic Diagram of one noise source made of I.C.'s only.

eliminated by drastically reducing the closed loop bandwidth of the amplifiers.

Through force of habit from the discrete component days, one could argue that the noise observed at the output of the noise source of Fig. 23 is basically that of the first two transistors in the differential input circuit, since any other noise would have to be beta times larger amplitude in order to be equally significant. Although a complete schematic of the particular operational amplifier used is available[43] with each "transistor" clearly marked, it is this author's opinion that such a discrete component analysis is of little interest for two reasons:*

a) The integrated circuit op-amp is an entity in itself; it is an electronic component which can survive no more surgical dissection than a single transistor or tube.

b) Although the first "stage" of amplification is mostly responsible for the observed noise, a more realistic and accurate view is to consider the entire op-amp as a "noise source".

One is thus referring to the noise properties of the amplifier.

9.3 Design of the Power Supply

In an attempt to prevent power-line voltage fluctuations from affecting the data, batteries were originally used to supply the Mark II

*The integrated circuit manufacturer could, of course, modify the design of the circuit and this would be of considerable interest, then.

noise source. Both dry and rechargeable nickel-cadmium batteries were tried; unfortunately, the batteries' voltage drift caused by gradual discharge and by room temperature fluctuations was excessive. A highly regulated power supply was thus constructed in the conventional pattern shown in Fig.24 below. Two cascaded stages of a series pass transistor driven by a differential voltage-sensing transistor-pair formed the heart of this supply which was used to power the Mark III noise source.

In the absence of any linear trends or oscillations in the raw data suggestive of regulator inadequacies, experimental measurements of the degree of regulation actually required were taken only later in connection with a new power supply for the ten integrated-circuit noise sources.

In keeping up with the technological improvements in integrated circuits, the supply which powered the ten integrated-circuit noise sources utilized integrated circuits itself. The μA723 monolithic voltage regulator made by Fairchild was selected; it consists of a temperature compensated zener, an error amplifier, a low-level series-pass transistor and some current limiting circuitry, all very much in the pattern of earlier discrete component designs; external series-pass power transistor was used to handle the current needed by all ten noise sources. The complete schematic shown in Fig. 25 has been measured to have a .05% voltage regulation; that is, for an input voltage fluctuation of 3V the output voltage fluctuation should not exceed 1.5 mV at any load. The need for a measure of the actually desired degree of regulation is now obvious. Is the above .05% truly representative of the behavior of the circuit? If so, is this regulation enough? How important

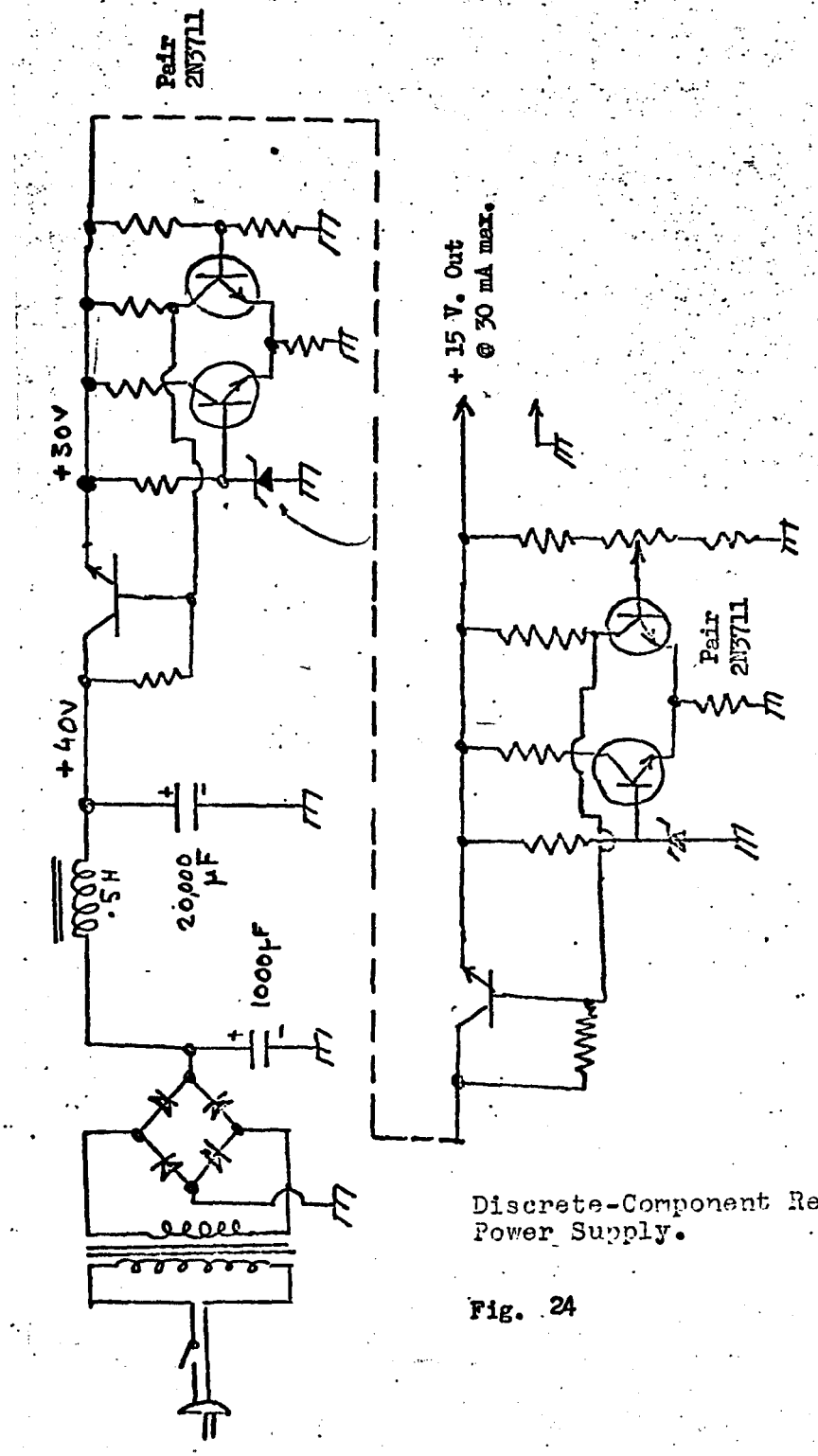

Discrete-Component Regulated Power Supply.

Fig. 24

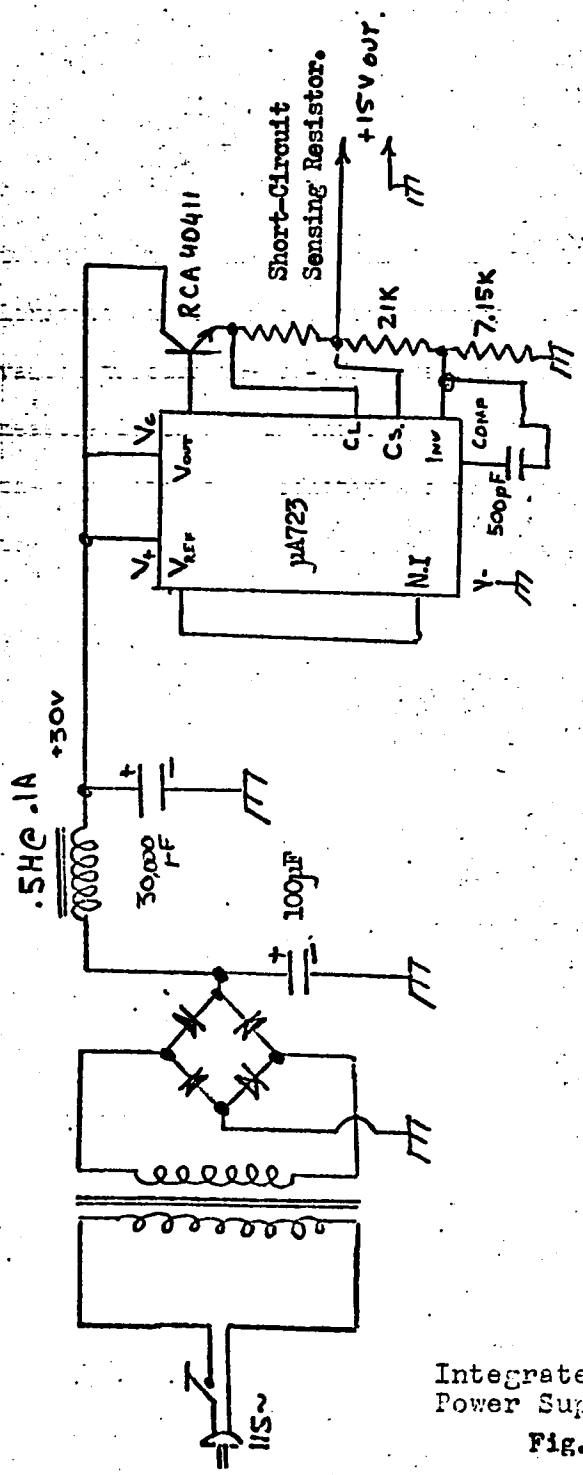

Integrated-Circuit
Power Supply

Fig. 25

is the fluctuation of the power supply's ambient temperature? These questions are all answered experimentally below.

The question of the true (measured) voltage-regulation characteristics of the voltage regulator is the simplest to answer. Assuming a linearity in the regulation characteristics, the input voltage was varied through the use of a variac, just enough to produce a reliably measurable change in the output; it was found necessary to reduce through the regulator the "constant" output voltage to less than 10 volts so as to gain an extra decimal figure of resolution in the digital voltmeter. The regulation was found to be well within the advertised limits mentioned earlier.

Direct measurement of the required voltage regulation by time-multiplexed recording of both the regulated voltage and of the noise sources is next to impossible with a four-digit digital volt meter; a fluctuation of $\pm \frac{1}{2}$ mV on a 15V d.c. voltage would simply not be detected.

A free-running multivibrator, followed by a cascade of frequency dividers was therefore constructed as shown in Fig. 26a, and was used to induce square wave voltage excursions of 40 mV p.p. amplitude and approximately 10 minute period on the nominally regulated B^+ line to the noise sources, as shown in Fig. 26b.

The time-multiplexed response of nine voltage sources and the offending stimulus were digitally recorded and are shown in Fig. 27 and 28. A 40 mV p.p. variation on the + side only of the power supply produces obvious output response of varying degrees, but of the order of 1V p.p. This amounts to an error-amplification of approximately 25. The

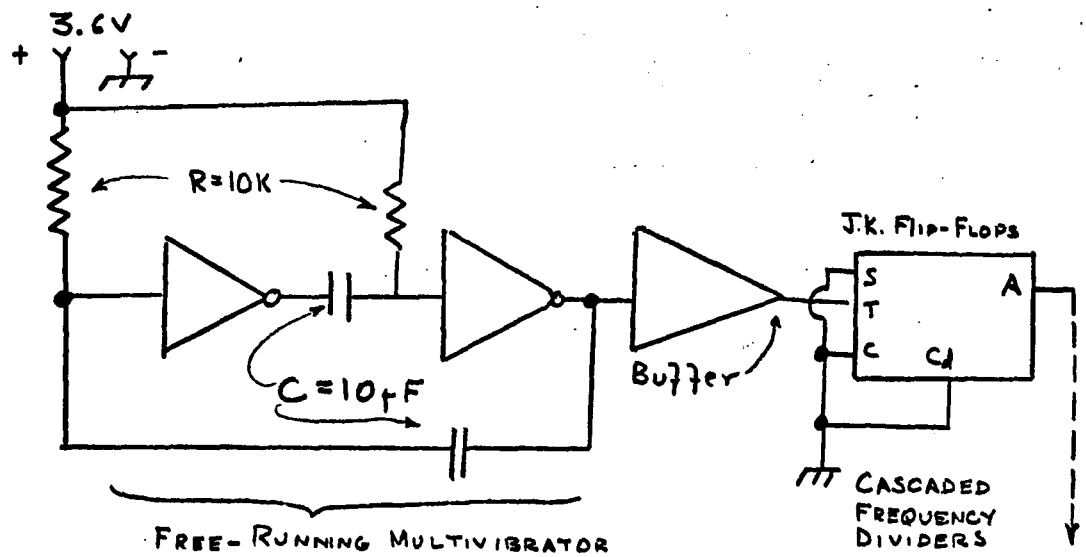

Fig. 26a

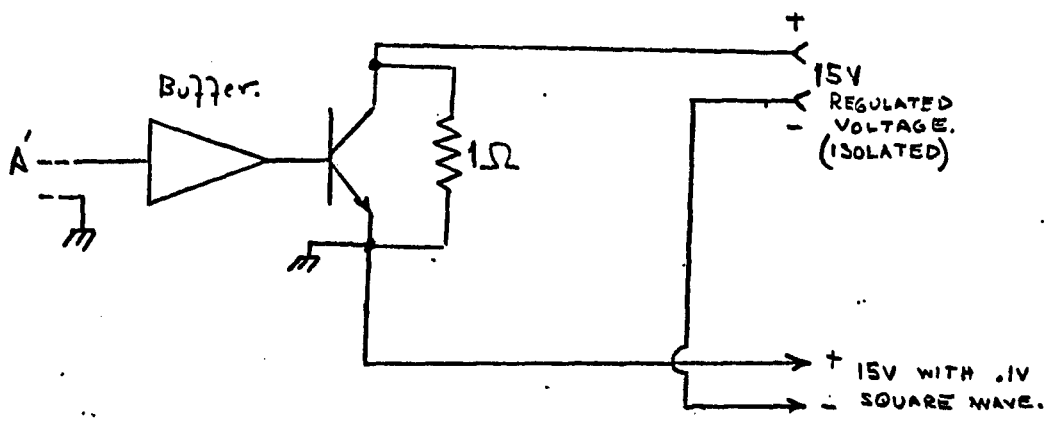

Fig. 26b

Very Low Frequency Square-Wave Generator Used to Test Noise Sources' Voltage Sensitivity.

Noise Source Sensitivity to Power Supply Fluctuations.

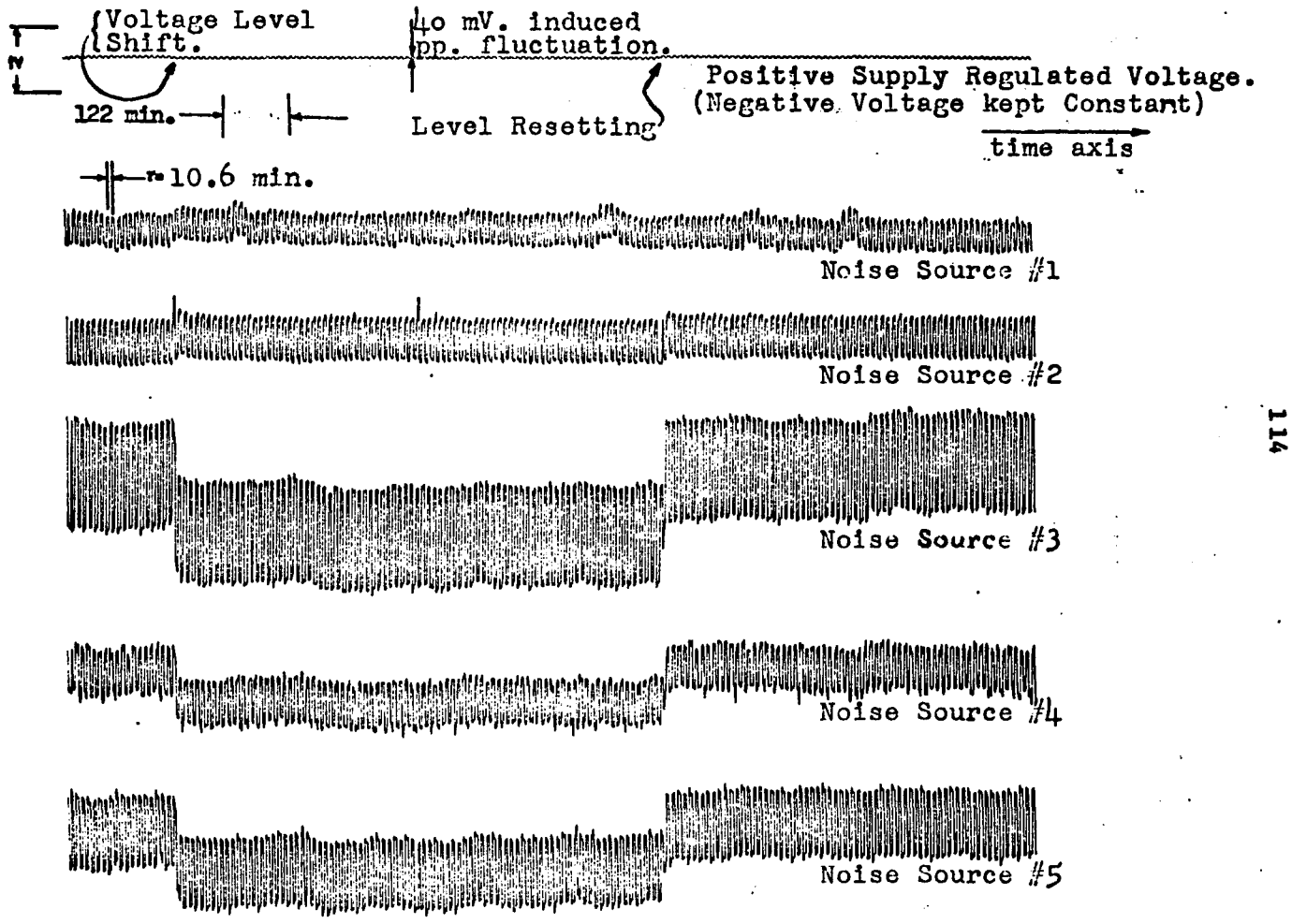

Figure 27

Sensitivities of Individual Noise Sources to Power Supply Fluctuations

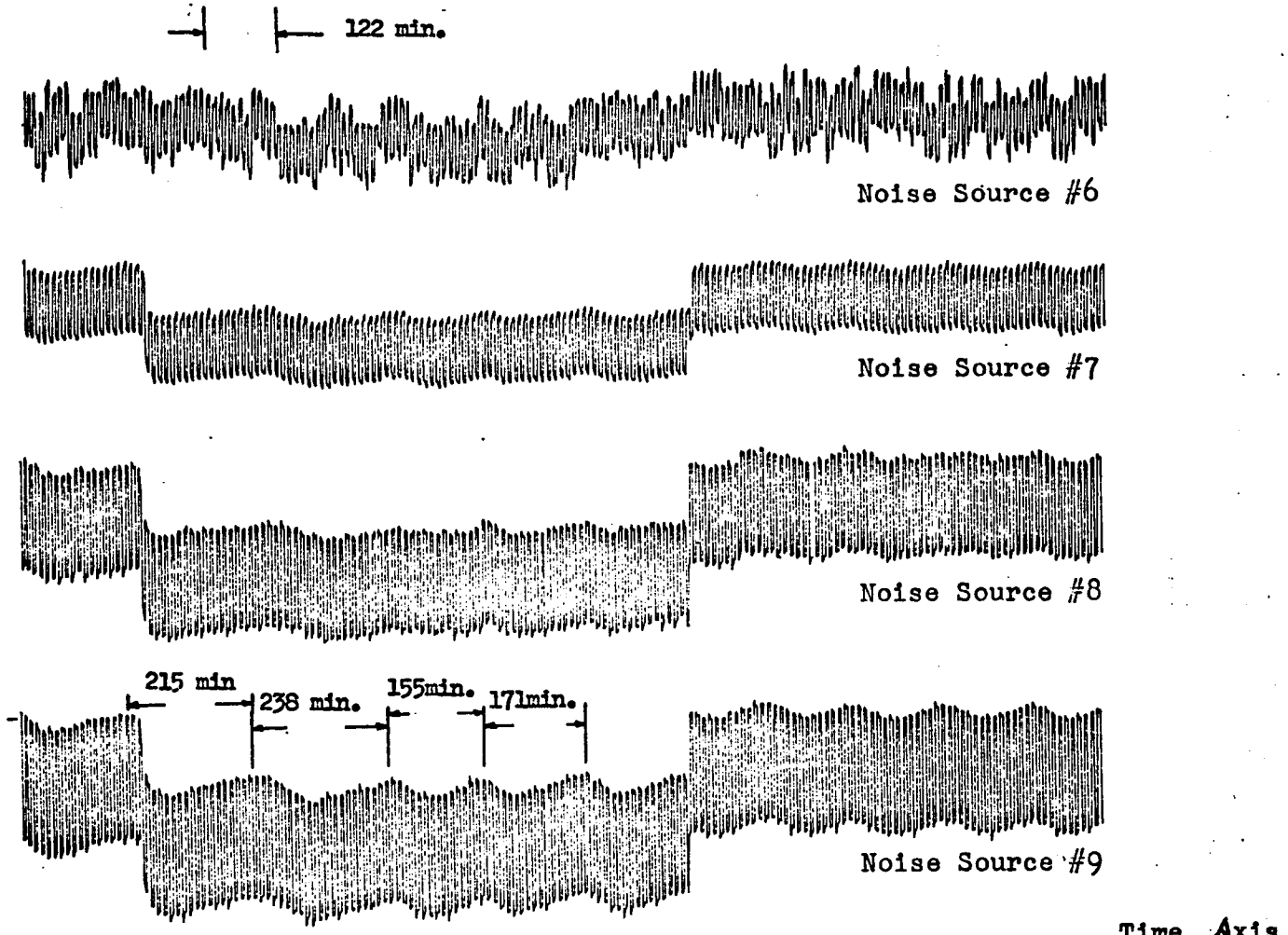

Figure 28

unregulated input voltage to the regulator, however, was measured and found not to exceed 1V p.p. over a period of 30 days; this amounts to

$$\left[\frac{\text{1V = unregulated voltage change}}{\text{2 = factor inserted because the negative voltage will also change in the algebraically opposite direction}}\right] \cdot \left[\frac{1.5\text{ mV}}{3\text{V}}\right] = \mu\text{A723 attenuation} = .25\text{ mV}$$

which, when amplified by the above-measured "error amplification" of 25, gives 6.25 mV maximum attributable to input voltage fluctuations.

However, the typical raw data output excursions are about 1V p.p. hence

$$\left[\frac{\text{power-supply caused maximum voltage excursions}}{\text{observed raw noise output voltage excursions}}\right] = .6\% \ .$$

This is <u>not</u> obviously negligible. Noise source #7 does not seem to be excessively sensitive to supply-voltage fluctuations in Fig. 28. Figure 37, however, appears to suggest that noise source #7 is quite sensitive to voltage fluctuations; this is not so, though, because noise source #7 is, in fact, responding to temperature fluctuations and not to voltage fluctuations; indeed, the voltage fluctuations observed in Figure 37 are themselves caused by the primary disturbance which is the temperature-regulating current applied to the thermostatically-controlled heater; this current-drain affects the line voltage which, in turn appears as a "power-supply-disturbance".

Noise source #7 was replaced for all subsequent runs as discussed in more detail later in this section.

It may be noticed from Figs. 27 and 28 that there is a sudden transition in the noise sources' outputs after about 2½ hours of data taking, and a subsequent return to the original state. These low changes of state were produced by deliberately altering the ambient temperature of the voltage regulators, so as to measure their exact susceptibility to such environmental changes.

By removing the forced-air cooling from the power supply, the surface temperature of the case of the μA723's was raised by 60°F, as measured by a contact thermocouple*. The effect on noise output as seen in Figs. 27 and 28 is, on the average, less than one volt; assuming a linear dependence over small temperature changes this amounts to 17 mV/°F, and since the typical raw noise output voltage amplitudes are about 1V, and the typical room temperature variations are about 2°F,

$$\frac{\text{Effect of room temperature on noise through power supply}}{\text{Observed raw noise output voltage excursions}} = 3.4\% \text{ max.}$$

The comments made earlier in this section in connection with the effect of the power supply variations on the final spectral estimate apply here, too. In this case of temperature fluctuations, however, experiments have revealed the presence of a single, rather well-defined, prominent frequency of approximately 1 cycle per 20 minutes. This rather unusual

*Precision calibrated thermocouple was borrowed through the courtesy of the Optical Radiation Corporation, 2626 S. Peck Road, Monrovia, Calif.

frequency was carefully traced and was found to be the frequency of the thermostatic system controlling the temperature of the liquid bath in which the noise sources were immersed . [The line voltage was also affected due to the non zero impedance of the 110V line; this indirect effect, however, is negligible because of the higher attenuation of the system to voltage variations (.6%) than to temperature fluctuations (3.4%)].

Since noise source #7 in Fig. 37 appeared to be affected quite significantly, it was replaced. No significent residual response was observed at this frequency in any of the final data-runs. In any case, a small component at this frequency would not affect the general trend of the spectral response in the range 1 cps to $10^{-6.3}$ cps, but would at most appear as a small peak near 10^{-3} cps.

A final word on the somewhat periodic excursions of noise source #9 in Fig. 28. As will be shown later in this chapter, noise source #9 is particularly sensitive to temperature fluctuations. The very low frequency sinusoidal fluctuations shown in Fig. 28 are believed to be caused by the slow time constant of the thermostat of the refrigerator itself, to be discussed shortly.

9.4 Temperature Regulation

Whereas a Dewar flask was chosen for the Mark II and Mark III noise sources based on intuitive notions of "thermal insulation", this sort of a passive attenuator was found unsuitable for the subsequent more careful work. Indeed, the thermal characteristic of an average size Dewar flask are such that a measured 1 watt of heat dissipated inside it can almost linearly raise the inside temperature to 160°F within three days and still keep raising it. Such an ambient temperature is hardly among the natural and average situations where a circuit is usually utilized.

The approach ultimately resorted to in this research was to combine active temperature control, to be discussed in detail in Section 9.4.2, with a more sophisticated passive attenuation scheme, to be discussed below.

9.4.1 Passive Attenuation

From an intuitive point of view, the properties desired from the attenuator's material are:

a) low heat conductivity, but not so low that the inside temperature builds up too high;

b) high specific heat capacity so that transients will be attenuated through dissipation.

The heat equation

$$\frac{\partial T}{\partial t} \cdot \frac{1}{k} = \nabla^2 T \tag{97}$$

where

$$\frac{1}{k} = \frac{\rho(\vec{r})\, C(\vec{r})}{k_o(\vec{r})} \tag{98}$$

ρ is the density

C is the specific heat capacity

k is the thermal diffusivity

k_o is the thermal conductivity

and $\vec{r}$ is the polar position vector

was thus resorted to.

In awareness of the notoriously slow convergence of the resulting infinite series for the heat equation, the geometry was severely simplified to the one-dimensional case illustrated in Fig. 29 below.

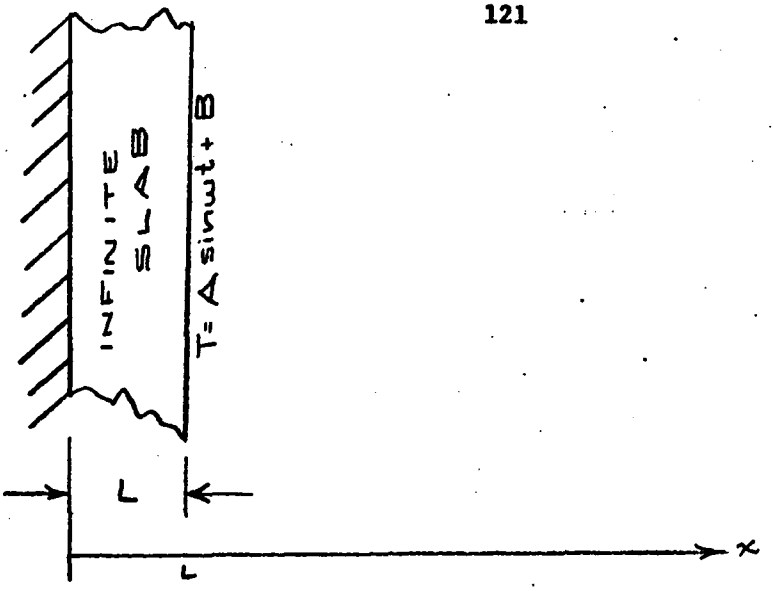

Fig. 29

Equation (104) then becomes

$$\frac{\partial T}{\partial t} = k \frac{\partial^2 T}{\partial x^2} \quad , \qquad T_o \equiv T(x,0)$$

$$\left.\frac{\partial T}{\partial x}\right|_{x=0} = 0 \tag{99}$$

$$T(L,t) = A \sin \omega t + B$$

The specific algebraic expressions are far too lengthy to make it worthwhile to repeat them here. There are some quantities of significant interest, though, which have been derived from the above. Assuming that the slab side next to the fluid is subjected to oscillations, it is interesting to know how the slab attenuates these oscillations as a function of frequency (by the time these oscillations have reached the other end of the slab.)

The steady state ratio of the amplitudes is, after a very considerable amount of algebra, found to be

$$R \simeq \sqrt{\frac{\omega^2 k^2 \pi^2}{L^4\left[\omega^2 + \frac{\pi^4 k^2}{16L^4}\right]^2} + 1 + \frac{-\omega^4}{\left[\omega^2 + \frac{\pi^4 k^2}{16L^4}\right]^2} - \frac{4\omega^2}{\pi\left[\omega^2 + \frac{\pi^4 k^2}{16L^4}\right]}} \qquad (100)$$

to a first approximation (neglecting higher order terms in the infinite series). As a quick check, one may notice that

a) $\lim_{L \to 0} R = 1$

b) $\lim_{\omega \to \infty} R = 0$

c) $\lim_{\omega \to 0} R = 1$

which agree with intuitive expectations.

Thermal properties of materials were then considered in an attempt to find a material of convenient cost, weight, mechanical properties, and noncorrosive, with precisely known thermal properties so that the exact effect of temperatures and heat flows could be found from the derivations of this section; the material would have to have high heat capacity and average conductivity. One-inch thick aluminum met all criteria except cost and weight. A special epoxy-like substance made locally to specifications, courtesy of the Magnetika, Inc. of Santa Monica, California, solved the problem.

To verify the existence of the advertised properties of the material, a 9-inch cube was constructed and placed in a controlled-temperature

bath; calibrated thermistors connected to the amplifiers shown in Fig. 30 constructed for that purpose were installed to measure the temperature of the outside and of the inside walls of the box; time-multiplexed digital recordings were then made of deliberately created temperature changes on the bath's temperature; plots of the "inside" and "outside" temperatures were then made. Finally, the digital computer was asked to simulate the characteristics of the above temperature-fluctuation attenuating box and to come up with a plot of what the inside temperature would have been if the parameters claimed and the associated mathematics summarized earlier in this section were correct.* For completeness, to eliminate the unlikely

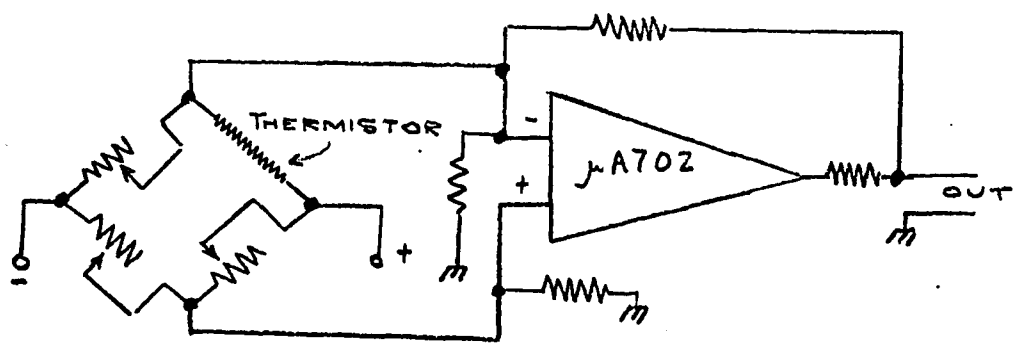

(Note: The high common-mode and supply rejection of this circuit give a null independent of supply voltage; null drift is negligibly small. The design is by Fairchild Applications Dept.)

Temperature Amplifier

Fig. 30

*A measure of the frequency response of the attenuating box was given by Eq. (100).

possibility of temperature spikes having been introduced extraneously or accidentally, all steps involved in, for example, the introduction of a cold bath-spike, were carried out except the actual pouring of cold liquid, and the response was observed. Figure 31 displays these results; the likeness between the computer simulated result and the actually obtained result is, indeed, striking. Appendix A has all the relevant mathematical details and discussion of the computer simulation.

A significant quantity, in the interest of assuring that the circuits be operating under normal conditions, is the steady-state temperature rise inside the passive attenuator.

In the steady state case where the outside temperature is held constant through active control, to be described later in Section 9.4.2, the applicable equation is a simplified version of the generalized heat condition equation

$$\rho(\vec{r})C_p(\vec{r})\,\frac{\partial T}{\partial t}(\vec{r},t) = Q(\vec{r},t) + \operatorname{div}[k(\vec{r},t)\,\nabla\vec{T}(\vec{r},t)] \qquad (101)$$

where

k = thermal conductivity in $\left[\frac{\text{calories}}{\text{sec-cm-degrees}}\right]$ *

$\frac{\partial T}{\partial t}$ = 0 for steady state

Q = internal energy source in $\left[\frac{\text{calories}}{\text{cm}^3\text{-sec}}\right]$

ρ = density in grams/cm^3

C_p = specific heat capacity

Equation (101) thus reduces to

$$Q(\vec{r}) + k\nabla^2 T(\vec{r}) = 0 \qquad (102)$$

---

*The C.G.S. system of units is invoked here.

Effects of Environmental Parameters on Temperature.

(Measured and Mathematically Estimated)

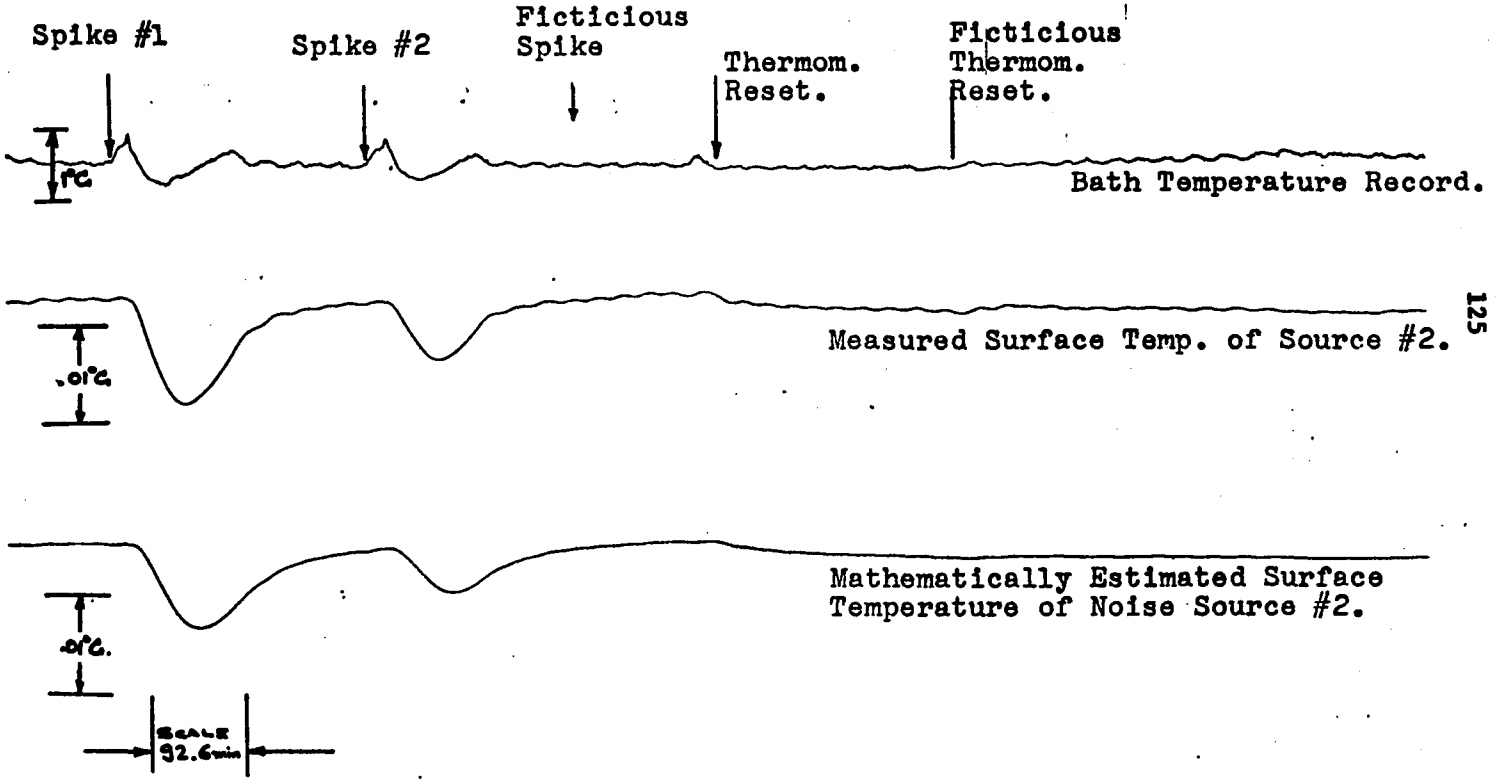

Figure 31

But

$$q = -k\nabla T(\vec{r}) \tag{103}$$

where k = thermal conductivity, assuming that heat flows from hot to cold, $k > 0$.

Solving for q in spherical coordinates yields an expression very similar to the electrostatic equivalent, namely

$$q = \frac{4\pi k r_o r_i}{r_o - r_i} (T_i - T_o) \tag{104}$$

where r_o = outside radius

r_i = inside radius

T_i = outside temperature

T_o = inside temperature

For the epoxy material chosen, $C_p = 0.38$ calories/^oC gram

$= 721.86 \frac{\text{watt} \cdot \text{sec}}{\text{lb} \cdot {}^oC}$

$= 0.00468$ watts/in.$\cdot {}^oC$

$= 0.825$ lbs/in^3

Therefore $k = 7.85 \times 10^{-5}$ is the thermal diffusivity. A $\frac{1}{4}$ - inch thick material was selected. For these values, approximating the 13" cube by a 13" diameter sphere, substituting values in Eq. (104), and solving for T , one obtains

$$\Delta T \cong 5^oC$$

for an assumed power consumption of 3W inside the box, a number very close to the measured power consumption of 2.86 watts of all ten noise sources.

9.4.2 Active Temperature Control, and Overall Setup

A stage of active temperature control in cascade with a stage of passive control is essentially one more buffer stage insulating the temperature-sensitive machine from the outside world's random temperature fluctuations, especially the very low frequency ones.

It has been maintained in the past[25] that active temperature control is difficult to accomplish and maintain over long periods of time; this indeed may be the case if analog devices such as thermistors are called upon to do the sensing. A mercury thermometer whose mercury column makes or breaks an electrical contact, however, presumably does not suffer from the aging that some analog devices, such as thermistors, are prone to. A commercially available device such as this, made by the Chemical Rubber Company, was purchased and used in this endeavor. Its advertised accuracy is $\pm.01^{\circ}C$. To maintain this accuracy throughout the temperature-controlled liquid, one cannot tolerate any temperature gradients in the liquid; furthermore, there should be no time delay between the thermometer's command to "warm up" tnd the uniform application of heat; since none of these conditions can be fully realized, an accuracy of $2 \times \pm.01^{\circ}C$ is a more realistic* measure for temperature fluctuations.

Many considerations enter into the design of a very accurate,

*The precision thermometer used has an advertised precision of better than $\pm.01^{\circ}C$; such a claim seems quite reasonable in view of the length of the mercury column, and no attempt was made to verify it using a higher precision instrument. In fact, this mercury thermometer was used to calibrate a thermistor circuit (discussed in Section 6.1.3); the thermistor was then used to measure the temperature variations of the circulating ethylene glycol. The accuracy figure of $2 \times (\pm.01^{\circ}C)$ is the direct result of these thermistor measurements.

practical - yet not prohibitively expensive - regulator of the temperature of the liquid surrounding a box:

a) The liquid must be highly nonvolatile to avoid constant adding; it must be noncorrosive, reasonably nonconductive, and of low viscosity to facilitate agitation to prevent temperature gradients. It must also not react with the common polyethylene plastic sheets used in "waterproofing". Pure ethylene glycol (anti-freeze) met all the above requirements and was thus selected.

b) The amount of liquid must be minimal so as to minimize time delays for a given amount of stirring, and to raise the frequency of the heating-cooling cycles so that the effect will be highly attenuated by the passive attenuator box surrounded by the liquid. At the same time, need for stirring calls for some extra liquid-filled space large enough for a propeller. This problem was solved by substituting a 20 gallon/min pump which created more than enough stirring, while requiring very little extra liquid.

c) Heating and cooling must be as evenly and uniformly distributed as possible. Furthermore, to keep the heating-cooling frequency high, a large amount of energy should be quickly going in and out of the liquid. While ohmic heating can easily handle the heating part, no efficient cooling analog seems to be available.*

---

*A small reverse-biased semiconductor cooler was tried; despite its power consumption of approximately 30W, its cooling ability was not sufficient for this experiment. Considering the cost and high D.C. power requirements of an adequately larger unit, a compressor-type refrigerator was judged to be more appropriate for the purposes of this experiment.

Figure 32 shows the physical setup used. The only reason the pump P is moved outside the refrigerator is that a strong 60 cps magnetic coupling was noticed when the pump was physically near the noise sources.*

The heater coil circuitry was somewhat of a problem; if a high current were to be switched on and off, it would be nice to use an SCR to avoid relay arcing; but then it would be imperative to use a.c. to commutate the SCR in a simple way; high current a.c., however, is most likely to be picked up by the noise sources! A happy compromise is shown in Fig. 33.

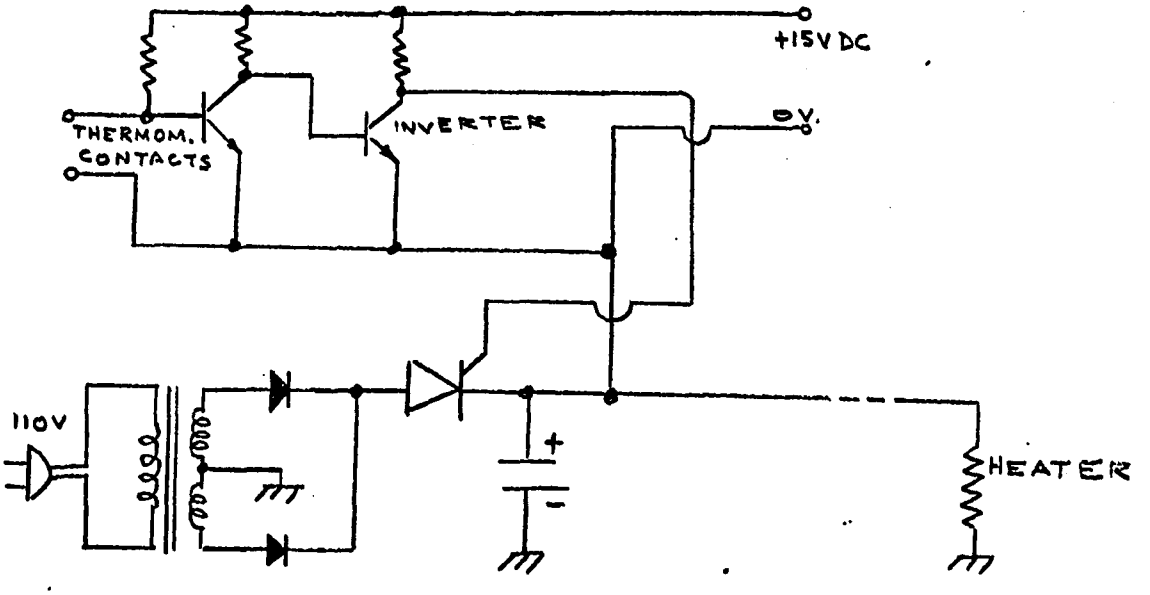

Heating System Regulation

Fig. 33

*The magnetic nature of the 60 cps coupling was first suspected because the relative orientation of the pump with respect to the noise sources was very pronounced.

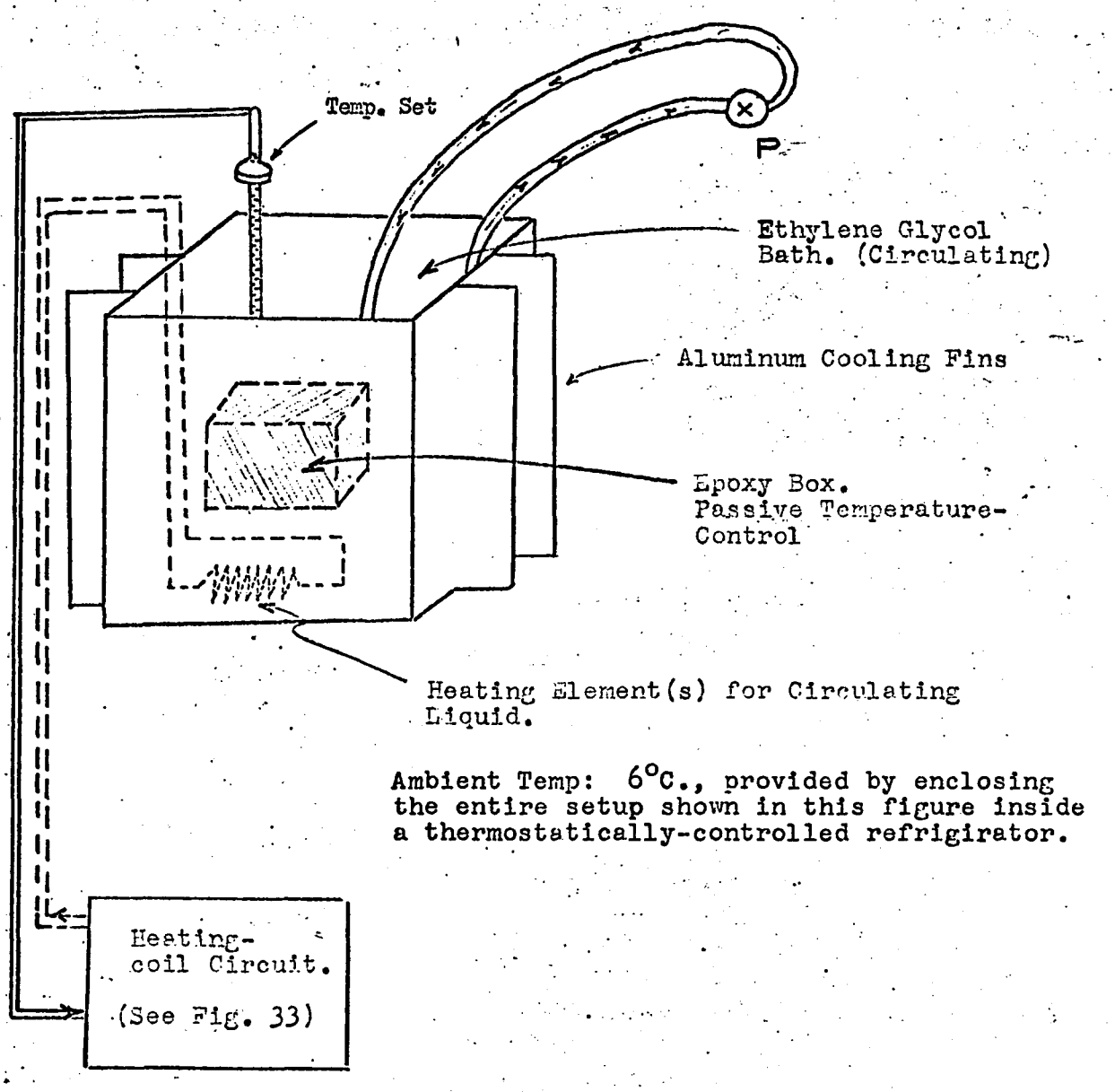

Block Diagram of Temperature-Control.

Fig. 32

Figure 34 shows a plot of the temperature of the bath, as monitored by a thermistor and plotted by a chart recorder. Indeed, the combination of time constants, heat capacities and slight temperature gradients involved is such that no square-wave output exists; yet it does not follow that this noisy output contains high frequencies alone.

Figure 35 shows the relation between the surface temperature change of a noise source (as measured by a calibrated thermistor in thermal contact with the first op-amp) and the raw noise itself. For that rather typical noise source, .01°C ambient change results in a noise source amplitude shift by no more than four times that source's standard deviation. As Fig. 36 shows, it took a .8°C peak to peak temperature hike in the surrounding bath to produce the aforementioned typical shift in the output of any noise source; were it not for the refrigerator-caused low frequency sinusoidal temperature variation first observed in Fig. 37 below, it would seem that the temperature control is indeed quite satisfactory.

9.4.3 Bias Due to Temperature Regulation

If the period of the heating-cooling cycle is prolonged by reducing the heating and cooling powers, the cycle will propagate through the passive temperature-stabilizer with less attenuation. Figure 37 is a set of concurrent raw-data plots of seven noise sources, of the noise source supply before the regulator and, at the bottom, of the bath temperature. The earlier "noisy look" of the bath temperature has been replaced by a fairly orderly on-off sequence of cycles with the usual

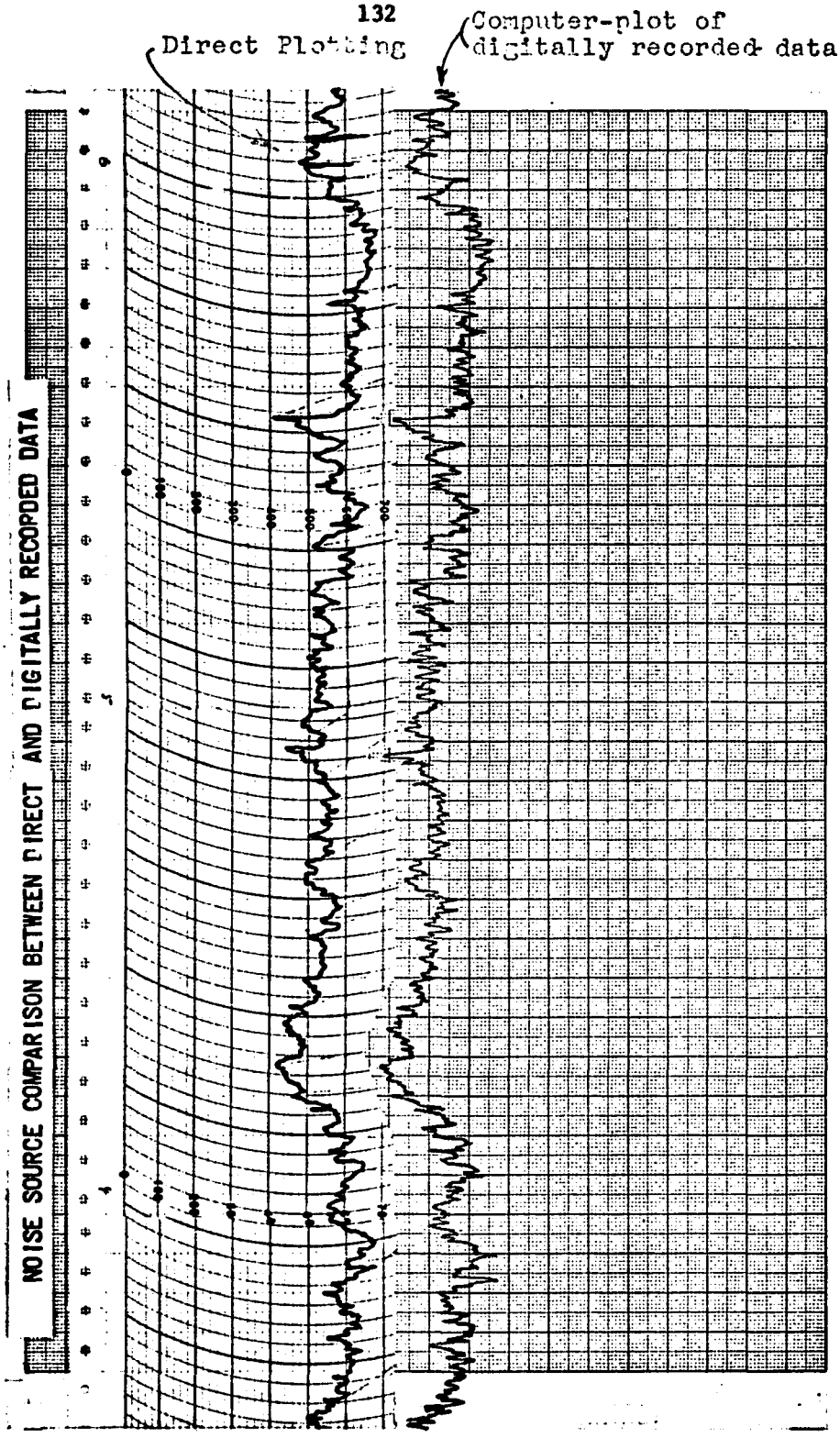
Direct Plotting
Computer-plot of digitally recorded data.
NOISE SOURCE COMPARISON BETWEEN DIRECT AND DIGITALLY RECORDED DATA

Figure 34

Temperature Effect on Raw Noise Output of Noise Source #2.

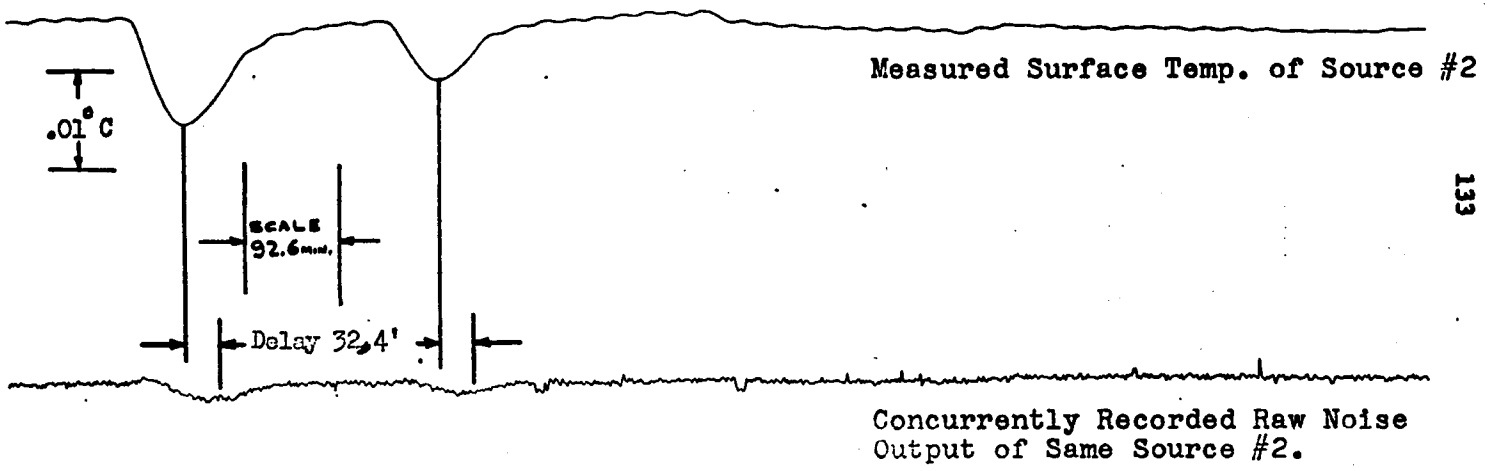

Figure 35

Response of Noise Sources' Output to Temperature Changes

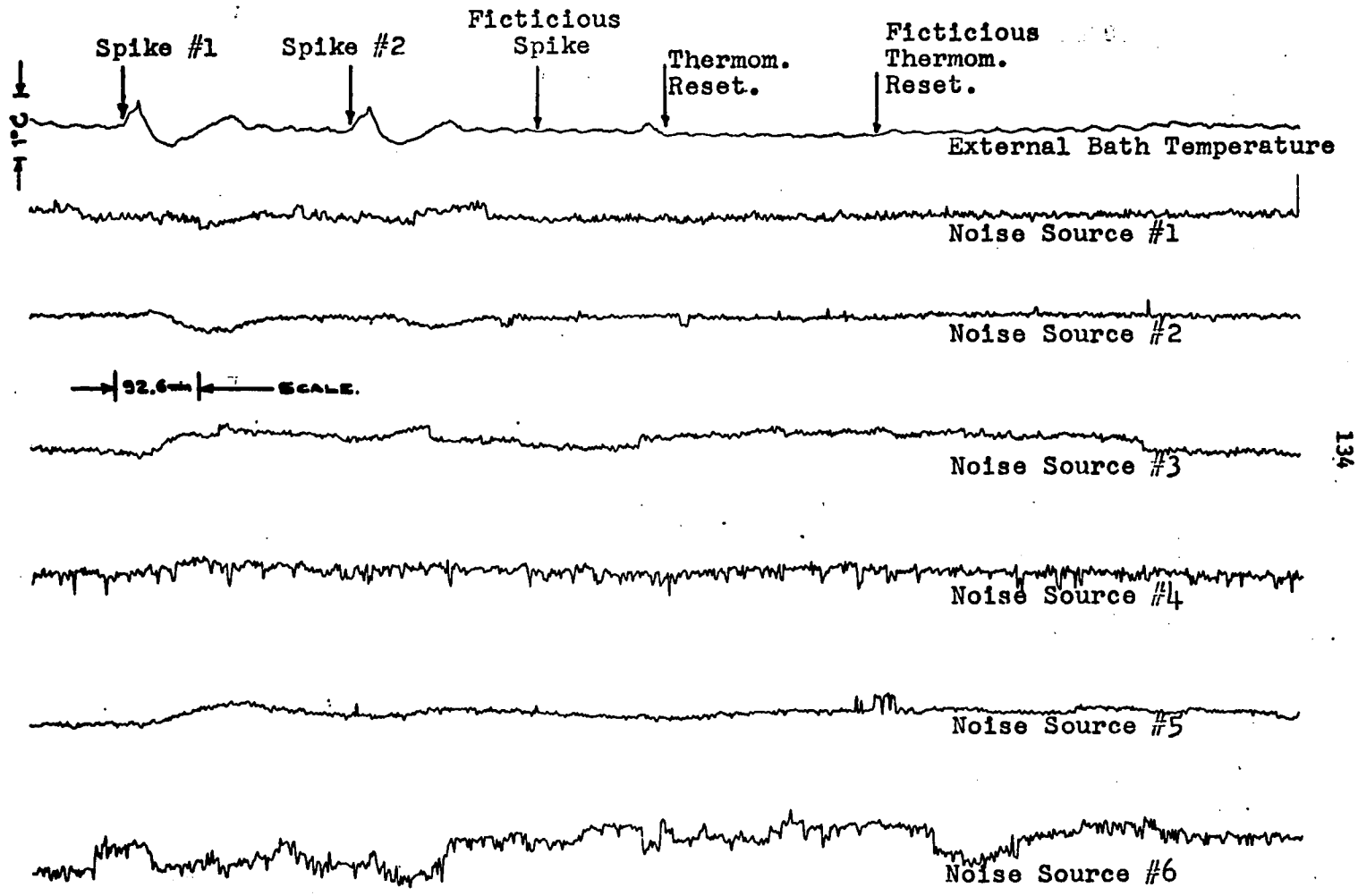

Figure 36

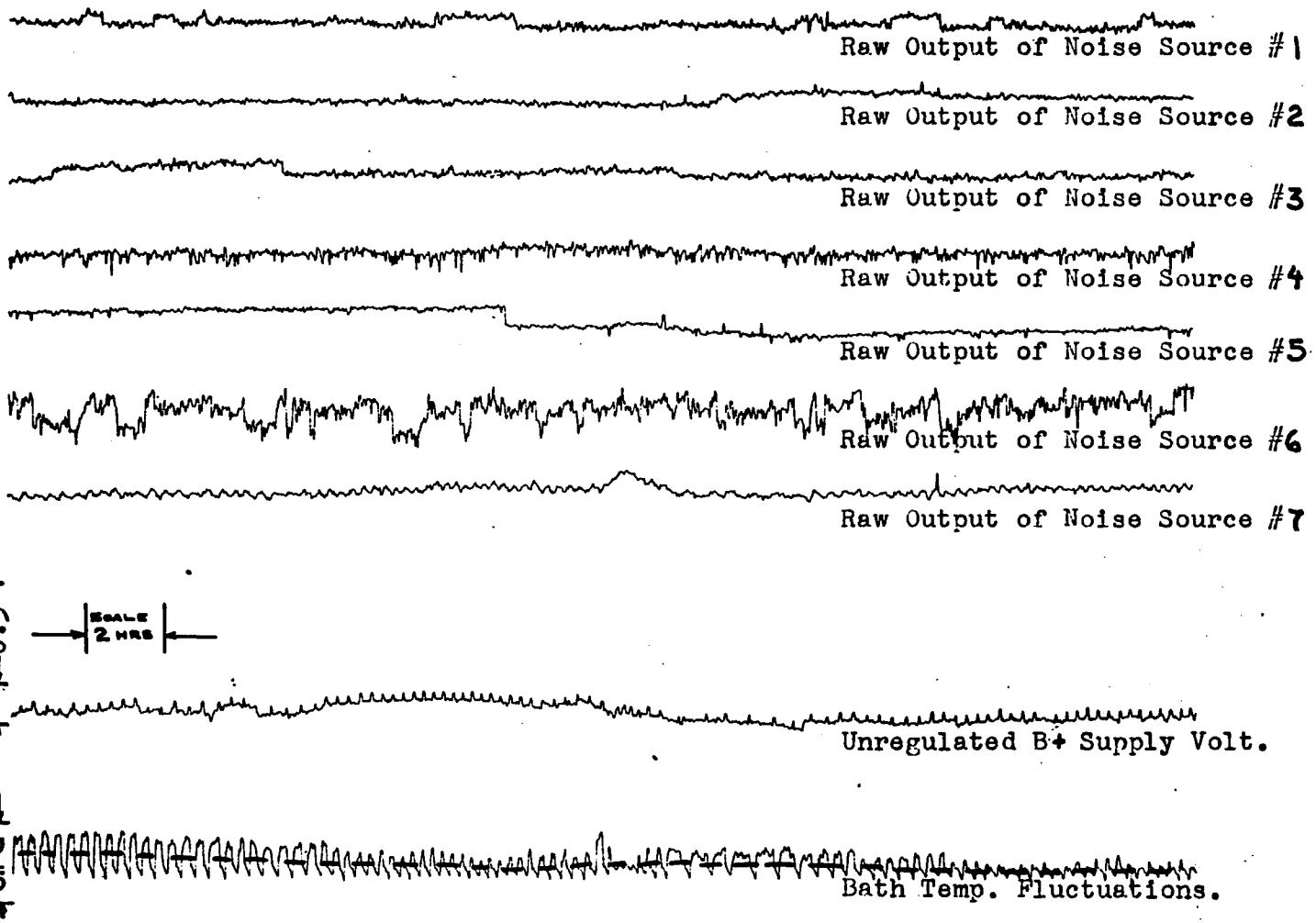
Raw Output of Noise Source #1
Raw Output of Noise Source #2
Raw Output of Noise Source #3
Raw Output of Noise Source #4
Raw Output of Noise Source #5
Raw Output of Noise Source #6
Raw Output of Noise Source #7
0.5 V
SCALE 2 HRS
Unregulated B+ Supply Volt.
0.1°C
Bath Temp. Fluctuations.

Figure 37

superimposed low frequency caused by the refrigerator's own thermostatic control.

This Fig. 37 shows quite predictably that each source has its own degree of sensitivity to temperature; one might, in fact, use this information in evaluating spectral estimates of individual noise sources.

The power spectrum of a source which is heavily affected by extraneous temperature and power-supply variations may or may not be $k/|f|$ in nature any more. In that case it is only logical to suspect that prewhitening and subsequent postgreening, both assuming k/f spectral densities, may not be the best scheme of data processing. With this in mind, the raw data of Fig. 37 were each processed in two ways: once with $1/f$ prewhitening, and once without. Figures 38 through 43 depict the results.

Noise sources #1, #2, #3, #6, and #7 of Figs. 38, 39, 40, 41 and 42, depict the typical effect of the absence of prewhitening: their unprewhitened estimates have singularly distorted frequency estimates at such peculiar periods at 167 minutes, 83 minutes, etc.

It is indeed quite obvious, in retrospect, that a stochastic process which is not exactly $1/f$ will be flatter and, consequently, best prepared for further processing by the Tukey algorithm if it is prewhitened than if it is left alone as $1/f^2$ or whatever it happened to be.

Unfortunately, this argument cannot be stretched to cover processes which are white in the first place or which go like $(1 - e^{-f})$, for example. A "cut and try" iterative procedure might be best in that case.

Prewhitened and Non-prewhitened Spectral Estimates for Noise Source #1.

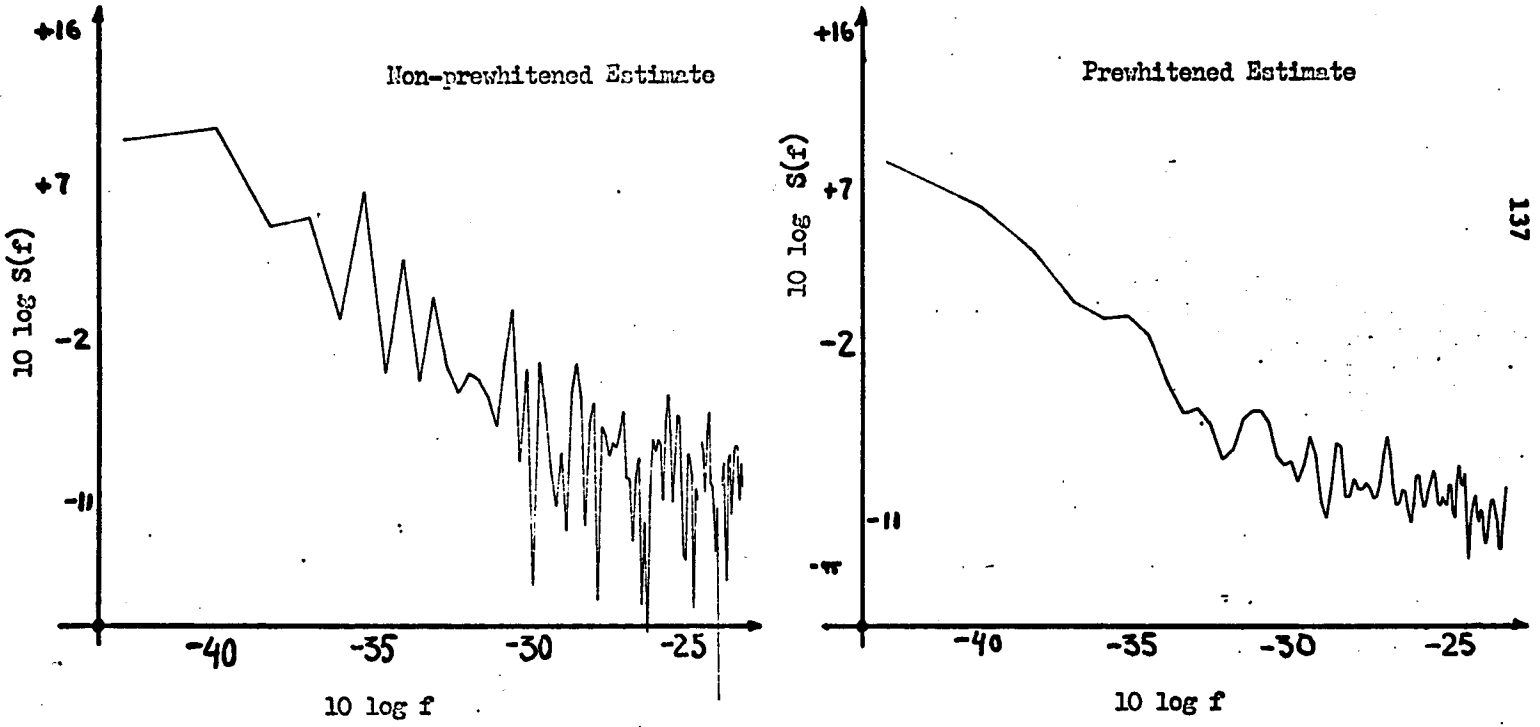

Figure 38

Prewhitened and Non-prewhitened Spectral Estimates for Noise Source #2

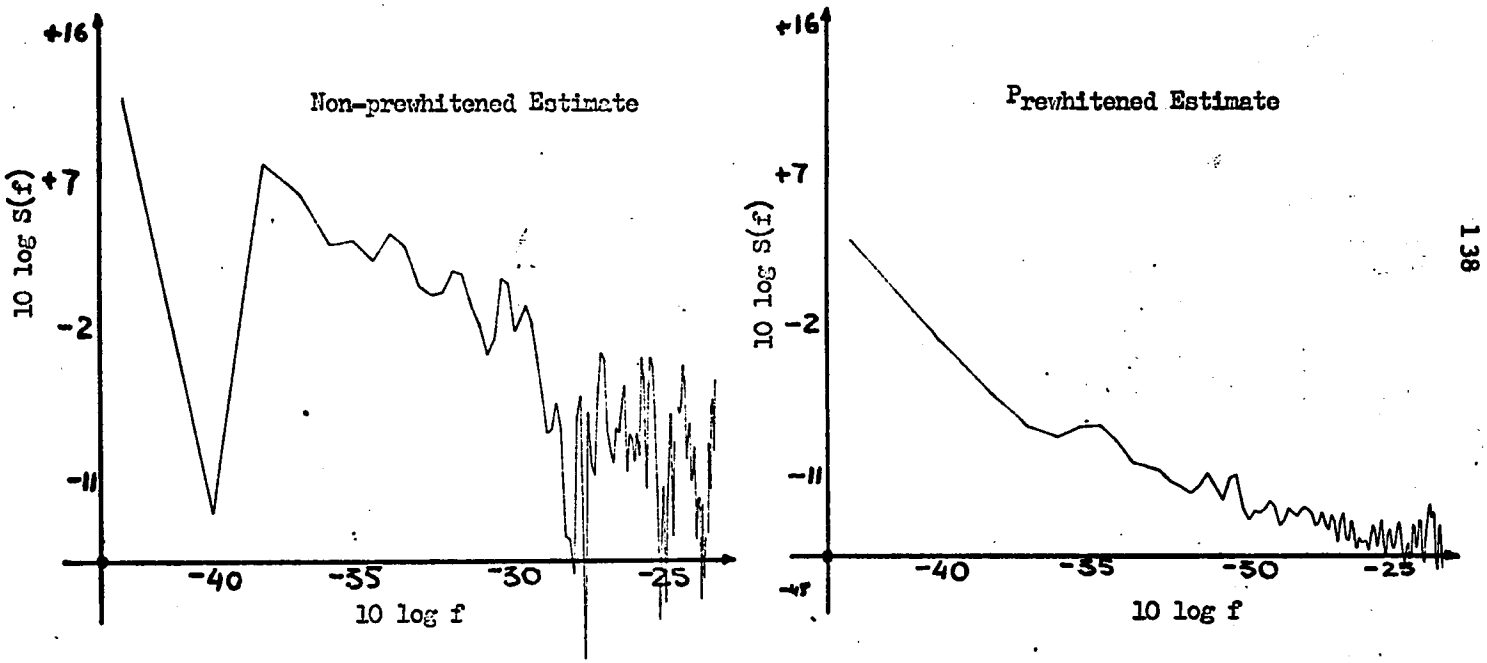

Figure 39

Prewhitened and Non-prewhitened Spectral Estimates for Noise Source #3

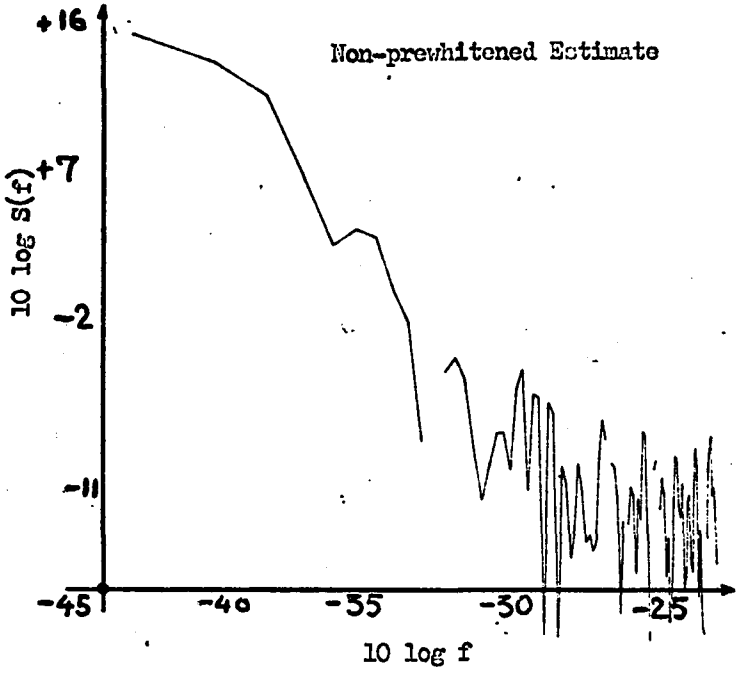

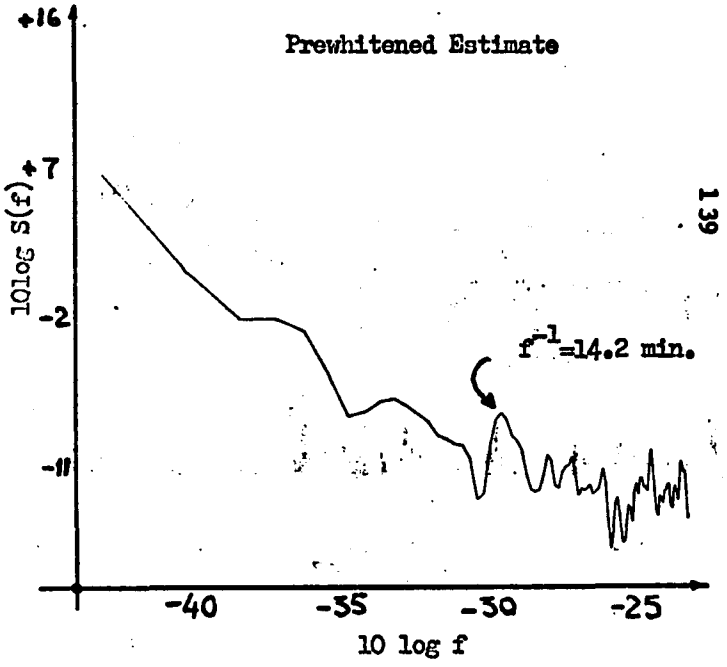

Figure 40

Prewhitened and Non-prewhitened Spectral Estimates for Noise Source #6

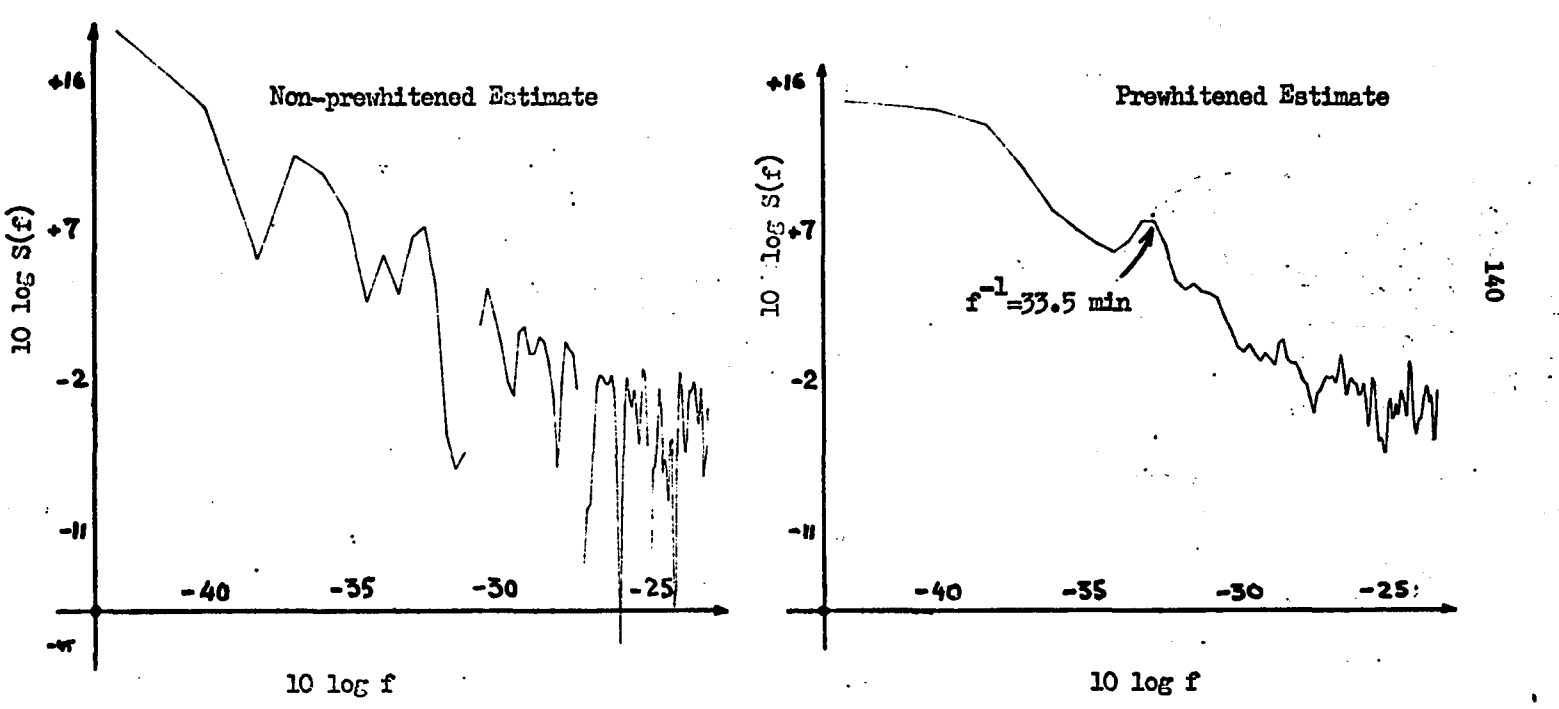

Figure 41

Prewhitened and Non-prewhotened Spectral Estimates for Noise Source #7

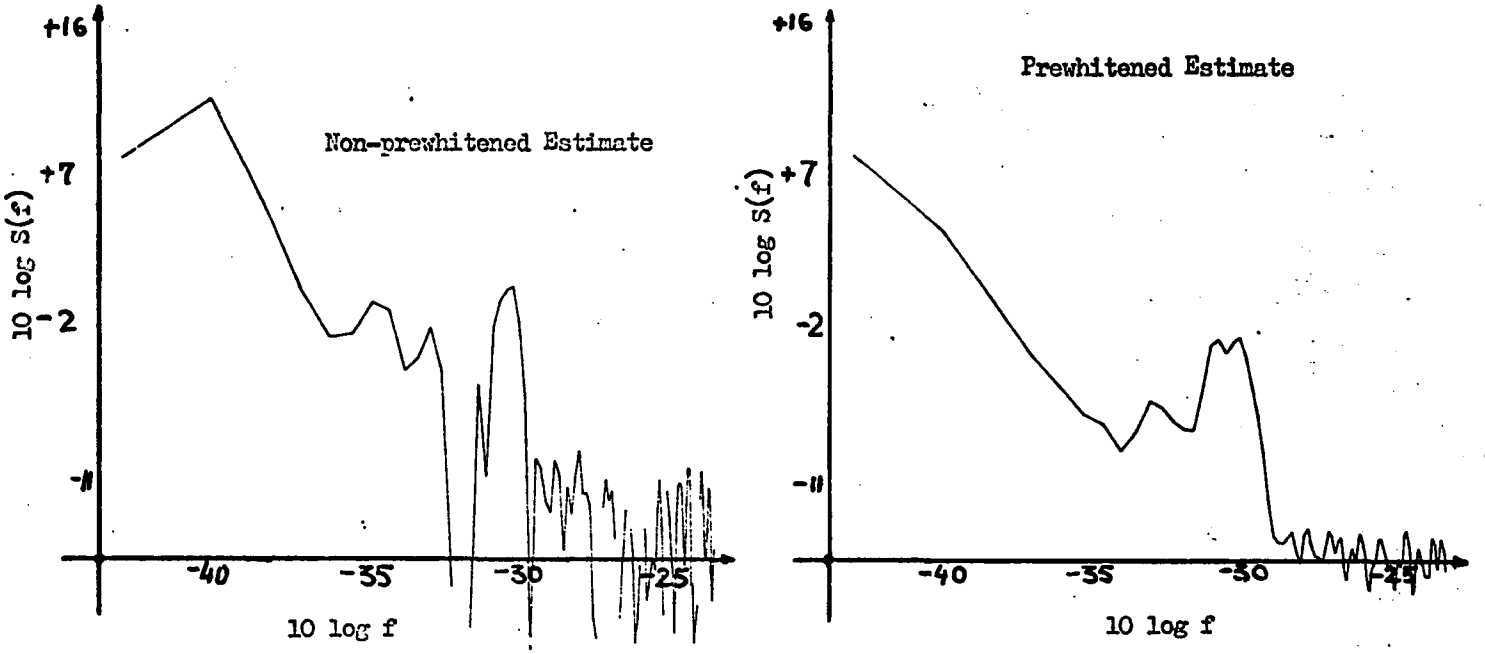

Figure 42

Prewhitened and Non-prewhitened Spectral Estimates of the Bath Temperature.

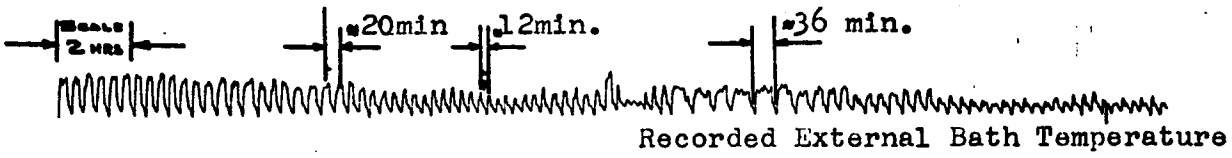

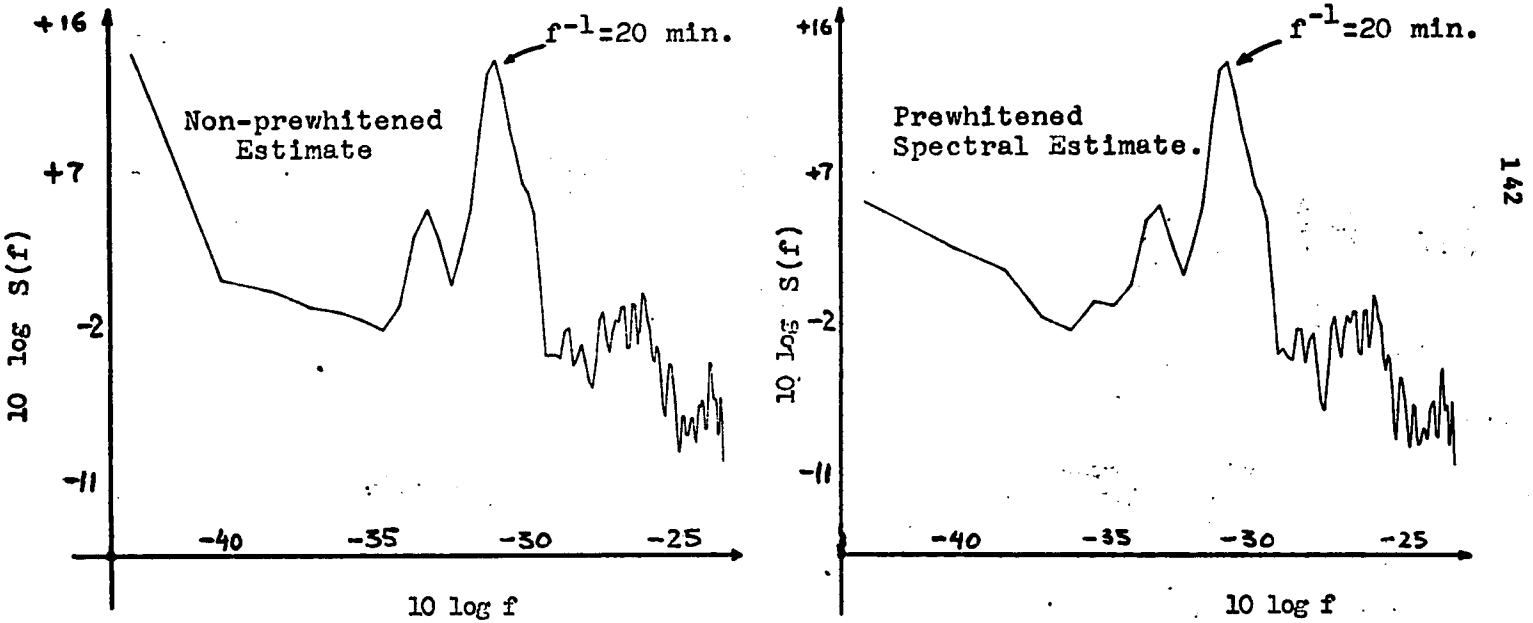

Figure 43

A typical example is the bath temperature shown on Fig. 43; both the unprewhitened and the prewhitened spectral estimates look almost identical, thereby suggesting that both approaches process a signal with similar lack of spectral flatness.*

Finally, just as all processes do not have to be k/f ones, there is no reason why some unlikely processes could not turn out to be k/f ones. Figure 44 depicting the spectral estimates of the unregulated supply voltage shows again the typical low frequency bias of the unprewhitened estimate; although no conclusions can really be drawn from that alone, it is mildly indicative that the true spectrum behaves something like k/f .

9.5 Automatic Data-Collecting Circuitry

As mentioned earlier, equidistant samples were used in this experimental project which utilized the Blackman-Tukey estimator of the spectral density of a process. Although the process of obtaining equidistant samples visually displayed on a digital voltmeter was trivial, the process of accurately recording these readings took a very considerable amount of time, which was spent to a great extent in the construction and troubleshooting of the electronics designed.

The problem is simple to state: as soon as the digital voltmeter (dvm for brevity) has settled on its reading consisting of four digits and scale, a "coupler" must look at one digit at a time, encode it to

*This argument is by no means conclusive, however, because the major effect of prewhitening is on the spectral estimates variance and not on its mean.

Prewhitened and Non-prewhitened Spectral Estimates of the Supply Voltage

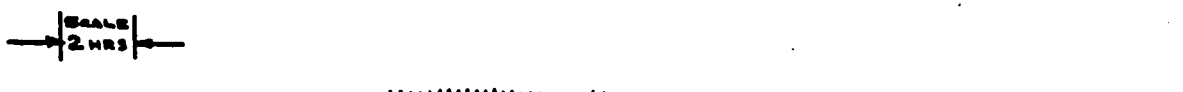

Recorded Unregulated B+ Supply Voltage

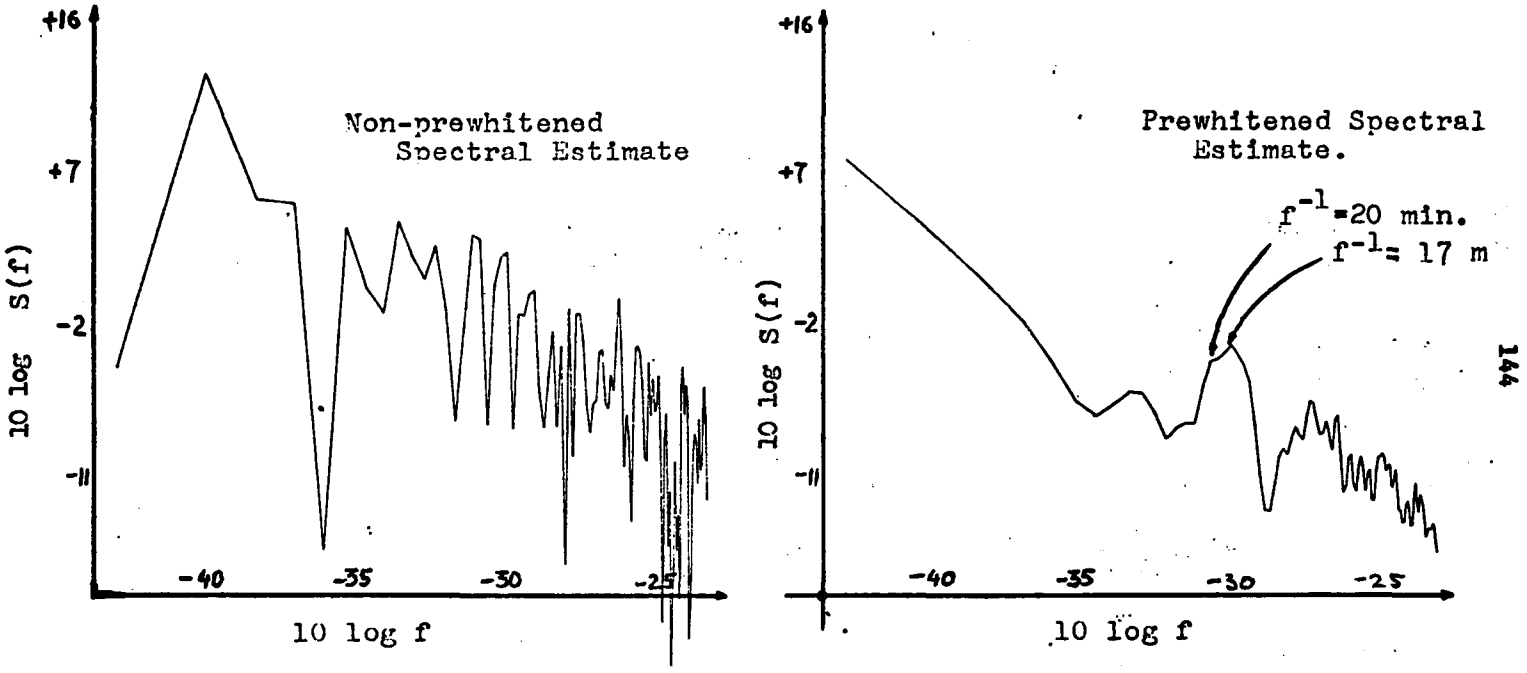

Figure 44

provide for single-error correcting automatically, then it must be synchronized with a rotating paper-tape punching machine, punch the first digit, and then return to do the same with the other digits and scale; at the end it must also punch an "end of reading" mark. For the case of ten multiplexed noise sources, an extra "end of round" mark is also desirable.

The four-digit digital voltmeter and the seven-channel high speed paper punching machine were selected mainly because of their availability; in fact, they were perfectly adequate for the purposes of this experiment.

Once the data had been collected in punched paper tape form, it was ready for the sequence of steps itemized in Section 3.2, carried out by the IBM 360/75 computer, with deliberately introduced need for human intervention between these steps. A block diagram of the data processing cycle is shown in Fig. 45. The diagram of Fig. 45 is meant to be read in a clockwise fashion starting from the bottom left.

The noise sources, the regulated power supply, the heater coil circuitry and the thermistor amplifiers have all been discussed individually in detail above.

The main precision-clock, whose detailed schematic is shown in Fig. 46, is composed of a 100 KHz crystal oscillator followed by a cascade of divide-by-ten frequency dividers; additional provision for 2x and 5x, the periods available from the aforementioned dividers, is made through appropriate digital circuitry shown in Fig. 46. The function of the inverter following the clock is to provide a 180° "phase" difference between the time the multiplexing relay is actuated and the time the volt-

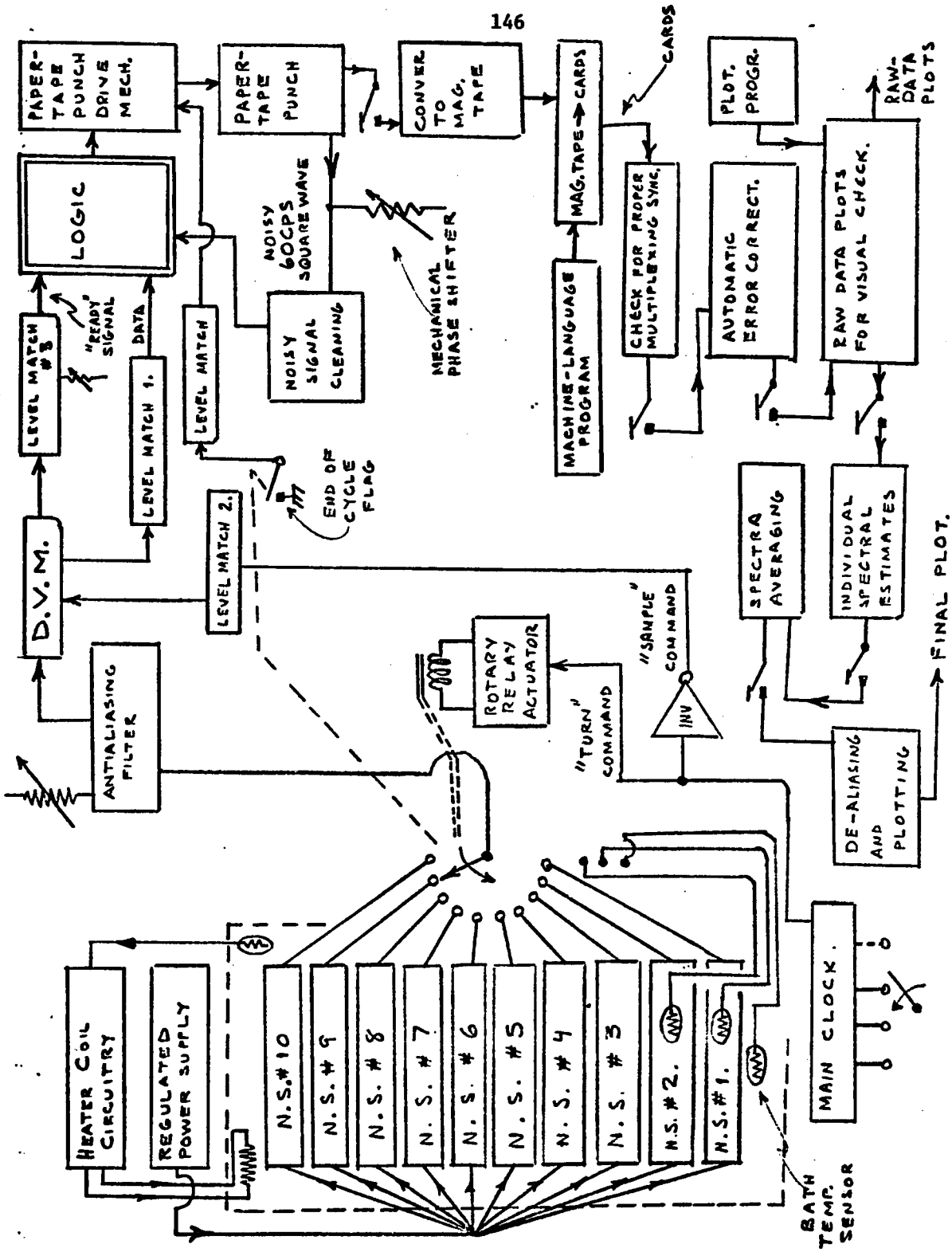
PAPER-TAPE PUNCH DRIVE MECH.
PAPER-TAPE PUNCH
CONVER TO MAG. TAPE
MAG. TAPE → CARDS
CARDS
PLOT. PROGR.
RAW-DATA PLOTS
LOGIC
NOISY 60CPS SQUARE WAVE
MECHANICAL PHASE SHIFTER
CHECK FOR PROPER MULTIPLEXING SYNC.
AUTOMATIC ERROR CORRECT.
RAW DATA PLOTS FOR VISUAL CHECK.
LEVEL MATCH #3
"READY" SIGNAL
DATA
LEVEL MATCH 1.
LEVEL MATCH
NOISY SIGNAL CLEANING
MACHINE-LANGUAGE PROGRAM
END OF CYCLE FLAG
D.V.M.
LEVEL MATCH 2.
SPECTRA AVERAGING
INDIVIDUAL SPECTRAL ESTIMATES
FINAL PLOT.
ROTARY RELAY ACTUATOR
"SAMPLE" COMMAND
INV
"TURN" COMMAND
ANTIALIASING FILTER
DE-ALIASING AND PLOTTING
HEATER COIL CIRCUITRY
REGULATED POWER SUPPLY
N.S.#10
N.S.#9
N.S.#8
N.S.#7
N.S.#6
N.S.#5
N.S.#4
N.S.#3
N.S.#2.
N.S.#1.
MAIN CLOCK.
BATH TEMP. SENSOR

Fig. 45

a) Basic Decimal Divider. (J-K Flip-Flops used throughout)

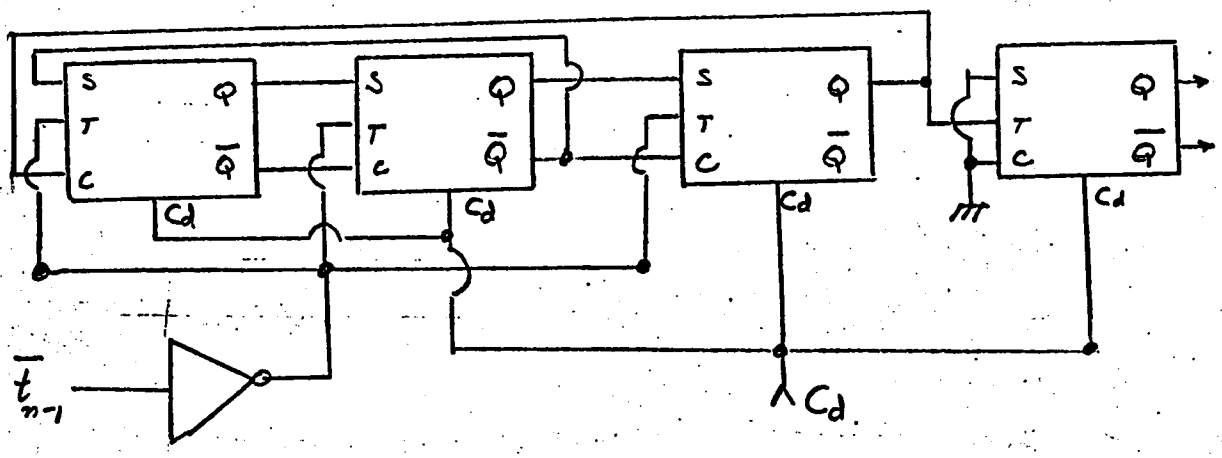

b) Crystal Oscillator Circuit used.

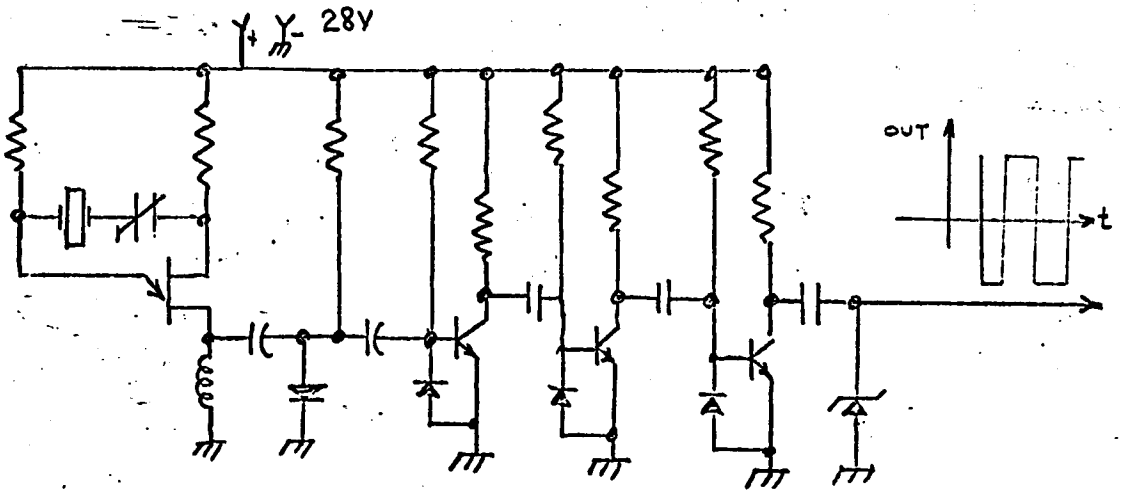

c) Overall Block Diagram.

Schematic diagram of Main Clock.
Fig. 46

meter is told to sample-and-hold.

As discussed earlier, an antialiasing filter is absolutely necessary even in 1/f noise measurements; a single low-pass R.C. filter was used in this work; the precise effects are discussed in detail in Chapter 10 in connection with the experimental results.

The various level-matching networks are essentially for compatibility between the inputs and outputs of different circuits; the logical "zero" of the digital voltmeter, for example, is -24V, and its logical "one" is -1V. These values must be converted to the input requirements of the Translator Logic which expects the logical zero to be 0.0V and the logical "one" to be +2V, ±1V, hence the need for the box marked "level matching 3". Similar considerations hold for the other "level matching" networks.

By far the most interesting, yet highly complicated device constructed, is the multiple function rectangle boxed with double lines in Fig. 45 above. The exact specification of the tasks to be performed by this device were briefly summarized earlier in this section and are specifically the following, listed in the order they ought to be performed:

a) Read-and-hold the entire reading of the digital voltmeter as soon as it is available as a B.C.D. output.

b) Get into "ready" position as soon as the digital voltmeter transmits the pulse indicating that it is ready to be read.

c) Wait for appropriate synchronizing signal from the paper tape punch; this is necessary because the coding and subsequent actual punching of the first peice of information will be practically instantaneous.

d) Upon receipt of the aforementioned first synchronizing pulse, code the first digit. The coding is discussed in detail in Section 9.5.1 below, since it carries the burden of error correcting and error detecting.

e) Synchronously activate the paper-advance relay and the proper relays to punch the coded first digit.

f) Upon receipt of the next synchronizing pulse, 1/60th second later, code the second digit. Repeat step (e) for that digit.

g) Repeat step (f) for the third and fourth digits and for the scale information.

h) Upon receipt of the sixth synchronizing signal, repeat step (e) to punch an "end of reading" mark.

i) Upon receipt of the seventh synchronizing signal, activate only the paper-advance relay so as to provide for a single-space separation between adjacent readings on the tape for subsequent visual inspection.

j) Upon receipt of the eight synchronizing signal, reset the synchronizing signal's counter so that it ignores any further such signals until it is ordered again into a "ready" position by the digital voltmeter for a new reading.

The complete schematic diagram of the circuit is shown in Fig. 47. A number of incidental constraints are partly responsible for its complexity:

a) The total number of bits required to fully describe a single-error-correcting and double-error-detecting coded decimal figure

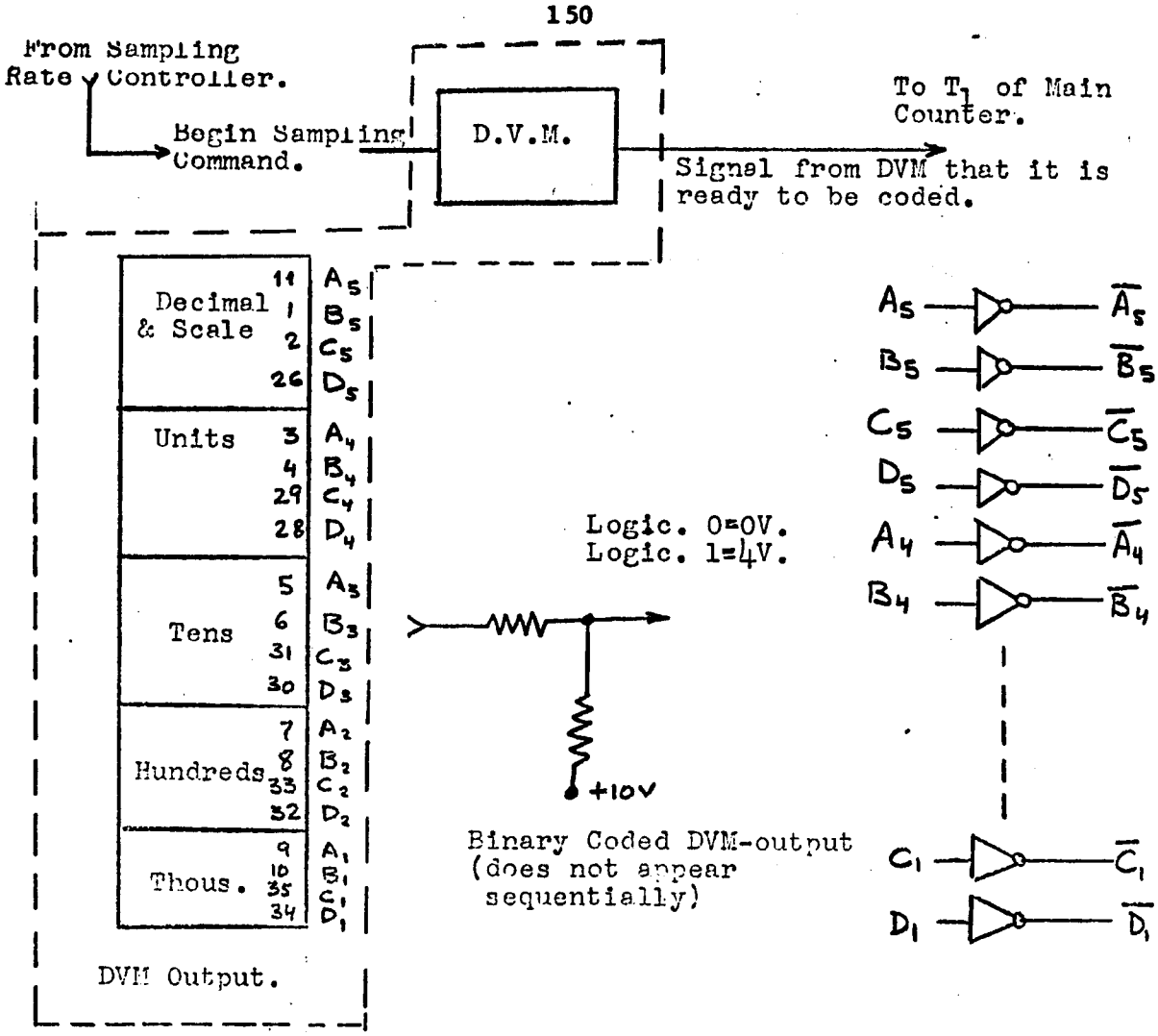

Digital Voltmeter's Truth Table.

PIN#	11	1	2	26	PIN#	A	B	C	D
						3,5,7,9	4,6,8,10	29, 31, 33, 35	28, 30, 32, 34
+1000v	0	1	0	0	1	1	0	0	0
-1000v	1	1	0	0	2	0	1	0	0
+100v	0	0	1	0	3	1	1	0	0
-100v	1	0	1	0	4	0	1	0	1
+10v	0	1	1	0	5	1	1	0	1
-10v	1	1	1	0	6	0	0	1	1
+1v	0	0	1	1	7	1	0	1	1
-1v	1	0	1	1	8	0	1	1	1
+.1v	0	1	1	1	9	1	1	1	1
-.1v	1	1	1	1	0	0	0	0	0

Figure 47 a

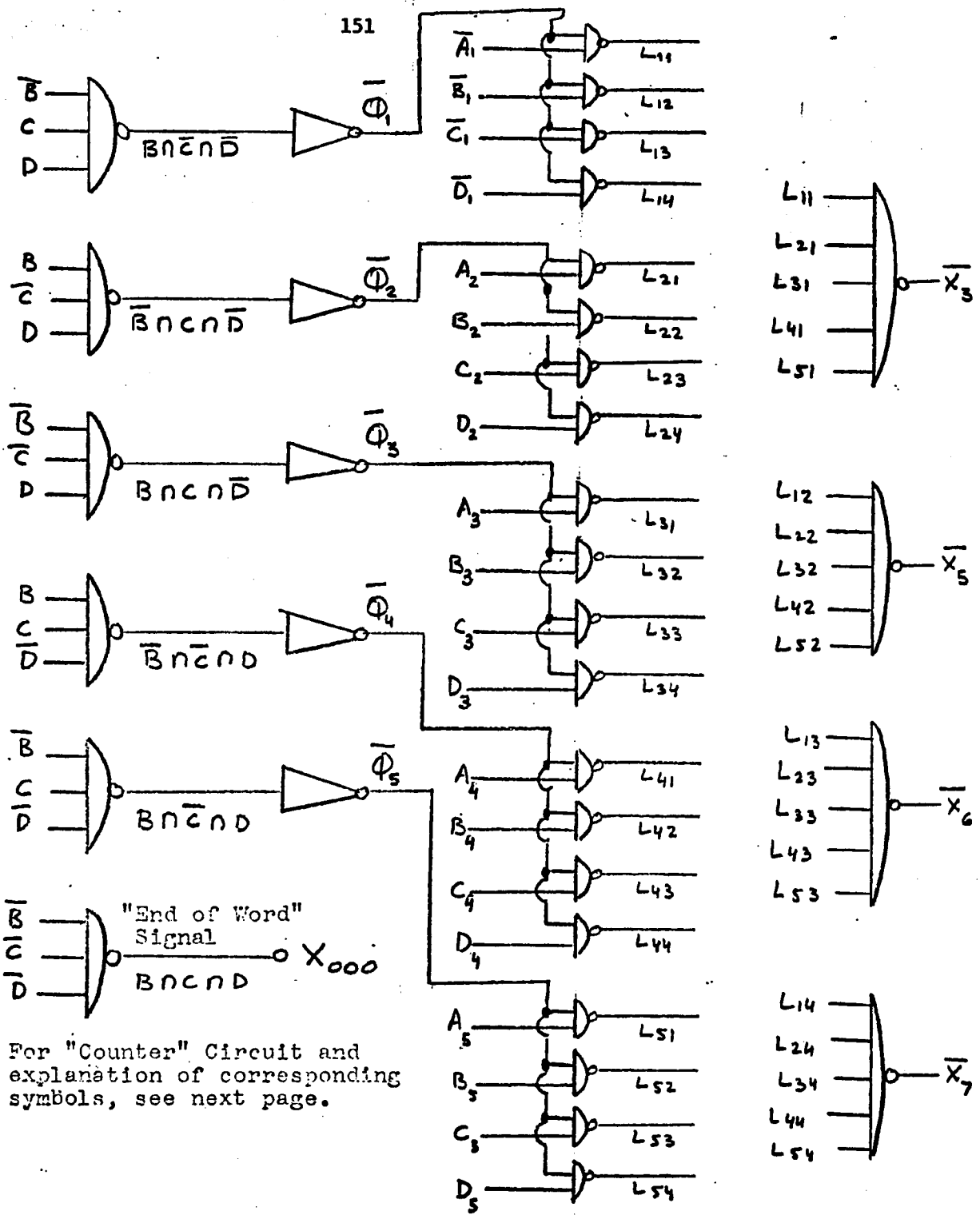

For "Counter" Circuit and explanation of corresponding symbols, see next page.

Fig. 47 b (Sequencing Circuitry)

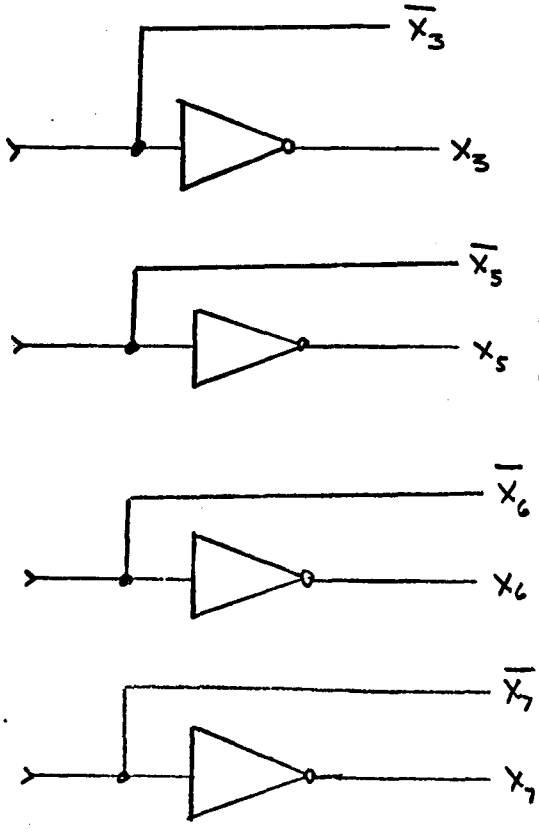

(Rest)

(Ready)

"Truth Table" of
Main Counter (sequencer).

A	B	C	D
1	0	0	0
0	0	0	0
0	1	0	0
0	0	1	0
0	1	1	0
0	0	0	1
0	1	0	1
0	0	1	1
0	1	1	1
1	0	0	0

Time Axis

Main Counter (sequencer) Circuit.

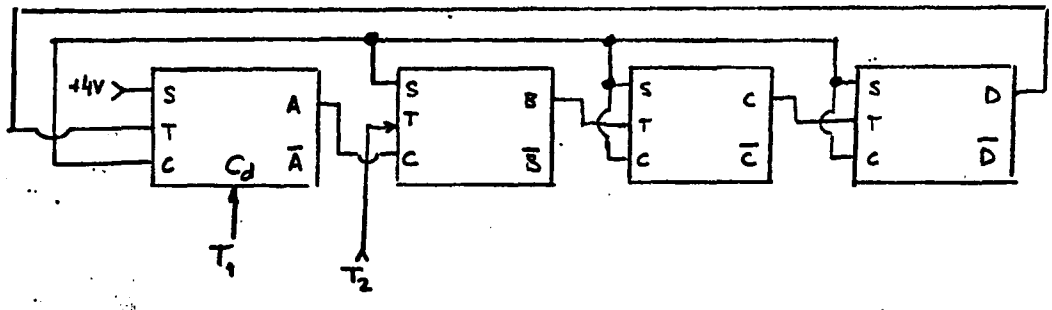

Fig. 47 c

Note: Since the number "zero" is so far coded into 'all zeroes' i.e. no holes on the paper tape, x_{oo} has been added to remedy this situation.

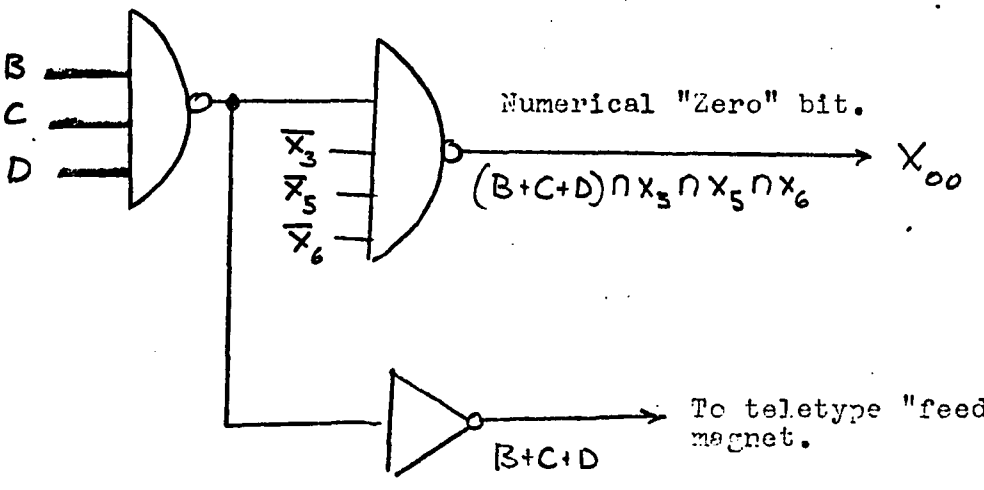

(The code at this stage is a 9-bit code-word one; since nine holes cannot be accomodated in just one column of the available paper tape, each code word is split into 2 parts.)

Fig. 47 a

Error Correcting and Error Detecting Bits

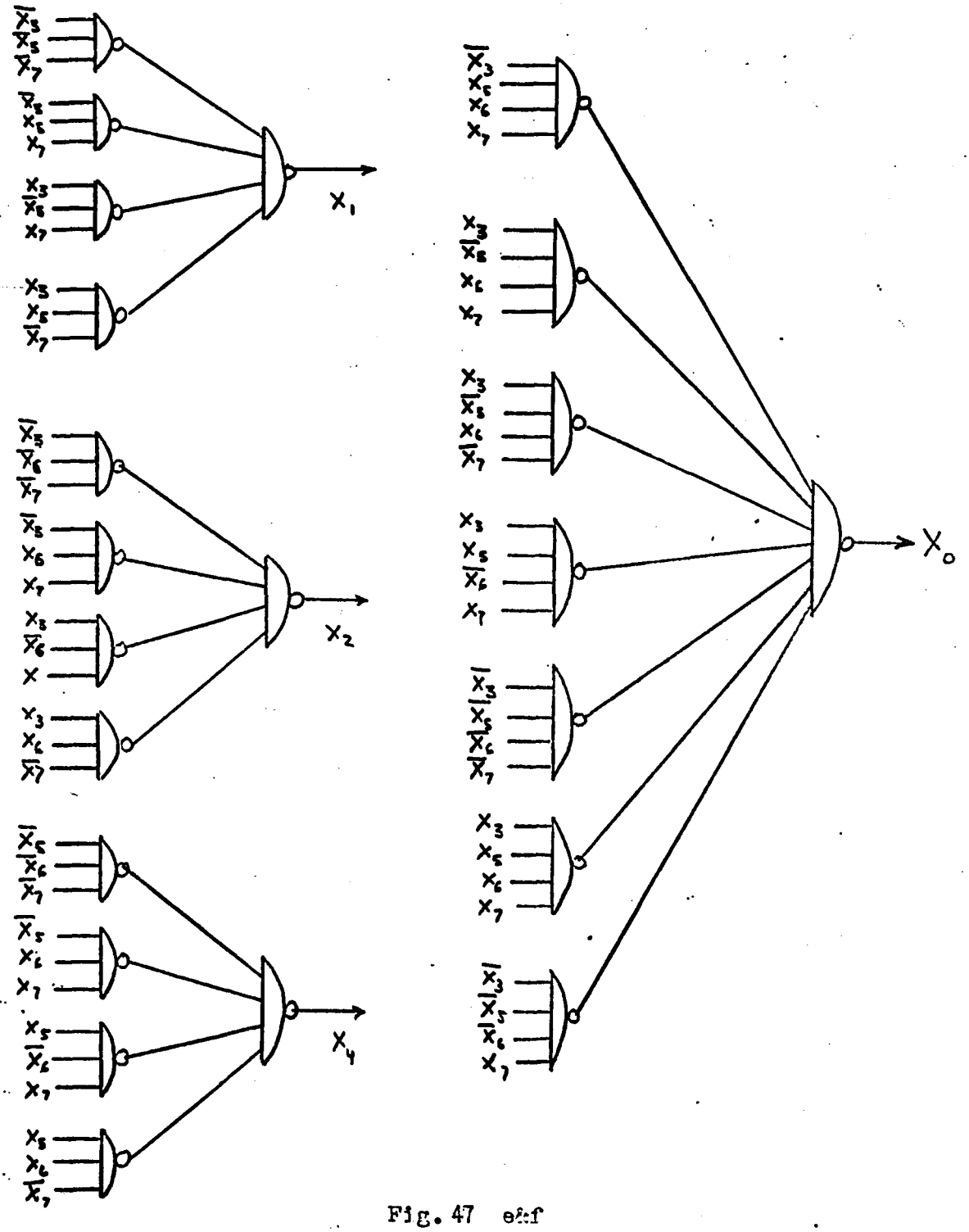

Fig. 47 eff

Code-Word Splitter

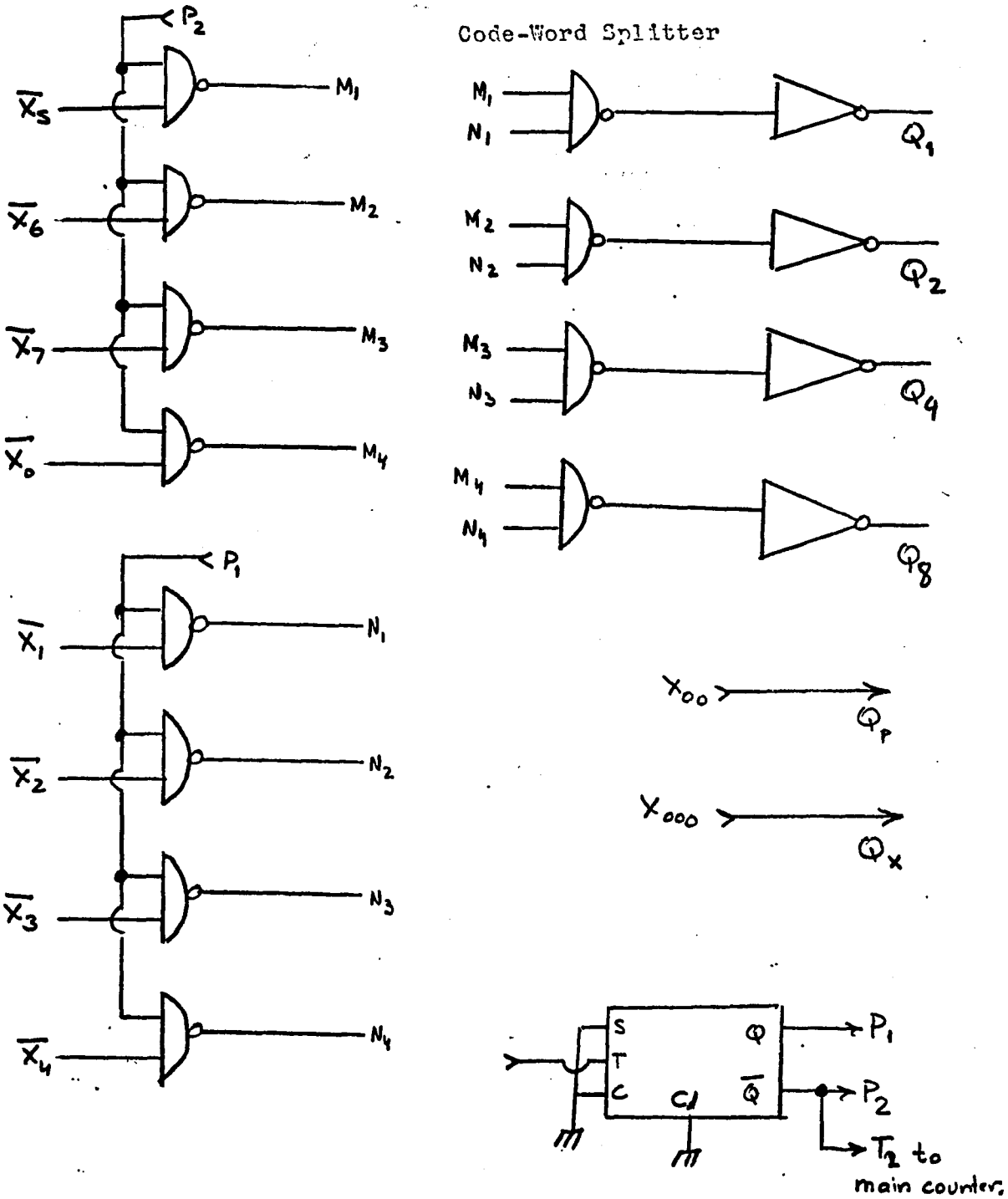

Fig. 47 g

exceeded the available number of bits per vertical column on the paper tape; each decimal figure, therefore, had to be split into two parts which were punched sequentially in two successive vertical columns of the paper tape.

b) No decimal or scale reading could be coded into a series of zeros (corresponding to no-hole on that column of the tape) because the paper tape reader automatically disregards such blanks.

c) Multiple function digital integrated circuits were not available at reasonable prices at the time of the construction of the unit, hence the entire logic circuitry was done with inverters, "nor-gates" and "J.K. flip flops", only.

9.5.1 Error Correcting Coding

Since the most frequent malfunction was caused by marginally-set synchronization timing resulting in an occasional punching-relay failure to activate in time, a single-error-correcting scheme was considered desirable; additional simple parity checking could then take care of double errors. The coding devised for the occasion is shown in Fig. 48. A total of 8 bits per word is needed per source symbol; an additional bit is required for an easily visible end-of-word flag, unless one is willing to settle for a visually unidentifiable flag coded into still another combination of the 8 bits above. The information carrying binary digits are x_3, x_5, x_y, x_7 , while the rest of the binary digits compose the error-correcting and detecting schemes mentioned above.

Decoding the pattern of holes on the paper tape is the job of a

(Double-Error Detecting Digit) (Information Carrying digits)

Single Error Correcting and Double Errror Detecting Code.

	X_0	X_1	X_2	X_3	X_4	X_5	X_6	X_7	X_{00}	X_{000}
0	0	0	0	0	0	0	0	0	1	0
1	1	1	1	1	0	0	0	0	0	0
2	1	1	0	0	1	1	0	0	0	0
3	0	0	1	1	1	1	0	0	0	0
4	1	0	1	0	0	1	0	1	0	0
5	0	1	0	1	0	1	0	1	0	0
6	1	1	0	0	0	0	1	1	0	0
7	0	0	1	1	0	0	1	1	0	0
8	0	0	0	0	1	1	1	1	0	0
9	1	1	1	1	1	1	1	1	0	0
+1000V	1	1	0	0	1	1	0	0	0	0
-1000V	0	0	1	1	1	1	0	0	0	0
+100V	1	0	1	0	1	0	1	0	0	0
-100V	0	1	0	1	1	0	1	0	0	0
+10V	0	1	1	0	0	1	1	0	0	0
-10V	1	0	0	1	0	1	1	0	0	0
+1000mV	1	1	0	0	0	0	1	1	0	0
-1000mV	0	0	1	1	0	0	1	1	0	0
+100mV	0	0	0	0	1	1	1	1	0	0
-100mv	1	1	1	1	1	1	1	1	0	0
Word End	0	0	0	0	0	0	0	0	1	1

Fig. 48

machine language program written by J. Hughes of the Caltech Computing Center. Four modulo-2 operations are performed in the set of eight digits into which each symbol is coded; these operations scan for errors, and they are

$$\begin{aligned} x_4 \oplus x_5 \oplus x_6 \oplus x_7 &= a \\ x_2 \oplus x_3 \oplus x_6 \oplus x_7 &= b \\ x_1 \oplus x_3 \oplus x_5 \oplus x_7 &= c \end{aligned} \qquad \oplus = \text{Modulo-2 addition} \qquad (105)$$

The binary number a b c indicates the exact position of the single error; e.g., if a = 1, b = 1, c = 0, digit x_6 is wrong and ought to be changed before any further processing. Digit x_0 alone takes care of detecting any even number of errors through simple parity check.

It may be noted from the coding table of Fig. 48 that the symbol zero is coded into no-holes-at-all, which is not permissible, as mentioned earlier. This oversight was found at a later time and was remedied by punching an x_8 whenever all x_i , $i \in [0,7]$ were logical zeros.

Fancy and convenient as this scheme may be - indeed, it was used extensively for all the work before the multiplexed noise sources were constructed -, it suffers from two disadvantages:

a) It consumes twice as much paper tape as a simple-minded scheme would, which would punch only the information carrying digits; this is most significant when ten noises have to be measured and the need to change reels in the middle of a run becomes very pronounced.

b) Data processing cost of carrying out the aforementioned four

modulo-2 operations and of implementing the error correcting rises unnecessarily high; this judgment is a consequence of the observation that single errors were actually present in approximately one out of 6000 symbols, and double errors were practically absent.

A simple circuit modification of the original diagram was thus performed which resulted in punching only the four information digits, all in one column, reserving one paper tape track for x_8, one for a readily visible end of reading mark, and one for "multiplexing cycle completed" mark. An error-detecting scheme was included in the new machine language program written by James Lo, then with Caltech's Computing Center staff; the error-detecting scheme simply checks for disallowed combinations of hole patterns and reports them as such on the computer printout.

The electronics implementing the logic were originally built on two double-sided p.c. boards, whose design and actual construction were done by this author. After a certain amount of "debugging" and replacing of 14-pin integrated circuits firmly soldered in thin copper, a duplicate was constructed by R. Dukelow with all wiring done with wires rather than thin copper strips.

9.6 Auxiliary Data Collecting Circuits

The "noisy signal cleaner" appearing in the block diagram of Fig. 45 is necessary because the pulse logic J.K. flip-flops need a clean-cut square wave to operate satisfactorily, whereas the mechanical contact-

created square wave from the tape punch is noisy.

The "signal cleaner" simply passes the noisy 60 cps from the tape punch through a tuned 60 cps LC filter which is subsequently squared again through a Schmidt trigger, or a cascade of saturated d.c. amplifiers. The circuit is shown in Fig. 50. The schematic diagram of the paper tape punch driver is also shown in Fig. 49; the few points of interest are:

a) Protective diodes across the relay coils are inadvisable despite the prevailing standard practice; they invariably prolong the activated state of the relay beyond 1/60 sec, thereby ruining the punched data.

b) In view of the high d.c. voltages present, experience has dictated the use of series diodes in the bases of the power transistors to protect the entire logic circuitry should something go wrong.

To obtain a tangible measure of the quality of the overall data collection system, the noise output of a source was sampled by the elaborate data-collecting scheme discussed in this section, and by a chart recorder (an Easterline Angus milliameter). The digitally processed data were plotted side by side with the analog-obtained one, and the results were identical.

9.7 The Paper-Punch Recorder.*

As has already been stated, the data were recorded on computer paper tape before any data processing. For the purposes of this experiment, namely the recording of data at relatively low rates, a recorder

*Teletype Corporation, Model BRP-2

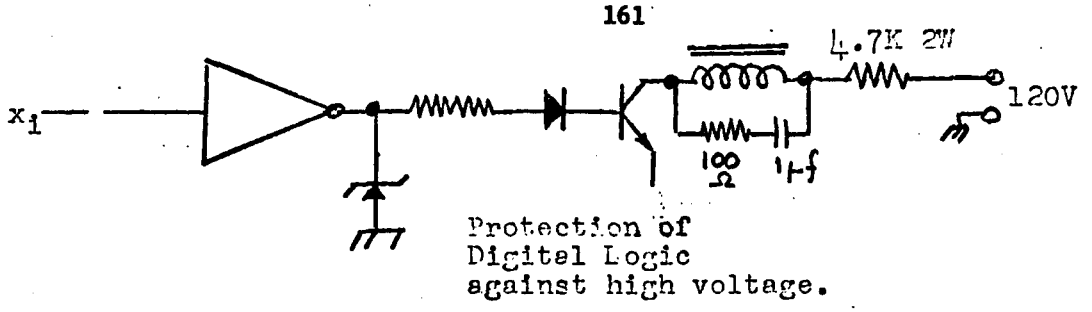

Fig. 49

Teletype Relay Actuating Circuit

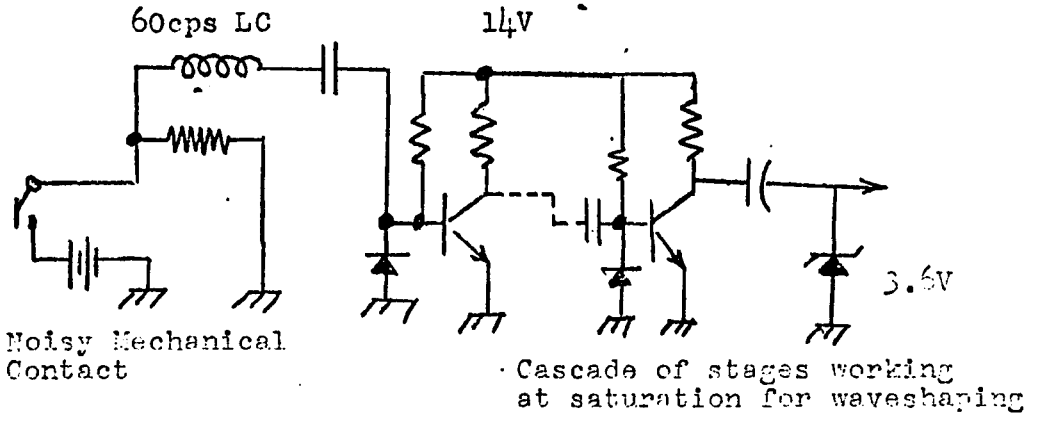

Fig. 50

Contact Noise Eliminator from 60cps Sync. Signal.

of this kind was perfectly adequate; the recorder used had a total of seven binary channels, that is, it could record a maximum of seven bits at a time. Four bits are adequate for any decimal digit (or any hexadecimal digit, for that matter); one channel was reserved for an "end of word" synchronization mark while still another channel was reserved for an "end of multiplexing cycle" synchronization mark. Some economy could clearly have been achieved through proper coding of these synchronization marks but this was considered undesirable because the synchronization marks would no longer be as obvious for visual inspection.

The most bothersome problem encountered in the use of the paper-punch recorder itself, was the wear and tear associated with its critical mechanical settings; this problem was, naturally, most pronounced during the long data-taking runs. Careful inspection of the (collected at the end of each run at various stages of the data-processing procedure insured against false data points.

It is this author's opinion that, should long data-taking runs be made in the future, the relatively-low cost and high mechanical reliability of magnetic-tape recorders would make them ideally suited for such applications. If it is further desired to extend the experiments to higher frequencies, a magnetic tape recorder will be necessary and perhaps even an analog-to-digital converter as well.

9.8 The Computer Program

The computer program used in this work is an expanded version of an earlier program.[25] In painful awareness of the truthfulness of the

slogan that "humans can make mistakes but it takes a computer to really foul things up",* the above "program" is really a sequence of programs with human intervention between them. Data processing is checked at 5 successive intermediate stages before it is allowed to proceed to the next stage. The above-mentioned stages are:

a) Convert punched paper tape into binary cards. Check for hole-punching errors and report each and its exact position. Check for multiplexer's synchronization, i.e., that no noise source was either skipped or punched more than once on the paper tape by mistake;* report any error and identify the suspected data point.

b) Print out the manually-corrected raw data in 10 columns, each column representing one noise source so that the data can be readily checked visually before any further processing.

c) Plot the above raw data to recreate the 10 noise sources' outputs so that the subsequent 10 individual spectral estimates can each be appropriately evaluated before spectral averaging.

d) Provide spectral estimates for each of the ten noise sources in punched cards, in computer-printed output, and in log-log plots for evaluation.

e) Average the individual spectra according to the algorithm indicated in detail earlier.

f) De-alias the estimate obtained from (c) above and plot it versus

---

*One typical reason why human intervention between successive segments of the data-processing algorithm is desirable is given in Section 9.8.

frequency on a log-log scale.

It is of interest to point out some pertinent details associated with the computer-processing of the data.

Except for punched-paper error detection, the transfer of information from paper-tape to binary data cards was done without any other processing; accordingly, the data points appeared on the cards in the order they were recorded, that is, time multiplexed. It would thus have been very desirable to have as many data points per computer-card as the number of multiplexed noise sources; this was unfortunately unfeasible because the maximum number of four-digit numbers, each accompanied by its sign, by the appropriate power to ten, and by the sign of that number is seven; this allows for a desirable one-blank spacing between successive four-digit numbers. It follows that if one data card was misplaced in the deck, this created a loss of the necessary synchronization for proper demultiplexing. It was considerations like this which made it desirable to inspect the data processing at various stages by dividing the overall data-processing into smaller segments. Furthermore, it is the above-discussed possible loss of the necessary synchronization for demultiplexing which prompted the analysis of Section 6 as to the effects of a step-function in the unprocessed data of any one noise source on its corresponding spectral density estimate.*

*Because of the deliberately set different mean output voltage of each different noise source (for purposes of identification), a loss of synchronization in demultiplexing clearly results in a step-function change in the unprocessed data of all ten noise sources.

CHAPTER 10

SEMICONDUCTOR NOISE EXPERIMENTAL RESULTS

This section concentrates on the results and their interpretation for the various semiconductor-noise sources measured in this work; these are: Mark II noise generator, Mark III noise generator, and the time-multiplexed noise sources constructed of integrated circuit operational amplifiers.

Extensive experimentation with, and spectral estimation of the actively controlled bath temperature, of the surface temperature of the noise-generating operational amplifiers, and of the unregulated input to the voltage regulator of the power supply have already been presented; they have appeared in the appropriate sections above pertaining to the temperature and voltage regulation used.

While Chapter 9 dealt with the experimental method used in obtaining spectral density estimates, this chapter deals almost exclusively with the presentation of the pertinent results obtained.

In an effort to avoid duplication, each experimental result presented in this chapter will not be followed by a repetition of the discussion of Chapter 9 as to exactly why each change in the experimental set up was made prior to the next series of experiments; it will be presumed that the reader has read Chapter 9 where all such points are clarified.

The experimental results are presented in their natural chronological order in which they were obtained.

The mathematical algorithm used has been discussed in great detail in earlier sections (see Section 3.2 for a comprehensive

summary) while the experimental implementation of the algorithm has been discussed in Section 9.7 above.

10.1 Preliminary Power Spectral Estimates (Mk. II and Mk. III)

Throughout the experiments associated with this work, various low pass R.C. filters were used; it follows that the amount of aliasing included in the preliminary results may vary from one experiment to another, depending on the R.C. characteristics used.*

The noise sources went through three basic stages of improvement: the first stage involved a discrete-component differential input configuration shown in Fig. 20, and used a discrete-component regulated power supply with two cascaded series-pass circuits (shown in Fig. 21). Temperature stability was achieved (to a limited extent only) through the use of a Dewar flask enclosing a 1/4-inch thick all aluminum enclosure of the single noise source.

Approximately 10,000 data points were taken for all single-source runs, and 100 frequency estimates were made at equidistant frequency intervals covering two frequency decades.

Figure 51 shows** the results obtained from that noise source, referred to as Mark II ("Mk I" stands for the noise source used by Blakemore[25] in his work.)

---

* For de-aliased runs the de-aliasing algorithm discussed earlier was properly tailored to the particular R.C. parameters used; a detailed example of de-aliasing is given in Appendix B.

** Figure 48 does not depict 100 estimates per run because it was plotted by hand using a selected few points from a computer printout. This was remedied in later experiments, excluding the one depicted in Fig. 49.

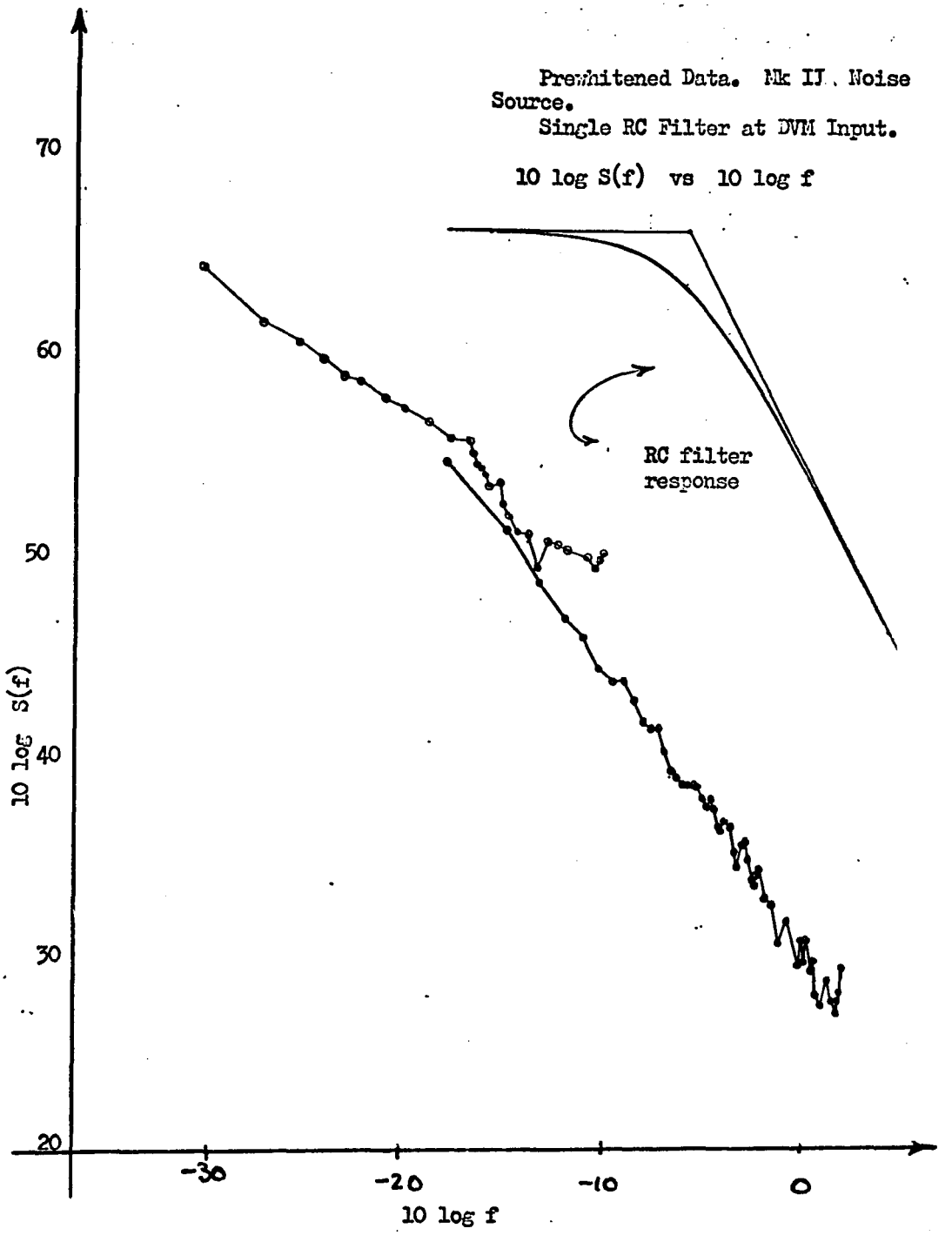
Prewhitened Data. Mk II. Noise Source.
Single RC Filter at DVM Input.
10 log S(f) vs 10 log f
RC filter response
70
60
50
40
30
20
10 log S(f)
-30
-20
-10
0
10 log f

Figure 51

The R.C. filter asymptotes on this figure are not aligned with the coordinates but merely indicate the associated attenuation slope; the 3 db point is at 1 cps for the higher-frequency run, and at another frequency for the low frequency run; as the purpose of this original set of estimates was basically to test the equipment and to obtain a crude measure of the required temperature stabilization and voltage stabilization, no detailed records were made of the specifications of the second low-pass filter, or of parameters which were not of direct interest at that time.

The above set up was found to be in need of improvement because of a persistent linear trend superimposed on the raw data; the most plausible explanation for this drift appeared to be a slowly rising temperature inside the Dewar flask.

Instead of radically revising the temperature regulation set-up, it appeared simpler to select a temperature-matched set of transistors housed in the same metal case so that any ambient temperature drift would not produce any drift from the differential amplifier. The power-supply, whose regulation was measured to be better than one part per thousand, was left intact.

Figure 52 shows the power spectral density estimate obtained with this source; again, as stated, 10,000 data points were recorded per run, and 100 discrete-frequency estimates were made per run, each run spanning two decades in frequency. This time a single R.C. filter was used for all four runs with 3 db point at 1.5 cps, hence the increasing aliasing-distortion as the sampling period is increased in successive runs. This noise source is referred to as Mk III.

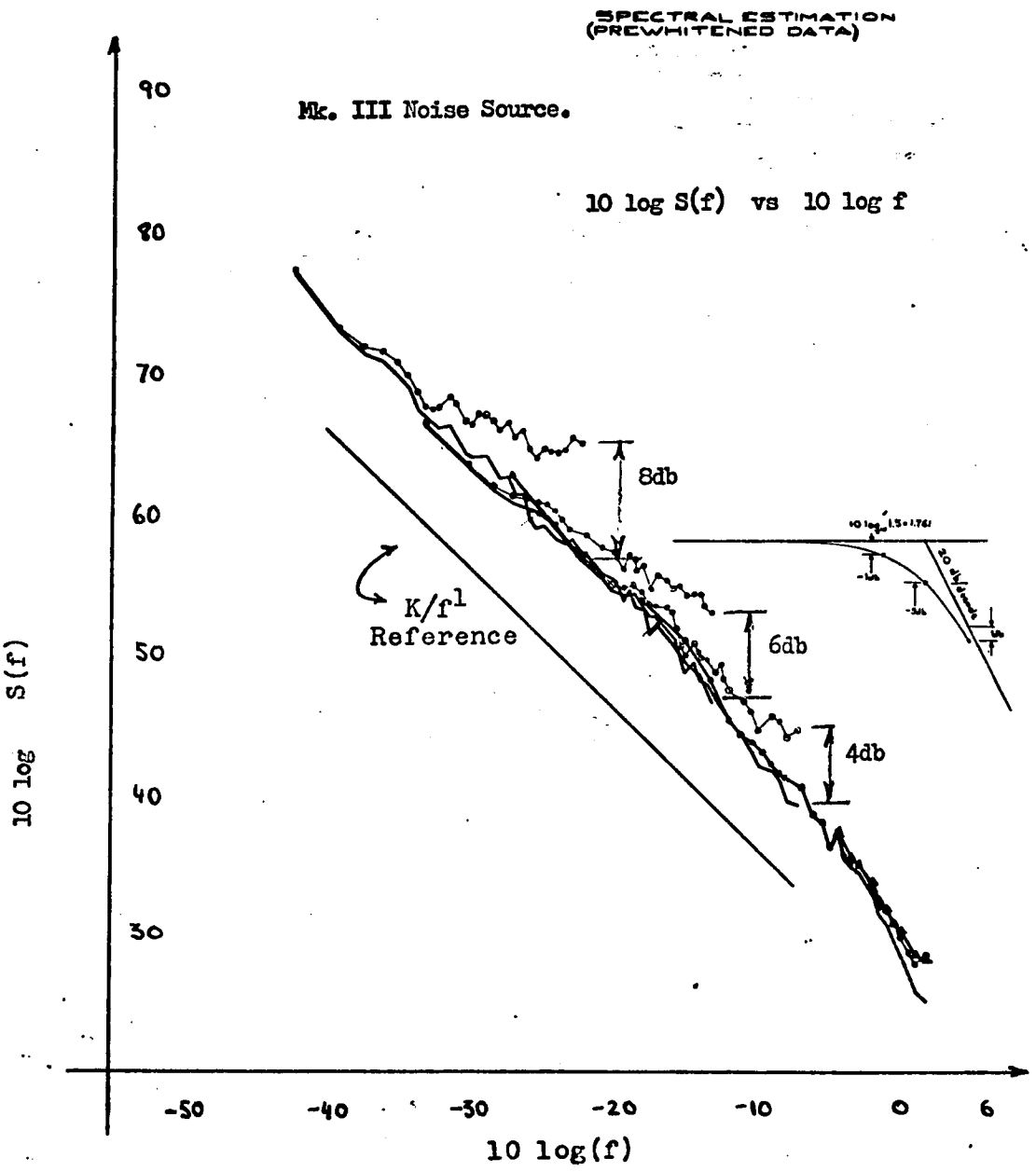
SPECTRAL ESTIMATION
(PREWHITENED DATA)
Mk. III Noise Source.
10 log S(f) vs 10 log f
90
80
70
60
50
40
30
10 log S(f)
8db
6db
4db
K/f^1
Reference
-50
-40
-30
-20
-10
0
6
10 log(f)

Figure 52

Instead of pursuing the problem using rather poor noise sources and measuring techniques it was decided to optimize both the quality* of the noise sources, and the quality of the entire apparatus. The latter would include improvements of the temperature stability, of the voltage regulation, and would use 10 time-multiplexed noise sources (see appropriate theoretical discussion on this point presented in Section 5.5 .)

10.2 Mark IV Time-Multiplexed Noise Sources

In painful awareness of the ever-present temperature build-up inside any insulated container, and of the separate problem of what can gently be referred to as "operator's fatigue" over the mere prospect of year-long data collection sessions**, radical improvements were undertaken before the next round of measurements.

The noise sources were redesigned with integrated circuit operational amplifiers of very low offset, large input common mode

---

*Strictly speaking, no noise source is "worse" than any other. The criterion implied here is that the noise source is desired to exhibit predominantly 1/f spectra; furthermore, its raw data output is desired to be free from the usual sources of bias discussed earlier in this thesis. Whereas the use of integrated circuits does not in itself improve the "quality" of the noise source, the small physical size of the integrated circuits makes it much easier to use 10 noise sources instead of just 1, thereby improving the overall experimental procedure as discussed earlier.

**If a single noise source were used to produce spectral estimates down to $10^{-6.3}$cps with the same variance as that required of the combined one of 10 noise sources, a run of about two years' length would be required.

range, high gain, low power consumption and exceptional temperature stability; the circuit appeared in Fig. 23 above and was amply analyzed in Section 9.2. The voltage regulation was, similarly, improved through the use of a precision integrated voltage regulator with a measured line regulation well within .05%, and low temperature drift through the use of a temperature compensated reference amplifier; this circuit which appeared in Fig. 25 above was discussed in Section 9.3. Temperature control, finally, was significantly improved upon, as discussed in detail in Section 9.4. Most important, the sensitivity of each and every noise source to both voltage and temperature was actually determined through the direct measurement discussed in Sections 9.3 and 9.4. In the interest of completeness, the effect of temperature on the power supply alone was also determined. Equipped with all these "case histories" of the noise sources one could rather easily spot any disorder in the raw data before any subsequent processing. It must be stated that during the initial phases of setting up the 10-noise-source experiment, many different op-amps were tried as noise sources; on the average, one out of every three was rejected because it either did not display 1/f noise, or it displayed the distorting biases discussed at length in Section 6. It follows, thus, that the numbers assigned to noise sources refer to "socket numbers" more than to any one op-amp, unless otherwise stated in the text.

Figure 53a shows the raw data output of noise source No. 5; its only peculiarity is the persistent presence of a sawtooth wave appearance; is it "noise", or not? A new measurement was thus made at a higher sampling rate, roughly equivalent to passing the raw data

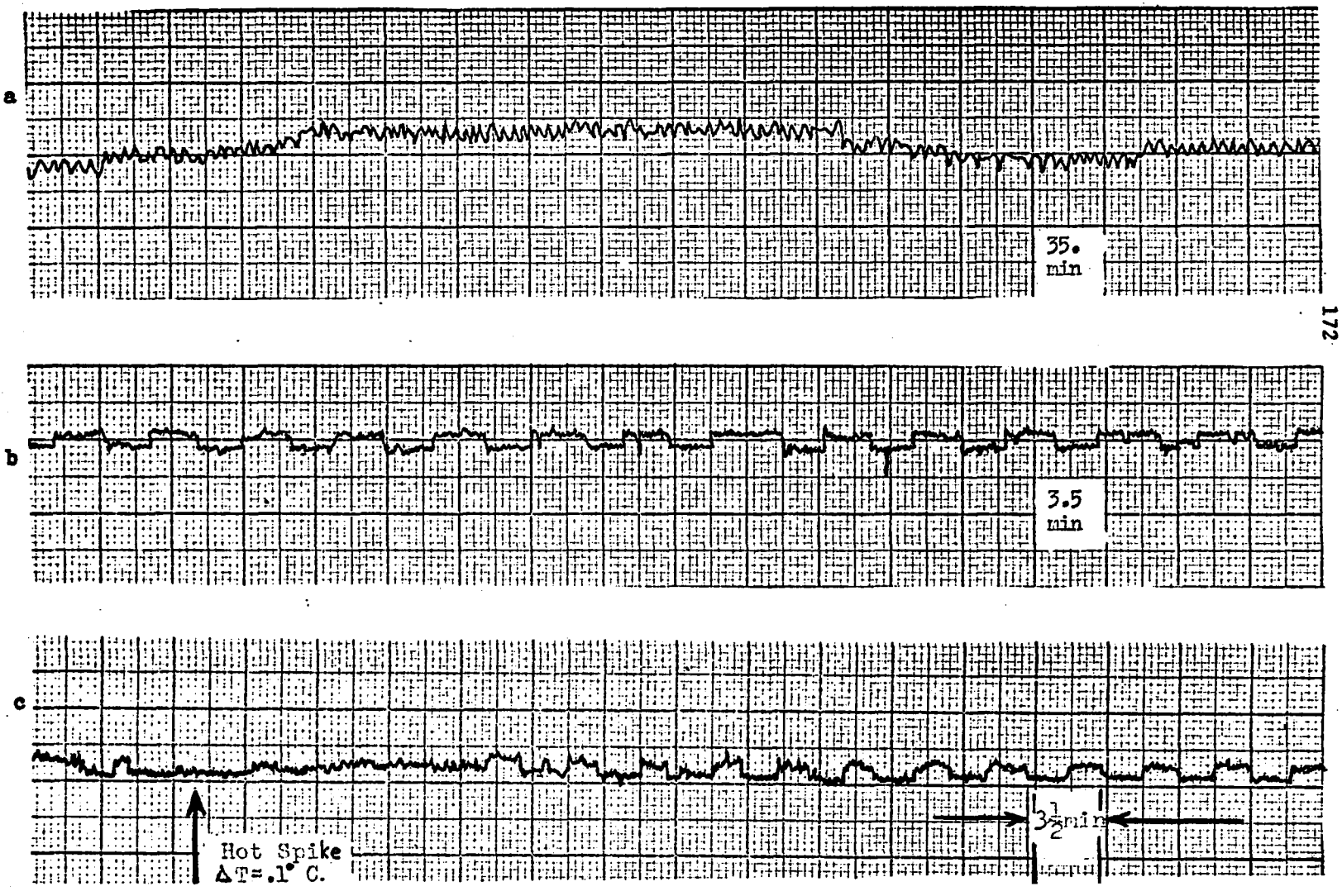

Figure 53

through a finer grid; the result shown in Fig. 53b hints what the cause* of the "sawtooth" wave may be; a ground-loop problem was then found to be the cause of the extraneous square wave. In order to settle the question of an additional possible "popcorning" noise, the graph of Fig. 53c was obtained; a hot "spike" was induced in the bath liquid, and the subsequent gradual response verified that the square wave was not "popcorn noise" but a response to thermostatic controls. The reason why the period is about 4 minutes and not the longer time specified earlier for the refrigerator's own cooling thermostat, is that this new disturbance is associated with the period of the heating circuit which heated the ethylene glycol bath with a thermostat of its own as discussed in Section 9.4 and Figs. 32 and 33. The period of 20 minutes of Fig. 43 is due to the refrigerator's cooling temperature control**.

The first series of spectral estimate measurements of 10 carefully chosen sources was completed in January 1970 and is depicted in Fig. 54. A single R.C. filter with a time-constant of .5 sec was used for all runs, each of which sampled each source at 1000 equidistant times. De-aliasing was done without the aid of a computer on a $K/f^{1.3}$ model which these sources appear to display and was based on

---

* The hint is that the superimposed disturbance is not a gradual one as the sawtooth wave suggested but an abrupt one; this implies that it is not a gradual temperature-propagation effect but an abrupt voltage change in all likelihood.

** The effect of the heater's thermostat was hardly noticeable in recordings of the temperature; it appeared here indirectly through a ground-loop.

Power Spectral Density Estimates
(aliased and hand-dealiased)

10 log S(f) vs. 10log(f)

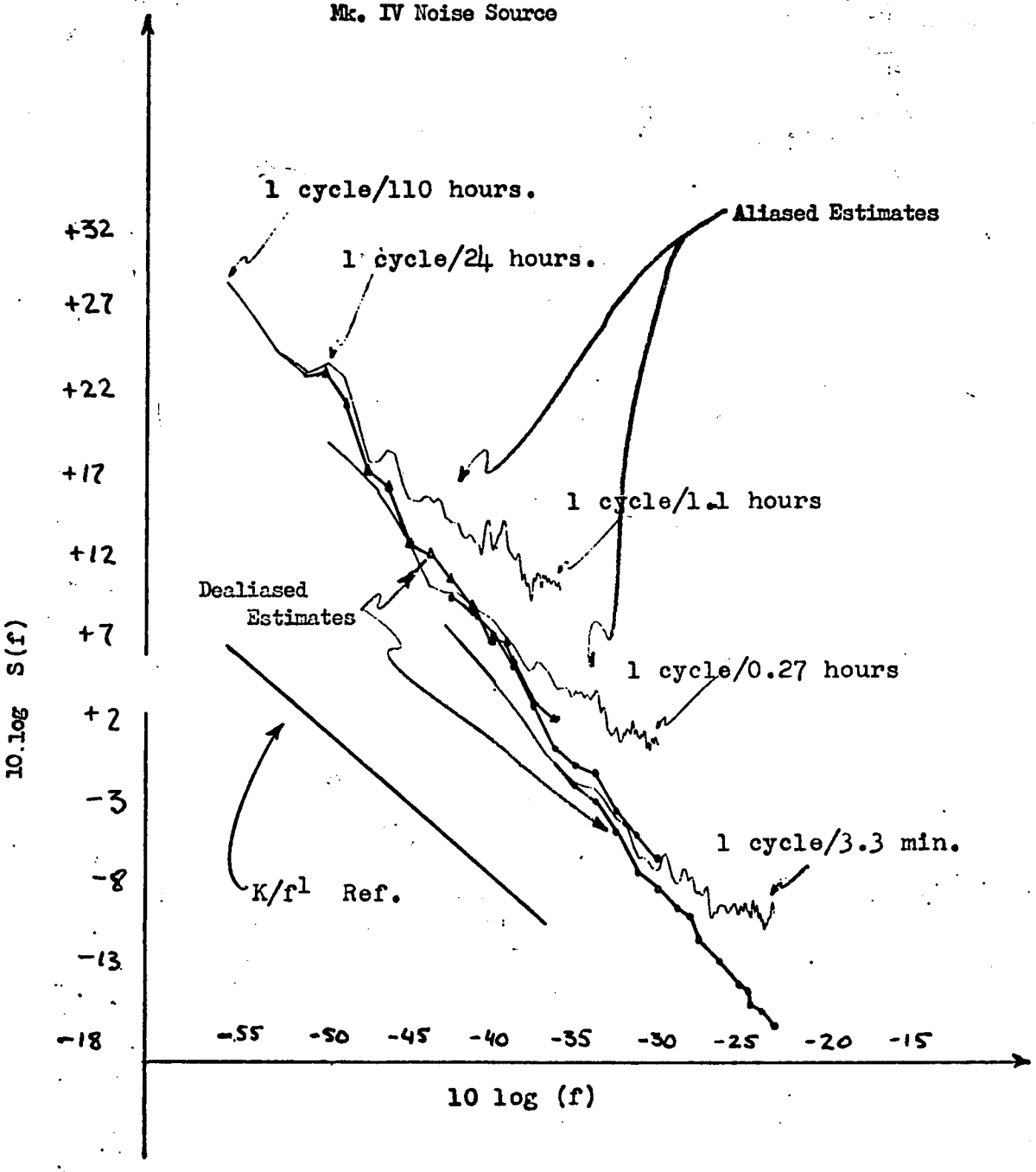

Figure 54

the discussion of Section 5.3; this manual de-aliasing was done only for a selected few points and even at those points it was only approximate because of the total amount of arithmetic involved. This set of plots (Fig. 54) was again made for trial purposes only in the sense of checking the new laboratory set-up and the new computer algorithms; accordingly no great emphasis was placed on precise de-aliasing.

A closer look was then taken at the raw data from which the three averaged-up spectral estimates of Fig. 54 resulted. These raw data, 1000 points per plot, are depicted in Figs. 55 through 64 and have the following two important characteristics:

(a) Not only the variance, but the "character" of the noise of each source is clearly different from that of another noise source.

(b) The sources designated as No. 2, No. 10, and especially No. 4 and No. 8 have a few very noticeable 1-volt spikes*; these clearly extraneous spikes are sufficient grounds for replacing these noise sources. Yet the very prospect of adjusting another group of sensitive d.c. amplifiers seemed to hint an alternate possibility. It was conjectured that one could perhaps "finger-print" each noise source by recording its raw data output so as to make appropriate allowances later for biases in their spectral estimates; this idea was abandoned, however, because it violated the assumption that all 10 noise sources had similar spectra. The offending sources were thus replaced by ones whose raw

*The magnitudes referred to are the amplitudes of the output of the noise sources; recall that each noise source is really a 100 db amplifier, approximately.

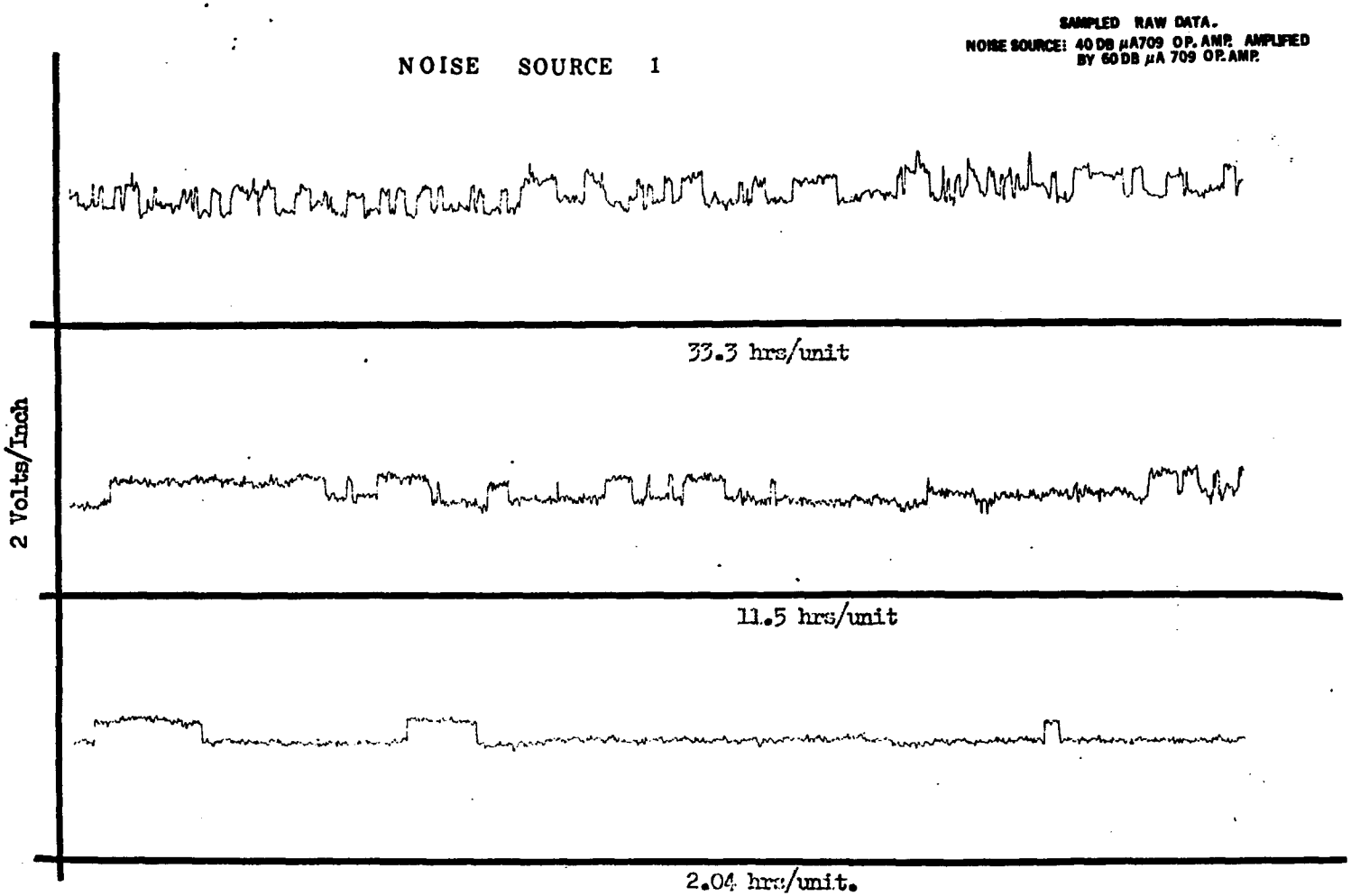

Note: One 'unit' is $\frac{1}{2}$ inch in Fig. 55 through 64

Fig. 55

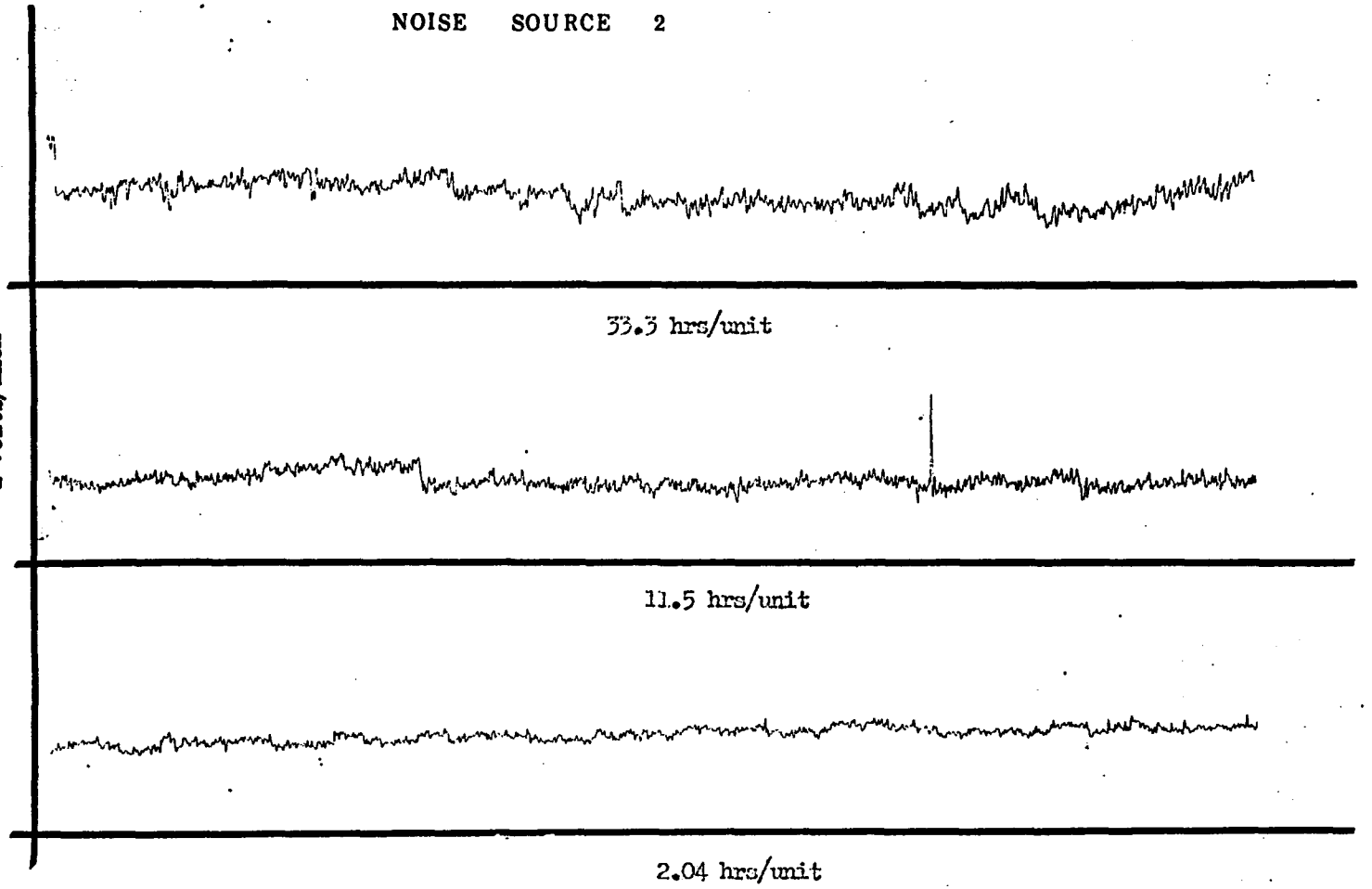
NOISE SOURCE 2
33.3 hrs/unit
2 Volts/Inch
11.5 hrs/unit
2.04 hrs/unit

Fig. 56

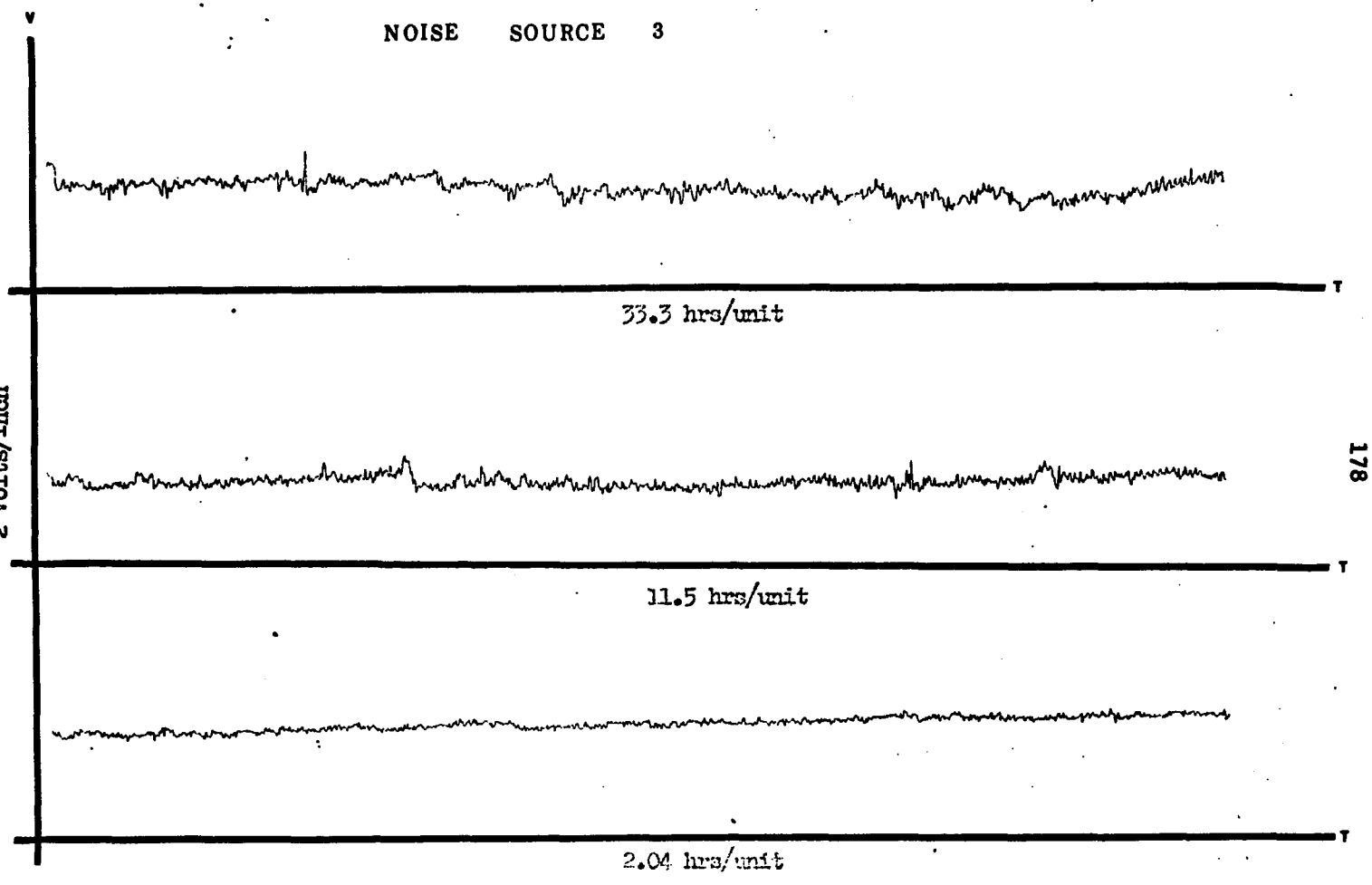
NOISE SOURCE 3
V
T
33.3 hrs/unit
2 Volts/Inch
11.5 hrs/unit
2.04 hrs/unit

Fig. 57

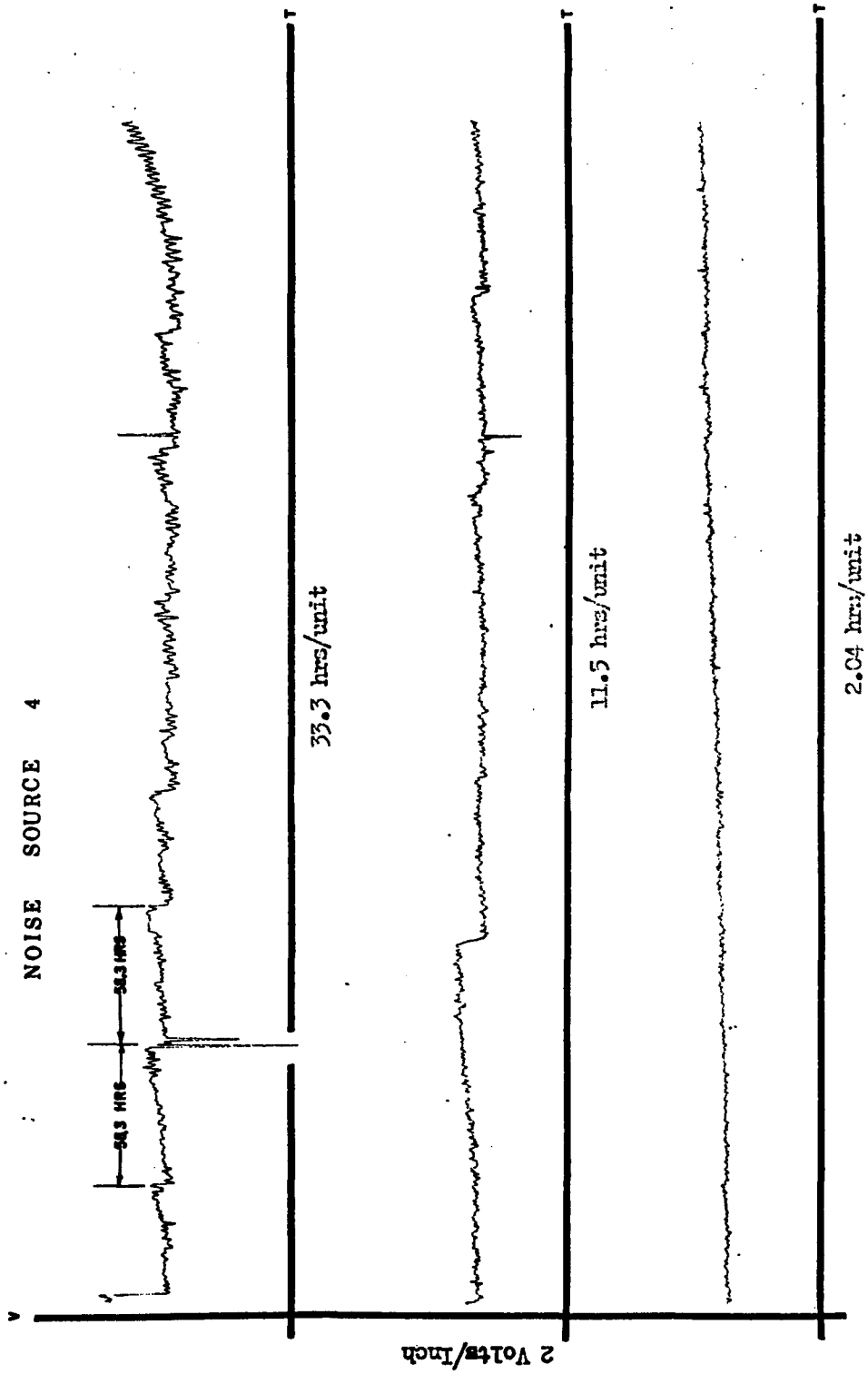
NOISE SOURCE 4
33.3 HRS
33.3 hrs/unit
11.5 hrs/unit
2.04 hrs/unit
2 Volts/Inch

Fig. 58

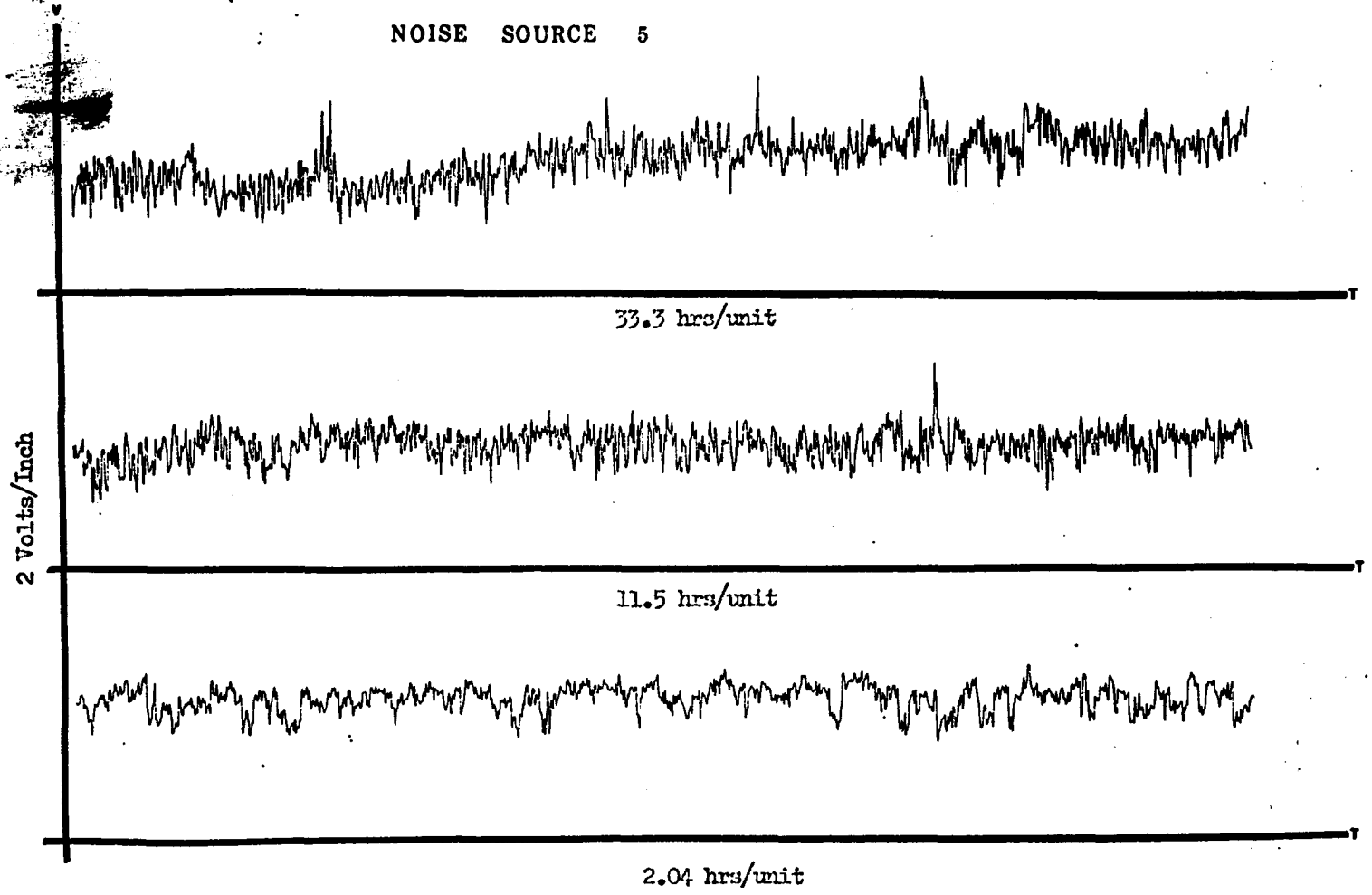
NOISE SOURCE 5
33.3 hrs/unit
11.5 hrs/unit
2.04 hrs/unit
2 Volts/Inch

Fig. 59

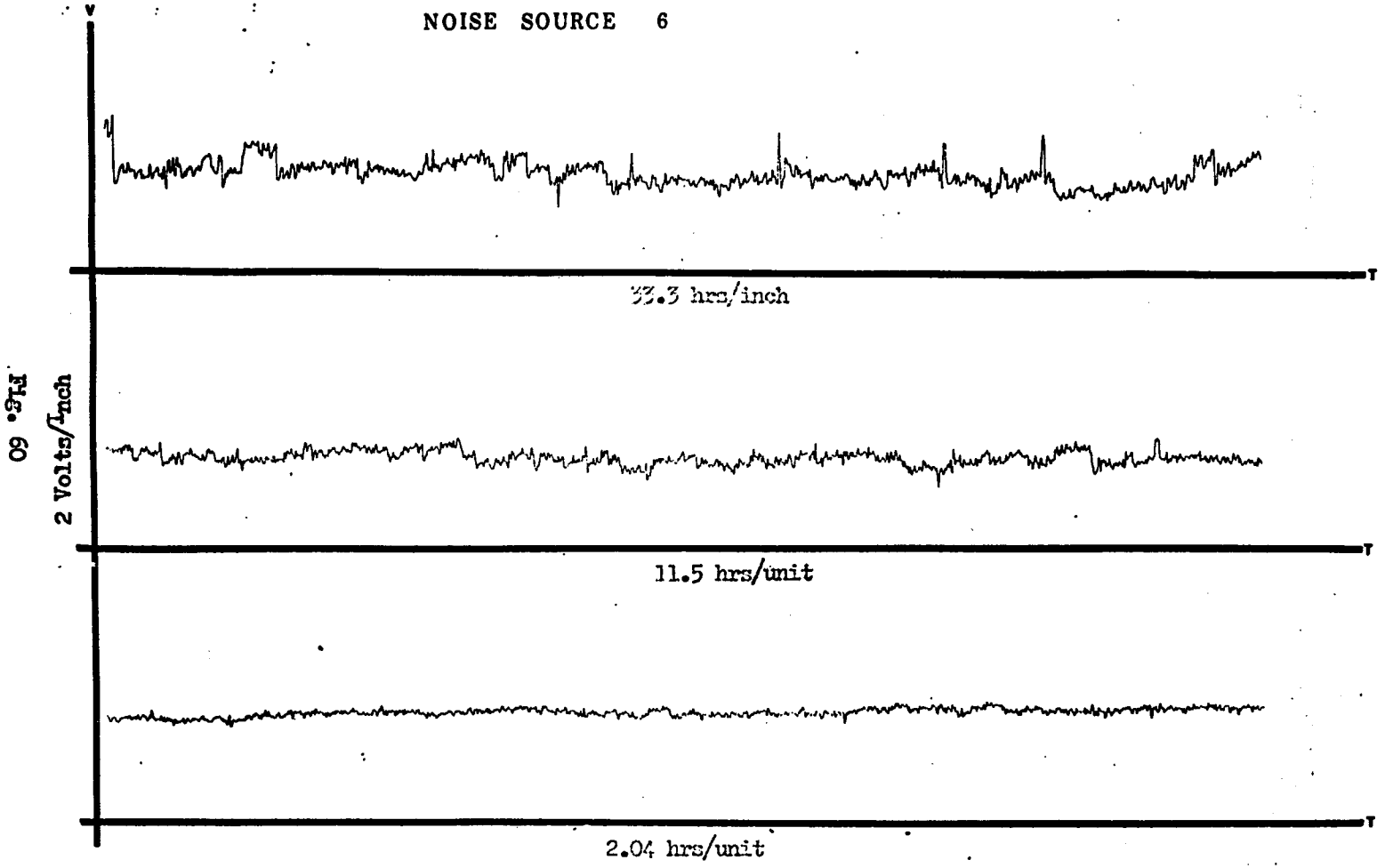
NOISE SOURCE 6
V
T
33.3 hrs/inch
2 Volts/inch
11.5 hrs/unit
2.04 hrs/unit

Fig. 60

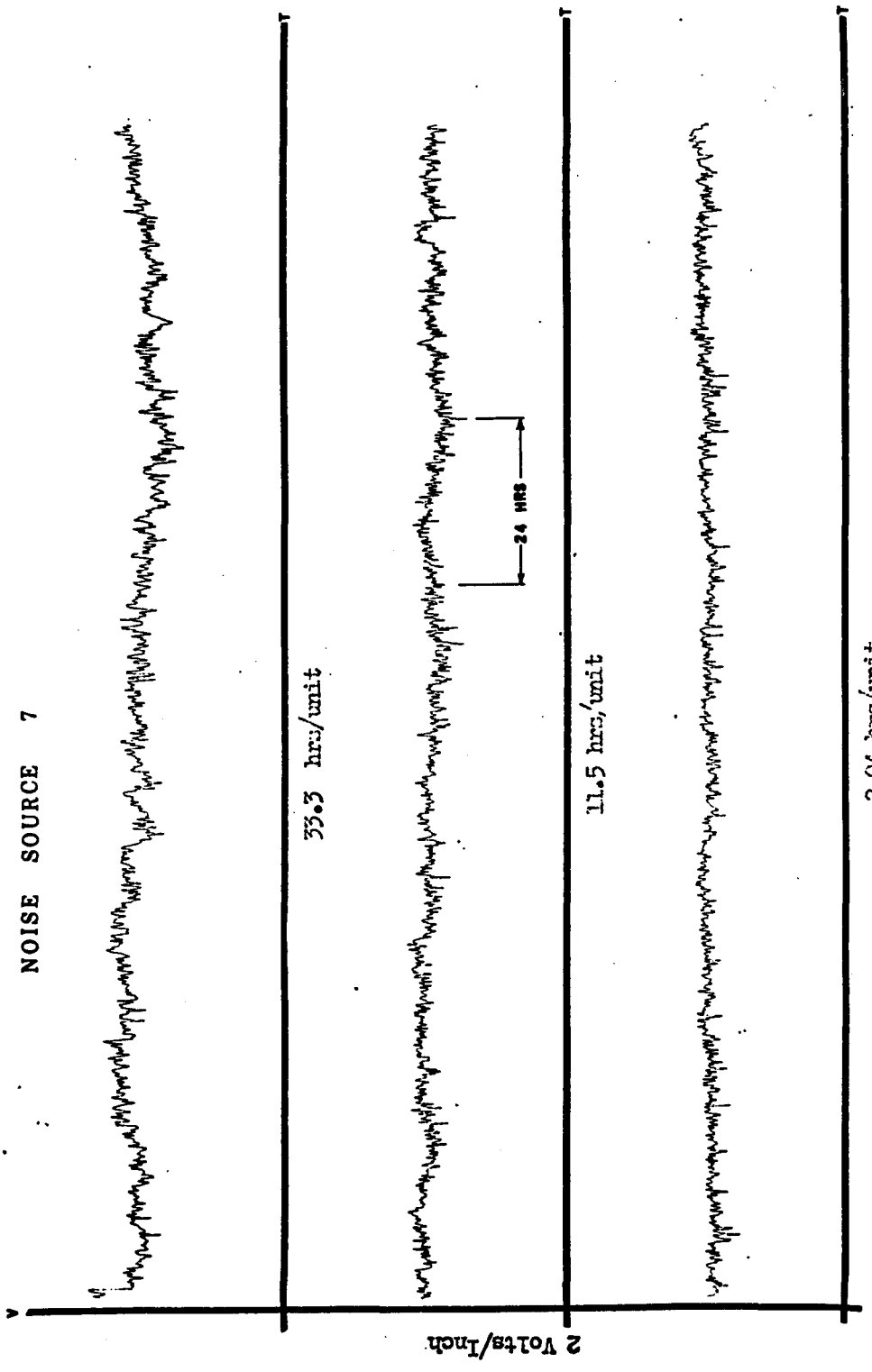
NOISE SOURCE 7
33.3 hrs/unit
11.5 hrs/unit
2.04 hrs/unit
24 HRS
2 Volts/Inch

Fig. 61

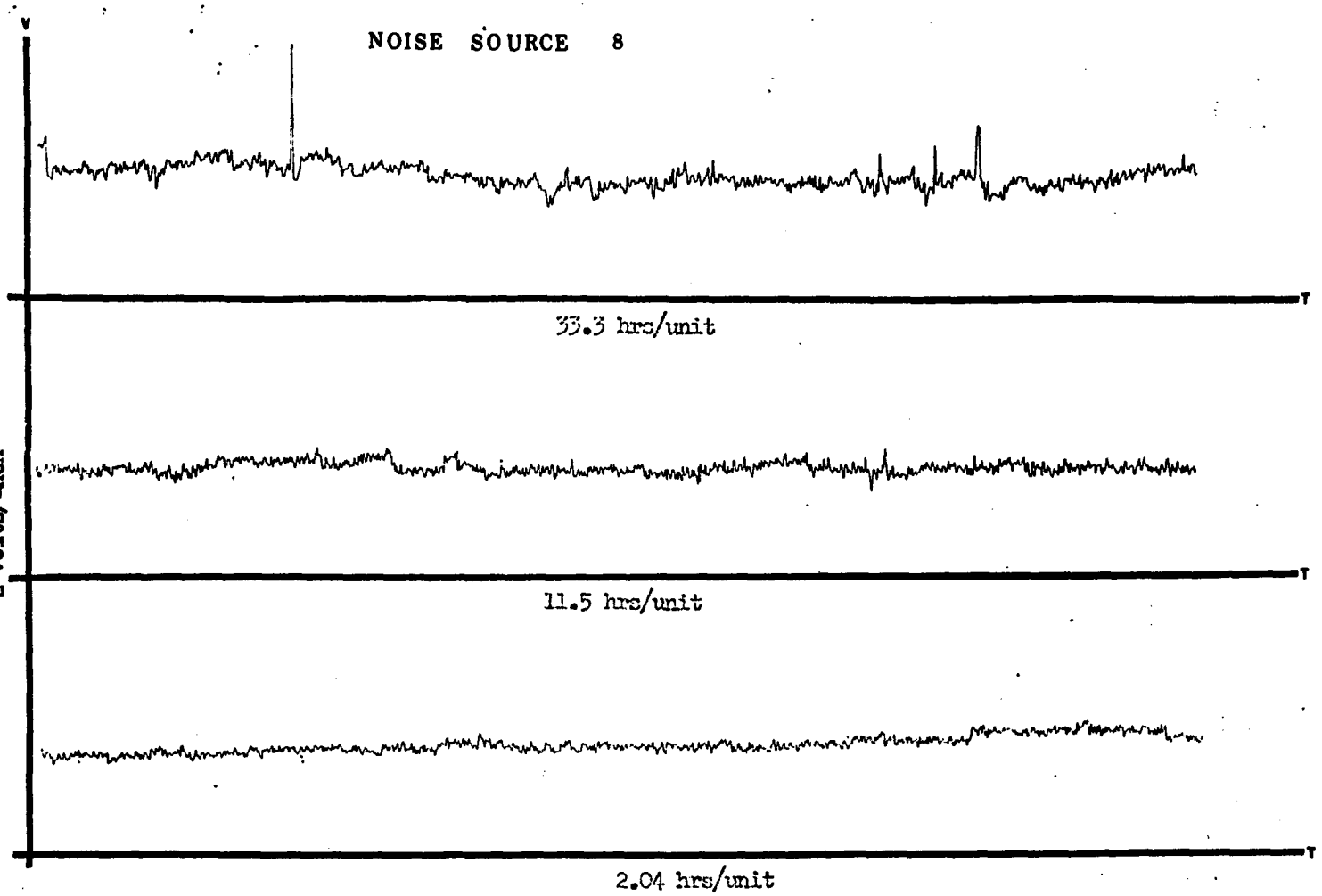
NOISE SOURCE 8
V
T
33.3 hrs/unit
2 Volts/Inch
11.5 hrs/unit
2.04 hrs/unit

Fig. 62

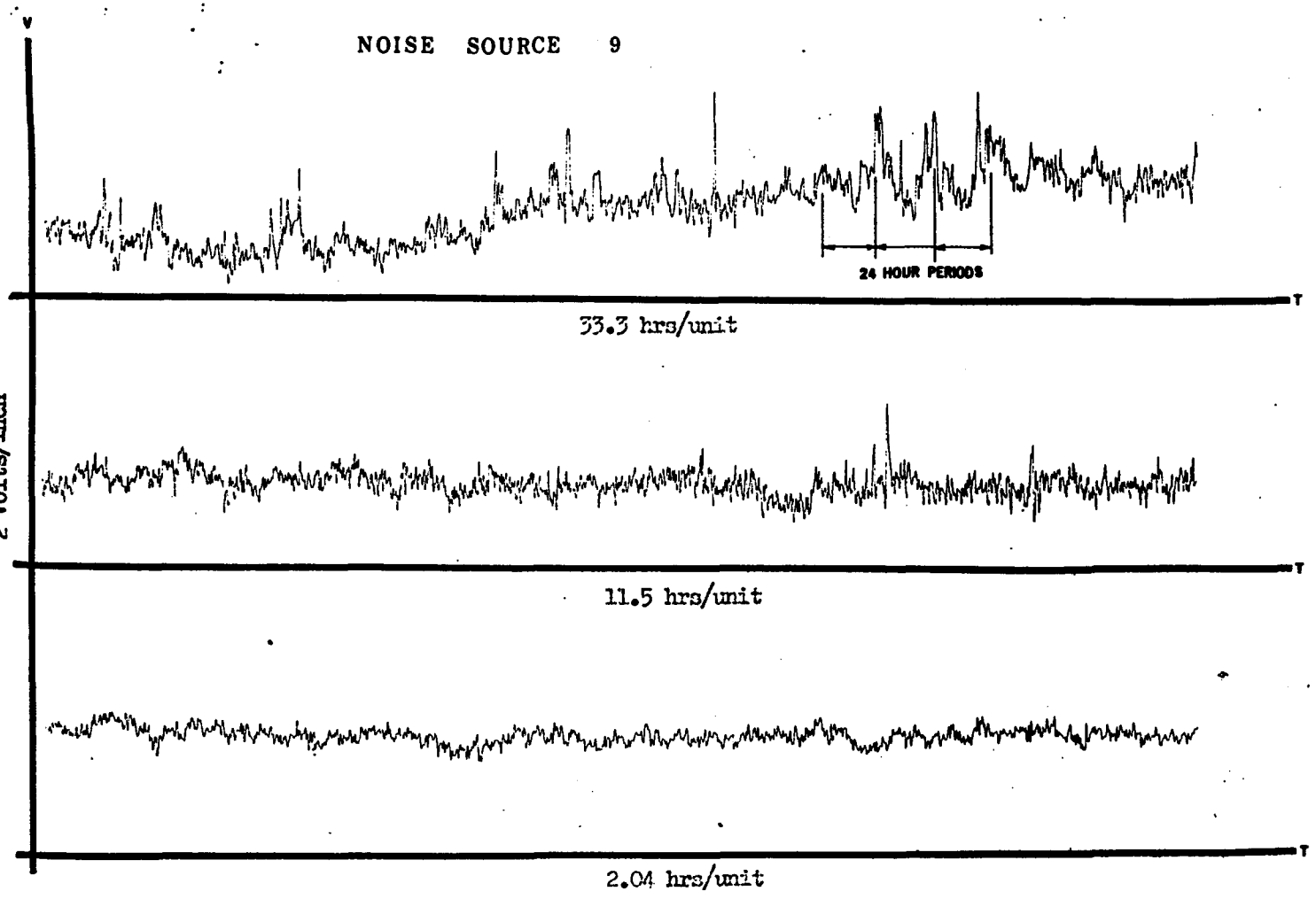
NOISE SOURCE 9
V
24 HOUR PERIODS
T
33.3 hrs/unit
2 Volts/Inch
T
11.5 hrs/unit
T
2.04 hrs/unit

Fig. 63

Fig. 64

2 Volts / Inch
NOISE SOURCE 10
24 HOUR PERIODS
22.3 hrs/unit
11.5 hrs/unit
2.04 hrs/unit

data outputs and preliminary spectral estimates did not indicate the presence of such bothersome biases.

A major series of data collecting runs were made at 5 different sampling rates*, each differing by an order of magnitude from the next**. In the interest of checking the variance of the results, the sampling rates were arranged so that at any one frequency in the range of interest there are exactly two available estimates, one or both of which may be just the line connecting two discrete adjacent frequencies at which estimates were made. The number of samples per noise source per run is about n = 1200. As the purpose of these experiments was to estimate reliably the very lowest frequencies' spectral densities, no effort was made to obtain estimates at any frequency which is higher than five decades above the lowest frequency considered. One reason why even such an extended frequency range was considered was to have solid evidence of the $K/|f|^{\alpha}$ behavior in high frequency estimates in order to accurately de-alias the lowest frequency estimates***; this argument can be invoked in support of obtaining still higher frequency estimates, but the aliasing effect is then almost absent due to the single low pass filter utilized. Of course, a five frequency-decade whose 3 db points were at 2 cps spectral estimate is

---

* $\Delta\tau$ = 1, 10, 100, 1000, and 10,000 sec for each source.

** Although the raw data outputs of these sources appear dissimilar, preliminary spectral estimates established that they all have similar spectra.

*** De-aliasing was done by the digital computer this time and was based on $K/f^{1.3}$ noise, where K was obtained through extrapolation at f = 1 cps; the technique of Section 5.3 was, naturally, used.

not redundant since it is not only the possibility of a low break-frequency (break in the K/f "law") which is of interest; the low-frequency spectral behavior as such is of just as much interest, too.

As indicated in Section 9.7, a rather extended sequence of steps is carried out, with various plotted auxiliary results being produced in the process, before the final "best" result (in the sense of Section 5.5) is determined. Each distinct sampling-rate run produced approximately 100 pages of computer-printout, a minimum of 10 raw data full page plots if the raw data contain no detectable errors, an additional 10 individual, aliased, spectral estimate plots, and one final de-aliased spectral density estimate plot; a total of 120, on the average, computer-generated pages are thus accumulated per sampling rate, or 600 pages for the entire experiment of five different sampling rates; a couple of hundred feet of chart recordings of the bath temperature is also produced by the Esterline Angus chart recorder to assure one of temperature stability without occupying any channel of the noise-source multiplexer. The quantities of greatest interest are:

a) All raw-data noise outputs.

b) The final spectral estimates, one for each sampling rate, all superimposed on the same sheet of graph paper.

c) Occasional records of peculiar behavior by the noise sources in support of arguments related to any otherwise inexplicable biases in the spectral density estimates.

Figures 65, 66, and 67, depict some of the raw data output of all noise sources on which the five final estimates are based.* Figures 68 through

Recorded Raw Noise Output.

Sampling Rate/Noise Source: 10 sec.
Number of Data Points/Source 1200.
Vertical Scale: 2 Volts per Inch.

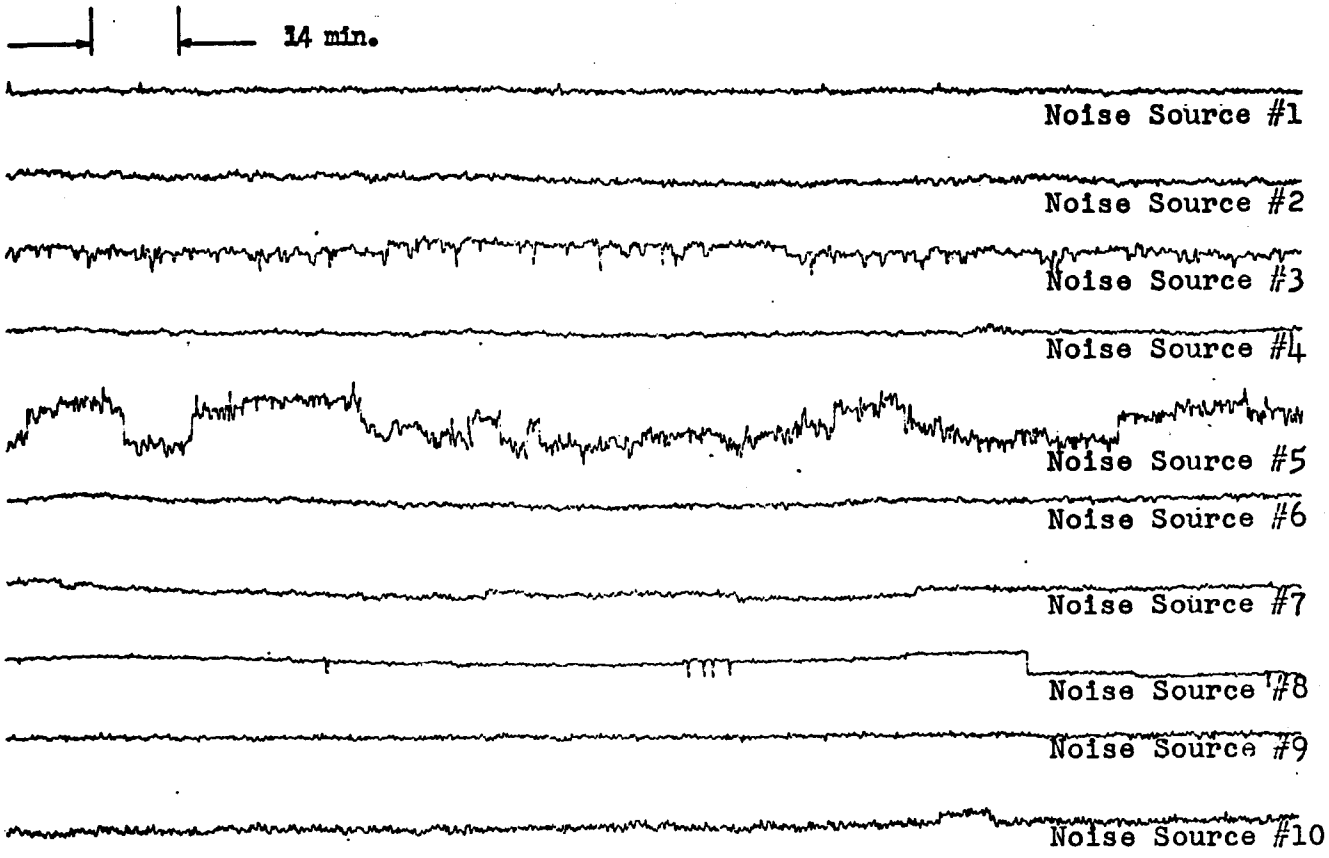

Figure 65

Recorded Raw Noise Output.

Sampling Rate per Noise Source: 100 sec
Number of Data Points/Noise Source 1200

Vertical Scale: 2 Volts per Inch.

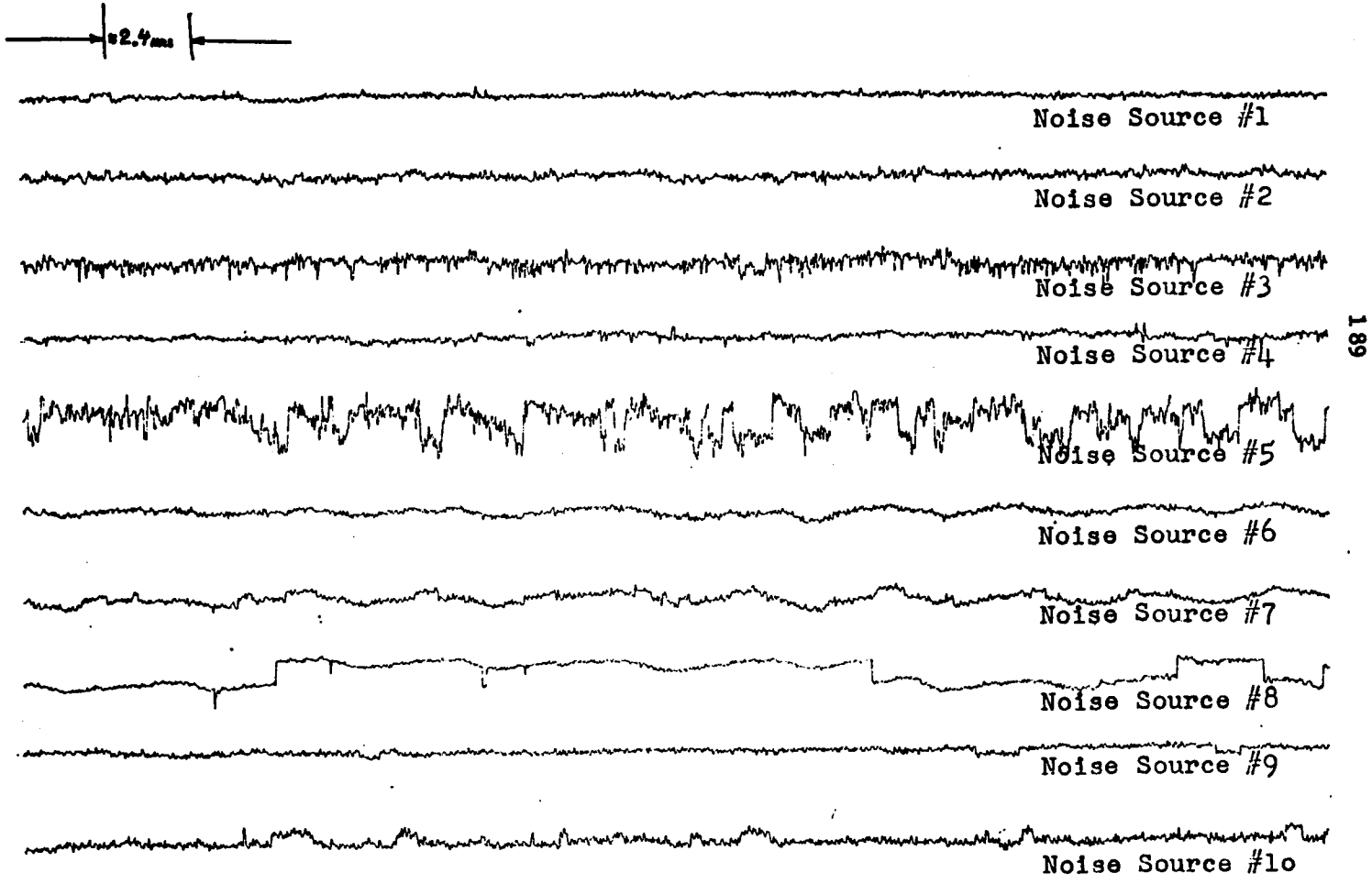

Figure 66

Sampling Rate per Noise Source: 1000 sec
Number of Data Points per Source: ≈ 1200

Recorded Raw Noise Output.

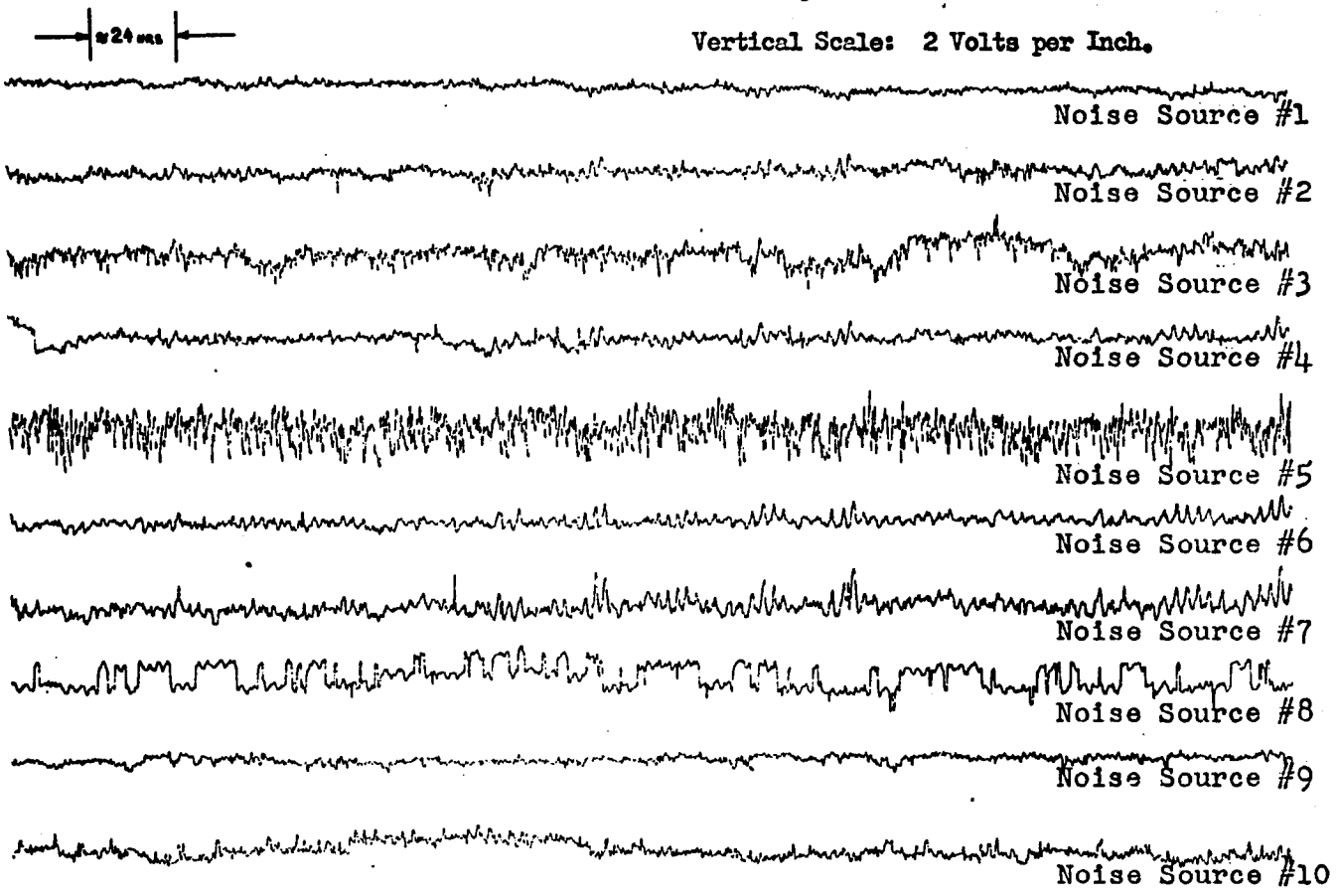

Figure 67

77 depict the aliased spectral density estimates for each of the 10 noise sources used in deriving the final, averaged spectral density estimate; it must be remembered that the variance associated with each of those individual estimates is approximately ten times as large as that of the final estimate. Figure 78 depicts the final dealiased spectral density estimate. Appendix B shows in detail how dealiasing was done by using the aliased spectral estimate of all individual noise source as an example.

10.3 Interpretations of Experimental Results of this Work

This final experimental result, depicted in Fig. 78, has the following interesting characteristic:

It depicts, for the first time, an estimate of the actual spectral characteristics of semiconductor flicker noise in the uncharted regions between 10^{-6} and $10^{-6.3}$ cps. The power spectrum appears to be of the $(1/f^{1.3})$ type over most of the frequency range, except the lowest decade where it appears to become a $(1/f^{1})$ spectrum.

The behavior, subject to variance considerations discussed below, is roughly $K/|f|^{\alpha}$ in character; this is still within the broad theoretical limits implied by the two major postulated models for flicker noise, i.e. the "physical" model which attributes the $1/f$ behavior to associated

ALIASED SPECTRAL DENSITY
ESTIMATES FOR NOISE SOURCE #1

10 log S(f) vs 10 log f

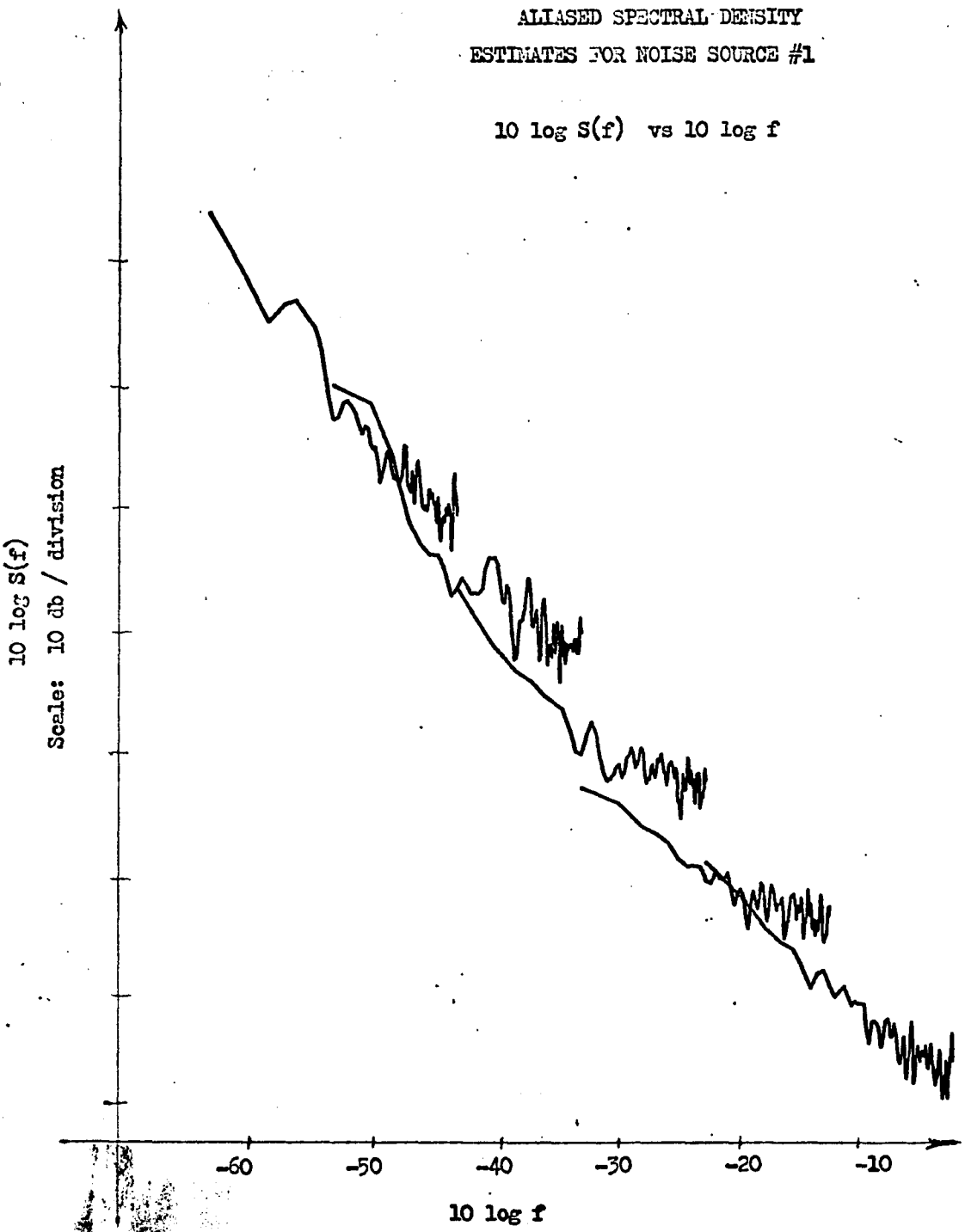

Fig. 68

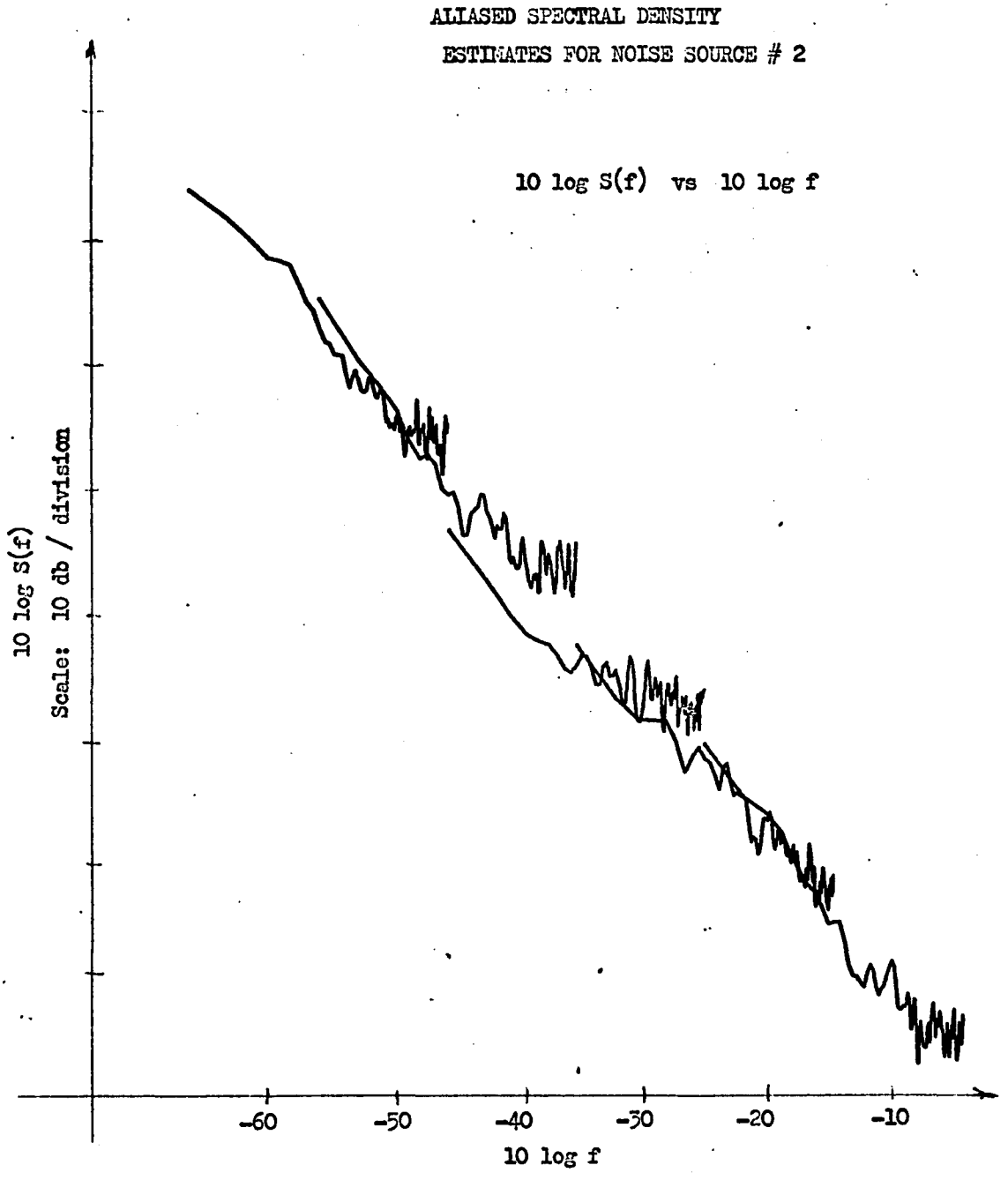
ALIASED SPECTRAL DENSITY
ESTIMATES FOR NOISE SOURCE # 2
10 log S(f) vs 10 log f
10 log S(f)
Scale: 10 db / division
-60
-50
-40
-30
-20
-10
10 log f

Fig. 69

ALIASED SPECTRAL DENSITY
ESTIMATES FOR NOISE SOURCE #3
10 log S(f) vs 10 log f

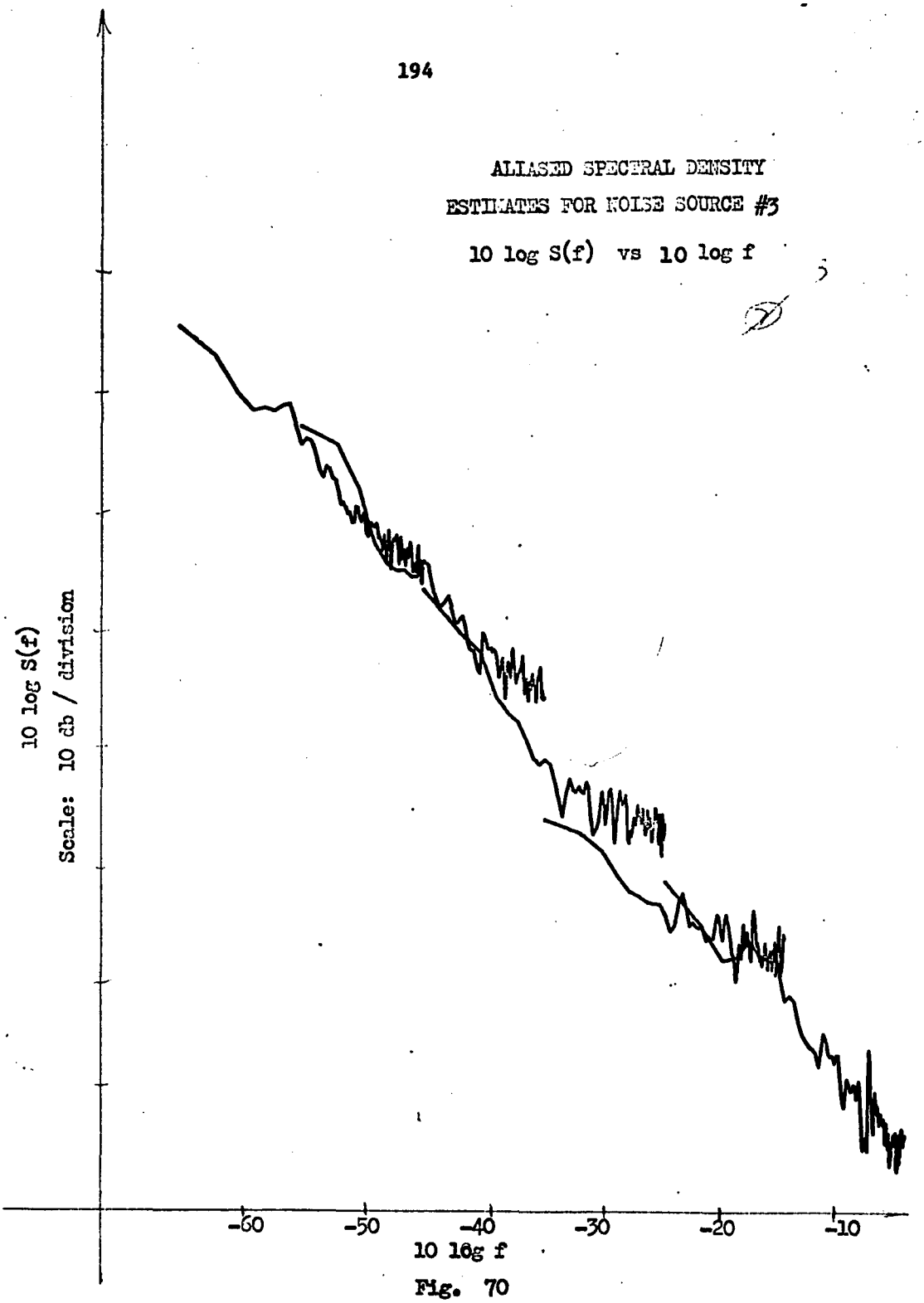

Fig. 70

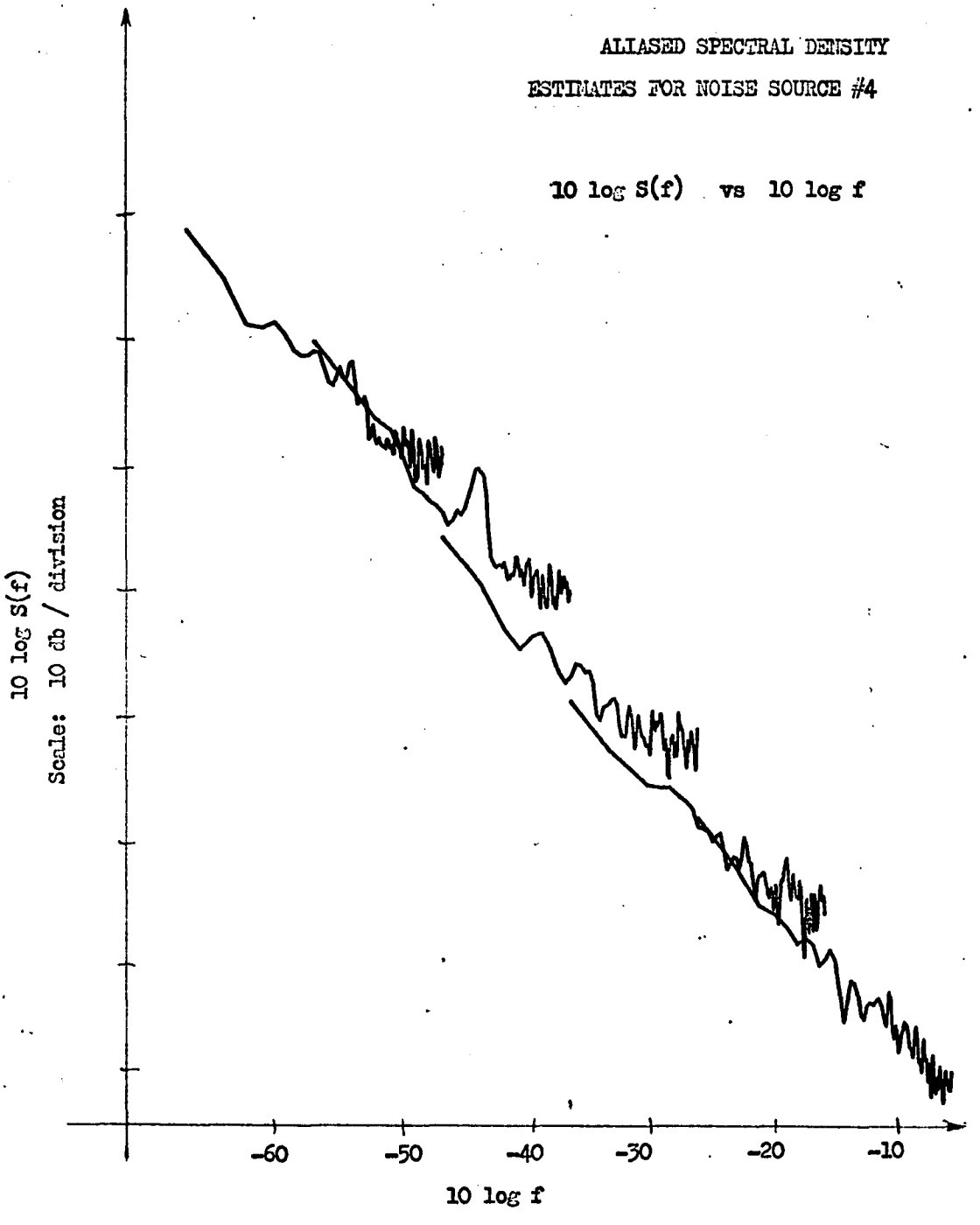
ALIASED SPECTRAL DENSITY
ESTIMATES FOR NOISE SOURCE #4
10 log S(f) vs 10 log f
10 log S(f)
Scale: 10 db / division
-60
-50
-40
-30
-20
-10
10 log f

Fig. 71

ALIASED SPECTRAL DENSITY
ESTIMATES FOR NOISE SOURCE #5

10 log S(f) vs 10 log f

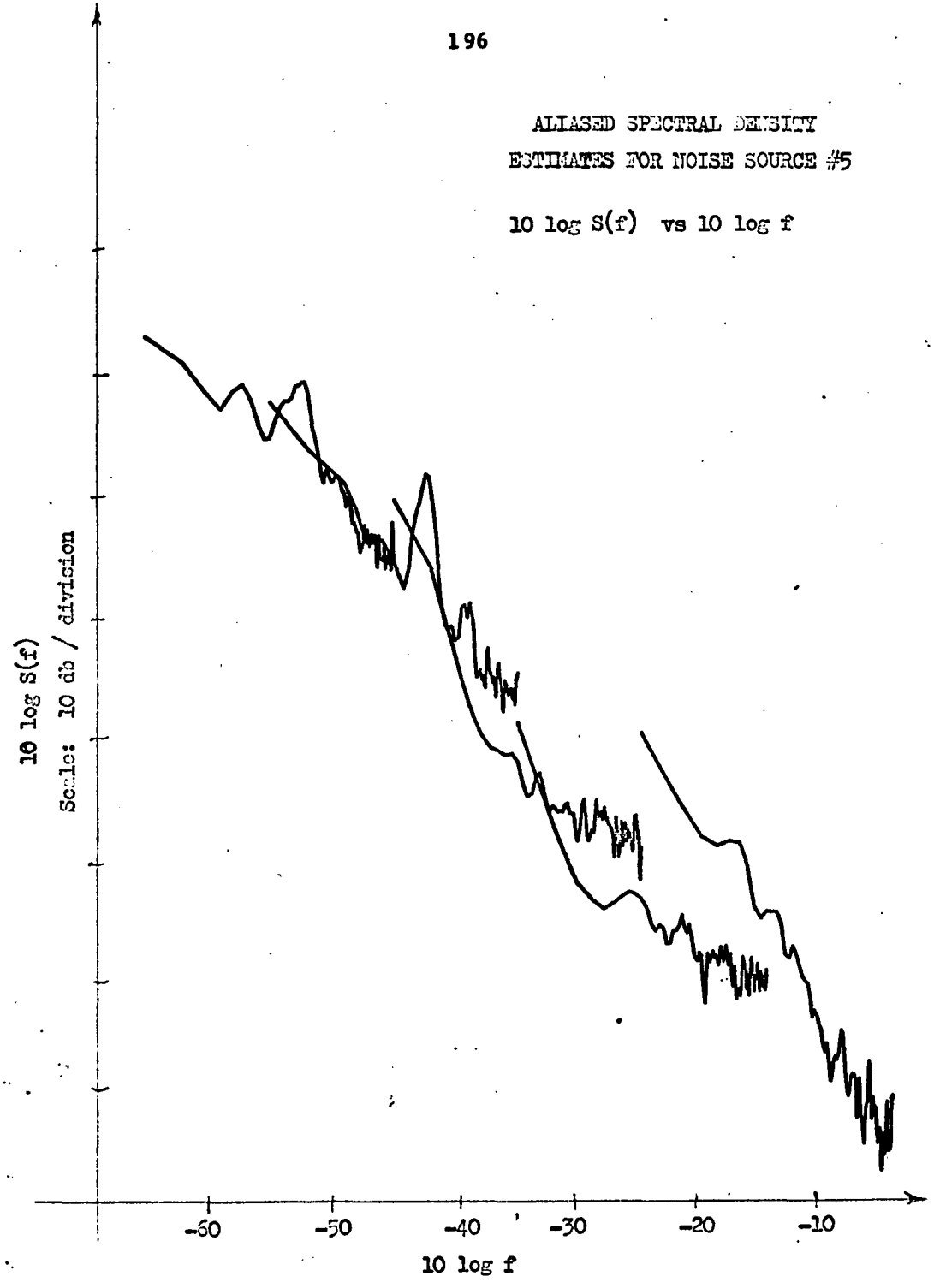

Fig. 72

ALIASED SPECTRAL DENSITY
ESTIMATES FOR NOISE SOURCE # 6.

10 log S(f) - vs 10 log f

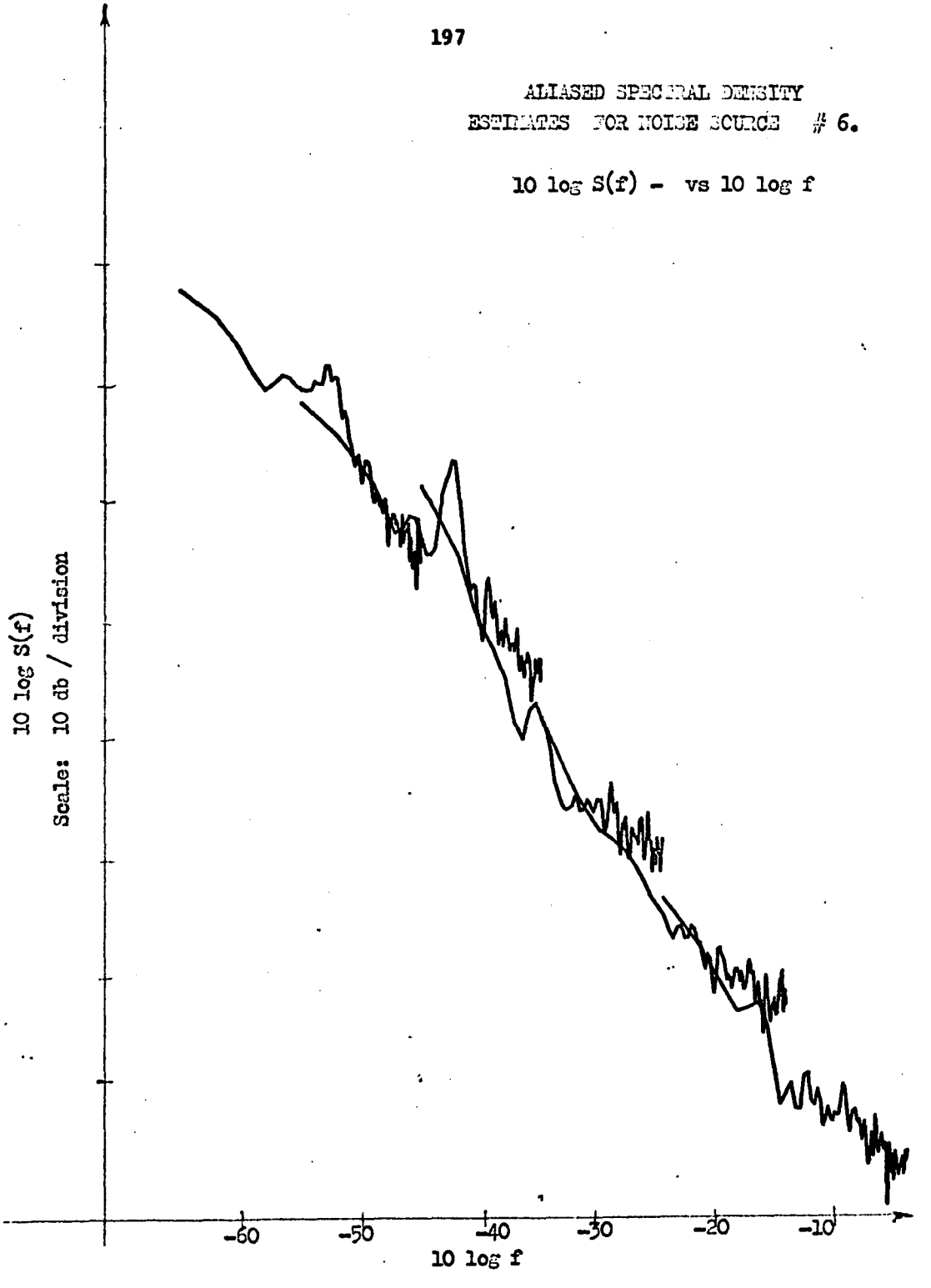

Fig. 73

ALIASED SPECTRAL DENSITY ESTIMATES
FOR NOISE SOURCE # 7

10 log S(f) vs 10 log f

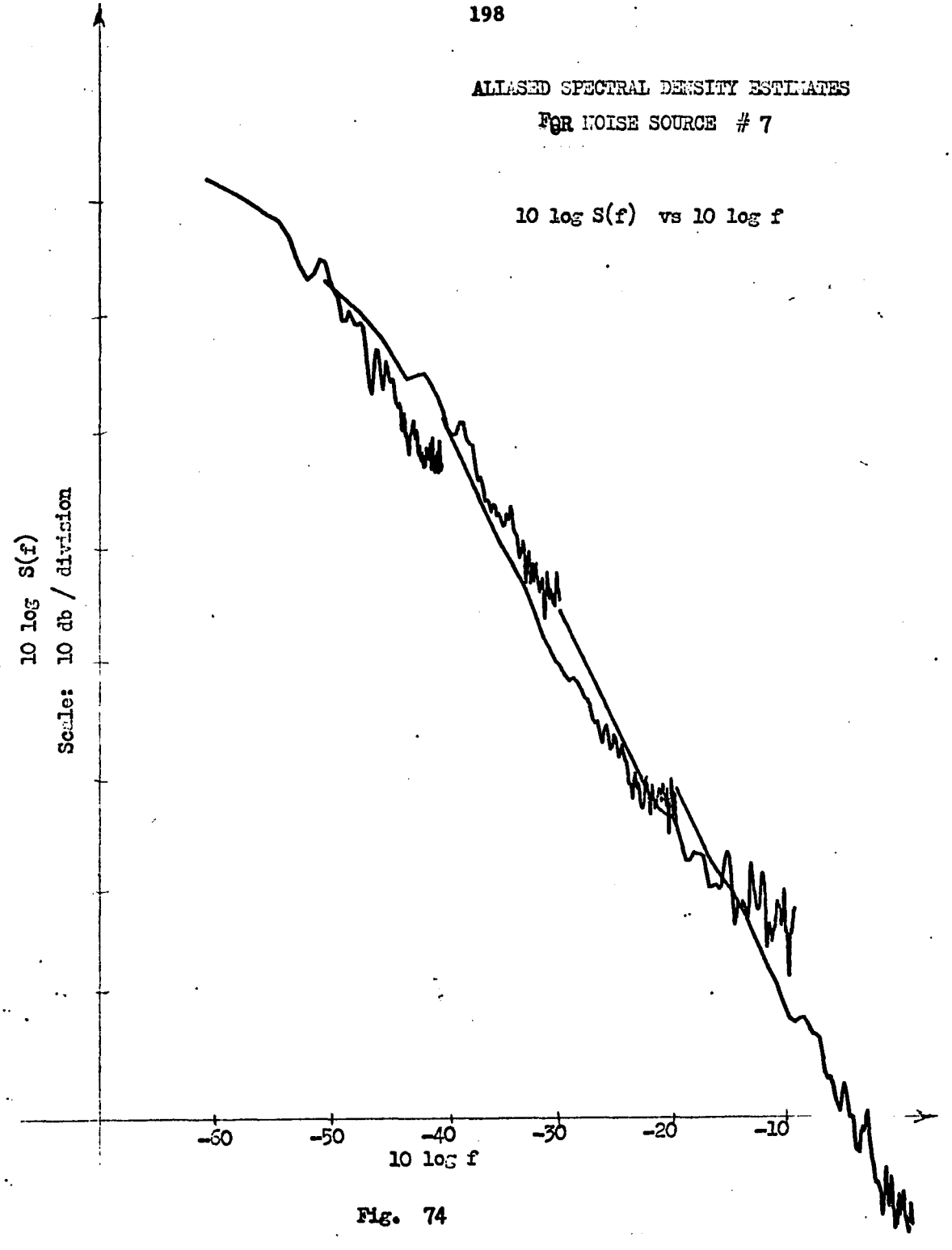

Fig. 74

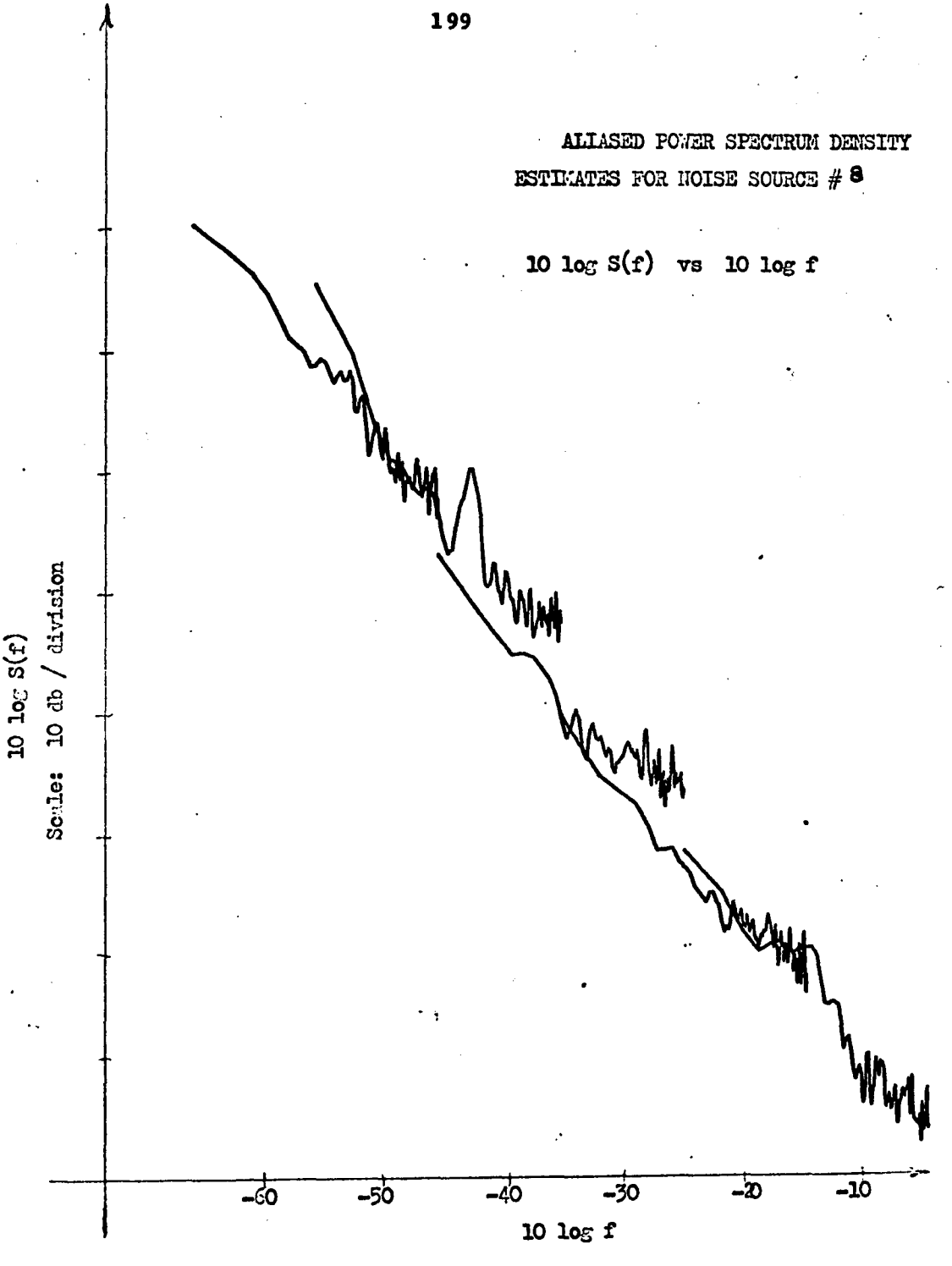
ALIASED POWER SPECTRUM DENSITY
ESTIMATES FOR NOISE SOURCE # 8
10 log S(f) vs 10 log f
10 log S(f)
Scale: 10 db / division
-60
-50
-40
-30
-20
-10
10 log f

Fig. 75

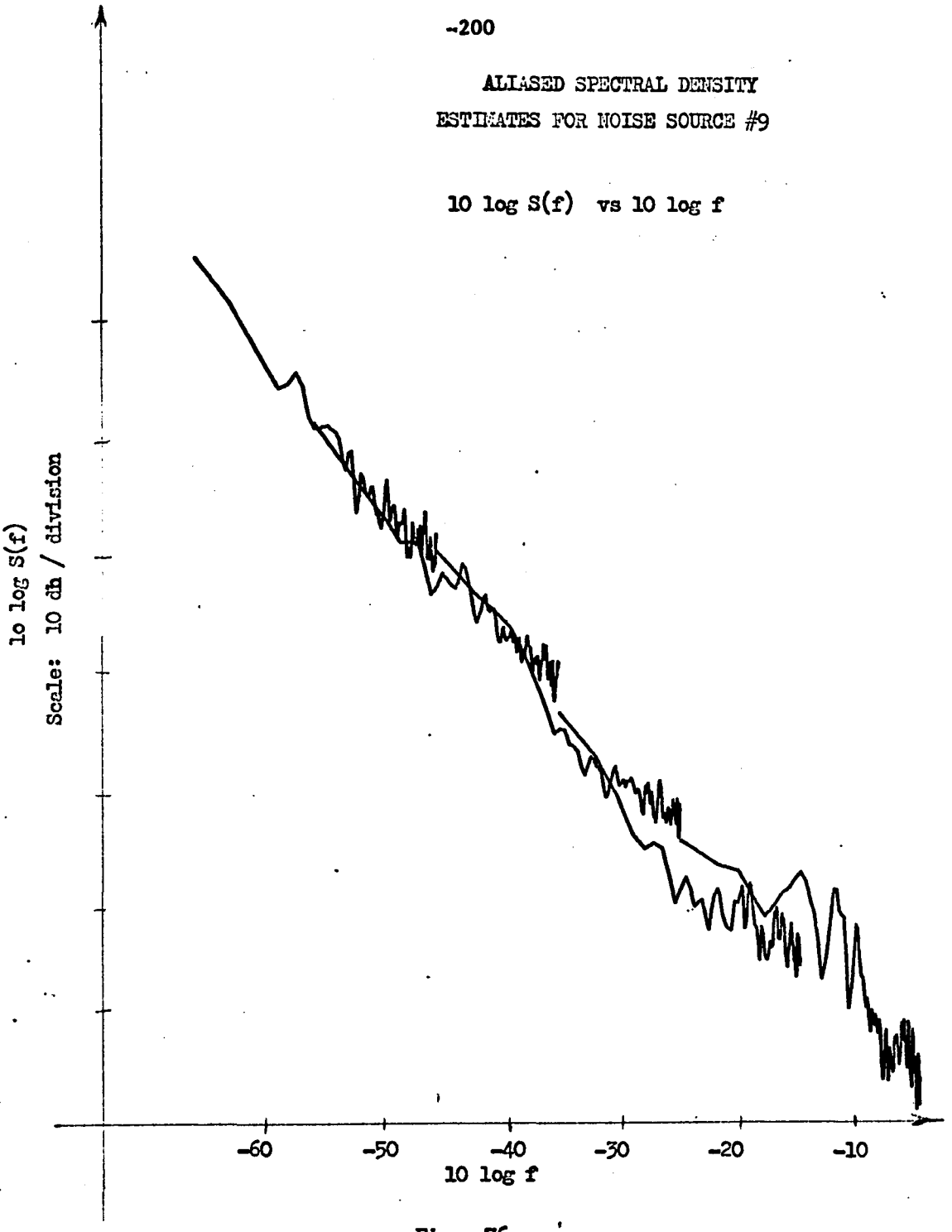
-200
ALIASED SPECTRAL DENSITY
ESTIMATES FOR NOISE SOURCE #9
10 log S(f) vs 10 log f
lo log S(f)
Scale: 10 db / division
-60
-50
-40
-30
-20
-10
10 log f

Fig. 76

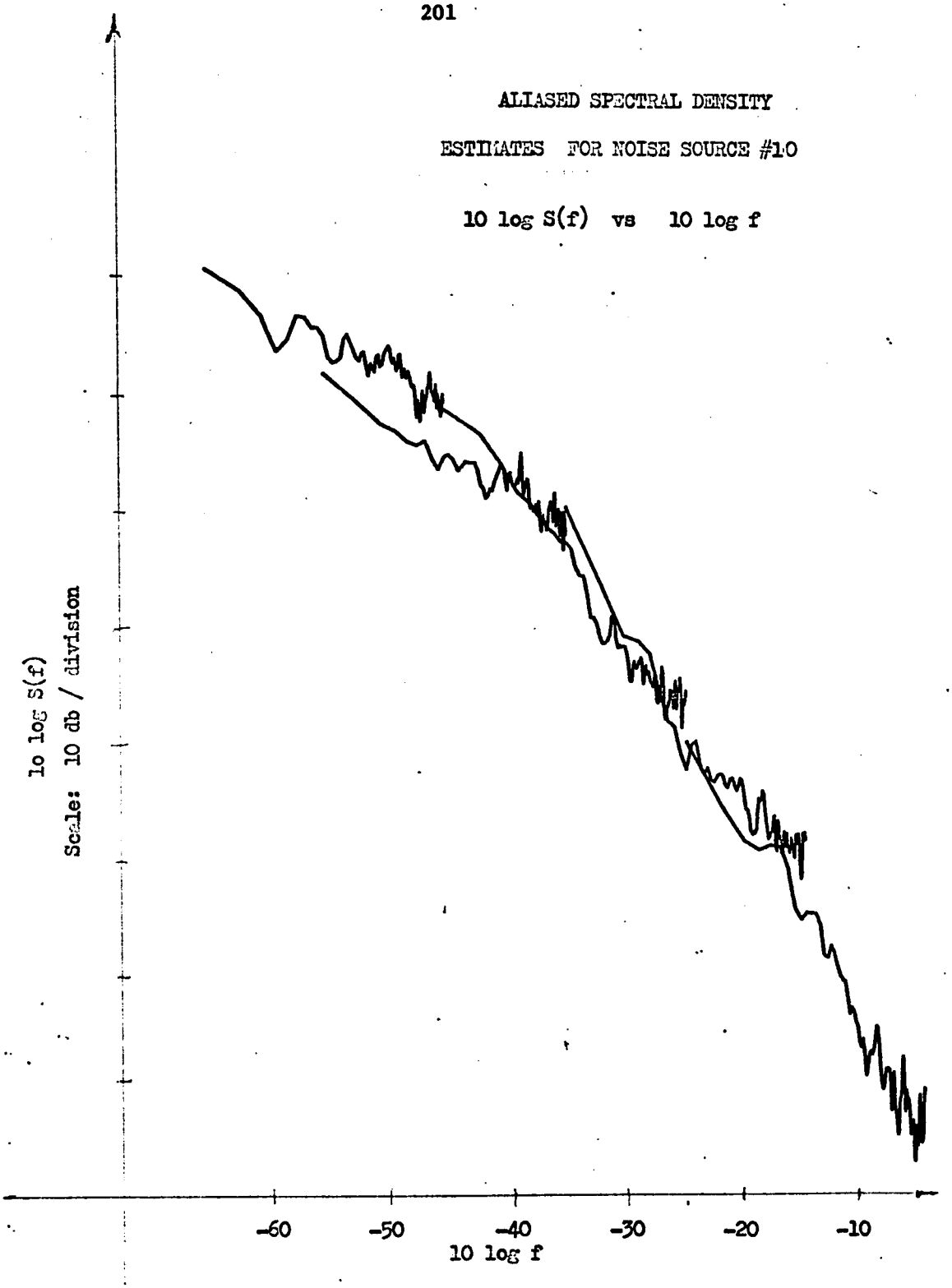
ALIASED SPECTRAL DENSITY
ESTIMATES FOR NOISE SOURCE #10
10 log S(f) vs 10 log f
10 log S(f)
Scale: 10 db / division
-60
-50
-40
-30
-20
-10
10 log f

Fig. 77

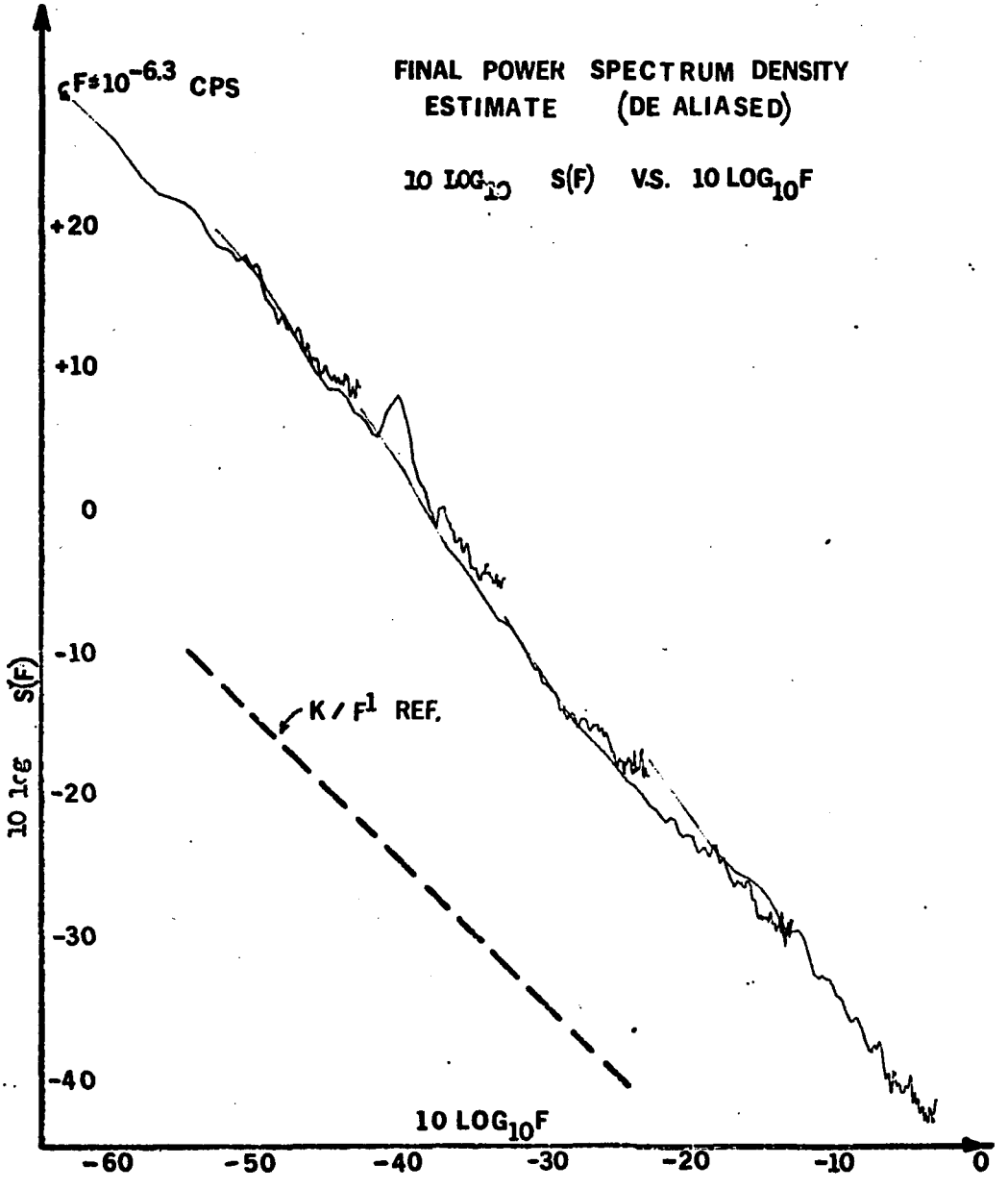
FINAL POWER SPECTRUM DENSITY
ESTIMATE (DE ALIASED)
10 LOG10 S(F) V.S. 10 LOG10F
F*10^-6.3 CPS
+20
+10
0
-10
-20
-30
-40
10 log S(F)
K / F^1 REF.
10 LOG10F
-60
-50
-40
-30
-20
-10
0

Fig. 78

long time-constants within the semiconductor lattice[1], and the "mathematical" model which views the 1/f behavior as a consequence of having used mathematics which are not applicable to the physical process under investigation.

In view of the theoretical results presented in this thesis in relation to the spectral estimate's variance, the experimental result of Fig. (78) can be expected to be within 17% of its average value, i.e. within ± 2.3 db, only 68% of the time. A subtle point worth mentioning is that "time" is also logarithmically rather than linearly depicted on the log-log scales of Fig. (78); that is, the linear length of the log-log plot of Fig. (78) is not proportional to the "time" that an estimate is expected to be within a certain band.

Two specific comments on the results of Fig. (78) are in order now before any conclusions can be drawn:

a) The apparently disturbing difference between the two estimates at $f \approx 10^{-4}$ cps is indeed explicable with the help of the individual spectral estimates of Figures (68) through (77). The spectral peak shown by one of the two estimates is a valid one, and it is present in the individual spectral estimates in varying degrees; the physical cause for it has been already identified earlier in this thesis. The reason why this spectral peak is not easily identifiable on the "lower" estimate in the plots is a matter of resolution: as it has been shown by Blakemore[25], the Blackman/Tukey estimator creates distortion in the detection and reproduction of narrow spectral peaks.

b) The entire graph, including the aforementioned region around

10^{-4} cps, is well within the theoretical limit of the variance established in this work.

It is interesting to discuss at this point why the theoretically predicted divergence of the variance of the spectral estimate of unprewhitened 1/f noise does not in fact appear in the experimental results pertaining to unprewhitened spectra. There can basically be three explanations given for this apparent discrepancy:

1) The variance is a statistical average and, consequently, the spectral variance need not diverge in any particular estimate or group of estimates.

2) The variance cannot be observed because the theoretically predicted divergence in this thesis did not take into consideration the actual algorithm used in collecting and processing the data.

3) The variance cannot be observed because of the inherent limitations of the noise source amplifiers and of the measuring equipment which would "clip" any data sample outside a given range.

While the first of the above explanations is, in principle, correct, it is not the only reason why the unprewhitened experimental results of this thesis do not seem to have an infinite spectral variance. In fact, the variance of the spectral estimates of unprewhitened 1/f noise obtained in the manner described in this thesis cannot be infinite.

It is, indeed, true that if one or more raw data samples were of infinite value the resulting spectral variance would be infinite; this cannot occur in an actual experimental situation, however, because any such value will be "clipped" by the noise source amplifiers or by the measuring equipment. Such clipping however, would register in the

raw data output as a readily distinguishable spike, and this was, in fact, never observed.

By far the most subtle reason why the spectral variance can never diverge if the data are processed in the manner described in this work is the algorithm itself. Specifically, the mean value of any one given noise source was approximately reset to a predetermined constant prior to each data-collecting run; any noise effect whose frequency is low enough to appear disguised as a drifting-mean is thus removed even before the data are recorded; the effect is the same as if a constant mean is removed from a prewhitened set of data points: the power spectrum of the noise source is effectively truncated at some very low frequency in the manner analyzed in detail in Ref. (25). It has been shown in the present work that a truncated $1/f$ process has spectral estimates whose variance does not diverge.

While it seems desirable, from a theoretical viewpoint, to never reset the mean value of a given noise source's output, significant experimental difficulties can be encountered if this is not done; these difficulties include the possibilities that:

a) the noise source's mean change is a result due to environmental only parameters; such a drift can only degrade the final spectral estimate.

b) The noise source's mean change is indeed a manifestation of very low frequency noise, but the amount of the change is such that the noise source is driven out of its linear operating region and into saturation.

CHAPTER 11

FURTHER WORK

Despite the time-saving benefits of time-multiplexing, first introduced in spectral estimation in this work, it appears that spectral estimates at a frequency substantially lower than the one presented in this work are not too likely to be calculated in the foreseeable future because of the data-taking times involved.

Optimization of a parameter of one's personal choice such as alias-free sampling through nonrandom sampling, or high resolution in frequency have been studied in detail only to show that data-reduction costs reach disproportionate levels.

One promising area for further work may cover the domain of recording only the zero-crossing times of the low-pass filtered stochastic process in question; the associated complexity of the experimental set-up need not be high at all; the mathematics for such a new data-processing algorithm may be quite challenging, though.

The growing popularity of the "Fast Fourier Transform" which is still in its developmental stage, suggests that faster data-processing technologies may later bring to actual life such rather exotic techniques as semirandom sampling. Indeed, there is a great demand for fast spectral analyses: Doppler-radar measurements of orbital objects or traffic, and seismic exploration are typical examples.

Many theoretical problems, some raised by results in this thesis, are of interest: Is there a physical law that explains why

the variance of a true $1/f'$ noise is infinite, while that of a $1/(f^{1-\delta})$ is not? Is there a physically underlying principle behind the multiplicity of natural processes exhibiting $1/f$ noise? This thesis has gone into considerable theoretical and experimental depth to answer some questions; in the process is has raised new ones of even greater interest.

Appendix A

Summary of the Computer Simulation of the Temperature Characteristics of the Noise Sources' Container

The heat equation is a distributed-parameter equation, and its infinite series solution is well known to converge notoriously slowly. A lumped-parameter model was thus substituted using electrical passive circuit elements, and it was this model which was simulated with the digital computer.

Realizing that a closed container behaves basically like a low-pass filter, a three-stage RC filter was analyzed whose six parameters were appropriately defined. An infinite cascade of RC's could provide an exact equivalent to the heat equation; a three-stage model, however, was chosen for the following reasons:

a) Its unit-step response could be easily obtained.

b) It successfully modeled the frequency fall-off obtained from the heat equation analytically.

c) It successfully modeled the three main layers of the actual container: the external polyethylene bag, the epoxy layer, and the air space.

The parameters of the three resistors and three capacitors were defined so as to match the true "low-pass" character obtained analytically from the heat equation*.

---

* The analytic expression giving the ratio of the amplitude of the exciting stimulus and that of the response as a function of angular frequency was actually used. This expression was derived in Section 6.1.3.

The circuit is

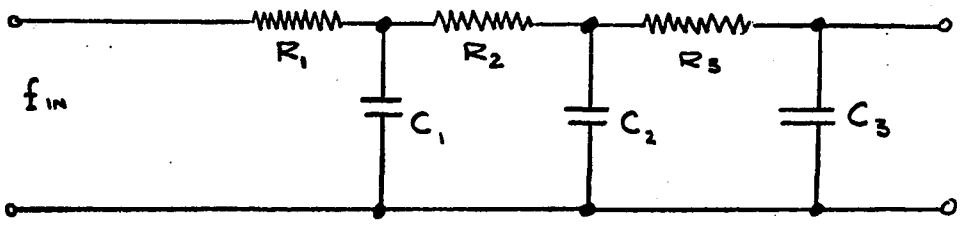

Defining

$R(t - \tau_k)$ = response of network at time t to unit step occurring at time $\tau_k \leq t$

and realizing that the quantity desired is the overall response to many successive step-stimuli of varying amplitudes, we can write

$$f(t=\tau_k) = \delta f_{in}(\tau_1)R(t-\tau_1) + \delta f_{in}(\tau_2)R(t-\tau_2) + \cdots \delta f(\tau_k)R(0)$$

where $R(0) = 0$ for realizability reasons. This can be rewritten as

$$f_{out}(t) = \sum_{k=1}^{t=\tau_k} [\delta f_{in}(\tau_k)]\ [R(t-\tau_k)]$$

The computer program implements exactly this last equation.

The quantity R is of some interest since it really involves solving a cascade of linear differential equations, one per stage.

For the first stage

$$\frac{dq}{dt} + \frac{1}{RC}\, q(t) = \frac{1}{R}\, e(t), \quad \text{where} \quad e(t) = \text{unit step.}$$

Using $\mu(t) = e^{t/RC}$ as integrating factor gives $V_1(t) = 1-e^{-t/RC}$. Using $V_1(t)$ as a forcing-term to obtain the output from the second stage gives

$$V_2(t) = 1 - \left(\frac{R_1C_1}{R_1C_1-R_2C_2}\right)e^{-t/R_1C_1} + \left(\frac{R_2C_2}{R_1C_1-R_2C_2}\right)e^{-t/R_2C_2}$$

Repeating the procedure once again with considerable algebraic manipulations yields

$$V_3(t) = 1 - \frac{(R_1C_1)^2}{(R_1C_1-R_2C_2)(R_1C_1-R_3C_3)}\, e^{-t/R_1C_1} -$$

$$\frac{(R_2C_2)^2}{(R_2C_2-R_1C_1)(R_2C_2-R_3C_3)}\, e^{-t/R_2C_2} -$$

$$\frac{R_3C_3}{(R_3C_3-R_1C_1)(R_3C_3-R_2C_2)}\, e^{-t/R_3C_3}$$

This concludes the essential derivations associated with this otherwise peripheral part of this work.

Appendix B

The aliased spectral estimates of the ten noise sources on which the final spectral estimate of Fig. 78 is based, were shown in Figures 68 through 77. This appendix focuses on the dealiasing requirements dictated by the particular low-pass filter used in the experimental runs which produced the final spectral estimate.

The following points are of interest in properly interpreting the discussion of this appendix:

a) The variance of the spectral estimate of any one source is approximately 10 times as large as that of the final averaged estimate. Specifically, for any one noise source

$$\frac{\sqrt{\text{var } S_i(f_j)}}{\overline{S_i(f_j)}} \simeq \sqrt{3x \frac{T_M}{T_N}} \simeq \sqrt{.30} \simeq .56$$

i.e., for a gaussianly distributed random variable $S_j(f_i)$ the estimate must be within 56% of its average value 68% of the time. (This applies to the dealiased estimate).

b) In view of the large variance of the estimate for any one source, and for computational economy, one dealiasing was performed on the aliased final spectral density estimate rather than one dealiasing for each noise source separately. This was done only after visually inspecting the 10 individual spectral estimates for the purpose of being assured that they were all similar in functional form. The dealiasing procedure shown in this appendix is to illustrate the

procedure used on the final estimate.

c) Dealiasing of the final estimate was done by the digital computer in view of the extensive summations required. The arithmetic results shown in this appendix are only approximate, although the mathematical procedure is the same.

d) A single R.C. filter was used for all data runs; its 3 db point was selected to be at 2 cps. As shown below, this results in a progressively larger aliasing effect as the sampling rate is decreased, especially on the "high frequency portion" of each data run's spectral estimate.

The aliasing effect will now be examined on each of the five sampling rates, given that the same low-pass filter was used for all. Since the summations involved are so extensive, a quantitative measure of the effect of aliasing will be given for the spectral estimates at the lowest and at the highest frequencies at which spectral estimates were obtained from each data run.

The fundamental aliasing equation has been shown to be

$$S_{\text{aliased}}(f) = S_{\text{true}}(f) + \sum_{q=1}^{\infty} S_{\text{true}}\left(\frac{q}{\Delta\tau} - f\right) + S_{\text{true}}\left(\frac{q}{\Delta\tau} + f\right)$$

Each sampling rate will be considered individually:

1a. Sampling Rate = 1 sample per second

If the true spectrum is K/f, the magnitude at the highest frequency at which an estimate is made is

$$\frac{K}{1/(2\Delta\tau)} = 2K = S_{true}(.5 \text{ cps})$$

$$S_{aliased}(f = \frac{1}{2\Delta\tau}) = S(.5) + S(.5) + S(1\tfrac{1}{2}) + S(1\tfrac{1}{2}) + S(2\tfrac{1}{2}) + \cdots$$

$$= 2K + 2K + \frac{2K}{3} + \frac{2K}{3} + \frac{2K}{5} + \cdots$$

$$= 2K \left\{2[1 + \frac{1}{3} + \frac{1}{5} + \frac{1}{7} + \frac{1}{9} + \cdots]\right\}$$

Approximating the R.C..filter for illustrative purposes as a cutoff filter at 3 cps, yields

$$S_{aliased}(.5) = S_{true}(.5) \left\{2[1 + \frac{1}{3} + \frac{1}{5}] = 3.1\right\} \qquad \text{(B.1)}$$

But 10 log(3.1) ≃ 5 db, hence a 5 db increase is to be expected at the high-frequency end of the estimate.

1b. Sampling Rate = 1/10 samples per second

Highest frequency estimate at f = .05 cps, with true magnitude $K/(1/2\Delta\tau) = 20K$.

$$S_{aliased}(.05) \tilde{=} S_{true}(.05) \left\{2[1 + \frac{1}{3} + \frac{1}{5} + \cdots + \frac{1}{59}]\right\}$$

where the approximating assumption was made again that the low pass filter is a cutoff filter at 3 cps. Then,

$$10 \log \left\{2[1 + \frac{1}{3} + \frac{1}{5} + \cdots + \frac{1}{59}]\right\} \simeq 7.1 \qquad \text{(B.2)}$$

Thus a 7.1 db increase is to be expected at the high-frequency end of this estimate.

1c. Sampling Rates: 1/100, 1/1000, 1/10000 samples per second

A similar analysis can be extended to these lower sampling rates; each such analysis involves a summation of ten times as many additive terms in equations of the form (B.1), (B.2), as the number of additive terms corresponding to the next highest sampling rate. The overall results are:

3.1 db are attributable to aliasing at $f = .5$ cps for $\Delta\tau = 1$ sec

7.1 db are attributable to aliasing at $f = .05$ cps for $\Delta\tau = 10$ "

8.8 db are attributable to aliasing at $f = .005$ cps for $\Delta\tau = 100$ "

10.0 db are attributable to aliasing at $f = .0005$ cps for $\Delta\tau = 1000$"

10.9 db are attributable to aliasing at $f = .00005$ cps for $\Delta\tau = 10000$"

A brief look at Figures 69 and 70 suggests that these quantities are indeed plausible within the increased variance limits for individual noise sources discussed above.

The effect of aliasing on the low-frequency end of each data run will be examined next.

2a. Sampling Rate = 1 sample per second

The lowest frequency at which an estimate is made is $1/[100 \cdot 2\Delta\tau] = 5 \times 10^{-3}$ cps; assuming again a true spectrum of K/f implies

$$S_{true}(5 \times 10^{-3} \text{ cps}) = 200K$$

$$S_{aliased}(5 \times 10^{-3}) = S(.005) + S(1 - .005) + S(1 + .005) + S(2 - .005) + S(2 + .005) + \cdots$$

$$S_{aliased}(5\times 10^{-3}) \simeq 200K + 2K[1 + \frac{1}{2} + \frac{1}{3} + \frac{1}{4} + \cdots] \qquad (B.3)$$

Invoking again the assumption that we have a cutoff filter at 3 cps yields

$$S_{aliased}(5\times 10^{-3}) \simeq 200K + 3.6K$$

i.e., the estimate is expected to be 1.8% larger, which on a logarithmic scale is less than .1 db.*

2b. Sampling Rates: 1/10, 1/100, 1/1000, 1/10000 samples per second

Similar considerations can be applied to the low-frequency ends of the remaining four sampling rates; the effect, again, is an increase in the number of additive terms in equations analogous to (B.3). The results are

		For $\Delta\tau$= (sec)
1.8% increase (.08 db) is due to aliasing and	$f = 5\times 10^{-3}$ cps	1
3.8% increase (.16 db) is due to aliasing and	$f = 5\times 10^{-4}$ cps	10
6.1% increase (.26 db) is due to aliasing and	$f = 5\times 10^{-5}$ cps	100
9.5% increase (.39 db) is due to aliasing and	$f = 5\times 10^{-6}$ cps	1000
12.9% increase (.53 db) is due to aliasing and	$f = 5\times 10^{-7}$ cps	10000

These quantities are quite small in a logarithmic scale, but are nonetheless compensated for in the actual dealiasing of the final spectral density estimate performed by the digital computer.

*This effect was, nonetheless, removed in the actual dealiasing performed by the digital computer.

(Dealiasing was done on each and every estimate for the result of Fig. 78). The program did not assume a sharp cutoff filter but, instead took into consideration the actual attenuation characteristics of the RC filter.

REFERENCES

1. A. van der Ziel, "Noise in Solid State Devices and Lasers", Proc. IEEE, Vol. 58, pp. 1178-1207, August 1970.

2. A. van der Ziel, "Carrier Density Fluctuation Noise in Field Effect Transistors", Proc. IEEE, Vol. 51, pp. 1670-1671.

3. J. B. Johnson, "The Schottky Effect in Low Frequency Circuits", Phys. Rev., Vol. 26, pp. 71-85, July 1925.

4. W. R. Attkinson, L. Fey, J. Newman, "Spectrum Analysis of Extremely Low Frequency Variations of Quartz Oscillations", Proc. IEEE, Vol. 51, p. 379, February 1963.

5. J. Brophy, "Statistics of 1/f Noise", Phys. Rev., Vol. 166, pp. 827-831, February 1968.

6. R. F. Borges, et al., "Valve and Circuit Noise", Radio Research Special Report 20, London: His Majesty's Stationary Office 1951.

7. A. van der Ziel, "Carrier Density Fluctuation Noise in Field Effect Transistors", Proc. IEEE, Vol. 51, pp. 1670-1671, November 1963.

8. A. van der Ziel, "Fluctuation Phenomena in Semiconductors", New York Academic Press, 1959.

9. A. van der Ziel, "Noise", Englewood Cliffs, N.J., Prentice Hall, 1954.

10. J. Bernamont, "Fluctuations in the Resistance of Thin Films", Proc. Phys. Soc., Vol. 49 (Suppl.) pp. 138-139, July 1937.

11. H. E. Derksen and A. Verveen, "Fluctuations of Resting Neural Membrane Potential", Science, Vol. 151, pp. 1388-1399, March 18, 1966.

12. D. Brouwer, "A Study of the Changes in the Rate of Rotation of the Earth", Astron. J., Vol. 57, pp. 125-146, September 1952.

13. H. V. Cottony and J. R. Johler, "Cosmic Radio Noise Intensities in the VHF Band", Proc. IRE, Vol. 40, pp. 1053-1060, September 1912.

14. D. Halford, "A General Mechanical Model for f Spectral Density Random Noise with Special Reference to Flicker Noise 1/f ", Proc. IEEE, Vol. 56, pp. 251-257, March 1968.

15. L. Cutler and C. Searle, "Some Aspects of the Theory and Measurement of Frequency Fluctuations in Frequency Standards", Proc. IEEE, Vol. 54, pp. 221-230, February 1966.

16. J. A. Barnes, "Atomic Timekeeping and the Statistics of Precision Signal Generators", Proc. IEEE, Vol. 54, pp. 207-220, February 1966.

17. D. W. Allan, "Statistics of Atomic Frequency Standards", Proc. IEEE, Vol. 54, pp. 221-230, February 1966.

18. A. L. McWhorter, "1/f Noise and Germanium Surface Properties", Semiconductor Surface Physics, R. H. Kingston, Ed., U. Pa. Press, 1956.

19. W. H. Fonger, "A Determination of 1/f Noise Sources in Semiconductor Diodes and Transistors", in "Transistors", Princeton, N.J., pp. 239-297.

20. T. B. Watkins, "1/f Noise in Germanium Devices", Proc. Phys. Soc. London, pt. 1, Vol. 73, pp. 59-68, January 1959.

21. D. Halford, "1/f Noise", Proc. IEEE, Vol. 56, March '68.

22. J. A. Barnes and D. W. Allan, "Statistical Model of Flicker Noise", Proc. IEEE, Vol. 54, pp. 176-178, February 1966.

23. B. Mandelbrot, "Some Noises with 1/f Spectrum, A Bridge Between Direct Current and White Noise", IEEE Trans. Vol. 17-13, pp 289-298, April '67.

24. R. B. Blackman and J. W. Tukey, "The Measurement of Power Spectra", New York: Dover, 1959.

25. D. Blakemore, "Microcycle Spectral Estimation", Ph.D. Thesis, Caltech, 1966.

26. Bingham, Godfrey and Tukey, "Modern Techniques of Power Spectrum Estimation", IEEE Trans., Vol. AU 15, No. 2, June 1967.

27. W. Davenbort, Jr., and W. Root, "An Introduction to the Theory of Random Signals and Noise", McGraw Hill, New York 1958.

28. A. Papoulis, "Probability, Random Variables, and Stochastic Processes". McGraw-Hill, New York, 1965, pp. 326-334.

29. A. Mood, "An Introduction to the Theory of Statistics", McGraw-Hill Book Co., New York, 1950.

30. J. Hancock and Paul Wintz, "Signal Detection Theory", McGraw-Hill, New York, 1966.

31. R. A. Fisher, "On the Mathematical Foundations of Theoretical Statistics", Phil. Trans. Royal Soc. - London, Ser. A., Vol. 222, p. 309, 1921.

32. H. Cramer, "Mathematical Methods of Statistics, Princeton University Press, Princeton, N. J., 1946.

33. A. Mood and F. Graybill, "Introduction to the Theory of Statistics", McGraw-Hill, New York, 1963.

34. J. N. Puckett, "An Electrical and Statistical Study of Burst Noise", Ph.D. Thesis, Caltech, 1971.

35. G. Newton, L. Gould and J. Kaiser, "Analytical Design of Linear Feedback Controls", John Wiley, Inc., New York, 1964.

36. J. Wozencraft and M. Jacobs, "Principles of Communication Engineering", John Wiley, Inc., New York, 1967.

37. J. V. Uspensky, "Introduction to Mathematical Probability", McGraw-Hill Book Company, New York 1937.

38. O. Mueller, "1/f Flicker Noise in Bipolar Transistors", General Electric Technical Information Series, No. R68-GPD-5, July 1968.

39. B. Mandelbrot, in Fluctuations in Solids Symposium, University of Minnesota, June 1966 (unpublished).

40. D. A. B. Bell, Proc. Phys. Soc. (London) B68, 690(1955).

41. Burr Brown Corp., "Handbook of Operational Amplifier Applications", Tucson, Arizona, 1963. (out of print)

42. "Handbook and Catalog of Operational Amplifiers", Arizona, 1969.

43. J. N. Giles, "Fairchild Semiconductors Linear Integrated Circuits Applications Handbook", Mountain View, California, 1967.

LIST OF FIGURES

NUMBER		PAGE
1	Modified Autocorrelation Function	13
2	Prewhitened and Non-prewhitened Spectral Density Estimates for Noise Source 4	31
3	(same) for Noise Source 5	32
4	Recorded Raw Noise Output	49
5	Amplitude Probability Distributions	53
6	Typical Raw Data Disturbances	61
7	Spectra of Distorted Outcut of Source 1	63
8	(same) for Noise Source 3	64
9	(same) for Noise Source 5	65
10	(same) for Noise Source 7	66
11	(same) for Noise Source 8	67
12	Spectra of Raw Noise of Source 1 with superimposed Linear Trend	71
13	(same) for Noise Source 2	72
14a	Autocorrelation and Spectrum of Semirandom Telegraph Signal	75
14b	Spectral Ripple from Superposition of Many Telegraph Signals	77
15a	Amplitude Distribution of Noise Source 4 on Probability Paper	85
15b	(same) for Noise Source 9	86
16	Relative Availability of Mean Lagged Products	91
17	Asymptotic Relative Availability of Mean Lagged Products	92
18	Autocorrelation for Uneven Sampling	93
19	Autocorrelation for Uneven Sampling	94
20	Schematic Diagram of Mk.II and Mk.III	103

LIST OF FIGURES (CONTINUED)

NUMBER		PAGE
21	Non-Inverting Op-Amp. Circuit	105
22	DC Balancing Circuit for Op-Amps	106
23	IC Noise Sources' Schematic Diagram	107
24	Discrete-Component Regulated Power Supply	110
25	IC Regulated Power Supply	111
26	VLF Square Wave Generator	113
27	Noise Sources' Voltage Sensitivity	114
28	(same) for More Sources	115
29	Unidimensional Heat Equation Geometry	121
30	Temperature Sensing Amplifier	123
31	Effects of Environment on the Temperature of the Noise Sources	125
32	Block Diagram of Active Temperature Control	130
33	Heating System Regulator	129
34	Direct Recording of Bath Temp. Fluctuations	132
35	Temperature Effects on Noise Source 2	133
36	Temperature Sensitivities of All Noise Sources	134
37	Time-Multiplexed Recordings of Temperature, Supply-Voltage, and Nosie Sources' Output	135
38	Prewhitened and Non-Prewhitened Spectral Estimates for Noise Source 1	137
39	(same) for Noise Source 2	138
40	(same) for Noise Source 3	139
41	(same) for Noise Source 6	140
42	(same) for Noise Source 7	141
43	(same) for Bath Temperature	142
44	(same) for Power Supply Voltage	144

LIST OF FIGURES (CONTINUED)

NUMBER		PAGE
45	Block Diagram of Automatic Data Collector	146
46	Schematic Diagram of Main Clock	147
47	Logic Diagrams for Automation Circuits	149
48	Error-Correcting and Error-Detecting Code	157
49	Teletype Relay Actuating Circuit	161
50	Mechanical Contact Noise Eliminator	161
51	Mk. II Spectral Density Estimate	167
52	Mk. III Spectral Density Estimate	169
53	Raw Noise Irregular Behavior	172
54	Mk. IV Spectral Density Estimate	174
55-64	Raw Noise Output of Sources used in Preliminary Spectral Density Estimates	176-185
65-67	Raw Noise Output of Sources used in the Final Spectral Density Estimates	188-190
68-77	Individual Aliased Spectral Density Estimates for All Finally Used Noise Sources	192-201
78	Final Spectral Estimate	202